

POLITECNICO DI TORINO

Master of Science in Energy and Nuclear Engineering

Master Thesis

**Calcium Looping Process as Thermochemical  
Energy Storage in CSP Plant: Integration  
Strategies and Preliminary Analysis**



Supervisors:

Ricardo Chacartegui

Vittorio Verda

Candidate:

Gabriele Colelli

March 2020



*A mio Nonno.*

*La Vita non mi ha lasciato il tempo di festeggiare un mio successo insieme a te.*

*Ti dedico questa Tesi, come risultato di un percorso di crescita in cui il tuo Ricordo ha sempre rappresentato un punto fermo a cui rivolgermi.*

## Abstract

The growing environmental concerns and the necessity to identify alternative energy sources besides traditional fossil fuels have placed increasing emphasis on renewable resources. Their discontinuous nature, however, requires the development of a storage system capable of responding to the demands of users even in conditions of absence of the resource.

The primary aim of the following report is to investigate the possibilities offered by the Calcium Looping (CaL) process and its application as thermochemical energy storage system. It consists of the cyclical repetition of reversible chemical reactions of calcination-carbonation using calcium carbonate as raw material, which is extremely abundant and easily available. The process consists in the splitting of  $CaCO_3$  into  $CaO$  and  $CO_2$  in the endothermic calcination reaction followed by the subsequent recombination of the two products in the exothermic carbonation reaction. The high energy density offered by the phenomenon and the ease of storage of the substances involved suggest the possibility of applying it to the development of a thermochemical storage system integrated with renewable resource power plants.

The analysis focuses on the integration of the Calcium Looping process into a concentrated solar power plant. Given the immaturity of the technology and the absence of similar installations to date, considerable attention is devoted to the two main reactors, calciner and carbonator, as well as the other components constituting the plant. Two different plant configurations are treated, one with high temperature solids storage system and the other with solids stored at ambient temperature. Each is investigated and modelled through the use of AspenPlus software. In both cases, the main power block is characterized by a Joule-Brayton cycle with gas turbine, exploiting the high thermal availability of  $CO_2$  resulting from the energy released by carbonation. The discussion continues through the implementation of an exergo-economic analysis of both configurations observed, with the aim of highlighting their strengths and possible opportunities for improvement. Moreover, the two configurations are also compared from an environmental point of view, through the realization of a cradle-to-grave LCA analysis, in order to understand the possible impacts generated. The compilation of the inventory required for the analysis was obtained from the combination of data regarding a comparable design plant (Gemasolar), hypotheses formulated with the assistance of the literature and results obtained from the simulations performed. Finally, the EROI (Energy Return On Investment) and EPBT (Energy PayBack Time) methodologies are applied in order to provide further information on the energy sustainability of the project, defining a valid tool for comparison with other plant technologies already widely established.



# Summary

INTRODUCTION .....	1
--------------------	---

## CHAPTER 1

### OVERVIEW ON ENERGY STORAGE

1.1. Energetic and environmental background .....	3
1.2. Importance of renewable resources .....	6
1.2.1. Focusing on solar thermal and CSP .....	8
1.3. Energy storage technologies .....	10
1.4. Thermal energy storage systems .....	11
1.4.1. Sensible heat storage systems .....	12
1.4.2. Latent heat storage systems .....	14
1.4.3. Thermochemical energy storage systems .....	15
1.4.3.1. Advantages and disadvantages .....	18
1.5. TES comparison .....	20

## CHAPTER 2

### THE CALCIUM LOOPING PROCESS

2.1. Introduction .....	21
2.2. Description of physical and chemical principles .....	24
2.2.1. Imperfect reversibility of the reaction .....	26
2.3. Integration in a CSP plant .....	30
2.2.2. Advantages of integrating CSP with CaL .....	30
2.4. Description of all systems, equipment and processes .....	32
2.4.1. Calciner .....	32
2.4.2. Carbonator .....	35
2.4.3. Heat exchangers .....	37
2.4.4. Storage systems .....	40
2.4.5. Solid-gas separation and solid transport .....	41
2.4.6. Power block .....	44
2.4.7. Different solar calciner for integration with CaL .....	46
2.4.7.1. Falling particle receivers .....	47
2.4.7.2. Centrifugal solar receivers .....	50

2.4.7.3. Fluidized bed receivers .....	52
--	----

## **CHAPTER 3**

### **SIMULATIONS OF CSP-CaL INTEGRATION**

3.1. CSP-CaL integration methodologies .....	54
3.1.1. Solar tower configuration .....	55
3.1.2. Solar Tower Plant simulation .....	58
3.2. Different CSP-CaL integration layouts analysed .....	59
3.2.1. CASE 1: CSP-CaL with high temperature storage systems	60
3.2.2. CASE 2: CSP-CaL with ambient temperature storage systems .....	67
3.2.3. Main differences and considerations .....	73
3.3. CSP-CaL integration on small scale: Beam-down .....	75

## **CHAPTER 4**

### **EXERGO – ECONOMIC ANALYSIS**

4.1. Goal and meaning of exergo-economic analysis .....	77
4.2. Description of the systems .....	78
4.2.1. CASE 1: 100 MW, high temperature storage system .....	78
4.2.1.1. CASE 1, main assumptions .....	78
4.2.1.2. CASE 1, functional and thermodynamic analysis .....	79
4.2.1.3. Differences between day and night configuration .....	84
4.2.2. CASE 2: 100 MW, low temperature storage system .....	85
4.2.2.1. CASE 2, main assumptions .....	85
4.2.2.2. CASE 2, functional and thermodynamic analysis .....	86
4.2.2.3. Differences between day and night configuration .....	91
4.3. Irreversibility calculation .....	92
4.3.1. Operational concepts .....	92
4.3.2. Irreversibility of CASE 1 .....	96
4.3.3. Irreversibility of CASE 2 .....	98
4.3.4. Considerations and comparisons .....	100
4.4. Exergy-cost calculation .....	101
4.4.1. Operational concepts .....	101
4.4.2. Exergy costs of CASE 1 .....	103
4.4.3. Exergy costs of CASE 2 .....	104
4.5. Cost allocation of different components .....	105
4.5.1. Cost estimation methodology .....	105

4.5.2.	Economic considerations .....	109
4.5.3.	Cost-rates of components .....	110
4.6.	Exergo-economic analysis .....	111
4.6.1.	Operational concepts .....	112
4.6.2.	Exergo-economic analysis of CASE 1 .....	114
4.6.3.	Exergo-economic analysis of CASE 2 .....	115
4.6.4.	Considerations and comparisons .....	116
4.7.	Sensitivity analysis and hypothesis discussion .....	121
4.7.1.	Analysis on heat exchangers .....	121
4.7.2.	Analysis on intercoolers .....	125
4.7.3.	Main results from previous considerations .....	126
4.7.4.	Analysis on input electricity cost .....	127

## **CHAPTER 5**

### **LCA OF CSP-CaL INTEGRATIONS**

5.1.	LCA, Life Cycle Assessment: main concepts .....	130
5.1.1.	Different LCA approaches .....	131
5.1.1.1.	Cradle-to-Grave .....	131
5.1.1.2.	Cradle-to-Gate .....	132
5.1.1.3.	Cradle-to-Cradle .....	133
5.1.2.	LCA recommended structure .....	133
5.1.2.1.	Goal and Scope definition .....	134
5.1.2.2.	Life Cycle Inventory (LCI) .....	135
5.1.2.3.	Life Cycle Impact Assessment (LCIA) .....	136
5.2.	Goal & Scope of the analysis .....	137
5.2.1.	Functional Unit .....	138
5.2.2.	System Boundaries .....	138
5.2.3.	Methodology and Indicators .....	140
5.3.	Life Cycle Inventory Analysis (LCIA) .....	141
5.3.1.	Solar Field .....	141
5.3.2.	Solar Tower and receiver .....	143
5.3.3.	Storage systems .....	144
5.3.4.	Power block .....	148
5.3.5.	End-of-life inventory .....	150
5.3.6.	Inventory conversion factor .....	150
5.4.	Life Cycle Assessment Analysis .....	151
5.4.1.	Assembly-Phase analysis .....	152

5.4.2.	Use-Phase analysis and results .....	153
5.4.2.1.	Comparison on normalized impact categories .....	153
5.4.2.2.	Impact share from main components .....	154
5.4.3.	End-Phase analysis and results .....	156
5.5.	Interpretation of the results .....	159

## **CHAPTER 6**

### **USEFUL INDICATORS FOR FUTURE COMPARISONS**

6.1.	Introduction .....	160
6.2.	Energy PayBack Time (EPBT) .....	161
6.2.1.	EPBT of CSP-CaL integrations .....	161
6.2.2.	Comparison with EPBT of other systems .....	162
6.3.	Energy Return On (Energy) Invested (EROI) .....	163
6.3.1.	EROI of CSP-CaL configurations .....	164
6.3.2.	Comparison with EROI of other systems .....	164
6.4.	Global Warming Potential (GWP) .....	165
6.4.1.	GWP of CSP-CaL configurations .....	165
6.4.2.	Comparison with GWP of other systems .....	166
6.5.	Sensitivity analysis .....	167
CONCLUSIONS .....		171
APPENDIX – MATRICES FOR EXERGO-ECONOMIC ANALYSIS .....		176
AKNOWLEDGEMENTS – RINGRAZIAMENTI .....		183
REFERENCES .....		185



## INTRODUCTION

The progressive depletion of underground fossil fuels reserves in conjunction with the impelling environmental issues encourage, in a constantly more decisive manner, the orientation of the energy and production sector towards the exploitation of the possibilities of renewable resources.

Among the main challenges associated with the decarbonisation process of the global energy scenario, the issue of the intermittence and discontinuity of renewable energy sources is a topic of wide debate. The dependence on natural phenomena and the impossibility of benefiting from a stable and constant energy resource unavoidably slow down an otherwise considerably less complex switch. In response to the problem mentioned above, a field of great ferment in energy research is represented by energy storage, devices capable of storing energy and releasing it when required, effectively extending the availability of resources even to periods of absence of the natural generator phenomenon.

One of the renewable technologies that could benefit the most from the capabilities offered by storage systems is the concentrating solar power plant, CSP, a solution of sure effectiveness and currently established mainly in Spain and the United States, with progressive interest also from many other countries. While thermal storage systems, especially the sensible heat type, are widely applied in integration with CSP applications, the research is recently directed towards a new interesting opportunity offered by thermochemical energy storage systems, devices which, as explained in *Chapter 1* of the following thesis, exhibit absolutely competitive characteristics and of considerable interest in terms of alternatives to traditional thermal energy storage systems.

More specifically, among the technologies included in the category of thermochemical energy storage systems, particular interest is offered by Calcium Looping (CaL). It consists of a concept based on the reversibility of calcination and carbonation reactions, using calcium carbonate, extremely available and easily processable, as raw material. Its main components, calcium oxide and carbon dioxide, can be easily stored in special deposits, making the process attractive for integration with a renewable resource power plant.

In this regard, in *Chapter 2* the analysis of the technology is deepened, addressing its theoretical principles and technical limitations, especially in relation to the degradation that the properties of sorbent may experience as a result of the iteration of reaction cycles. Moreover, with a view to its application in a CSP system, space is dedicated to the discussion of the main components and equipment that should be used to make the integration effective.

Calcium Looping offers characteristics capable of guaranteeing various possible types of plant configurations. Starting from this concept, in *Chapter 3* two main solutions are studied: Calcium Looping used as high temperature thermochemical energy storage system in a CSP plant and Calcium Looping used as ambient temperature thermochemical energy storage system in a CSP plant. In order to analyse the integration operation, plant modelling using software is adopted with the aim of investigating the effective behaviour and cooperation with the necessary components.

The main aim of the following discussion is to address the concept of CSP-CaL integration following an analytical approach based on the evaluation of its effectiveness in terms of exergo-economic and environmental performances, with particular attention to the concept of energetic sustainability. The two proposed configurations are then compared in order to enrich the knowledge with results in addition to those obtained from plant modelling and energy operations studies. In this regard, an exergo-economic analysis is carried out in *Chapter 4*, with the objective of providing information about the operation of the components of the proposed systems and suggesting possible areas for potential future modifications and improvements.

In the subsequent *Chapter 5*, instead, an LCA analysis is implemented on the two CSP-CaL configurations. Various environmental indications can be obtained through this method, enabling a comparison in order to evaluate the impacts generated in each phase of the plant life cycle and to perceive the situations of greater sensitivity on which to intervene to improve environmental performance.

In conclusion, the information obtained from the analyses carried out permits the calculation of some important indicators, such as GWP (Global Warming Potential), EPBT (Energy PayBack Time) and EROI (Energy Return On Energy Invested), which allow the comparison of the two CSP-CaL plant solutions with other types of power generation plants existing in the international production scenario. Therefore, *Chapter 6* also reports some data obtained from the literature, through which to evaluate the possible advantages of the proposed plant in terms of energetic and environmental sustainability.

# CHAPTER 1

## OVERVIEW ON ENERGY STORAGE

### 1.1. Energetic and environmental background

The 21st century is an era characterised by a dramatic evolution of the energy and production system, in adaptation to a substantial transformation of global living habits. The introduction of increasingly efficient tools and progressively more sophisticated equipment means an advancement in the process of integrating technology into the everyday life of each person, making it an essential part and indispensable component.

The information age and its particularities inevitably affect an energy sector that has to face a growing and increasingly diversified demand, thus complexing the response mechanism.

On the other hand, although technological progress ensures the implementation of cutting-edge generation processes, increasingly high production efficiency rates and continuously evolving operation techniques, climate change and the environmental emergency are holding back fervent development and are bringing ever more topical problems back into vogue.

From the analysis of the data reported in "Energy Transitions: Global and National Perspectives" [1], it is clear that the global energy production sector is, up to now, still deeply dominated by the intensive exploitation of fossil resources.

As shown in the graph below (*Figure 1*), the increase in energy demand has caused a consequent growth in primary energy consumption. However, despite the incredible potential of renewable resources, their penetration in the global production sector is still extremely marginal compared to the intensive use of fossil fuels.

Although the possibilities offered by alternative energy sources are in wide and constant development, the exploitation of traditional sources of energy is still of primary

importance, especially in view of the exhausting industrialisation process faced by current developing countries.

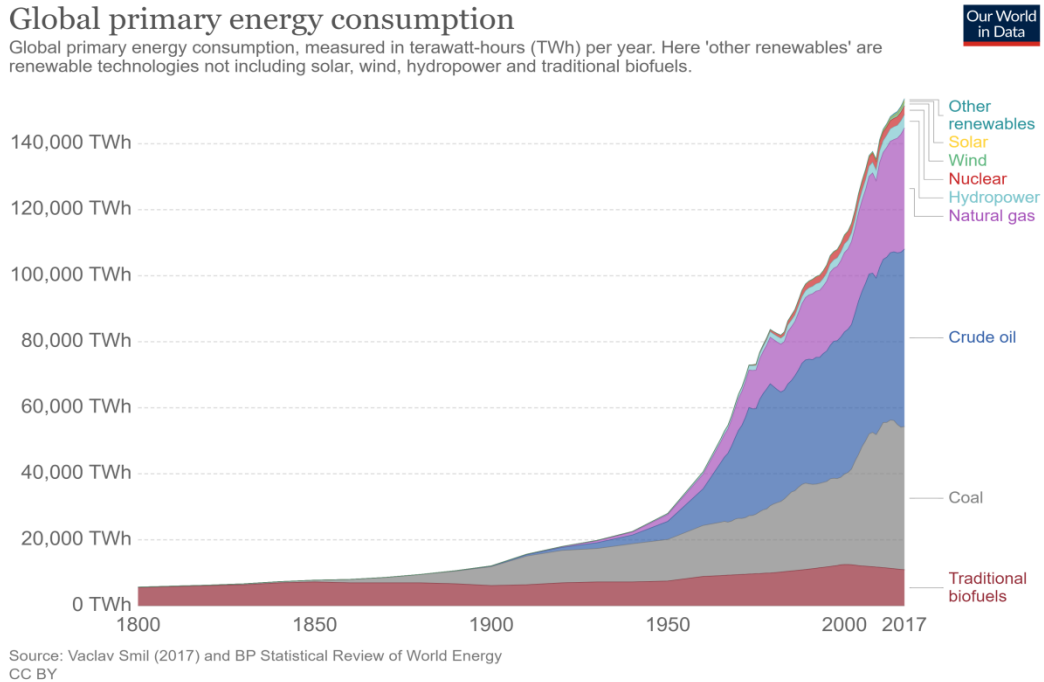


Figure 1 - Global primary energy consumption [1], [2]

The main concern arising from a similar arrangement of the energy system is the significant environmental damage caused by emissions from the combustion of traditional fossil fuels. The following table shows the specific carbon dioxide emissions of some of the most frequently used fuels (Table 1).

Type of fuel	Emissions [(kgCO <sub>2</sub> )/kWh]	Emissions [(kgCO <sub>2</sub> )/GJ]
Hard Coal	0.34	94.6
Fuel oil	0.28	77.4
Diesel	0.27	74.1
Gasoline	0.25	69.3
Liquid petroleum gas	0.23	63.1
Natural gas	0.20	56.1

Table 1 - Specific carbon dioxide emissions of various fuels [3]

Unavoidably, due to the widespread use of fossil fuels, the amount of emissions into the atmosphere proceeds at an unsustainable rate, resulting in environmental emergencies, climate change and meteorological disturbances.

It is possible to investigate the situation in greater detail by observing the following graph (Figure 2). It shows the marked increase in carbon dioxide emissions on a global scale, mainly from the last years of the 20th century.

The considerable contribution of developing countries to the total result is particularly evident, registering a growing trend, in opposition to the urgent need for environmental protection.

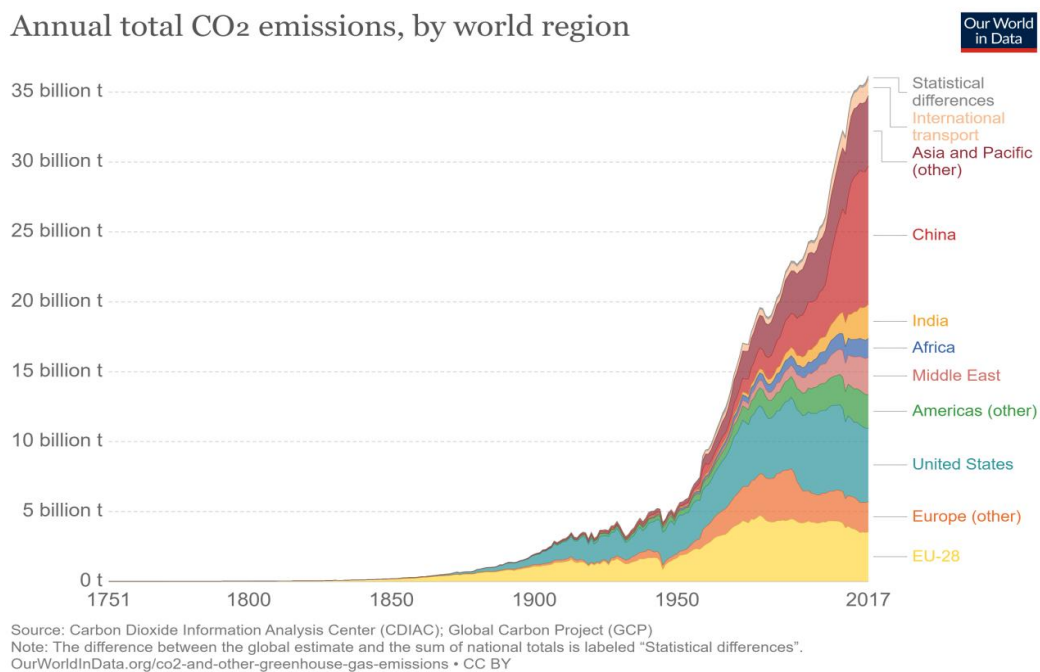


Figure 2 - Annual total CO2 emissions, by world region [4], [5]

This trend is further underlined by the diagram below, which shows the contribution of the various production regions to the overall amount of carbon dioxide emissions (Figure 3).

More specifically, it is particularly noticeable how the contribution of carbon dioxide emissions on a global scale by the Eurozone countries has been drastically reduced, mainly since the 20th century. In principle, the tendency is justified by the intensive process of industrialization of the United States, a new emerging economy in direct competition with European countries. Recently, however, coinciding with the end of the 20th century, a gradual increase in the magnitude of the emissions generated by China

and Asian countries can be observed, reflecting the high level of industrial intensity of their growth process.

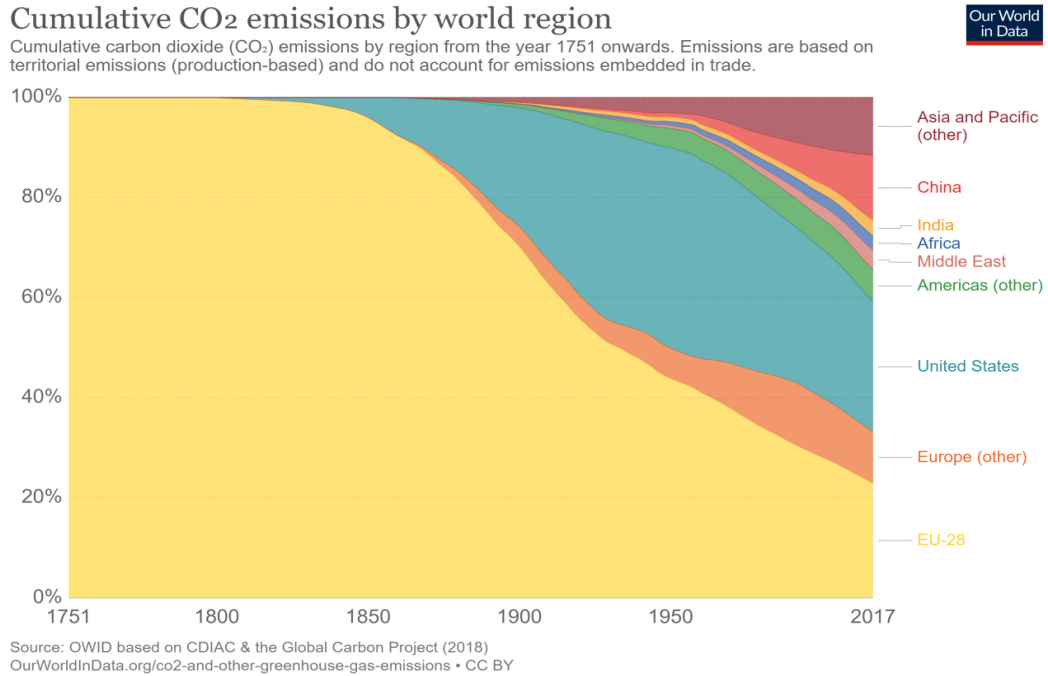


Figure 3 - Cumulative CO<sub>2</sub> emissions, by world region [4], [5]

In accordance with the evident situation of climate emergency, it is absolutely necessary to completely overturn these trends through a radical change in the production and energy sector, with a view to a deep decarbonisation that favours a mitigation of climate-altering effects.

## 1.2. Importance of renewable resources

The urgent environmental issues require a solution that provides an effective restructuring of the energy system towards sustainable processes in order to reduce the current amount of pollutant emissions. The aim is to mitigate the phenomenon of global warming, defined as an increase in the average temperature level of surface air and surface water in a time period of at least 30 years. The topic was widely debated at the Paris Climate Conference (COP21) in December 2015, leading to the approval of the

Paris Agreement, a treaty that reinforces the concept of global warming and preaches the urgency of solving the problem. Specifically, the objective is set to keep the 21st century temperature increase at least below 2°C above pre-industrial levels, with further efforts to improve profitability by reducing the target to 1.5 °C.

An analysis of the report published by IPCC - Intergovernmental Panel on Climate Change, specifically the special report "Global Warming of 1.5 °C" (2018), demonstrates how anthropogenic activities caused an average increase in surface temperature of about 0.85 °C in the period between 1880 and 2012 (Figure 4). More in detail, there are also more marked regional temperature increases, with some geographical regions having already largely reached the level of 1.5 °C over a continuous time period long enough to be considered effective.

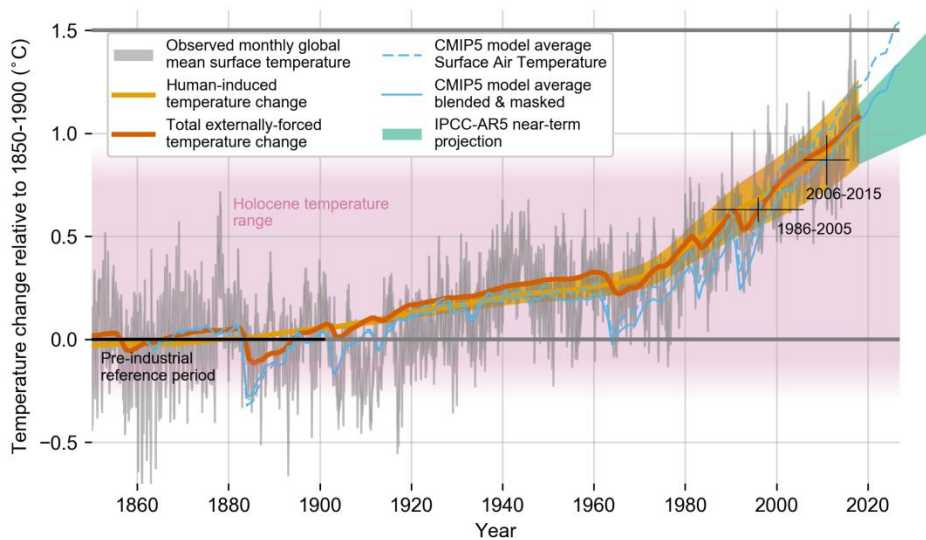


Figure 4 - Evolution of global mean surface temperature (GMST) [6]

Among the various methodologies proposed to address the problem, the intensive exploitation of renewable resources is a valuable solution. Modern technologies guarantee a rapid development of the sector, introducing conversion techniques with increasing conversion efficiency. In addition, manufacturing processes are becoming more and more standardised, resulting in a reduction of previously high costs. State incentives and environmental benefits are additional aspects in favour of their development.

The following chart (Figure 5) shows the growth trend of the main renewable resources in the current energy sector. It is noticeable how recently there has been an important development in the wind and solar sectors.

## Renewable energy generation, World

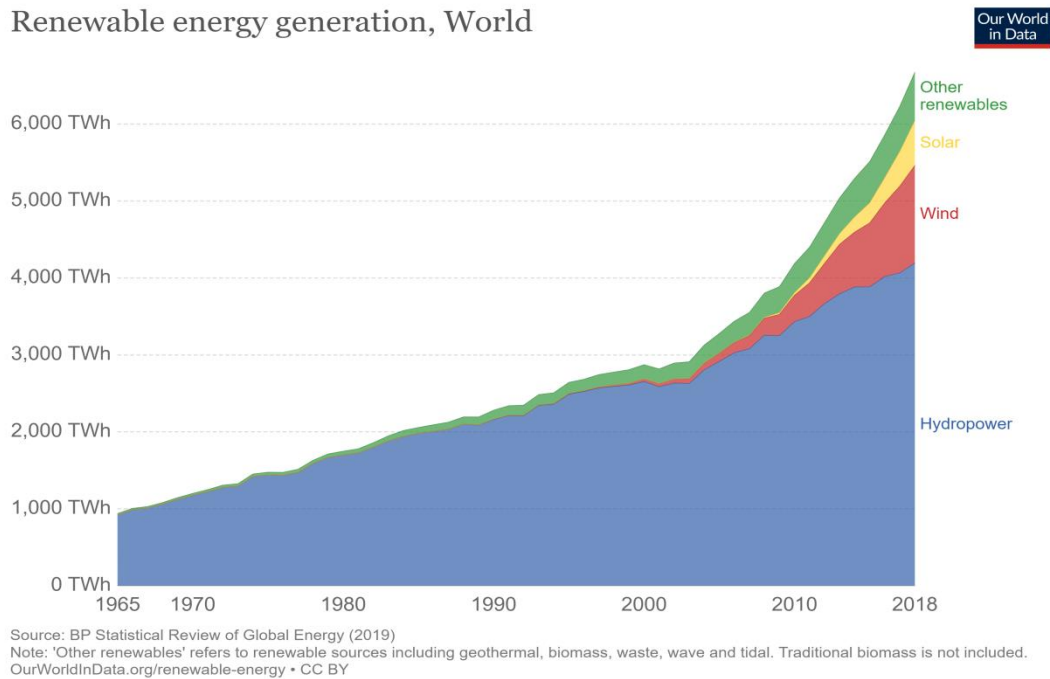


Figure 5 - Renewable energy generation, World [7], [8]

Solar technology, in particular, represents the field in which research is, nowadays, largely active in order to improve its performance and ensure its diffusion on a large scale. Its incredible potential and the wide range of applications that characterize it, makes solar energy a very interesting alternative energy resource. Moreover, its peculiarities make it remarkably complementary with the topics discussed in the following treatise, which is why it is considerably advantageous to dedicate additional consideration to it.

### 1.2.1. Focusing on solar thermal and CSP

Among the alternative energy sources, solar thermal is certainly an interesting option in view of environmental concerns and the climate change process. The concept behind its use consists in exploiting the thermal availability of solar radiation with the aim of obtaining a high amount of thermal power to evolve in a subsequent power cycle. Basically, the operating scheme is similar to that of common fossil fuel plants, with the difference that the primary resource, solar radiation, does not require combustion processes, making the system potentially carbon free.

Concentrated solar power is clearly one of the most interesting applications of the solar thermal concept. The technology bases its operation on the concentration of solar radiation, ensuring the achievement of significantly higher temperatures than traditional

methods in the field of solar thermal. The process of exploitation of thermal heat in the power cycle is therefore advantaged, with higher plant efficiency.

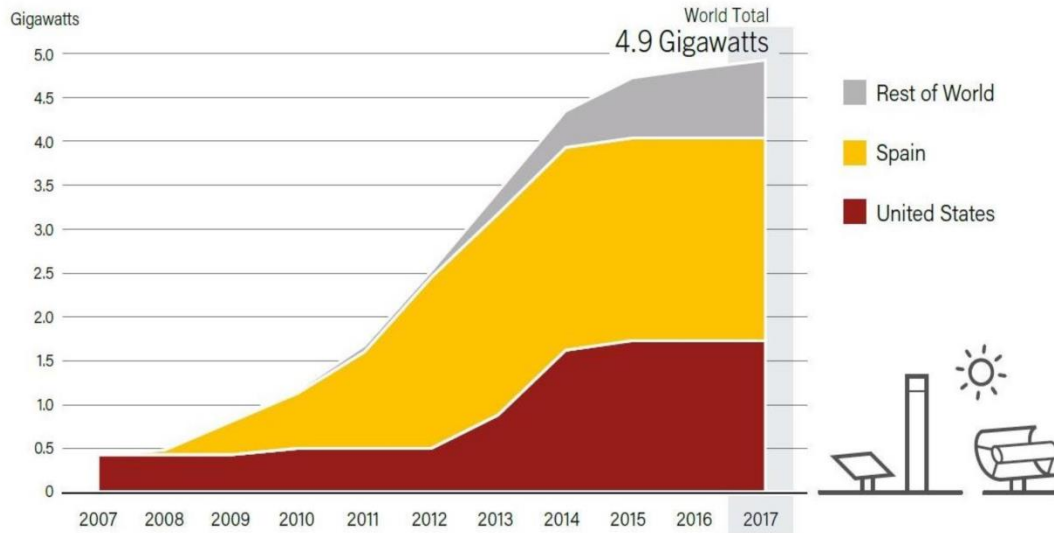


Figure 6 - Concentrating solar thermal power global capacity by country and region over the period 2007–2017 [8]

The above diagram (*Figure 6*) demonstrates the growing interest in CSP technology. Its implementation remains reasonably limited to geographical areas with a high availability of direct normal irradiance (DNI), confirming the evidence that Spain and the United States are the countries in which the plant design is most widely used today [8].

The mechanism for generating energy from solar thermal and, more specifically, from concentrated solar power, however, is strictly dependent on the availability of solar radiation, limiting its use to daylight hours only. The problem, actually, is extended to most of the renewable resources, whose main disadvantage is the intermittence of the source due to the dependence on climatic conditions and the occurrence of natural phenomena.

A solution to the problem of discontinuity of resources may be identified through the introduction of an adequate energy storage system. A plant which is dependent on an intermittent renewable source, if integrated with a storage system, would produce energy during the periods of availability and at the same time would guarantee the possibility of accumulating an adequate quantity to satisfy demand even in the absence of external input. Specifically, equipping a CSP plant with a thermal energy storage mechanism would allow the conservation of thermal energy useful for the generation of electricity even in the absence of incident solar radiation, giving the plant greater

flexibility and increasing its competitiveness compared to traditional fossil fuel generation processes.

### 1.3. Energy storage technologies

Energy storage represents a fundamental factor in the establishment of production plants based on renewable resources. Its integration guarantees a mitigation of power peaks, an increase in system flexibility and encourages the conservation and distribution of energy obtained from intermittent alternative sources. In this way it is possible to balance the energy demand by placing a smaller impact on the distribution network and at the same time amortizing construction, transmission and distribution costs.

Generally a storage system is composed of a storage medium, a power conversion system and a balance of system. Different storage technologies can be distinguished: electrochemical, chemical, mechanical, electrostatic, electromagnetic and thermal [12].

Electrochemical storage systems, which are commonly indicated as batteries, are devices that transform the chemical energy of the substances contained within them into electrical energy. Essential elements of batteries are anode, cathode and electrolyte. The properties of the device are inevitably influenced by the chemical species that make it up [11]. Among the fundamental characteristics that a battery must exhibit there are high charge and discharge efficiency, low self-discharge and long life cycle. The connection of several batteries in series and parallel enables a device with the required voltage and capacity values to be manufactured. Electrochemical storage systems include nickel-cadmium, nickel-hydrogen, nickel-metal hydride, nickel-zinc, lead-acid, sodium-sulphur, sodium-nickel chloride and lithium-ion batteries [11].

A similar mechanism of operation is displayed by chemical storage systems. They base their theoretical principle on the storage of chemical compounds with high chemical potential. The most important exponents of this category are the fuel cells, which share with common batteries the production of power from the stored substances, but they differ because the energy storage systems are separated from the power generation apparatus, thus exceeding the limit imposed by the internal storage capacity of the battery.

Mechanical storage systems include flywheels energy storage (FES), compressed air energy storage (CAES) and pumped hydraulic systems. While the former belongs to the

category of kinetic energy storage, basing its mechanism on the accumulation of energy by capturing the momentum of a rotating mass, the other two systems are part of the potential energy storage. They provide storage by accumulating potential energy within large pressurized reservoirs [12].

The field of electrostatic energy storage includes capacitors, which store energy in a magnetic field, rather than in chemical potential between reactants such as in batteries. Specifically, energy is stored by separating electric charges between two electrodes. Compared to batteries they have a very low energy density but a very high power density, thus offering the possibility to operate with very high current values although for rather reduced time ranges. Supercapacitors and ultra-capacitors share the same operating principle, however they exhibit higher capacity values in a smaller size [11].

Electromagnetic storage systems, or superconductive magnetic energy storage (SMES), benefit from the properties of the magnetic field to store energy. Specifically, a coil of cryogenically cooled superconductive material is charged with direct current. Therefore, through its discharge it is possible to obtain energy and transfer it to the grid. The main problems associated with this technology are the high cost of the superconducting coil and the high energy expenditure to obtain cryogenic cooling, which is why a SMES is commonly used for energy storage with a restricted period of operation [11].

As far as thermal energy storage systems (TES) are concerned, they are the most widely used category of energy storage in the field of energy accumulation from renewable sources, especially with a view to possible integration with a solar-type resource. They are divided into sensible heat storage, latent heat storage and thermochemical heat storage and will be analysed below.

#### 1.4. Thermal energy storage systems

Thermal energy storage systems base their operating scheme on the heating or cooling of a storage medium with the aim of storing thermal energy for subsequent reuse in order to produce a useful effect, regardless of whether it is a further heat exchange or power generation. It is particularly common to integrate a TES mechanism with renewable resource systems to provide a solution to the problem of intermittence of the resource through thermal energy storage for subsequently generating electricity in a power cycle, depending on user demand.

By virtue of the possibility of storing thermal energy, otherwise dissipated in the environment, saving fossil fuels necessary for its production in the absence of alternative energy sources, thermal energy storage systems guarantee both environmental and economic advantages. First of all, they reduce the costs associated with the purchase of combustible materials. In addition, they prevent the emission into the atmosphere of pollutants generated by combustion processes [14].

Thermal energy storage systems can be grouped into three categories [13]:

- Sensible heat thermal storage systems: they involve a temperature change in the storage medium;
- Latent heat thermal storage systems: they use phase change materials to store energy in the form of latent heat;
- Thermochemical heat storage systems: they exploit the thermodynamic properties of chemical reactions to acquire and release heat.

#### 1.4.1. Sensible heat storage systems

In sensible TES, the thermal storage mechanism consists in the temperature variation of the storage medium through the exchange of thermal energy. Substances that can be used as storage medium are: water, air, oil, rock beds, sand, bricks and soil. The choice of the medium is implemented in order to ensure correspondence between its thermodynamic properties and the operating conditions of the plant.

Water, for example, displays a relatively high heat capacity ( $\sim 4.2 \text{ kJ/kgK}$ ), consequently it represents a reasonable choice in applications in which the thermal range is within its operating limits, as in domestic heating processes. Ceramic materials, on the other hand, although they offer a considerably lower heat capacity ( $\sim 0.84 \text{ kJ/kgK}$ ), are considerably more suitable for situations with high operating temperatures [13].

The thermal process that takes place in a sensible TES is described in the following relation:

$$Q = m\bar{c}_p\Delta T = \rho\bar{c}_pV\Delta T \quad (1.1)$$

Where  $m$  is the mass of the storage medium,  $\bar{c}_p$  [ $\text{J/kgK}$ ] is its thermal capacity,  $\Delta T$  is the temperature variation to which the medium is subjected,  $\rho$  is its density and  $V$  its volume.

The characteristics of the sensible TES make it a technology particularly appropriate for integration in CSP systems. Among the storage mediums most frequently used for this purpose, the most common are molten salts. They provide high volumetric heat capacity, high boiling point and very high thermal stability, guaranteeing a satisfactory performance at very high operating temperatures, with a consequent increase in power cycle efficiency. They are furthermore suitable to be used simultaneously as TES and as heat transfer fluid, thus conferring elasticity to the plant [14].

Other materials that may be used as sensible TES in CSP plants are liquid metals. They are metals with a melting temperature low enough to be processed in liquid form, but at the same time a boiling point high enough to ensure a high operating temperature range. Although they have advantageous thermodynamic properties in terms of cycle efficiency and receiver functionality, cost, toxicity and corrosivity represent some problems that limit their diffusion [14].

In accordance with the functionality of a CSP system, it is also appropriate to mention the use of solid materials as sensible TES. Specifically, concrete, sands and castable ceramics have thermodynamic characteristics that guarantee an adequate operational response even at the high temperatures reached in a solar tower plant. The low cost and simplicity of manufacturing constitute favourable factors for their application, although some physical properties may suffer degradation as a result of thermal processes.

In the figure below (*Figure 7*) some possible ways of using sensible TES in CSP plants are represented. More specifically: (a) liquid metal as receiver with salt TES and (b) Direct TES system using liquid metal.

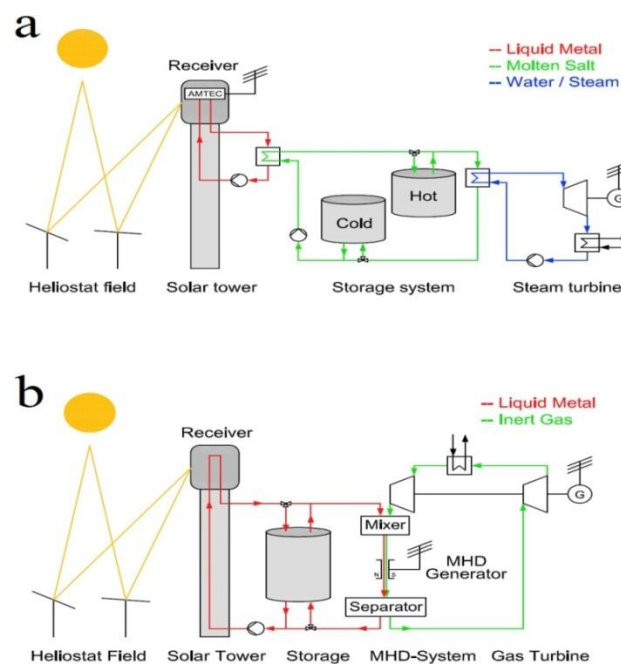


Figure 7 - Conceptual CSP plant using liquid metal (a) Liquid metal as receiver with salt TES and (b) Direct TES system using liquid metal [14]

#### 1.4.2. Latent heat storage systems

The latent TES are special devices that exploit the latent heat of the phase change of some substances for the implementation of heat exchange processes. The physical transformation that characterizes them is described in the following relation:

$$Q = mL = \rho VL \quad (1.2)$$

Where  $m$  indicates the mass of the storage medium, with density  $\rho$  and volume  $V$ .  $L$  [J/kg], on the other hand, represents the value of the corresponding latent phase change heat.

The storage mediums used in a latent TES are commonly known as Phase Change Materials (PCM). Their particularity consists in being able to accumulate a considerable amount of thermal energy through a phase change, thus achieving a substantially isothermal transformation. The technology is essentially based on solid/liquid or solid/solid transformations. PCM materials exhibit considerably advantageous characteristics when compared to sensible TES, due to an achievable storage capacity of  $100 \text{ kWh/m}^3$  compared with  $25 \text{ kWh/m}^3$  of sensible TES, and a process efficiency of up to values of 75-90% [12]. The possibility, moreover, of carrying out thermal storage transformations in an isothermal manner makes PCMs possible candidates for integration with solar systems, thus cushioning the limitation associated with high operating temperatures. The main disadvantage of PCMs is their low thermal conductivity value, generally between  $0.2 \text{ W/mK}$  and  $0.7 \text{ W/mK}$ , thus requiring the integration of technologies for the promotion of heat transfer [15].

The advantage of a latent TES over a sensible TES is adequately analysed in the following figure (*Figure 8*). Specifically, it is evident that performance improves further when the latent TES is realized by assembling different PCMs with increasing phase change temperature.

Substances commonly used as PCM are paraffin waxes, fatty acids, esters, glycols and salts. In conclusion, latent TES constitute a particularly promising technology, demonstrating important advantages such as high energy storage density and the possibility to perform transformations with a minimum temperature variation. Up to now, however, their applications are in the research and development phase, limiting their widespread diffusion on a large scale.

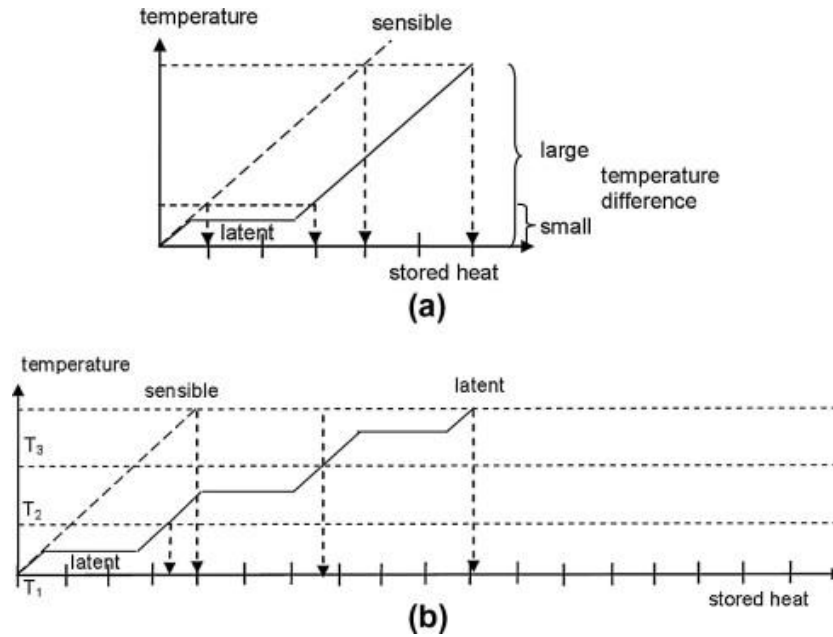


Figure 8 - Comparison of stored heat between sensible heat storage and latent heat storage: (a) With a single PCM; (b) With cascaded latent heat storage [15]

### 1.4.3. Thermochemical energy storage systems

Another interesting energy storage systems technology includes the thermochemicals. They base their operation on the energy exchange that occurs after the formation and breakage of chemical bonds in exothermic and endothermic reactions. They are therefore able to accumulate and release energy by exploiting reversible thermochemical reactions between appropriately selected chemical substances.

Compared to sensible and latent heat storage systems, thermochemicals offer a significantly higher energy density, in the order of  $300 \text{ kWh/m}^3$ , with equally considerable process efficiency values (75-100%) [12].

During the charging phase of the storage system, the chemical compound is dissociated into its components according to an endothermic chemical reaction, as expressed below:



The process requires an external energy input, corresponding to the  $\Delta H_R$  of reaction for the specific compound used, necessary so that the chemical bonds can be broken favouring dissociation.

The storage discharge phase, on the other hand, is described by the reverse reaction:



The recombination reaction of the products is an exothermic process and the amount of heat energy gained is equal to:

$$Q = n_{AB} \Delta H_R \quad (1.5)$$

With  $n_{AB}$  which indicates the number of moles of the generic compounds AB.

The comprehension of the mechanism is further facilitated by a thermodynamic study of chemical processes. Specifically, a generic thermodynamic transformation equation is the following:

$$\Delta G_R^0 = \Delta H_R^0 - T \Delta S_R^0 \quad (1.6)$$

It expresses Gibbs' free energy variation as a function of the corresponding changes in enthalpy and entropy. The identification of the transition temperature, defined as the temperature at which the reaction equilibrium constant is a unit value,  $K_a = 1$  (expressed in terms of activity), can easily be derived from Gibbs' definition of free energy. It is defined by the relationship:

$$\Delta G_R^0 = -R T \ln K_a \quad (1.7)$$

In thermodynamic equilibrium conditions,  $K_a = 1$ , then it results  $\Delta G_R^0 = 0$ . By imposing this condition in (1.6), the transition temperature  $T^*$  is immediately obtained:

$$T^* = \frac{\Delta H_R^0}{\Delta S_R^0} \quad (1.8)$$

The transition temperature provides important information about how the reaction should take place. Specifically, if  $T > T^*$ , the dominant process is decomposition, identifying the charging phase of the storage. Vice versa, if  $T < T^*$ , the synthesis transformation is favoured, with consequent discharge of the system [14].

Another significant parameter is the operating pressure inside the reactor. A decrease in this parameter would result in a reduction in the transition temperature. The reactor is generally equipped with a vacuum pump in order to control the internal pressure. In addition, this methodology also guarantees the possibility to vary the transition temperature, if necessary, simply by acting on the pressure.

In the description of thermochemical energy storage, it is appropriate to mention the considerable advantage resulting from the possibility to store the dissociation products for a very long period after the reaction. This feature allows not only to extend the availability of the resource to any time period of demand, but also contributes to improving the efficiency of the process, ensuring long-term storage with negligible thermal losses [14].

There are currently numerous chemical candidates to be used for thermochemical energy storage systems. Among the key properties for an efficient process, high chemical reversibility, large chemical enthalpy change and simple reaction conditions should be highlighted. In the table below (*Table 2*), some of them are presented, together with the corresponding values of energy density and reaction temperature, two factors of primary importance in the selection of the most suitable compound for the particular application treated.

<i>Thermochemical material (AB)</i>	<i>Solid reactant (A)</i>	<i>Working fluid (B)</i>	<i>Energy Density [<math>\frac{GJ}{m^3}</math>]</i>	<i>Reaction temperature [°C]</i>
$MgSO_4 - 7H_2O$	$MgSO_4$	$7H_2O$	2.8	122
$FeCO_3$	$FeO$	$CO_2$	2.6	180
$Ca(OH)_2$	$CaO$	$H_2O$	1.9	479
$Fe(OH)_2$	$FeO$	$H_2O$	2.2	150
$CaCO_3$	$CaO$	$CO_2$	3.3	837
$CaSO_4 - 2H_2O$	$CaSO_4$	$2H_2O$	1.4	89

*Table 2 - Promising materials for Thermochemical Energy Storage [17]*

The comparison is further investigated in the following illustration (*Figure 9*), proposed by (Pardo et al.), in which several possible reactants are compared in terms of mass energy density and volume energy density, assuming a packed bed porosity of 0.5 and a bulk density for solid reactants.

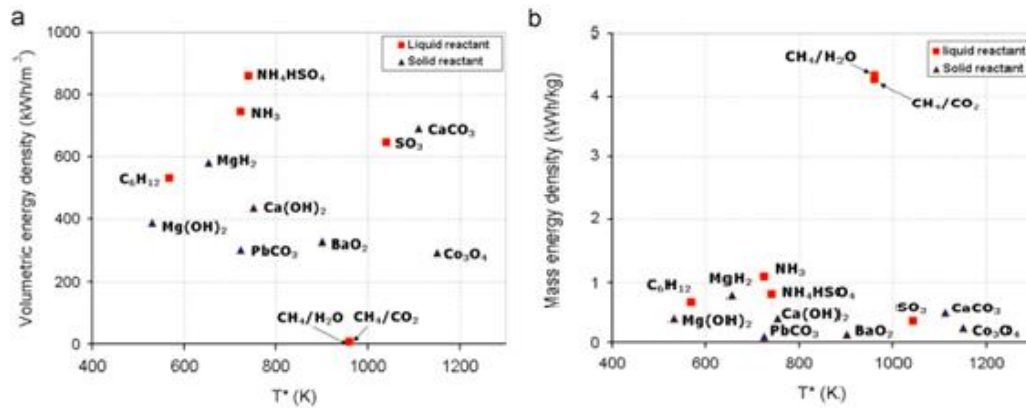


Figure 9 – Volumetric (a) and mass (b) energy density versus turning temperature [16]

#### 1.4.3.1. Advantages and disadvantages

Thermochemical energy storage systems are an emerging, innovative and undoubtedly interesting technology. Despite many advantages over traditional TES, it is also worth mentioning their various weaknesses in order to obtain an adequate comparison framework.

Thermochemical energy storage systems are very advantageous in terms of simplicity of storage of substances. Components A and B obtained after the dissociation reaction can be stored separately at ambient temperature after appropriate cooling processes. This guarantees an extension of the time of storage and increases the generation elasticity of the system. In addition, storage conditions of this type drastically reduce heat losses, which represent a significant challenge in traditional storage systems. Finally, another remarkable characteristic is the high energy density value, which allows a greater amount of energy to be stored in the same volume in comparison to sensible and latent TES. The latter property is particularly relevant in applications where there are space limitations. The following graph (Figure 10) confirms what has just been described, classifying the various thermal storage systems according to energy density.

However, the deployment of thermochemical energy storage systems is not yet completely consolidated. The technology comprises problems that are still under analysis and research, including: complexity of reactor design, low long-term durability due to degradation of reaction reversibility, chemical stability not completely reliable, corrosion caused by some of the candidate chemical substances, poor heat and mass transfer performance, in addition to typically relatively significant production and manufacturing costs.

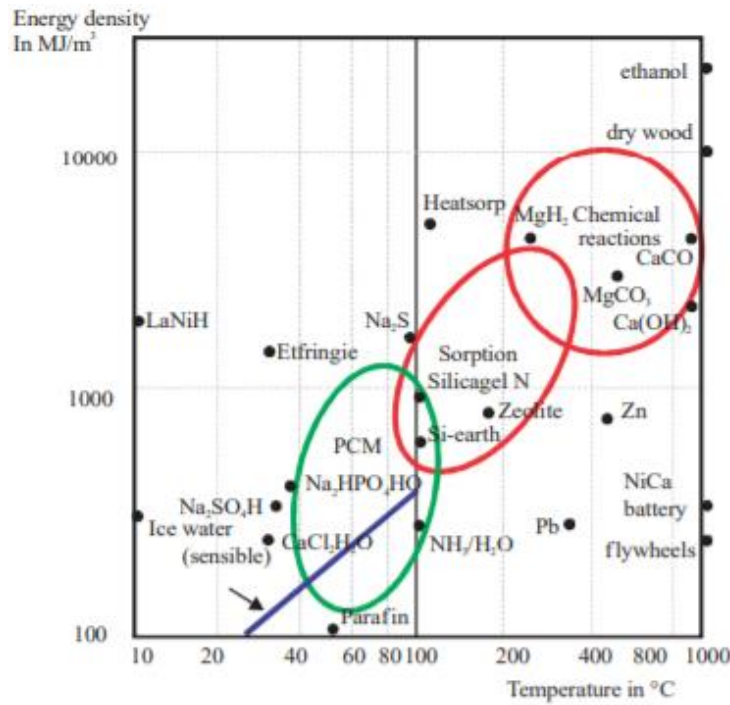


Figure 10 – Energy density for different TES [16]

The problems mentioned above therefore relegate thermochemical energy storage systems to laboratory applications for research purposes, reducing their commercial spread in waiting for greater guarantees. The immaturity of the technology and the lack of experience in the sector reduce its appeal in the industrial field, causing an increase in costs with a consequent rise in investment risks. However, its promising characteristics, in line with environmental requirements and the growth of solar thermal technologies, suggest the possibility of future developments and consequent affirmations in the energy industry.

## 1.5. TES comparison

The table below (*Table 3*) shows a comparison between the main characteristics of the different thermal energy storage systems analysed.

	<i>Sensible TES</i>	<i>Latent TES</i>	<i>Chemical TES</i>
<b>Storage density</b>	<i>Small ~ 0.2 GJ/m<sup>3</sup></i>	<i>Medium ~ 0.3 – 0.5 GJ/m<sup>3</sup></i>	<i>Large ~ 0.5 – 5 GJ/m<sup>3</sup></i>
<b>Storage temperature</b>	<i>Charging phase temperature</i>	<i>Charging phase temperature</i>	<i>Ambient temperature</i>
<b>Storage period</b>	<i>Limited (thermal losses)</i>	<i>Limited (thermal losses)</i>	<i>Hypothetically unlimited (no thermal losses)</i>
<b>Lifetime</b>	<i>Long</i>	<i>Limited due to PCM cycling</i>	<i>Limited due to reactant degradation</i>
<b>Technology</b>	<i>Basic</i>	<i>Medium difficulty</i>	<i>Advanced and complex</i>
<b>Maturity</b>	<i>Available commercially</i>	<i>Limited commercial availability</i>	<i>Mostly in research and development phase</i>
<b>Cost</b>	<i>~ 0.1 – 10 €/kWh</i>	<i>~ 10 – 50 €/kWh</i>	<i>~ 8 – 100 €/kWh</i>
<b>Transport distance</b>	<i>Short (thermal losses)</i>	<i>Short (thermal losses)</i>	<i>Hypothetically unlimited (no thermal losses)</i>
<b>Advantages</b>	<i>Low cost; Large materials availability; Simple technology.</i>	<i>Good storage density; Isothermal processes; High efficiency;</i>	<i>High storage density; Negligible thermal losses; Long storage period; Long transport distance possibility.</i>
<b>Disadvantages</b>	<i>High thermal losses; Low storage density.</i>	<i>High thermal losses; Corrosivity;</i>	<i>More complex technology; Still under development; Higher capital cost.</i>

*Table 3 - Thermal energy storage systems comparison [17]*

## CHAPTER 2

### THE CALCIUM LOOPING PROCESS

#### 2.1. Introduction

Calcium Looping is an innovative chemical and energetic process that has acquired considerable importance in the industrial and productive panorama of recent years. Its properties, especially in virtue of the possibility to realize processes with a significantly reduced environmental impact, have guaranteed its rapid development and growing application, mainly in integration with existing technologies.

The recent environmental situation, the urgent climate emergency and the need to identify alternative production methods that guarantee a reduction in atmospheric emissions make Calcium Looping (CaL) technology an essential resource in the context described. In this regard, its use as a CO<sub>2</sub> capture system is highly regarded, especially in view of the possibility of coupling it with a fossil fuel power plant, a solution that would make potentially carbon-free the exhaust fumes released into the atmosphere [18] [19]. There is no doubt that the CO<sub>2</sub> capture and storage (CCS) technique is a mode with considerable potential for reducing global greenhouse gas emissions. According to the International Energy Agency (IEA), CO<sub>2</sub> capture from fossil fuel emissions represents about 19% of the total potential for emissions reduction for a 2050 low-emission scenario [19].

Analysing, moreover, the trends related to CO<sub>2</sub> emissions in recent years, it can be seen that, due to the increasing industrialization, the growing energy demand and the gradual intensification of production in developing countries, the quantities of greenhouse gases and CO<sub>2</sub> in particular are constantly growing globally.

In relation to CO<sub>2</sub> emissions from fossil fuel power generation processes, the situation can be further investigated by analysing the graph proposed by IEA and reported below (*Figure 11*). Looking at the emission trends, it is possible to see that if OECD countries have achieved an overall, albeit modest, reduction in terms of emissions from fuels, recording a decrease from 12.6 Gt CO<sub>2</sub> in 2000 to 11.6 Gt CO<sub>2</sub> in 2018, at global level

the situation is decidedly less comforting. Over the same period, in fact, a substantial increase can be seen from 23.2 Gt CO<sub>2</sub> in 2000 to 33.4 Gt CO<sub>2</sub> in 2018 [20].

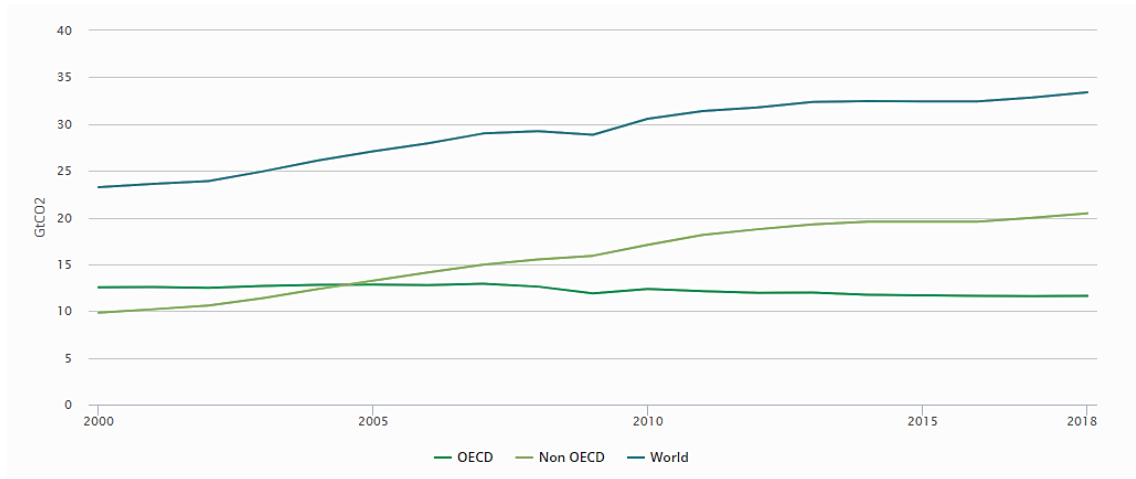


Figure 11 - CO<sub>2</sub> emissions from fuel combustion, IEA [20]. All rights reserved.

Analysing the data more in detail, it can be observed that the trend of emissions of OECD countries in recent years has remained stable at 11.6 Gt CO<sub>2</sub> per year, with no substantial variations. An explanation of the identified behaviour is provided by the following graph (*Figure 12*), provided by IEA, in which the change in annual CO<sub>2</sub> emissions for OECD and non-OECD countries in recent years is recorded. It can be seen that in the recent period 2017-2018 OECD countries have reversed the trend, showing a considerable increase in emissions (+ 52 Mt CO<sub>2</sub>) compared to the results achieved in previous years.

This chart, added to the marked increase in the emission levels recorded for non-OECD countries in recent years, explains the reason for the growing emission trend and puts further emphasis on the urgency of finding useful solutions to reduce the quantities released [20].

In this context, Calcium Looping is one of the most promising technologies in the current energy landscape, basing its functionality on a cycle of calcination and carbonation reactions using CaCO<sub>3</sub>, a material easily found in nature in substances such as limestone and dolomite [21]. This particularity attaches great importance to technology, because of undoubtedly favourable environmental aspects in a current emergency situation. The fundamental mechanism is based on the capture of CO<sub>2</sub> from the exhaust gases leaving production plants and its subsequent reaction with CaO in the ultimate production of CaCO<sub>3</sub> in a high-temperature carbonation process (650°C) [23].

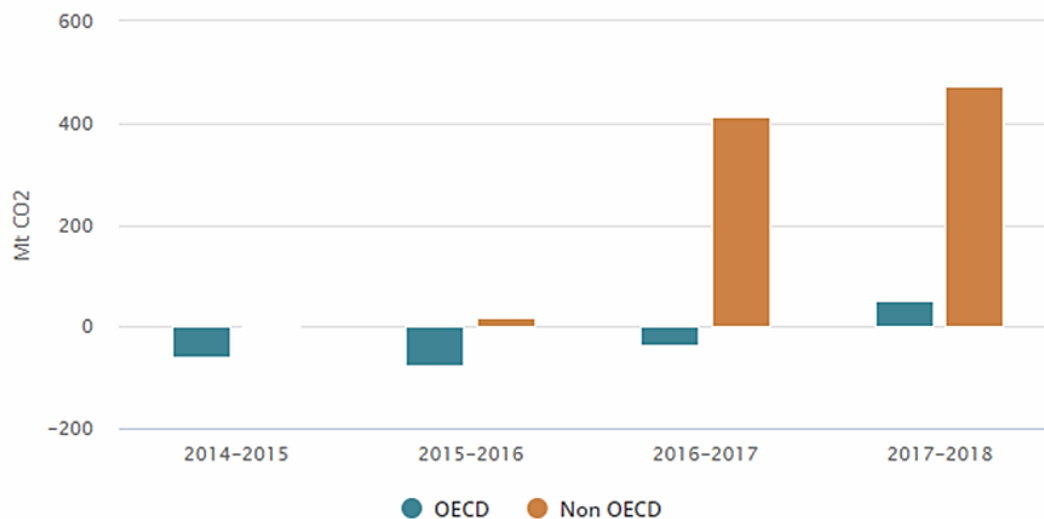


Figure 12 - Annual change in CO<sub>2</sub> emissions for OECD and non-OECD countries, IEA [20]. All rights reserved.

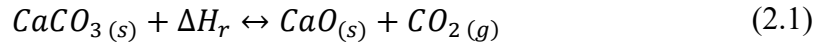
Due to the high temperatures required in the calciner (950°C), the use of the CO<sub>2</sub> capture system requires the integration with a heat production system, which can possibly be characterized by an alternative source, tendentially renewable, optimized with an internal network of heat exchangers that ensure the exploitation of the high operating temperatures of the fluids used [23].

Considering, moreover, the production of CaO in the cycle, it is immediate to consider the boasting deriving from a connection of the process with the cement industry, guaranteeing considerable energy savings in the otherwise necessary transformation of limestone into CaO, a fundamental compound in the operations of the above mentioned sector.

The range of application of Calcium Looping is wide and involves other possible branches and developments in the energy sector. Of great academic interest is, for example, the integration of the process in the production of hydrogen [24], which benefits from the catalytic gasification of coal, an activity currently abundant especially in China and developing countries. By virtue of the growing importance of hydrogen as a future energy source in its many applications, this scenario also inevitably increases the visibility and versatility of the Calcium Looping process.

## 2.2. Description of physical and chemical principles

The Calcium Looping process is based on a cycle of calcination and carbonation reactions involving calcium carbonate  $CaCO_3$ , calcium oxide  $CaO$  and carbon dioxide  $CO_2$ , as indicated in the formula below:



The raw material needed to start and implement the process is calcium carbonate ( $CaCO_3$ ). It is a material widely available in nature, being the second most abundant on Earth after water. Substances such as limestone and dolomite are, in fact, extremely rich of it [25][26], and consequently it constitutes a great advantage in terms of product availability, environmental sustainability and economic convenience.

The process begins in the calciner, which is a component whose function is to provide the initial  $CaCO_3$  separation reaction in the  $CaO$  and  $CO_2$  compounds. The process is endothermic and consequently requires an external energy supplement to occur, as specified by the following equation:



In view of a future integration of Calcium Looping in a thermochemical storage system, the thermal energy obtained from a solar receiver of a solar concentration system is certainly a way to feed the reaction. Following the same principle, it is immediate to identify why Calcium Looping has such a wide range of possibilities in the field of  $CO_2$  capture. If, in fact, integrated in a power generation plant powered by fossil fuels, the high amount of energy generated by combustion, in combination with the high availability of fuel, meet the requirements for starting the reaction.

The continuation of the cycle can take place immediately, sending the  $CaO$  and  $CO_2$  compounds directly into the carbonator for the reverse reaction, or after some time after their storage in special storage systems. The latter solution is particularly recommended in the case of integration of the Calcium Looping process in a solar concentration system. The mechanism would in fact guarantee the storage of the thermal energy collected by the plant in the form of potential chemical energy, which can be converted back into the carbonator whenever required.

The carbonator is a component in which  $CO_2$  and  $CaO$  are subjected to the ideal thermodynamic conditions so that the reverse chemical recombination reaction with consequent formation of  $CaCO_3$  can occur. The following formula explains the chemical mechanism that takes place at this stage:



It is an exothermic reaction, through which it is possible to convert the chemical potential stored in the form of  $CaO$  and  $CO_2$  reagents into thermal energy generated by their reaction.

The thermodynamic conditions under which the calcification and carbonation processes are conducted can be variable and depend on plant regulation. According to (Berger) and (Valverde and Medina) considering an integration of the Calcium Looping process in a solar concentration plant for the realization of a thermochemical storage system, the carbonation process should be conducted at high partial pressure of  $CO_2$  and high temperature (about 850 °C or higher) [27] [28]. The process would be speeded up by increasing the operating temperature in line with a concomitant change in the partial pressure of  $CO_2$  [29], ensuring a higher overall electricity generation efficiency.

Calcination, instead, should be performed at a lower temperature (about 700°C) using gases easily separable from  $CO_2$  [28] or alternatively, in accordance with the thermochemical equilibrium, a pure  $CO_2$  atmosphere with particularly high temperatures (above 950°C) [29][30] would be required in order to ensure a rapid reaction. Due to the high enthalpy value under consideration, the system would require integration, presumably with an auxiliary combustible, to provide the energy quantity required by the process.

In general it could be thought to reduce the partial pressure of  $CO_2$  by adding easily separable gases, such as helium or steam [27], which, being inert, facilitate the separation phase. In the case of steam utilisation it would be possible to proceed with condensation processes, while in the presence of helium it would be better to use selective membranes or Pressure Swing Adsorption, paying attention to the fact that the energy expenditure of these last cases does not make them much more convenient than the accessory combustion.

A further option is to supply the heat necessary for calcination indirectly through a heat exchanger system [31], consequently avoiding the necessity to use auxiliary fuel, although the limitations of the heat exchanger system arrangement do not guarantee the possibility to consider this as a definitive solution. The realization of calcination in

partial vacuum condition [32], finally, requires the resolution of problems related to the possible losses that could occur to the system.

The advantages of using calcium looping as a storage system are several. From an energy point of view, the analysed process results to have a theoretical energy density around  $3 - 4 \text{ GJ}/\text{m}^3$  [33][34] depending on the thermodynamic storage conditions. Comparing the data with the energy density of a common solar concentration system with tower technology with molten salts ( $0,4 \text{ GJ}/\text{m}^3$  [35]), it appears evident that the convenience of the illustrated technology is remarkable.

### 2.2.1. Imperfect reversibility of the reaction

One of the main problems concerning the Calcium Looping process involves the fact that the carbonation reaction between lime and carbon dioxide is not completely reversible. In particular, the properties of  $\text{CaO}$  sorbent undergo a progressive deterioration, increasing with the number of calcination/carbonation cycles performed, preventing a complete recombination reaction and causing the accumulation of a high amount of inactive sorbent [36].

Numerous investigations have been carried out to examine the behaviour of  $\text{CaO}$  when subjected to a particularly important series of reaction cycles. According to (Abanades and Alvarez), as a result of experiments based on TGA thermogravimetric analysis, it appears that the chemical reaction between lime and  $\text{CO}_2$  is characterized by a certain conversion limit, somehow related to the variation of porosity of the sorbent as a function of the variation of its pore size. The results demonstrate how the repeated cycles of calcination/carbonation involve a continuous change in the pore size of the sorbent  $\text{CaO}$ , typically generating larger pores than those observed at the beginning of the reaction [36].

The results obtained are generally expressed as a variation of the "*sorbent reactivity*", or capture capacity, in function of the number of cycles. The sorbent reactivity  $X$ , calculated through the TGA analysis, is defined by the following relationship:

$$X = \frac{\text{mol CaO reacted}}{\text{mol CaO stoichiometric}} \quad (2.4)$$

It is an index of fundamental importance in the evaluation of sorbent performance. It gives an indication of the molar fraction of sorbent actually involved in the reaction, perceiving as a consequence the amount left inactive.

Important results were obtained by (Grasa and Abanades) regarding the relationship between sorbent reactivity and number of cycles, by conducting experiments on various limestone samples subjected to calcination reaction with calcination temperatures below 950 °C, as summarized by the following graph.

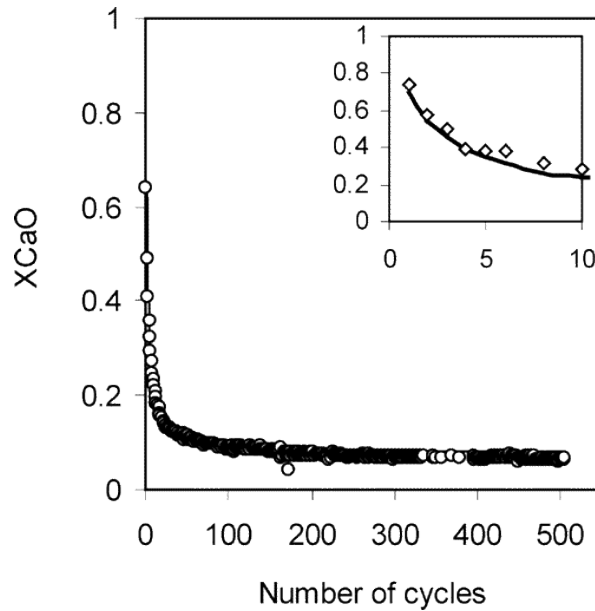


Figure 13 - Sorbent reactivity vs number of cycles [37]

The trend demonstrates a drastic reduction in sorbent capture capacity in the first 20 cycles before showing a stabilization with the increase in the number of cycles, remaining constant at a value of 0.075 - 0.08 for the next 500 cycles. [37].

A similar result for low number of cycles and progressively increasing and higher calcination temperatures is obtained by (Blamey et al.), as shown in the figure (*Figure 14*). The experiment concerned was conducted using a fluidized bed reactor and establishing at 900 s the duration of the calcination and carbonation reactions, with a total pressure of 101.3 kPa and  $CO_2$  concentration of 15%. The results indicate that the solid reactivity of the sorbent tends to vary its behaviour not only according to the number of cycles but also to the reaction temperature. It emerges that the decrease is more accentuated in higher sintering calcination environments, proportional to the increase in temperature [38].

In addition to temperature, another parameter that influences the behaviour of the sorbent in the calcination/carbonation reaction cycle is the presence of steam in the reactor. In particular, (Champagne et al.) as deduced from his experiments how the presence of water in the calcination phase affects the properties of the sorbent and leads to variations in the conduct of the carbonation reaction [39].

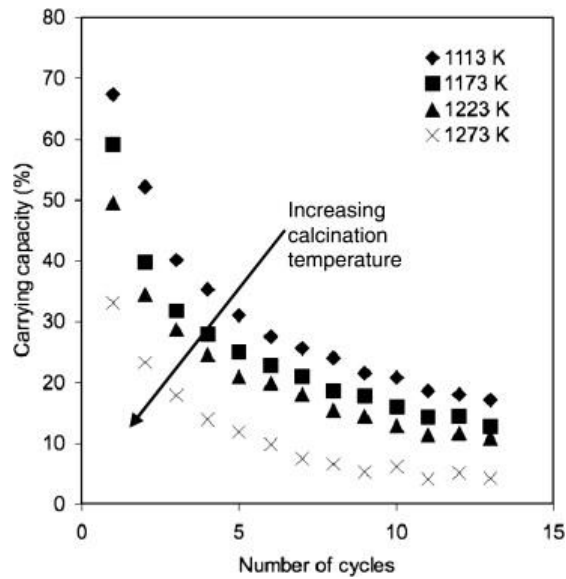


Figure 14 - CaO carrying capacity vs number of cycles [38]

The results demonstrate, specifically, how the introduction of water into the calciner, under specific temperature conditions (925 °C and 875 °C are the cases studied), leads to an increase in the reactivity of the sorbent. The following figure summarizes the results obtained after TGA tests with calcination at 925 °C and 60% of  $CO_2$  [39].

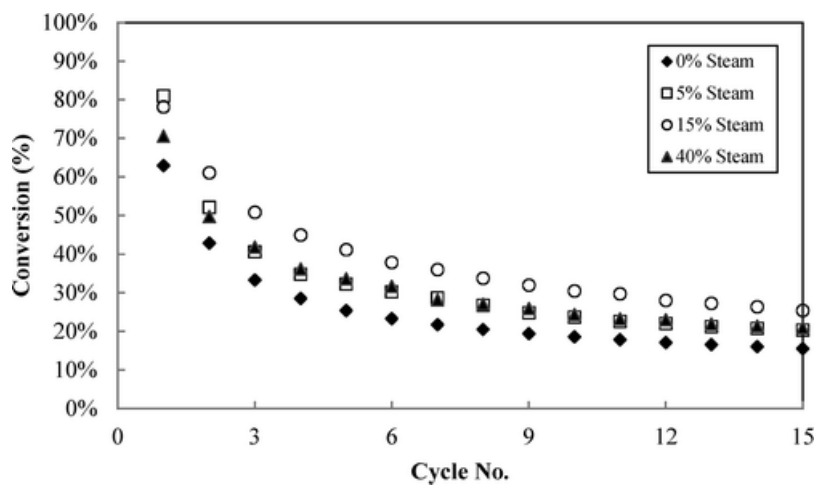


Figure 15 - Sorbent conversion from TGA tests with calcination at 925 °C, 60%  $CO_2$  for different steam percentages [39]

From the diagram it emerges that, among the vapour concentrations studied, 15% constitutes the value for which a greater influence on the carrying capacity of the sorbent is obtained.

In the same study, moreover, it is explained how the injection of steam in the calcination phase involves a change in the morphology of the sorbent, causing an

increase in the size of the pores with a consequent increase in carbonation reactivity [39].

As mentioned above, the partial pressure of  $CO_2$  in the reactor is also a relevant parameter in the study of reaction kinetics. Experiments useful for the discussion were conducted by (Valverde et al.), investigating the existing correlation between partial  $CO_2$  pressure and reaction temperature in the calciner for a given residence time. The result is the following graphic trend.

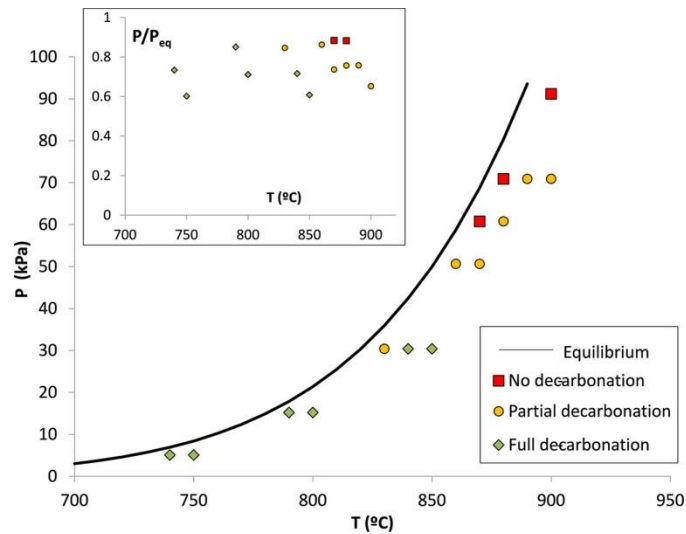


Figure 16 -  $CO_2$  partial pressure vs temperature in calcination [40]

From the experiment it is possible to observe not only the relationship between partial  $CO_2$  pressure and reaction temperature during the reaction, but also how, depending on the thermodynamic situation defined by the two variables, in the 60-minute residence time at which the experiment was conducted, the de-carbonation reaction may develop completely, partially or not at all [40].

Ultimately, what emerges from the analyses presented is how the sorbent generally tends to lose reactivity with the progression of cycles, leading to a reduction of material actually involved in the reaction to the benefit of the increasing accumulation of inactive substance. In view of an integration with a solar concentration plant for a possible use of the Calcium Looping process as a thermochemical storage system, it is therefore legitimate to consider the necessity of a periodic partial renovation of the quantity of solids involved in the process. Due to the considerably long life of the plant and the therefore high number of cycles that the sorbent would have to undergo, it is undeniable that an excessive reduction in reactivity would have considerable repercussions on the plant performance. A gradual replacement is an eventuality to be taken into account, therefore, when designing an integrated system of this type.

## 2.3. Integration in a CSP plant

In addition to the well-known application of calcium looping as a method to capture  $CO_2$  in an attractive integration in fossil fuel plants with the aim of making them potentially carbon free, its combination with a concentrated solar power plant certainly represents an innovative frontier of technology development.

### 2.3.1. Advantages of integrating CSP with CaL

The integration of a concentrating solar power plant with a thermal storage system plays an increasingly important role with the growing importance given to solar power as an alternative energy source. Its availability limited to daylight hours with clear sky makes it necessary to find a technical solution that would extend its functionality to satisfy any demands even in the absence of solar radiation. In this context, thermal storage, as previously stated, is a useful instrument to increase the production of energy even in non-operational panel conditions, consequently being able to respond to the demands of users ideally at any time of the day.

Among the storage systems useful for the conservation of thermal energy, the most interesting are the thermochemical storage (TCES), which are able to realize the charging and discharging processes simply through the development of reversible chemical reactions powered by the solar radiation collected by the plant. TCES applied to CSP uses the heat collected by the solar receiver to perform an endothermic reaction. When energy is requested, the by-products of the reaction are combined together at the necessary conditions for the reverse exothermic reaction to occur, which releases the previously stored chemical energy for power production [41].

The integration of CaL in a CSP system is an interesting solution and its characteristics enable an advantageous coupling.

On the one hand, CaL is a technology that requires a certain amount of energy to start the separation processes in the calciner. In addition, it is necessary to consider the additional consumption required for  $CO_2$  compression and solids transport. CSP could be an interesting resource in this context. Thanks to the availability of thermal energy with extremely high thermodynamic quality, the integration would guarantee the supply to the cycle directly from a renewable resource, thus increasing the attractiveness of the technology [42].

On the other hand, calcium looping is also an advantage for the CSP system itself. Thanks to the great chemical potential developed in the reactions that are performed in

calciners and carbonators, CaL is configured as a possible electrochemical storage system, useful for the conservation of the energy obtained from the solar plant, providing, in fact, the resource with the important qualities of constancy and continuous availability, providing a solution to the alternating and discontinuous nature of solar radiation [21].

The solar radiation collected by the receiver is used, in the form of thermal energy, to activate the chemical dissociation reaction inside the calciner.  $CO_2$  and  $CaO$  thus generated are then stored in special storage systems. When energy is required by the user, the substances are conveyed to the carbonator where the recombination reaction and the subsequent formation of  $CaCO_3$  takes place. Being a strongly exothermic reaction, the energy generated is useful to activate a turbine in a power cycle, in order to respond to the energy demand of the network.

An example diagram of the operating mechanism of the process in integration with a solar system is shown in the following figure.

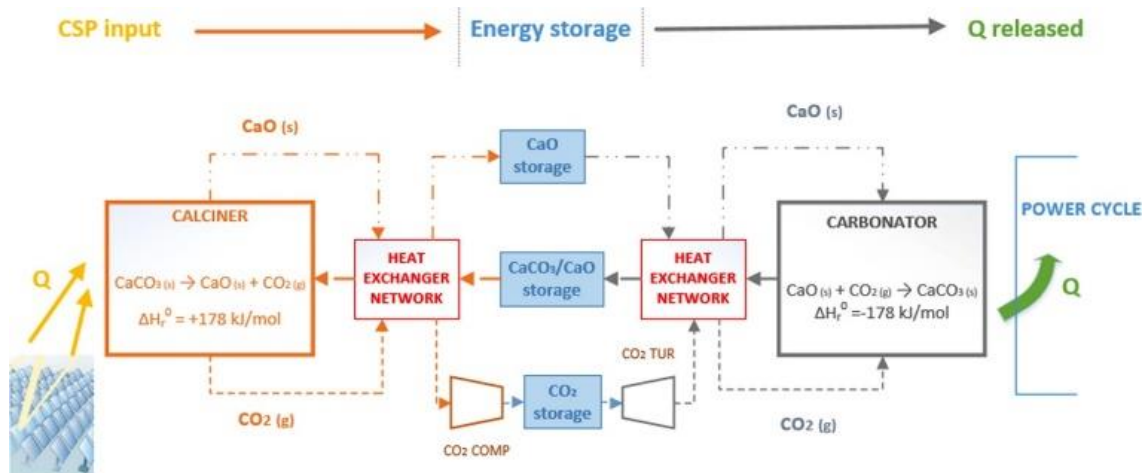


Figure 17 - CSP-CaL conceptual scheme [43]

One of the advantageous points of the integration of CaL in the CSP consists in the possibility of calibrating the system according to the characteristics of the network, therefore being able to operate in response to the peak demand, as well as in a continuous and constant way for the ordinary demand and over time. The characteristics of the CaL, in fact, make it possible for the integrated storage systems to be maintained at ambient temperatures, thus extending the storage time and giving the resource a remarkable seasonal operating characteristic [44].

## 2.4. Description of all systems, equipment and processes

Regardless of the purpose for which the calcium looping process is applied, there are some fundamental components required in order to apply the technique.

Commonly, as shown in the previous image (*Figure 17*), a system that exploits the potential of calcium looping requires the presence of a calciner, a carbonator, storage systems for  $CO_2$ ,  $CaO$  and  $CaCO_3$  as well as a network of exchangers useful to optimize the process and ensure adequate heat exchange.

Therefore some theoretical indications are given on the main components that compose the system.

### 2.4.1. Calciner

The implementation of an appropriate and highly efficient calcium looping process requires calcification to be conducted appropriately and successfully. The calciner is the component responsible for this, as it must achieve the splitting of  $CaCO_3$  into  $CaO$  and  $CO_2$ . Since it is an endothermic reaction, it requires an external energy supplement for this to happen. In this context, the way in which the thermal energy is supplied to the system depends on the type of integration and the purpose of the process.

Regarding calcium looping applied as a  $CO_2$  capture medium, in the calciner the reaction requires the satisfaction of extremely high enthalpy values, with operating temperatures above  $900^\circ C$  in a pure  $CO_2$  environment. Unavoidably, a backup system with oxy-fuel supply is necessary to obtain the required amount of energy [45]. The system could possibly be optimized by the addition of inert gases into the calciner's atmosphere, which would reduce the partial pressure of  $CO_2$  and consequently lower the operating temperature to values around  $725^\circ C$  [46]. The possible integration of this solution with an indirect heating system using heat exchangers would reduce the necessity to employ oxy-fuel combustion.

In the application of calcium looping for  $CO_2$  capture, the type of calciner used tends to be the rotary klin, characterized by operating temperatures around  $2000^\circ C$  and variable sizes capable of producing a flow rate of 3600 ton/day [47]. Usually it is integrated with particle preheating mechanisms, exploiting the high temperature of the gases coming out of the calciner to preheat those entering the rotary klin.

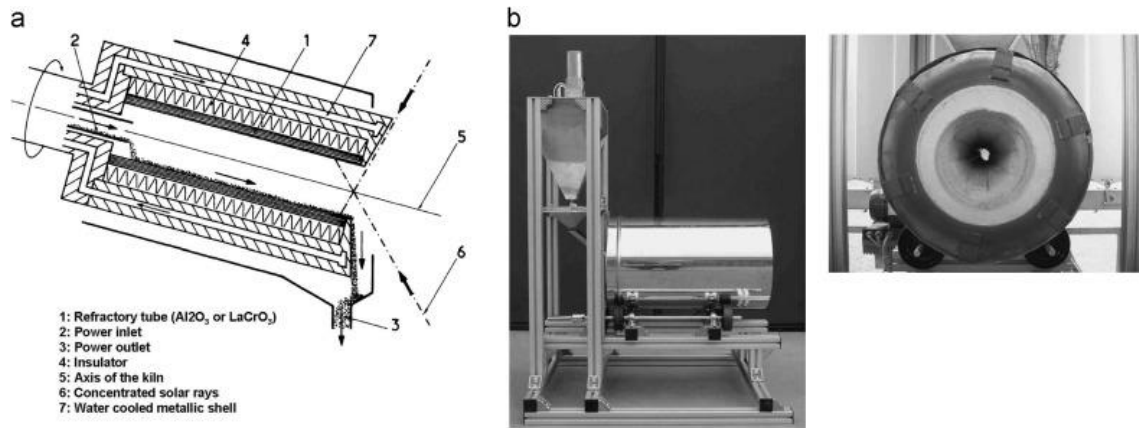


Figure 18 - Solar rotary klin examples [48]

(Shimizu et al., 1999) also proposes the possibility of using a fluidized bed reactor as a calciner [49], whose main advantage lies in promoting gas-solid contact by stimulating the heat exchange process.

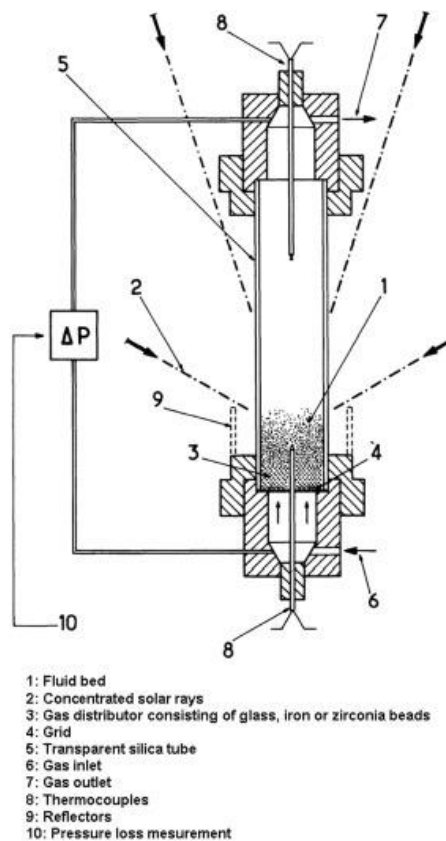


Figure 19 - Solar fluidized bed reactor [48]

The topic is further investigated by (Hanak et. Al., 2015)[50], who analyses various types of possible reactors, such as Moving Bed, Circulating Fluidized Bed, Bubbling Fluidized Bed. What emerges from the discussion is the potential problem deriving from particle size, a parameter that particularly affects the operating conditions of the component [51].

In general, a properly designed calciner should be able to ensure a sufficiently long residence time for particles in order to reach high operating temperatures correctly, ensure a rapid and defined calcination process, guarantee an appropriate heat exchange by minimising thermal gradients and losses, prevent the formation of particle agglomerations and ultimately achieve a thermodynamically controlled and correct transformation.

The integration of the calcium looping process with a concentrating solar power plant is mainly implemented in the functionality of the calciner. In this case, the energy needed to supply the chemical reaction derives directly from the solar radiation intercepted by the solar receiver, with clear overall gains for the system in terms of fuel consumption, environmental sustainability and independence from an auxiliary energy backup system [42].

The correct design of the calciner is an essential step in the process of integrating calcium looping with a CSP plant, due to the fact that the overall efficiency of the system is significantly influenced by the operational mechanisms that take place in the chemical splitting reaction of  $CaCO_3$ . Currently the optimal sizing and characterization of such a calciner is still in the process of completion. One of the most important issues is the thermal losses that may result from the particular operating conditions of the component. For this reason, significant radiative losses can arise due to the extremely high temperatures reached during the process as well as conduction losses, which are strictly dependent on the geometry and structure of the calciner [29].

In accordance with what has been argued by (Flamant et al.), some issues of primary importance in the design of a calciner perfectly integrated with a concentrating solar power system concern the necessity to ensure the particles a residence time long enough for the high operating temperatures required by the process to be reached, while avoiding the plausible thermal losses due to radiation and conduction and the definition of unfavourable thermal gradients. Adequate thermodynamic management of the operations would ensure the exclusion of any formation of particle agglomerates, which would compromise the overall efficiency of the process, also guaranteeing the absence of deposits that could cause consequent structural damage [52].

## 2.4.2. Carbonator

The carbonator is another essential component for the proper performance of the calcium looping process. It represents the device in which the carbonation reaction useful for the production of thermal energy previously stored in the form of chemical potential takes place.

The sizing and design phase is also of primary importance for the carbonator. The efficiency of the process and the way  $CaO$  reacts with  $CO_2$  in the formation of  $CaCO_3$  depends on the reaction conditions as well as the residence time of the particles in the component. The carbonator recombines the  $CaO$  and  $CO_2$  releasing heat to a heat transfer medium, eventually air or gas, in order to expand it into a gas turbine. Between calciner and carbonator there are storage vessels for  $CaCO_3$ ,  $CaO$  and  $CO_2$ , whose sized is chosen to provide buffer storage so that the solar calciner can consume  $CaCO_3$  and produce  $CaO$  and  $CO_2$  during daylight hours, while the carbonator/turbine can run 24 h a day with varying load as required and satisfy the grid demand [53].

The majority of carbonation processes take place in Fluidized Bed type reactors, in which fluidization plays a fundamental role to ensure the achievement of high carbonation efficiency values.

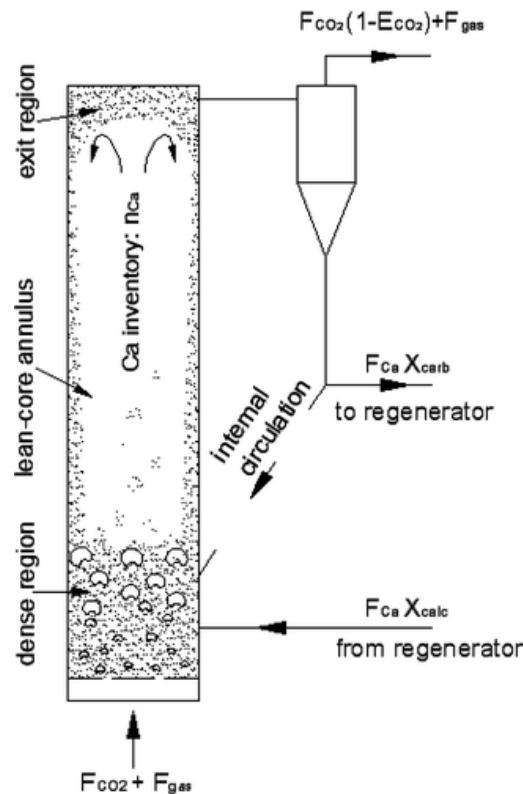


Figure 20 - Continuous fluidized bed carbonator scheme [54]

Eventually, in agreement with (Valverde et al., 2013) and (Romano, 2012), the performance could be further increased by assisted fluidization methods and the application of high intensity acoustic fields, useful to avoid the formation of particle agglomerations that would reduce the optimal success of the process [55][56].

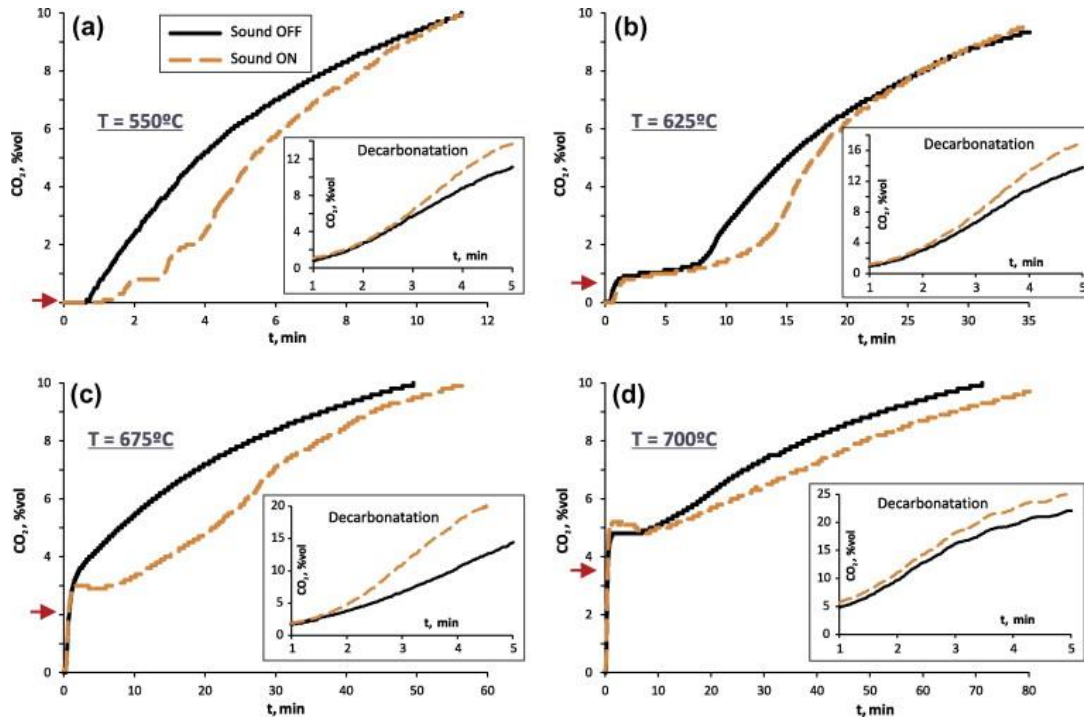


Figure 21 - CO<sub>2</sub> breakthrough curves measured during the carbonation stage in the absence of acoustic field and with an acoustic field applied [55]

As shown in the previous figure, the results of the experiments demonstrate that the use of sound waves with the aim of facilitating the carbonation process effectively guarantees a faster reaction, favouring heat and mass transfer and consequently reducing the quantity of CO<sub>2</sub> in the exhaust gases. This is a very important result in application to CO<sub>2</sub> capture systems [55].

A more in-depth analysis of the carbonator's operating mechanism allows the process to be divided into two distinct phases. Initially the reaction develops on the free surface of the solid through the formation of CaCO<sub>3</sub> molecules following the combination of CaO and CO<sub>2</sub>. The process speed, in this case, is determined by the chemical kinetics of the reaction in question. This phase is relatively rapid and ends when the free surface of the CaO molecules is completely affected by the initial formation of CaCO<sub>3</sub>. At this point follows the second, much slower phase, characterized by a solid-state diffusion of CO<sub>3</sub><sup>-</sup> and O<sub>2</sub><sup>-</sup> ions through the formed layers, ensuring a subsequent continuation of the reaction [57].

Ultimately, the carbonator, as well as the calciner, constitutes an element of fundamental importance within the process dynamics of calcium looping. The construction of a reactor of this type on a large scale requires essential characteristics so that the process can be carried out in a complete manner maximizing overall efficiency. In this context, it is appropriate to ensure sufficient residence time for the molecules to reach the required temperatures, controlling the thermodynamics of the process to avoid the formation of accumulations and maintaining appropriate fluidization. From a thermodynamic point of view, it is necessary to avoid losses and dissipations, reducing thermal gradients and allowing a homogeneous heat exchange to the reactor's wall. The power production as a result of the carbonation reaction will consequently be able to take place under ideal conditions, guaranteeing a satisfactory success.

#### 2.4.3. Heat exchangers

Accessorizing the Calcium Looping plant engineering process with an appropriate network of heat exchangers is an essential part of system development. The exploitation of hot flows and heat recovery guarantee the possibility of optimizing the process, reducing the amount of energy required from the outside and making it easier to carry out the different phases with increased efficiency.

From the analysis of the design of a common plant based on Calcium Looping, it definitely emerges the availability of heat in the hot flow of  $CO_2$  coming out of the calciner, for which it is convenient to provide cooling before sending it to the storage system. On the other hand, it can be observed that the  $CaCO_3$  entering the calciner could be preheated to reduce the required energy supply and facilitate and speed up the operations in the reactor. The thermal availability of the  $CO_2$  stream in question is such as to enable further plant modifications, assuming, for example, the integration of a power cycle with steam for the production of energy needed to self-sustain the compression of the same  $CO_2$  in the storage for which it is intended. The  $CO_2$  coming out of the storage could similarly be preheated to facilitate the operation of the carbonator. In this case, the thermal availability of  $CaCO_3$  leaving the carbonator would guarantee the resolution of the problem. The  $CO_2$  outgoing from the carbonator, also at a high thermal level, could finally be destined to a power cycle before exploiting its properties to preheat the stream of the same gas coming out of the carbonator and direct to the carbonator.

Ultimately, the typical plant design of a calcium looping process allows the integration of heat exchangers in various ways and different arrangements. In the same configuration it is possible to simultaneously install:

- Gas/gas heat exchangers: are mainly involved in the power cycles, in the  $CO_2$ /Steam heat exchange and in the pre-heating of the  $CO_2$  stream coming out of the storage. The main heat transfer vector is the flow of hot  $CO_2$ , both from the calciner and the carbonator. Typically the type of heat exchanger most widely used for this purpose is the "flat plate" heat exchanger. The limitation in its application lies in the flow rates involved. If the volumetric flow rate is not within the limits indicated by the manufacturer, generally "U-tube" type heat exchangers are used [44];

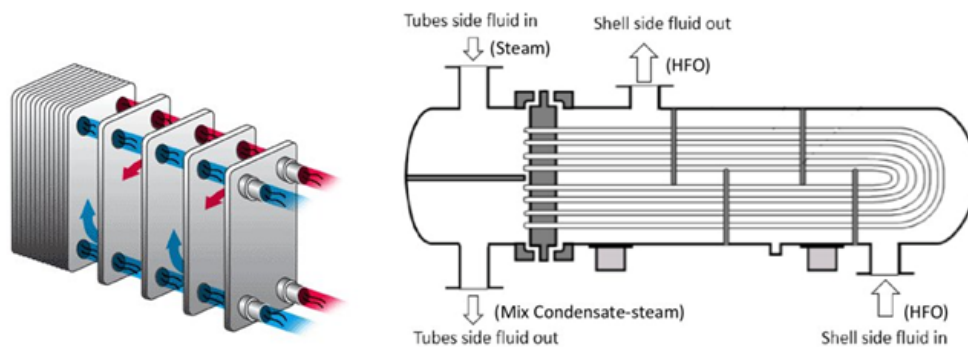


Figure 22 - Flat plate [59] and U-tube [60] heat exchanger

- Gas/solid heat exchangers: are used in the  $CO_2$ /solids coupling and ensure heat exchange between gas and solid particles. They are used both during the heating of  $CO_2$  by the  $CaCO_3$  coming out of the carbonator and in the opposite direction to pre-heat the  $CaCO_3$  entering the calciner. In the first case, it is essential to have an indirect heat exchanger that avoids direct contact between CaO and  $CO_2$  in the carbonator with the risk of causing partial and incomplete carbonation reactions, with consequent reduction of the useful power produced by the cycle;
- Solid/solid heat exchangers: They would ensure further plant improvement by promoting heat exchange between solid substances. They represent a technology that is still being developed and further explored. An often highly accredited configuration consists in coupling two solid/gas heat exchangers with an intermediate heat transfer fluid circulating between the two solids. Typically, due to the high temperatures, liquid metals can represent a good solution for this process [58].

Very common technologies of solid/gas heat exchangers are the suspension preheaters [61], which develop in different cyclone stages and are particularly useful in the preheating of  $CaCO_3$  particles. The hot stream leaving the calciner flows through the

various stages of the cyclone from bottom to top. At the same time, the  $\text{CaCO}_3$  particles are inserted and ensured to heat up before the cyclone is activated to separate them from the gas again. The suspension preheater guarantees extremely high levels of contact surface area, therefore the heat exchange achieved in this way is remarkable. The advantages of the technology lie in its maturity and reputation, being extremely widespread in the cement industry, as indicated in the following picture (Figure 23).

Another type of heat exchanger widely used is the grate preheater, in which the particles, arranged on a horizontal support sliding inside a closed tunnel, are invested by the flow of hot exhaust gases coming out of the calciner. The process guarantees a considerable cooling of the fluid with consequent significant preheating of the particles [62][63].

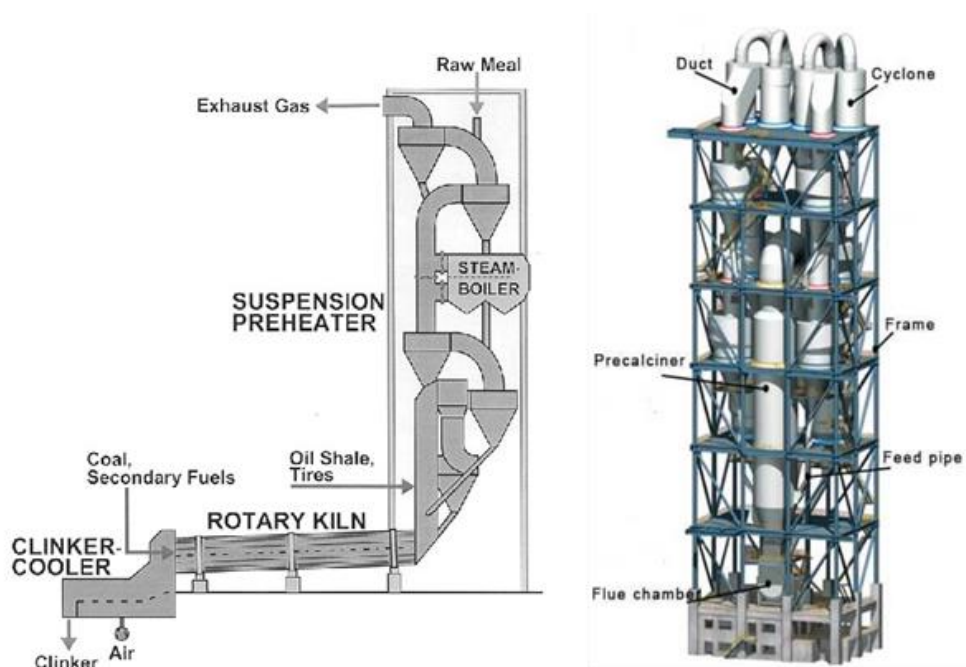


Figure 23 - Suspension preheater scheme [64]

In conclusion, the dimensioning and the choice of an appropriate heat exchanger system to be integrated in the plant appears to be a primary prerogative in order to increase the performance of the cycle and disconnect it from the necessity of using backup energy systems. The possibility of exploiting the thermal availability of the hot flows circulating in the configuration studied, gives independence to self-sustainability of the process, although with the shrewdness to realize connections and couplings in a perspective of continuous design optimization.

#### 2.4.4. Storage systems

A correct application of Calcium looping systems requires the integration of a series of storage devices useful to allow the iteration of operations. A common installation of this type generally includes three main storage technologies:

- $CO_2$  storage: it consists of a typically pressurized storage, suitable for storing the  $CO_2$  coming out of the calciner following the dissociation reaction of  $CaCO_3$ . The pressure level applied (around 75 bar) [65] is generally such as to ensure that supercritical  $CO_2$  conditions are reached at ambient temperature, an important solution to save volume compared to otherwise bulkier storage for gaseous substances. The use of lower pressures, in fact, would make it necessary to proceed with liquefaction by means of thermal reduction, with unavoidable energy expenditure and reduction in system performances [41]. A technology for storing  $CO_2$  at atmospheric pressure inside large vinyl buildings is also being developed [66];
- $CaO$  storage: it represents a storage for solids, in this case the  $CaO$  coming out of the calciner;
- $CaCO_3/CaO$  storage: it is also a storage facility for solids, but it is intended for the storage of the  $CaCO_3$  coming out of the carbonator as a result of the carbonation reaction, as well as a fraction of  $CaO$  remaining dissociated.

The calculation of the storage system integrated in the calcium looping process is fundamental and varies according to the utilization characteristic of the system. It can in fact be calibrated to satisfy peak demand, for intermediate operation or to adapt to standard energy demand. In addition, the calciner operates exclusively in solar radiation conditions, while the carbonator, and consequently the power cycle associated with it, is designed to ensure continuous production throughout the day, possibly adapting to the needs of users. Some of the most important advantages of integrating the calcium Looping process with a thermal concentrated solar power plant can indeed be found in the storage system. A TCES plant integrated with CaL, in fact, has a higher energy density than a more common molten salt scheme, allowing a reduction in volume of the size of the storage used, an improvement that unavoidably is also reflected in a reduction in costs. In addition, the possibility of storing substances at ambient temperature through compression processes provides the system with an important seasonal configuration, thus not restricting its operation to a restricted amount of time.

In the construction of the components, stainless steel is generally used for solids deposits, while the  $CO_2$  tank can be designed of as a cylindrical pressure vessels made of chromium and molybdenum doped stainless steel [67].

Among the various measures required during the design and sizing of the various storage devices included in the calcium looping process, some of the most relevant features to be monitored are their capacity, discharge rate and frequency, mixture and material uniformity, material friability, pressure and temperature differences, safety and environmental concerns, and construction materials [65].

#### 2.4.5. Solid-gas separation and solid transport

In the view of an integration of the calcium looping process with concentrated solar power, due to the fact that  $CO_2$  and  $CaO$  are allocated to different storage systems subsequently to the chemical dissociation reaction of  $CaCO_3$ , it is fundamental to perform a gas/solid separation at the calciner output. Tendentially a widely used methodology consists in the application of Cyclones, instruments that operate the separation using centrifugal forces generated by a rapid rotation of the mixture. The particles accumulate on the walls of the device and are then collected through an opening at the bottom. Due to the presence of particularly small particles, generally below 10 microns [68], the removal efficiency of common cyclones may not ensure adequate success in the process. For this reason it may be advisable to apply secondary processes to improve the result. As proposed in (Jo et al.) and (De Souza et al.), the integration of post-cyclone processes would ensure a higher gas flow purification with removal efficiencies up to 96-98% for medium-sized particles around 1.6 microns [69][70].

The transport of solids is another crucial point in the description of the operation of the calcium looping system. There tend to be a number of issues that need to be addressed in order to ensure the optimal success of the process.

First of all, one of the most challenging processes is the transport of  $CaO$  particles from the calciner to the  $CaO$  storage system and subsequently from this to the carbonator. The fundamental circumstance to avoid is a possible carbonation of the substance before entering the carbonator. This would cause a considerable reduction in the performance of the plant and a decrease in the efficiency of the power cycle. Considering the presence of an atmosphere rich in  $CO_2$  in the whole analysed process, a special attention in the handling of  $CaO$ . A possible solution to reduce the eventuality of problems could be represented by replacing the  $CO_2$  atmosphere with a nitrogen one, realizing an inertization of the system with a consequent reduction of storage temperatures before carbonation.

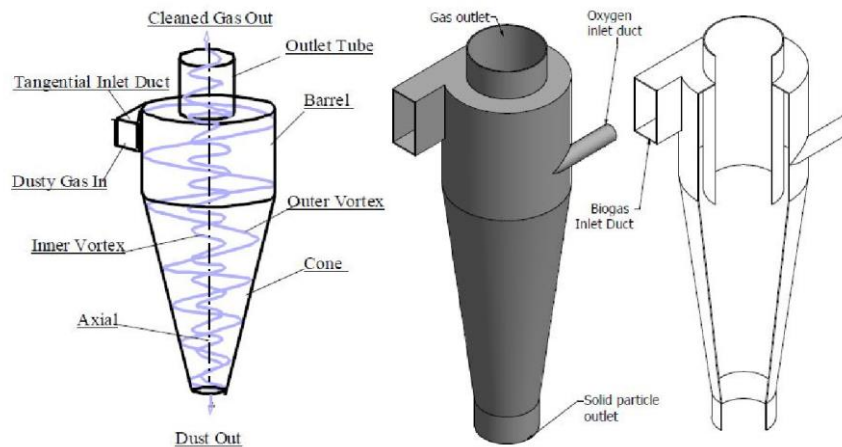


Figure 24 - Cyclone separator conceptual scheme [71]

The conveying mechanisms commonly used in calcium looping processes are divided into mechanical conveyors and pneumatic conveyors. Mechanical conveyors typically have a higher investment cost but a significantly lower operating cost than pneumatic conveyors.

Available technologies to transport high temperature particles up-down the receiver include mine hoist, bucket elevator, pocket elevator, screw conveyor, pneumatic conveyors, conveyor belts, cleated conveyor belts, metallic belted conveyors, masses elevators, bucket wheels, linear induction motor powered elevators and electromagnetic field conveyors [90].

Among the most widely applied mechanical transport mechanisms in calcium looping, the screw conveyors is a highly functional solution. It consists of a method that uses a rotating helical screw blade, generally positioned inside a tube, to move granular materials, as in the case of solids involved in calcium looping, or liquids. Often, when the installation space allows it, the screw conveyors can operate in an inclined position. Specifically, if the material flow is oriented upwards, the screw conveyor is an optimal method for elevating and conveying processes. The integration of a screw conveyor into the plant is typically studied from a mathematical point of view by calculating the characteristic volumetric curve [72], for which key parameters such as the trajectory angle of particle motion and the theoretical maximum mass flow rate are utilized. A possible contraindication related to the use of screw conveyors for a calcium looping system integrated in a solar power plant is due to the discontinuous nature of the radiation, which would make the operation of the component variable and its performance mechanically inefficient. [44].

Among those belonging to the screw conveyors category, the OLDS elevators exhibit peculiar characteristics that are suitable for the technical requirements needed in a calcium looping process. An OLDS is a vertical screw conveyor particularly suitable for the transport of solid substances at high temperature, especially in plant configurations where the calciner is positioned at the top of the solar receiver. The device consists of a circular casing that rotates around a stationary screw or propeller with a small parasitic energy consumption. [44].

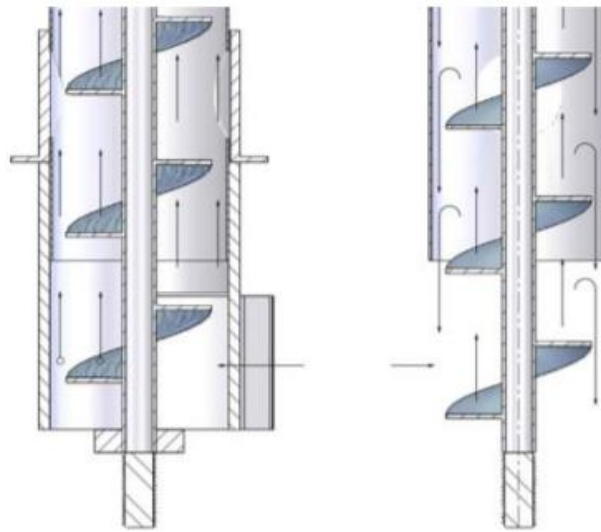


Figure 25 - Comparison between OLDS elevator (left) and conventional rotating screw elevator (right) [74]

Another potentially valid type of conveyors comprises belt conveyors (*Figure 26*), which base their operation on the transport of solid particles on conveyor belts. The convenience of their use, however, is proportional to the operating time, the capacity of the conveyed material and the distance covered. It is generally economically advantageous for long distances and significant material flow rates. [73].

Ultimately, the correct design of a system using the calcium looping mechanism also requires attention when integrating solids transport systems. They must be chosen in such a way as to ensure a continuous service, efficient and adapted to the requirements of the process, they must preserve the transported products by moving them under controlled conditions and, above all, they must be dimensioned in such a way as to minimize the total energy consumption. Providing the system with accessory equipment with a high energy consumption value would significantly reduce the overall performance, making the technology less attractive.

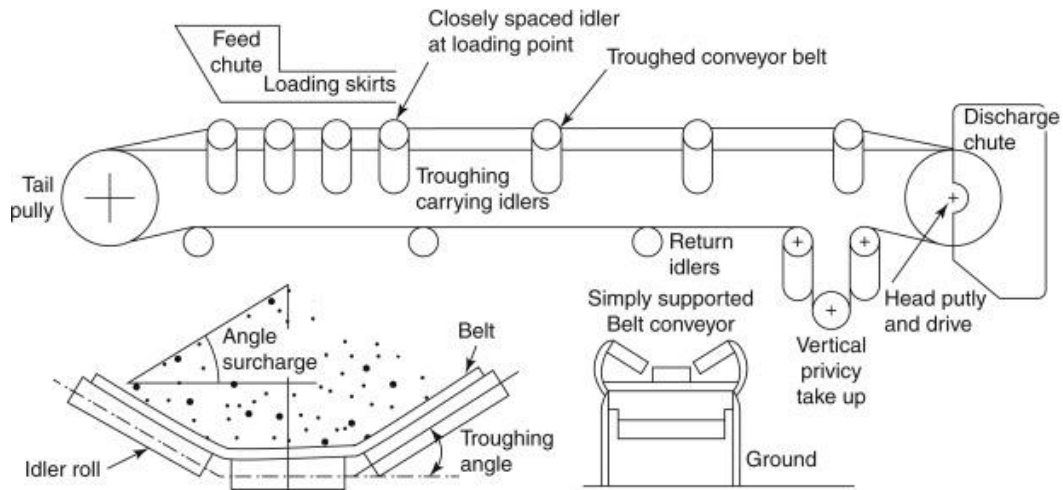


Figure 26 - Typical belt conveyor scheme [75]

#### 2.4.6. Power block

In order to successfully integrate the calcium looping process into a concentrating solar power plant, it is necessary for the system to be able to provide the energy supply whenever it is required by the user. The phenomenon that develops in the carbonator is an exothermic process which, consequently, occurs with the production of a high quantity of energy, in accordance with the chemical reaction analysed. In this context, the main challenge lies in being able to exploit the energy obtained to activate a power cycle that might ultimately contribute to the production of electricity to be supplied to the grid.

Several possible configurations are available through which this type of process can be developed. The most effective in an integrated CSP-CaL system consists of a direct energy production through a Brayton cycle that exploits the high thermal availability of the  $CO_2$  flow exiting the carbonator by activating the operation of a gas turbine. Once the process has been completed, the outgoing  $CO_2$  will be conveyed to a heat exchanger where it is possible to exploit the residual thermal availability to preheat the solid  $CaO$  entering the carbonator, increasing in this way the overall efficiency of the cycle. According to the information provided by (Ortiz et al., 2017), in such a configuration, the carbonator operates in a pure  $CO_2$  environment. Consequently the minimum pressure of the carbonator coincides with the partial pressure of  $CO_2$ , thus carrying out the carbonation reaction at a temperature around  $950\text{ }^\circ\text{C}$  for absolute pressures at 2.2 bar and around  $890\text{ }^\circ\text{C}$  for pressures above atmospheric pressure. The closed Brayton cycle has excellent overall efficiency values around 44-45% [41].



#### 2.4.7. Different solar calciner for integration with CaL

One of the most important aspects to be evaluated when designing and sizing a possible project for the integration of the calcium looping process in a concentrated solar power plant is the choice of the solar receiver to install in the plant.

The functioning of the calciner and consequently the way in which the calcium looping process may, in general, be successful, strictly depend on the performance of the solar receiver, which is responsible for supplying the thermal power required to carry out the operations by receiving and absorbing the incident solar radiation.

In general, potentially applicable solar receivers differentiate depending on whether the particles are irradiated directly or indirectly and, consequently, whether or not there are heat exchange and heat transfer mechanisms. The operational characteristics of a solar receiver intended for the functioning of a solar calciner in a calcium looping process depend mainly on the thermodynamic properties of the substances and the reaction conditions, which are necessary for the evaluation of the correct residence time of the particles so that the calcination of  $CaCO_3$  can be performed satisfactorily.

There are many challenges to be faced when dealing with high temperature solar receivers. In particular, it is necessary to consider issues such as the development of geometric designs, the minimization of thermal losses, the maximization of solar irradiance and absorptance, the exigency of high thermal resistance and high reliability when subjected to temperatures above one thousand degrees and for many operating cycles as well as the necessity to identify a heat transfer fluid suitable for the realized process. Moreover, during the design phase it is necessary to evaluate the convenience of direct or indirect heating. The former would allow to reduce exergetic losses by means of the intermediate heat transfer process. Direct heating, on the other hand, has as a fundamental advantage the possibility to carry out the processes directly with the heat transfer fluid, which can therefore also be used for conservation in storage systems and, when required, contribute to the production of power by participating directly in the power cycle. [72].

In order for the processes of calcination and carbonation to be completely carried out, a large availability of thermal energy is required, with the consequent application of a solar receiver that could operate at high temperatures. By virtue of this necessity, typically calcium looping is a process applied to concentrated solar power systems with tower technology, because in this configuration the concentration of solar radiation in the receiver is such as to ensure the satisfaction of the thermal requirements of the system. It represents so far the most widespread CSP plant construction technology on the market, as well as the one whose energy gain is maximized [77]. It is also advisable to take in account that a relevant solar concentration ratio on the receiver and reduced

radiation losses are critical to endure high thermal efficiencies at temperatures above 650 °C [72].

To date, among the various types that can be used in a concentrated solar power plant with integration of a calcium looping system, relevant candidates are the falling particle receiver, the centrifugal receiver and the fluidized bed receiver.

#### 2.4.7.1. Falling particle receivers

The falling particle receivers base their operation on the direct heating of falling solid particles, on which a concentrated beam of solar radiation, reflected on the receiver by the solar field heliostats, is directed. Particle receivers are currently being designed and tested as a means to achieve higher operating temperatures (>700 °C), inexpensive direct storage, and higher receiver efficiencies for concentrating solar power technologies, thermochemical reactions, and process heat [72].

Unlike conventional solar receivers with indirect functioning, in which the transfer of thermal energy is normally entrusted to a heat transfer fluid that flows inside tubular receivers, in the particle receivers the process is carried out in a direct way using a flow of particles directly invested by the incident solar radiation. Once heated, the particles can therefore be stored in a storage system, to allow the production of useful power even in the absence of solar radiation in the case of demand from the user, or they can be employed as a heat source to give thermal availability to a thermovector fluid operating in an accessory power cycle.

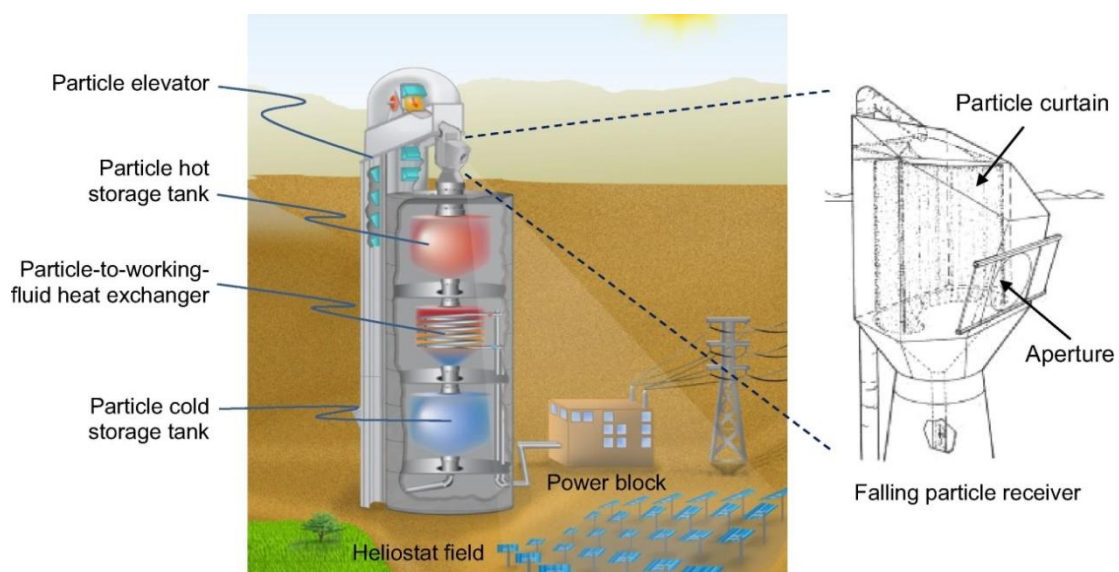


Figure 28 - Example of integration of falling particle receiver [72]

The advantages of using a falling particle receivers are particularly reflected in the installation costs. The possibility to conserve heat through the heating of solid particles of inexpensive and widely available substances in nature permits to considerably amortize the high cost related to the integration of a thermal storage system. On the other hand, however, it is necessary to consider the costs that may potentially derive from the necessity to provide for subsequent cycles of heating of the particles to ensure the achievement of higher operating temperatures. The most obvious solution, in case of wanting to increase the temperature reached by the solid particles used, consists in modifying the residence time of these particles inside the receiver, with a consequent increase in the amount of solar radiation collected. The geometric conformation of the receiver and its operating mechanism, however, make the problem difficult to be solved. It is possible, eventually, to think of a mechanism of recirculation of the particles exposing them several times to the light beam and subjecting them to a considerably higher thermal dispersion [78]. On the one hand, however, this would result in a higher thermal efficiency of the system, but on the other hand it would require the integration of transport and handling structures for the particles, with a consequent increase in costs and additional energy expenditure. A practical example of the problem in question is offered by (Ho Clifford K, 2016), analyzing a test recently conducted in which a solar receiver with recirculation of particles of the size of  $1\text{ MW}_{th}$  is studied, guaranteeing the achievement of temperatures of the order of  $700\text{ }^{\circ}\text{C}$  and thermal efficiencies with a value varying between 50% and 80%.

Another relevant aspect to be considered when sizing the falling particle solar receiver is the flow rate of particles to be introduced into the solar radiation beam. With reference again to the test conducted by (Ho Clifford K, 2016), it emerged that the particle temperature rise and thermal efficiency are dependent on the particle flow rate and irradiance. Specifically, by increasing the particle flow it happens that the particles are distributed in the receiver cavity forming a layer with growing opacity, which allows a smaller and smaller fraction of the incident solar beam to filter through. If the phenomenon would suggest an increase in the heat absorption achieved, on the other hand it is necessary to take into account the simultaneous increase in thermal losses due to shading and blocking, which consequently reduce the bulk outlet temperatures of the flow at a given irradiance [72].

A further useful method to increase the residence time of particles in the solar receiver is the so-called "Obstructed particle receivers" (*Figure 29*). It is characterized by the presence of obstructing material, such as obstacles or porous structures, whose role is to prevent the particles from falling freely and to slow down their motion, thus increasing the residence time in the cavity in contact with the solar beam. In this regard it is interesting to observe the results achieved in a test conducted in 2015 by (Ho et al., 2016), using a particle receiver consisting of a staggered array of stainless-steel

chevron-shaped mesh structures [79]. The peak temperature reached, over 700 °C, was located approximately in the centre of the receiver, thus indicating a very good functioning of the solution, however some problems emerged in the peripheral areas of the particle flow. Due to the presence of obstacles, in fact, the distribution of irradiance was inevitably not uniform, causing a reduced temperature increase in the lateral portions.

An additional obstructed solar receiver design, suitable for beam-down technology, is characterized by a screw elevator that lifts the particles towards an opening. The particles are irradiated by concentrated sunlight before flowing into the screw elevator for the subsequent heat exchange and reaction process [72].

In addition, always remaining in the field of solar receivers suitable for beam-down technology, another possible design is characterized by a spiral ramp in which particles move due to the effect of gravity and mechanical vibrations (*Figure 30*). Tests conducted on this mechanism show that temperatures of the order of 650 °C have been reached with a residence time of about 30 minutes at a radiant power of 5 kW<sub>th</sub> and a thermal efficiency of about 60% [80].

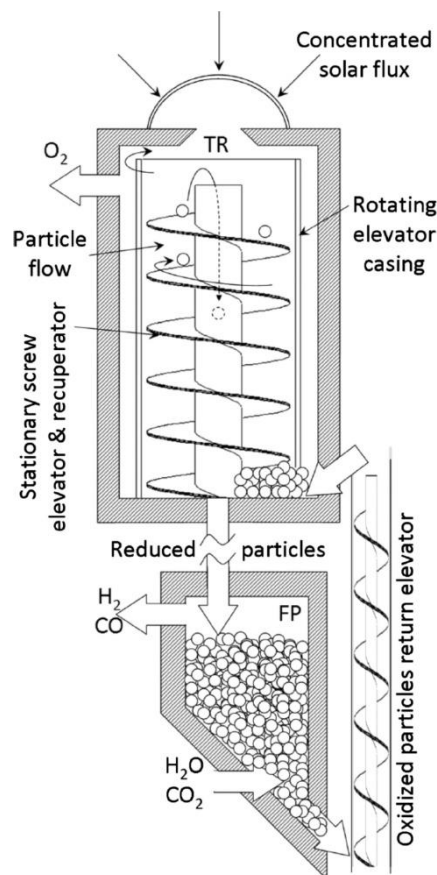


Figure 29 - Obstructed solar receiver with screw elevator [72]

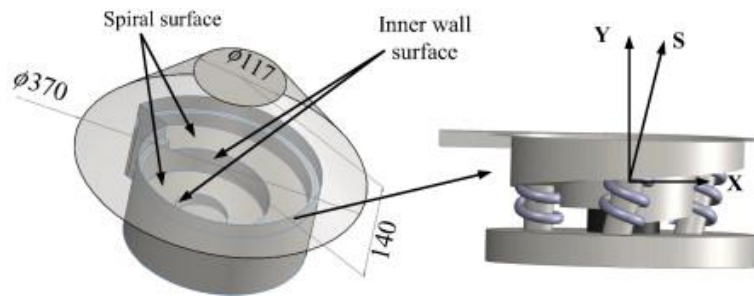


Figure 30 - Configuration of Spiral solar particle receiver [80]

In conclusion, falling particle receivers are extremely interesting devices, because of their marked installation simplicity compared to other solar receivers technologies, their considerable development and innovation possibilities and their relatively low costs thanks to the use of typically economical materials that are widely available in nature. They represent a technology of sure development, although their integration with a calcium looping system using  $CaCO_3$  particles is still in the evolution phase.

#### 2.4.7.2. Centrifugal solar receivers

Centrifugal solar receivers (CentRec) constitute a class of components which realize the heating of solid particles by solar radiation using the centripetal forces generated by swirling rotations. CentRec technology is based on the use of a rotary receiver. The particles are inserted from the top of the component and in their gravity fall motion they are invested by solar radiation. A rapid rotation of the receiver facilitates the exercise of a centripetal force that pushes the particles towards the cylindrical wall, holding them in position. They therefore exit through the opening at the bottom of the component. By varying the speed of rotation it is possible to modify the motion and trajectories of the particles, calibrating the actual incoming solar radiation and consequently ensuring a specific output temperature, constant up to  $1000^{\circ}C$  [81]. In order to keep constant the outlet temperature at all load conditions, it is possible to proceed by varying the mass flow rate by regulating the operation of a valve and defining an optimal retention time obtained by changing the rotation speed of the chamber [82].

As a result of gravitational force, the particles fall slowly downwards along the wall in an axial direction while being heated by the incident solar radiation beam. Exposure to light is extended by the resistance to motion guaranteed by centripetal force. The cylindrical receiver can be positioned at inclinations between  $10^{\circ}$  and  $90^{\circ}$  to the horizon. In this way, it is possible to identify the optimal orientation so that convection losses can be minimized and the efficiency of the heliostatic field increased [83].

(Wu et al.) Proposed a prototype of CentRec, consisting of a 170 mm diameter and 260 mm height inner tube with receiver function, fixed by two holding rings between the outer steel tube. The receiver is made of a high temperature nickel-based alloy in order to resist at the very high temperatures expected. In addition, a cylindrical outlet is properly designed to minimize particle loss. Regarding conduction heat losses, they are treated incorporating microporous insulation in the spaces between inner and outer tube. The rotation of the receiver is provided by a DC motor, while a double-walled feeding cone equipped with sixteen fins between the walls is included to accelerate the input particles and to make them reach the proper speed [83].

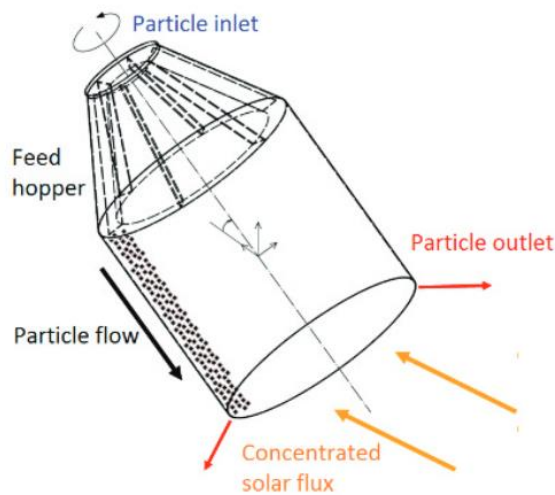


Figure 31 - Centrifugal solar receiver [82]

Solar calcination using a centrifugal reactor was studied also by (Meier et al.), who proposed two solar reactors of  $10 \text{ kW}_{th}$ , one of them directly irradiated while the other indirectly irradiated. The results show that a higher maximum conversion value of 38% is obtained in the indirect irradiation case, while a 20% of conversion factor is reached in the other situation (input of solar flux of  $2000 \text{ kW}/\text{m}^3$ ). Furthermore, the indirectly irradiated solar reactor represents a very suitable solution for CSP-CaL integration, since  $\text{CO}_2$  emissions are avoided [84].

In conclusion, the centrifugal receiver is a technology whose advantages significantly increase its attractiveness, especially with a view to a possible integration CSP-CaL. Specifically, the analysis carried out shows that the use of a rotary klin ensures substantial control of operations, thanks to the possibility of varying the residence time of the particles in the chamber by calibrating the rotation speed and mass flow rate of the flow introduced. These strategies allow an effective regulation of the thermal power

transmitted, ensuring an almost constant particle output temperature. The design, geometry and materials with which the cavity is designed confer a considerable resistance to high temperatures, and also the direct contact of the rotating particle bed with hot tube walls promotes heat exchange [85].

#### 2.4.7.3. Fluidized bed receivers

The fluidized bed receivers represent a further application possibility in the realization of solar receivers for a potential integration of a calcium looping system in a concentrating solar power plant. They are instruments used in many industrial applications and their most important feature, the use of a heterogeneous medium for the realization of the heat exchange process, confers them considerable heat exchange abilities and high energy density [87].

An accurate description of the operating mechanism is offered by (Ma et al.), analysing a fluidized bed receiver used in a high temperature CSP system with solar tower configuration. The proposed receiver is comparable with the operating mechanism of a fluidized-bed boiler, in which the gas fluidifies the solid particles in contact with the boiler heat exchanger and through the fluidized bed flows to the riser. Once heat is transferred to the heat transfer fluids, the mixture of gas and solid particles is conveyed into a separator in order to divide the solid fraction from the gaseous fraction. The solid particles thus obtained, having transferred the previous thermal availability in the heat transfer process encountered, are stored in cold storage. In the presence of solar radiation, the cold particles are consequently moved to the solar receiver, where they are invested by the solar beam, they increase their temperature and are therefore conveyed to the hot storage while waiting for a subsequent heat exchange process in the fluidized bed heat exchanger [86].

A CSP system integrated with a receiver of the fluidized bed type, therefore, can benefit from the development of a two phase gas/solid process which guarantees the implementation of heat exchange phenomena considerably more efficient than in single-phase transformations, due to the high heat exchange coefficient of the fluidized solid particles involved. This translates into the possibility of using compact and low cost fluidized bed heat exchangers, with consequent plant engineering advantages. It can be seen, therefore, that the successful integration of a fluidized bed in a CSP system depends on the ability to identify the correct design of the heat exchanger in order to maximize the heat exchange coefficient and the efficiency of the process, while including an optimization aimed at reducing costs and dimensions [86].

(Briongos et al.) proposes instead an application of fluidized bed receivers in a different installation context, considering CSP beam down systems. In this case, the ground

receiver consists effectively of a fluidized bed, on which the incident solar radiation coming from above is concentrated, according to a very different scheme compared to the solar tower configuration. The incident solar radiation heats the particles in the receiver and causes the formation of a surface layer of hot particles. To promote heat exchange and maximize the gas-solid mixing rate, the receiver operates in bubbling conditions. In this way the hot layer is propelled downwards of the fluidized bed, in a transient process that stabilizes when the energy transferred to the fluidizing gas equals that captured by the solid particles. This process of heat transmission and movement of the surface layer of hot particles are, however, the issues currently under discussion regarding possible improvements in the integration of the fluidized bed receiver into a beam down system. [87].

(Matsubara et al.) provides a useful description regarding the execution of a test on a fluidized bed prototype receiver with a solar simulator of the size of  $3 kW_{th}$ , in preparation for a field test at the Miyazaki beam down system. The experiments carried out show how the particles inside the receiver are heated up to temperatures above  $900^{\circ}C$  and how an increase in the central gas velocity favours a reduction in excess temperatures around the particle bed surface [88].

Ultimately, fluidized bed receivers represent a powerful alternative in optimizing the operation of a CSP system, especially because of the possibility of application in both a solar tower system and a beam down configuration. Generally, in order for the operation of the fluidized bed to be optimal and appropriate to be used as a solar receiver, it is required to be suitable for particle sizes desired by receiver, to guarantee a high heat exchange with low percentages of heat losses and parasitic power consumption, simultaneously ensuring reasonable design costs [89].

## CHAPTER 3

### SIMULATIONS OF CSP-CaL INTEGRATION

#### 3.1. CSP-CaL integration methodologies

The integration of the calcium looping process with a concentrating solar power plant and its implementation as a thermochemical energy storage system represent extremely interesting opportunities in the development and success of both technologies. Although their characteristics are clearly compatible and their combined use leads to mutual benefits, it is necessary to undertake a more comprehensive investigation into integration strategies and application methods in order to optimise the process and maximise results.

An effective strategy to assess the effects of the parties' combination consists in carrying out model simulations with the support of AspenPlus V8.8 software. The running of customised plant models and the possibility of implementing modification and optimisation procedures guarantee the identification of ideal layouts in the investigation of the subject.

The possibilities of the Calcium Looping mechanism in terms of thermochemical energy storage system will be explored in depth considering two different configurations: concentration solar plant with high temperature thermochemical storage system and concentration solar plant with ambient temperature thermochemical storage system.

The integration is achievable through different technologies of the CSP type solar plant. Specifically, in the proceeding of the study a system with solar tower technology will be considered and a total thermal power supplied to the calciner, net of losses, of  $100 MW_{th}$  will be assumed. Therefore, a discussion on further insights on the plant scheme is addressed later on, in order to provide a solid theoretical basis.

The storage system, on the other hand, represents an essential component in a CSP plant. It ensures that the system's operations are extended over time, allowing energy demand to be met even in non-radiation conditions and, at the same time, ensuring a cushioning of demand, especially during peak periods. It is therefore immediate to discern the obvious possibility of integration offered by the characteristics of the two technologies.

In addition, the flexibility of the Calcium Looping process is capable of ensuring proper functionality even for calciner input thermal power below the  $100 \text{ MW}_{th}$  considered. In this regard, it is interesting to clarify the possibility of applying the integration scheme on a small scale for lower size plants. In virtue of this consideration, it is convenient to add information about the realization potential and, specifically, to discuss the Beam-down technology, which is rapidly spreading among the solar concentration plant schemes.

#### 3.1.1. Solar tower configuration

Solar tower technology is one of the most interesting application possibilities in a CSP system. Its operating mechanism is based on the arrangement of the receiver on a considerably high tower (commonly it can exceed 100 meters in height), on which the solar radiation is reflected by a field of heliostats placed on the ground [91]. The height of the tower is an essential parameter in the design phase, because it allows to vary not only the extension of the heliostat field, but also the distances between the different mirrors and between them and the tower, in order to minimize shadowing and blocking phenomena. The heliostatic field consists of reflective structures oriented towards the receiver and equipped with a movement mechanism useful to arrange them according to the optimal orientation. The exact position of the tower and the orientation of the (mobile) mirrors depend mainly on the geographical location of the system and the inclination of the incident solar radiation. The closer the plant is located near the equator, the more the tower will be placed in the centre of the heliostatic field.

To provide an overview of the system articulation in question, the Gemasolar installation in Fuentes de Andalucía (Spain) is characterised by a central tower 140 metres high and a heliostatic field of 2650 heliostats for a total of  $304750 \text{ m}^2$ . It consists of a plant using molten sodium and potassium salts as heat transfer fluid, with a nominal turbine capacity of 19.9 MW [92]. The following figure (*Figure 32*) shows a photo of the installation. Of significant importance is the considerable extension of the solar field around the tower, whose position is not precisely in the centre for the reasons specified above.



Figure 32 - GEMASOLAR plant, owned by Torresol Energy (© Torresol Energy)

The considerable temperature reached in the receiver promotes the availability of a significant amount of thermal energy, which tends to be transferred through a heat transfer fluid with the aim of performing the subsequent thermodynamic processes. The application mode of solar tower technology probably, to date, more widespread involves the use of molten salts to transfer heat useful for the generation of steam to evolve into a Brayton cycle for the production of power [92]. The figure (Figure 33) shows a plant example of the configuration just described.

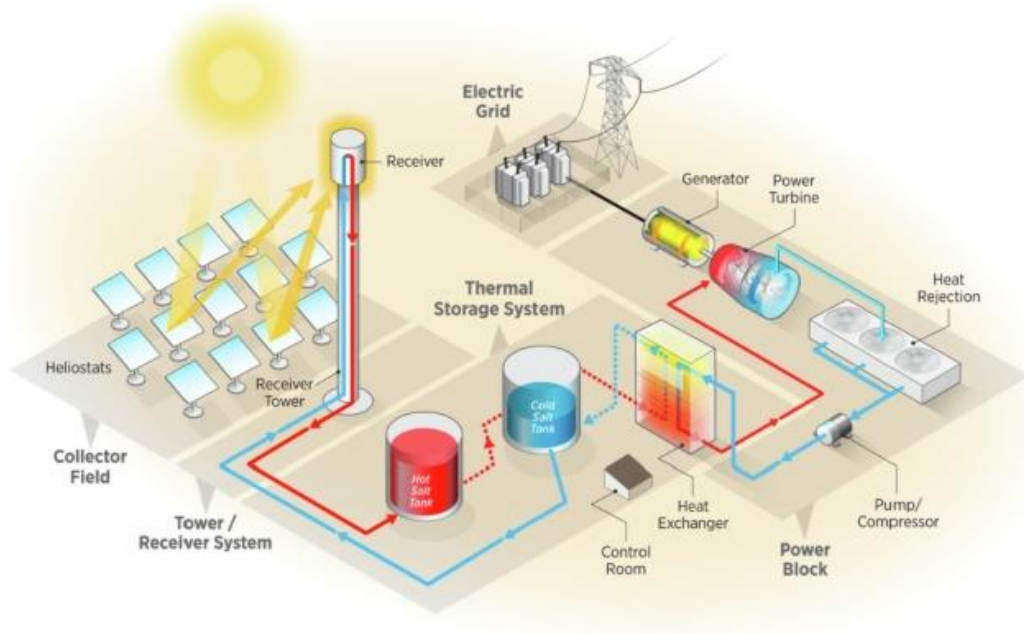


Figure 33 - CSP molten-salt power tower with direct storage [92]

With reference to the integration with the calcium looping process, on the other hand, the receiver has the function of supplying the calciner with the thermal power necessary for the calcination reaction and the decomposition of  $CaCO_3$  into  $CaO$  and  $CO_2$ . Differently from the scheme with molten salts just described, in the CSP-CaL situation the power production is performed in a Rankine cycle that exploits the high thermal availability of the  $CO_2$  stream heated by the carbonation reaction, evolving into a gas turbine.

The solar tower configuration represents the CSP plant methodology through which it is possible to reach the highest temperature values inside the receiver (up to 1000 °C and higher), with consequent higher efficiency in the production of useful power from the gas/steam turbine cycle. While on the one hand the energy and productive advantages are evident, on the other hand the solar tower configuration requires, however, the facing of investment costs that tend to be higher than the other plant solutions, especially due to the huge expenses necessary for the construction of the tower and the vertical system for the conveying of substances.

Spain, strengthened by favourable climatic conditions and suitable land morphology, has become one of the most involved countries in the exploitation of the technology's potential. In addition to the GemaSolar described above, the two installations PS10 and PS20, part of the Abengoa Solar complex located in the region of Andalusia, are equally important [93]. The Solar tower Jülich, located in the German state of North-Rhine Westphalia in the town of Jülich, also plays an important role in Europe. Although it consists of a small-sized plant (60 meters high for a solar field of about 18000  $m^2$ ), it provides a useful example of the application of the technology using air as heat transport medium [94].



*Figure 34 - Solar tower Jülich [94] and Abengoa Solar PS10 and PS20 plants*

### 3.1.2. Solar Tower Plant simulation

As a theoretical reference in the design of a CSP plant with solar tower technology with a view to integration with the Calcium Looping process, it is possible to rely on the simulations described in detail in (Ortiz et al.) [95]. The study consists in the complete characterization of a possible solar plant according to the characteristics described and with the target to reach a thermal power delivered to the calciner of  $100 \text{ MW}_{th}$ . The simulation is carried out with the support of the SolarPILOT software, using the summer solstice in Seville as the reference day. Some of the inputs used in the implementation of the simulation, and important for the continuation of the analysis in this treatise, and some of the results obtained are listed in the following table:

<i>Assumptions</i>	<i>Value</i>
<i>Heliostats area (<math>m^2</math>)</i>	$36 \text{ m}^2$
<i>Tower height (m)</i>	$100 \text{ m}$
<i>Design DNI (<math>W/m^2</math>)</i>	$790 \text{ W/m}^2$
<i>Field type</i>	<i>Surrounded</i>
<i>Minimum / maximum field radius (m)</i>	$75/597$
<i>Results</i>	<i>Value</i>
<i>Solar Power (MW)</i>	$212,3$
<i>Power for calcination (MW)</i>	$100,1$

*Table 4 - Main inputs and SolarPILOT results, adapted from [95]*

According to the results provided by (Ortiz et al.), the result is a total solar field consisting of 6081 heliostats with an optical efficiency of 67,4 % [95].

Other information relevant for the continuation of the analysis concerns the estimation of the storage system. It is calibrated according to an 8-hour period of operation in solar radiation availability, followed by 16 hours of night-time operation. The storage system is therefore designed to be large enough to ensure sufficient material for the 16 hours of absence of radiation. This results in quantities of 3050 and 3409 tonnes, respectively for  $\text{CaO}$  and  $\text{CaCO}_3$ , corresponding to storage volumes of  $3062 \text{ m}^3$  and  $2097 \text{ m}^3$ , taking into account packing density and solids porosity [95]. Finally, the pressurised  $\text{CO}_2$  tank, maintained at  $25 \text{ }^\circ\text{C}$  and 75 bar, is estimated to have a volume of  $462 \text{ m}^3$  and designed as a cylindrical pressure vessel made of chromium and molybdenum doped stainless steel [95].

### 3.2. Different CSP-CaL integration layouts analysed

In the following paragraphs an analysis of the plant layouts related to the integration of the calcium looping process in a solar tower technology concentrating solar system is described. Their analysis is treated considering a calciner power of  $100 MW_{th}$  and two different solutions, one with high temperature storage system and the other with ambient temperature storage system.

Despite the following configurations are analysed from a static point of view, it would be advisable to linger over the dynamic nature of the proposed integration. The presence of a storage system, in addition to the intermittence of solar radiation, results in an unavoidable differentiation between daytime and night-time operations of the system. If in the presence of solar radiation, the storage systems receive input substances, in conditions of lack of resource, the system is still able to continue to produce energy through the consumption of what has been previously stored in the tanks. This results in an operational division into two daily time periods. In order to simplify the study, it is assumed to consider the plant in operation for all 24 hours per day, dividing them proportionally into 8 hours of radiation availability and 16 hours of "night" operation. A distribution of this type simplifies the proportioning of the quantities of substances subdivided between storage systems and calcination and carbonation reactors. No other causes are therefore considered that could reduce the contribution of solar radiation during the 8 hours of light established, neglecting all sorts of meteorological phenomena and other possible obstacles to the efficient operation of the receiver.

In addition, the study is streamlined by assuming the almost ideal functioning of some components. Specifically, no significant losses are considered in the processes of mixing or splitting flows through components such as mixers and splitters.

Each of the two configurations is analysed by means of a description of the main components that constitute the plant layout. Specifically, particular attention is given to the reactors responsible for the calcination and carbonation reactions, the related heat exchanger networks and the  $CO_2$  compression systems. Each component is therefore characterized by the input and output flows involved in its operations and the related thermodynamic characteristics.

At the end of the analysis, a final paragraph of comparison between the two configurations is proposed, with the aim of highlighting the main differences and therefore observe the contexts of greater convenience for their use.

### 3.2.1. CASE 1: CSP-CaL with high temperature storage systems

The plant configuration analysed in this paragraph describes the integration of the Calcium Looping process with a solar concentration system. Remaining in the hypothesis of using solar tower technology, the simulation is carried out with a thermal power transmitted to the calciner equal to  $100 \text{ MW}_{th}$ . The results of the model provide information about flow rates and thermodynamic conditions of the various streams circulating in the system. They represent a direct consequence of the initial conditions imposed on the calciner in terms of the way in which the chemical calcination reaction takes place.

In this case (CASE 1), the substances, both solid and gaseous, stored in the storage systems are conserved at high temperature. This certainly implies a greater plant simplicity compared to the case with storage at ambient temperature (CASE 2, analysed later), due to the reduced heat exchange processes required for the subsequent heating of the substances. On the other hand, however, it reduces the flexibility of the system by shortening the duration of possible storage times without an excessive lowering of the temperature of the stored materials.

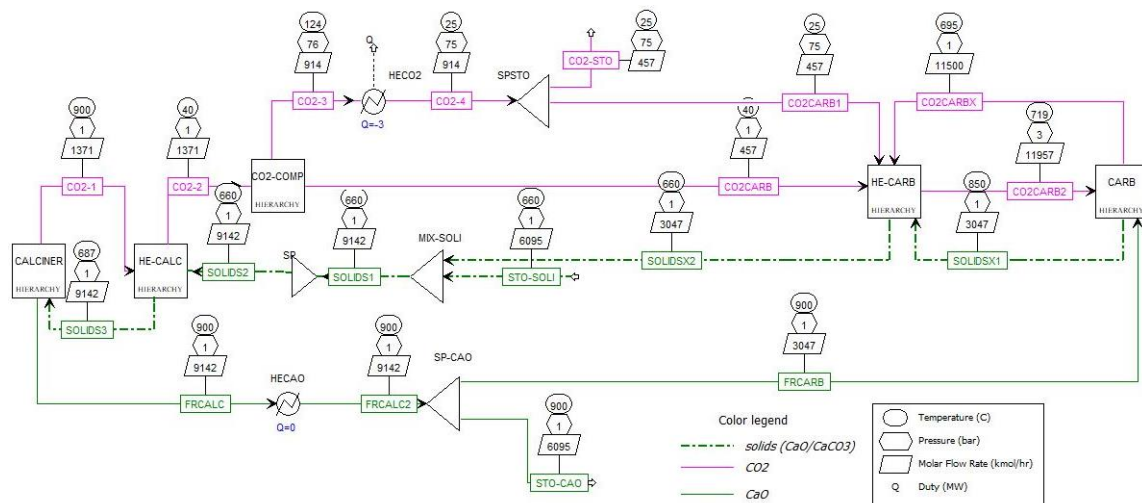


Figure 35 - CASE 1, main layout

From the plant layout shown in the figure (Figure 35) it can be seen that five main blocks can be distinguished in the configuration: CALCINER, HE-CALC, CO2-COMP, HE-CARB, CARB. They in turn enclose more or less complex circuits comprising different components useful for carrying out the operations. Therefore, a more detailed description of each of them will be provided below.

The process begins in the calciner, which is the component where the chemical calcination reaction is performed in order to dissociate the initial amount of calcium carbonate  $CaCO_3$  into the  $CaO$  and  $CO_2$  compounds. The reaction is endothermic and the amount of energy required for its accomplishment is obtained through the absorption of the incident solar radiation.

In order to increase process efficiency and with a view to plant optimization, it is advisable to pre-heat the  $CaCO_3$  stream before distributing it to the reactor. In this way, the thermal power obtained from the solar radiation is targeted to the reaction, without using it excessively for the preheating of the substances. In this regard, the scheme is completed with a heat exchanger system (HE-CALC), which ensures that the thermal availability of the high-temperature  $CO_2$  flow resulting from the dissociation reaction is exploited to increase the temperature of the  $CaCO_3$  reactant.

Specifically, according to the simulation carried out,  $CaCO_3$  is promoted from an initial temperature of 660 °C (SOLIDS1) to 687 °C (SOLIDS2) after exchanging heat with the  $CO_2$  stream.

The operating diagram of the heat exchangers system in question is shown below (Figure 36):

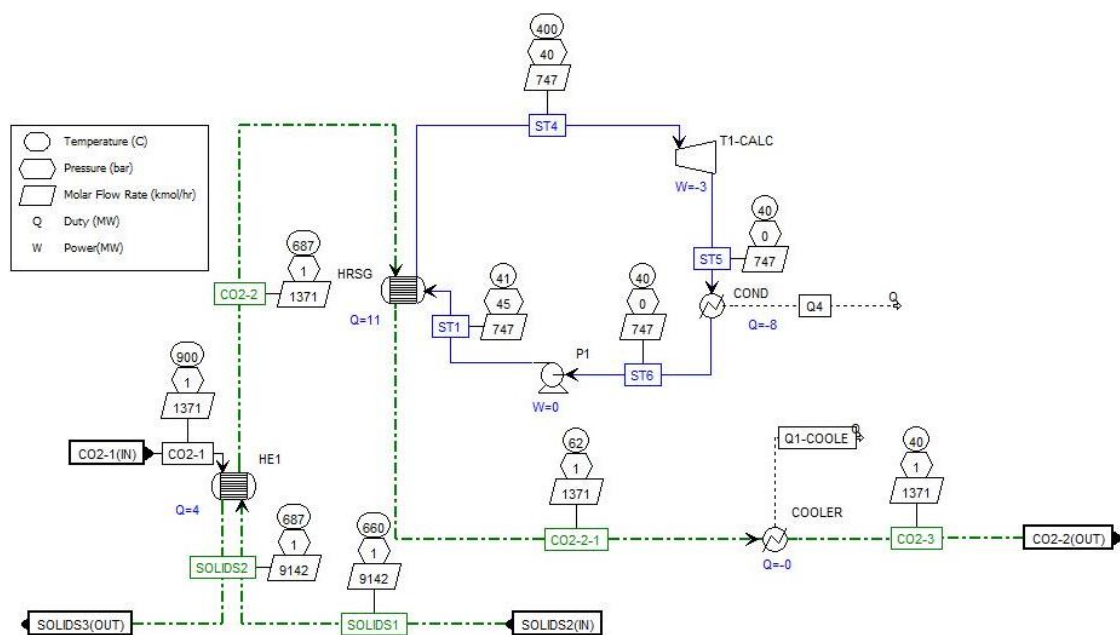


Figure 36 – CASE 1, HE-CALC

From the diagram shown in the figure it can be seen that the flow of  $CO_2$  entering the HE1 heat exchanger and leaving the calciner (CO2-1) has a temperature of 900 °C and a flow rate of 1371 kmol/hr. It passes into a heat exchanger where it transfers heat to the stream of  $CaCO_3$  (SOLIDS1). Respecting the rules of pinch analysis, it follows that the

hot flow of  $CO_2$  at the outlet, with obviously similar flow rate, has a residual temperature of  $687\text{ }^\circ\text{C}$  (CO2-2). Similarly, the stream of  $CaCO_3$ , with a flow rate of  $9142\text{ kmol/hr}$  increases its temperature from  $660\text{ }^\circ\text{C}$  to  $687\text{ }^\circ\text{C}$  and is consequently directed to the chemical dissociation reaction in the calciner.

As a result of the heat exchange process, however,  $CO_2$  still exhibits a temperature of  $687\text{ }^\circ\text{C}$  which is reasonably high. Its considerable thermal availability makes it possible, in this particular configuration, to include an additional power cycle with steam turbine, to further improve plant performances and increase the energy production. In this regard, the  $CO_2$  stream (CO2-2) enters a second heat exchanger (HRSG) which operates as a steam generator and heats a flow of  $H_2O$  (ST1), with a flow rate of  $747\text{ kmol/hr}$  from a temperature of  $41\text{ }^\circ\text{C}$  to  $400\text{ }^\circ\text{C}$  (ST4).

The high thermal quality steam is consequently expanded in a steam turbine (T1-CALC) with an operating capacity of  $3\text{ MW}_{el}$ . A configuration of this type, therefore, guarantees electricity production even in components that are not properly part of the power cycle building block.

The flow of  $CO_2$  (CO2-3), following the double heat exchange process, then leaves the system at a temperature of  $40\text{ }^\circ\text{C}$ , after being further processed in a cooler with water as refrigerating medium.

After preheating, the stream of  $CaCO_3$  is then injected into the calciner, at  $687\text{ }^\circ\text{C}$  and with a flow rate of  $9142\text{ kmol/hr}$ . The operating scheme of the block (CALCINER), including the calciner, used in the analysed configuration is the following (Figure 37):

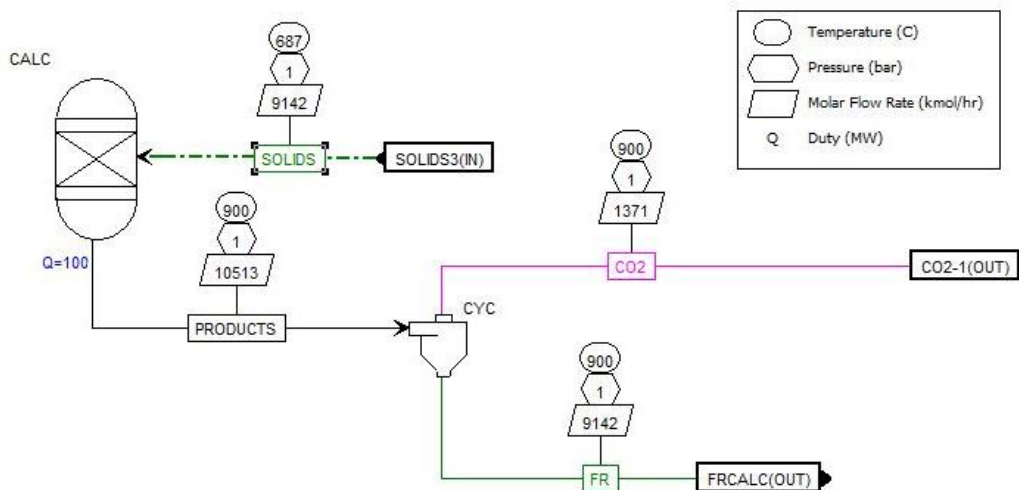


Figure 37 – CASE 1, CALCINER

From the graph it is further understandable the process developed in the calciner. The input solids stream (SOLIDS) undergoes the endothermic chemical dissociation reaction

due to the power provided by the incident solar radiation and splits into two distinct streams of  $CaO$  and  $CO_2$ , initially included in a single stream of matter (PRODUCTS), with a flow rate of 10513 kmol/hr and a temperature of 900 °C. The flow is then directed to a cyclone separator (CYC) from which the two different product streams originate: the portion of  $CaO$  (FR) at 900 °C and 9142 kmol/hr and the portion of  $CO_2$  ( $CO_2$ ) at 900 °C and 1371 kmol/hr. The cyclone separator is considered, in this simulation, as an ideal component with no mass or energy losses.

The quantity of  $CaO$  obtained is partly destined to be deposited in storage systems (6095 kmol/hr) while the remaining fraction (3047.5 kmol/hr) is sent to the carbonator for the subsequent carbonation reaction. The configuration, more precisely, is calibrated to divide the total amount of  $CaO$  into 1/3 for the carbonation reaction and 2/3 for storage, as a result of the daily division into 8 hours of operation with solar radiation and 16 hours of absence of the resource.

The  $CO_2$  flow leaving the heat exchangers system ( $CO_2-2$ ), at 40°C and 1371 kmol/hr, is directed to a by-pass system ( $CO_2BYPASS$ ) which splits it into two distinct flows: a 457 kmol/hr and 40°C ( $CO_2-1-1$ ) flow directed to the carbonator for subsequent recombination chemical reactions, and a 914 kmol/hr and 40°C ( $CO_2-1-2$ ) flow which is instead sent through various compression stages to the  $CO_2$  storage system. The first flow is used in the daytime operation of the system, in the presence of incident solar radiation. The second, on the contrary, being contained in the storage system, is used in night-time applications. Specifically, also in this case the system is regulated to send 2/3 of the initial quantity of  $CO_2$  to the storage and the remaining 1/3 to the carbonator.

The following figure (Figure 38) explains the plant articulation in relation to the series of transformations experienced by  $CO_2$  in the  $CO_2-COMP$  block:

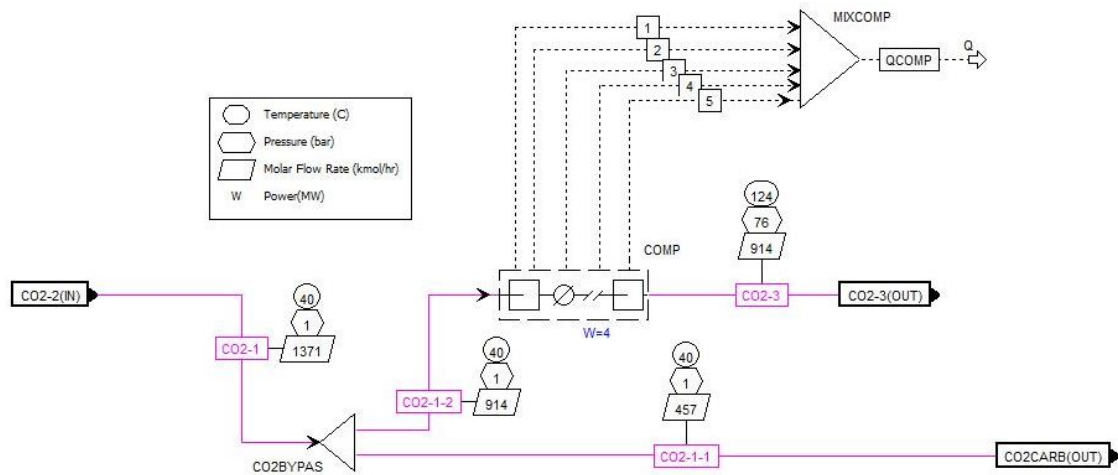


Figure 38 – CASE 1,  $CO_2-COMP$

Before carrying out the operations inside the carbonator, the material flows involved are processed in a second network of heat exchangers (HE-CARB), whose role is to exploit any residual thermal availability to increase the efficiency of the process. Specifically, the primary purpose is to pre-heat the  $CO_2$  flow to be sent to the carbonator in order to reduce the irreversibilities and thermal losses generated by an otherwise excessive temperature difference between reactants and products in the carbonation reaction.

In the heat exchanger network considered, two distinct flows of  $CO_2$  are conveyed: one at 457 kmol/hr, 1 bar and 660 °C (CO2CARB) coming directly from the heat exchangers after the calciner, and one of similar flow rate (457 kmol/hr), 25°C and 75 bar from the  $CO_2$  storage system (CO2-STO). The prevalence of one over the other undoubtedly depends on the operating conditions of the system and the presence or absence of incident solar radiation.

The plant layout of the network of heat exchangers preceding the carbonator is shown in the following figure (Figure 39).

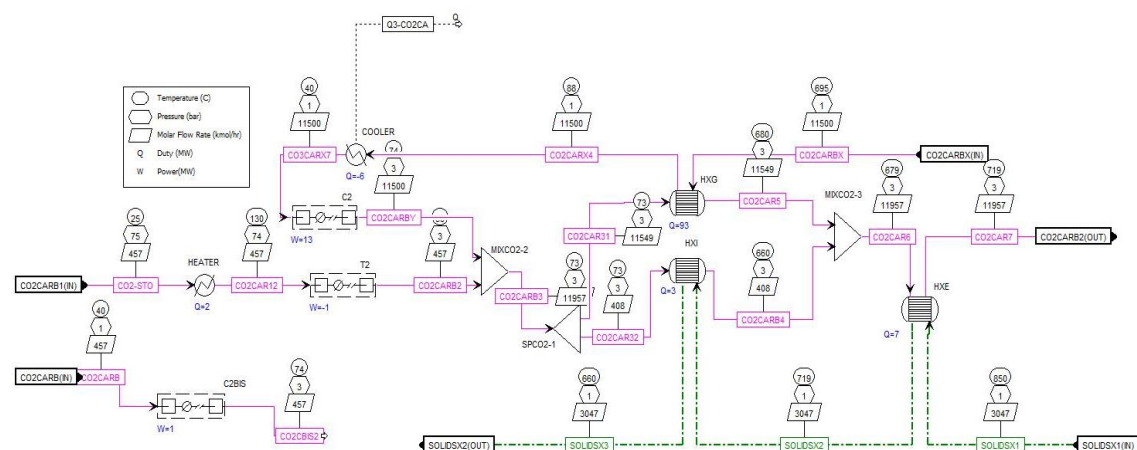


Figure 39 – CASE 1, HE-CARB

Under daytime operating conditions with solar radiation availability, the system supplies the carbonator with a flow of  $CO_2$  coming directly from the heat exchanger network after the calciner (HE-CALC). Consequently, the flow to be considered is CO2CARB, with a flow rate of 457 kmol/hr and a temperature of 40 °C. It undergoes preheating and compression stages by means of a compressor (C2BIS) that lead it to a temperature of 74 °C and a pressure of 3 bar (CO2CBIS2).

In night conditions, on the other hand, the  $CO_2$  flow comes from the storage system (CO2-STO), with a flow rate (457 kmol/hr) equal to the quantity supplied by the calciner, but with a lower temperature (25 °C) due to the conservation in ambient

thermal conditions and the thermal losses which can be counteracted in the component. The initial heating by heater is therefore higher than in the previous case, recording a thermal input of about 2 MW to reach a temperature of 139 °C. In addition, the  $CO_2$  storage system is a pressurized component such that the output flow registers a high level of residual pressure (75 bar). This high availability makes possible the introduction of a small gas turbine (T2), placed after the heater, with a production capacity of about  $1 MW_{el}$ . The  $CO_2$  flow then expands in the component, reaching a final pressure of 3 bar, similar to that of the  $CO_2$  flow from the heat exchanger system on the calciner side (HE-CALC).

The stream of  $CO_2$  fed into the network then enters a mixer, in which it is combined with the  $CO_2$  coming out of the power cycle (CO2CARBY).

A series of heat exchange stages through various gas/gas and gas/solid heat exchangers promote the increase in  $CO_2$  temperature by exploiting the thermal availability of  $CaCO_3$  leaving the carbonator, which registers an initial temperature of 850 °C (SOLIDSX1) reduced to 660 °C after passing through the various heat exchangers (SOLIDSX3). The  $CO_2$  flow, ultimately, enters the carbonator with a temperature raised to 719 °C and a total flow of 11957 kmol/hr (CO2CAR7).

Consequently, there follows the chemical reaction of carbonation carried out inside the carbonator, whose plant scheme is shown in the following figure (Figure 40).

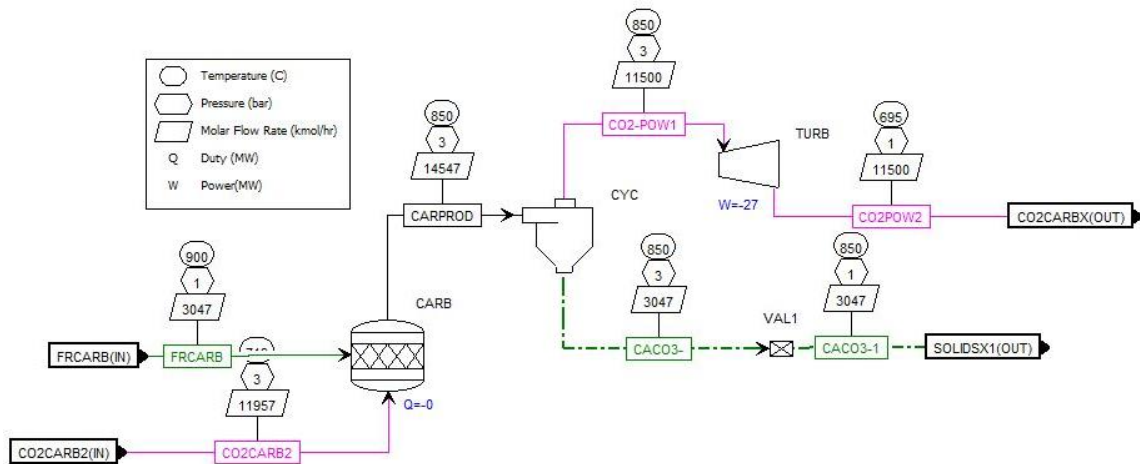


Figure 40 - CASE 1, CARB

The function of the carbonator is to realize the chemical reaction of recombination of  $CO_2$  and  $CaO$  with consequent reforming of calcium carbonate  $CaCO_3$ . The process is exothermic and the large amount of energy released is used to heat a large stream of

$CO_2$ . The high thermal quality purchased by the latter therefore allows the development of the power cycle and the production of electricity in the dedicated gas turbine.

As shown in the figure, the flow of  $CO_2$ , 11957 kmol/hr at 719 °C, leaving the HE-CARB heat exchanger (CO2CARB2) enters the carbonator together with the flow of  $CaO$ , at 900 °C and 3047 kmol/hr.

Stoichiometrically the  $CO_2$  is in excess, which is why only a portion of the incoming  $CO_2$  is actually used in the reaction, specifically an amount equal to 457 kmol/hr. This is a very important datum, because in order to guarantee the iteration of the cycle it is necessary that in the carbonator a quantity of  $CO_2$  is added, time by time, at least equal to that used in reaction. The remaining part of the incoming  $CO_2$  flow, 11500 kmol/hr, is heated in the carbonator thanks to the thermal energy released during the chemical reaction, raising its temperature from 719 °C to 850 °C. In addition, the compression experienced in the HE-CARB heat exchangers system has allowed its pressure to rise to the final value of 3 bar, taking advantage of the operation of a compressor (C2) with a size of around 11 MW. The flow of  $CO_2$  with high thermal availability thus generated (CO2-POW1) is consequently used in the power cycle, expanding into a turbine whose net capacity is 27,19  $MW_{el}$ . Afterwards, the  $CO_2$  flow exits the cycle with reduced temperature at 695 °C (CO2-POW2) and pressure of 1 bar and is recirculated in the HE-CARB heat exchanger.

The  $CaCO_3$  produced in the carbonator, on the other hand, has a temperature of 850 °C and a flow rate of 3047 kmol/hr (CaCO3-1). It follows a path similar to  $CO_2$ , passing through the HE-CARB heat exchangers system and finally being conveyed to the solids storage tank while waiting for the start of a new cycle.

### 3.2.2. CASE 2: CSP-CaL with ambient temperature storage systems

The plant configuration described below follows several of the characteristics of CASE 1 previously discussed. Once again the possibility of integrating the Calcium Looping process into a concentrated solar power plant as a thermochemical energy storage system is examined. The thermal power transmitted to the calciner from the heliostat field is also in this case assumed to be  $100 MW_{th}$ . Below are the results of the simulation, carried out by running the model using AspenPlus software. The thermodynamic values that characterize the flows and components involved in the system are a direct consequence of the operating conditions set and the input provided to the calciner.

Differently from CASE 1 discussed in the previous paragraph, in the following CASE 2 the solid substances are conserved in storage systems maintained at ambient temperatures. This difference in articulation results in a roughly more elaborate plant configuration, mainly in relation to the heat exchanger networks at the two calciner and carbonator reactors. This result derives from the necessity to increase the heat exchange processes to ensure the achievement of adequate operating temperatures for the solids streams. On the other hand, however, such an approach guarantees flexibility and elasticity to the plant, due to the possibility of considerably expanding storage times compared to CASE 1. As a result, the plant offers an improved ability to adapt to the requirements of the grid.

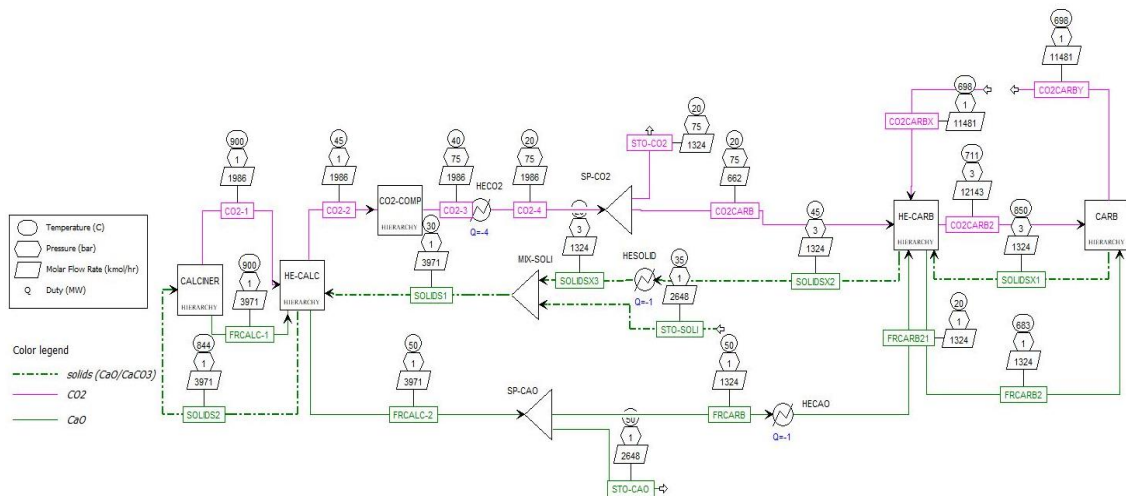


Figure 41 – CASE 2, main layout

The diagram shown in figure (Figure 41) highlights the presence of some fundamental blocks: CALCINER, HE-CALC, CO2-COMP, HE-CARB and CARB. In accordance with the methodology adopted in the CASE 1 study, in the following these blocks are analysed individually in order to clarify the implant articulation that characterizes them.

Calciner is the component in which the process begins. The flow of  $CaCO_3$  is fed into the reactor and thanks to the thermal power provided by the incident solar radiation, the necessary physical conditions are achieved for the chemical calcination reaction to take place, resulting in the production of  $CaO$  and  $CO_2$ .

As already discussed in the previous configuration, also in this second case it is advantageous to provide a heat exchanger system in order to optimize the process and maximize the overall performance. Taking advantage of the high thermal availability of the  $CO_2$  coming out of the calciner, it is once again realized a pre-heating process of  $CaCO_3$  flow.

In this second configuration, the preheating is even more convenient, in terms of performance improvement, because the solids storage system is maintained at low temperature. As can be deduced from the simulation carried out and from the results reported in the picture (Figure 42), the stream of  $CaCO_3$  and  $CaO$  solid substances deriving from the storage system (SOLIDS1) enters the HE-CALC heat exchanger system with a total flow rate of 3971 kmol/hr and a temperature of only 30 °C, considerably lower than the 660 °C of the previous case.

The operating diagram of the heat exchanger network concerned is shown below (Figure 42),

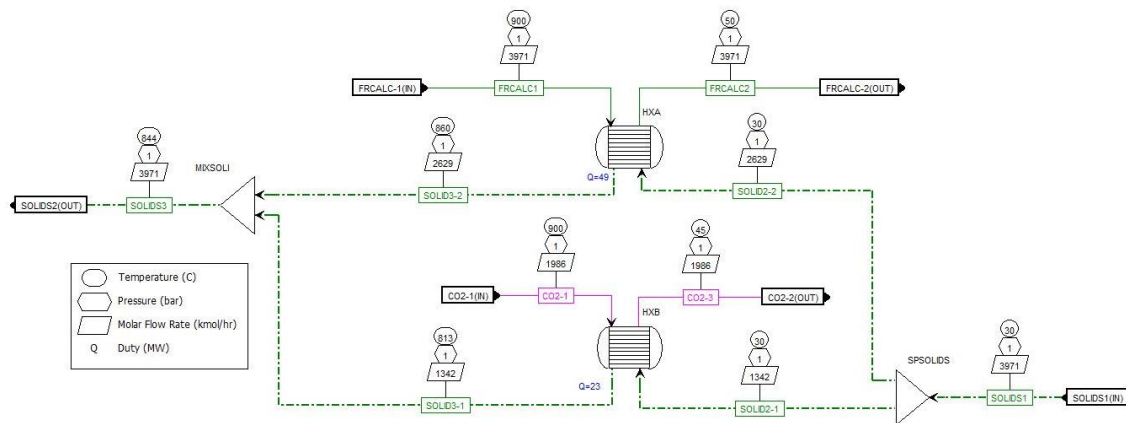


Figure 42 – CASE 2, HE-CALC

Analysing the graph, it appears how also in this case the  $CO_2$  flow leaving the calciner (CO2-1) exhibits a high thermal availability, with a temperature of 900 °C. However, because of the low temperature of the storage system, the input solids stream (SOLIDS1) at 30 °C requires an extremely intensive heating process in order to achieve the ideal thermodynamic conditions to facilitate the calcination reaction in an appropriate manner.

In order to ensure the success of the heat exchange, it would be convenient to subdivide the flow of solids entering the heat exchanger network. This not only optimizes the process, making the required heating possible, but also provides the cooling of the  $CaO$  stream exiting the calciner (FRCALC1), which requires a necessary temperature reduction in order to be stored in the storage used in this configuration.

Consequently, of the 3971 kmol/hr in input, a flow of 1340 kmol/hr (SOLID2-1) is directed to a heat exchanger in which it will face a heat exchange process with the  $CO_2$ . The outgoing stream (SOLID3-1) then records a final temperature of 813 °C. The  $CO_2$  flow, on the other hand, after the heat exchange varies its temperature from 900 °C to 45 °C (CO2-3) and then leaves the exchanger network.

The remaining part of the initial quantity of solids entering the network constitutes a flow (SOLID2-2), with a flow rate of 2629 kmol/hr, for which the thermal availability of the  $CaO$  stream coming out of the calciner is used instead. As a result of the heat exchange process, the incoming solids increase their temperature up to 860 °C (SOLID3-2), while the  $CaO$  stream is cooled down to 50 °C and then sent to the storage system (FRCALC2). In this situation it is therefore necessary to use a solid/solid heat exchanger. This is a disadvantage of the configuration analysed, due to the current absence of components of this type on an industrial scale, as the technology is still in the research and development phase.

The two solids streams thus generated, SOLID3-1 and SOLID3-2, convey into a mixer (MIXSOLI), from which a total flow of 3971 kmol/hr and 844 °C (SOLIDS3) is produced, ready for the chemical reactions that will take place in the calciner. The following figure (*Figure 43*) shows the plant layout of the block including the calciner in operation in this configuration:

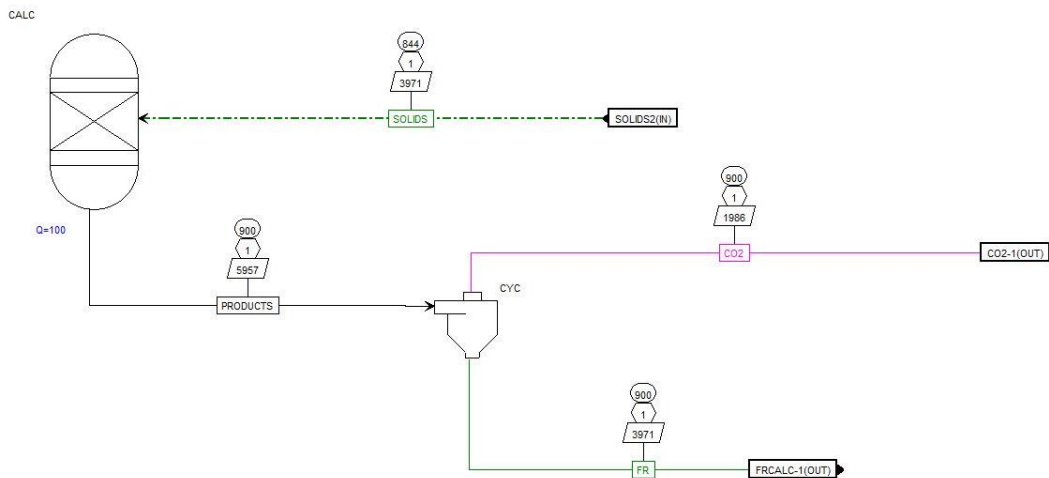


Figure 43 – CASE 2, CALCINER

As previously specified, also in CASE 2 the calciner is calibrated to operate with supplied thermal power equal to  $100 \text{ MW}_{th}$ . The incoming solids flow, following the heat treatments undergone in the heat exchanger network (HE-CALC), enters the reactor (CALC), where it faces the chemical reaction that leads to the dissociation of the initial  $\text{CaCO}_3$  in the two compounds  $\text{CaO}$  and  $\text{CO}_2$ .

The two products come out of the calciner in a single flow of matter (PRODUCTS) with a total flow rate of  $5957 \text{ kmol/hr}$  and temperature of  $900 \text{ }^\circ\text{C}$ .

Through the operation of a cyclone separator (CYC), the two component flows are separated. The  $\text{CaO}$  flow (FR) shows a flow rate of  $3971 \text{ kmol/hr}$  and a temperature of  $900 \text{ }^\circ\text{C}$ . The  $\text{CO}_2$  flow (CO2), on the other hand, is produced with a flow rate of  $1986 \text{ kmol/hr}$  and a temperature of  $900 \text{ }^\circ\text{C}$ .

The  $\text{CaO}$  flow, due to the elevated temperature, is initially exploited for the preheating of the solids entering the calciner, as previously mentioned. In this way, it reduces its temperature from  $900 \text{ }^\circ\text{C}$  to  $50 \text{ }^\circ\text{C}$  and can therefore be sent to the low-temperature storage systems. Specifically, the  $3971 \text{ kmol/hr}$  stream produced in the calciner is split into a  $2648 \text{ kmol/hr}$  stream for storage and a  $1324 \text{ kmol/hr}$  stream which is directly used for power generation operations in the carbonator. This configuration, in particular, is also calibrated to divide the entire  $\text{CaO}$  into  $1/3$  for the carbonation reaction and  $2/3$  for storage, in accordance with the assumption of 8 hours of solar radiation availability per day and 16 hours of subsequent absence.

As a consequence of the heat exchange processes occurred in the HE-CALC heat exchanger network, the residual  $\text{CO}_2$  flow records a temperature of  $45 \text{ }^\circ\text{C}$  and a flow rate of  $1986 \text{ kmol/hr}$  (CO2-2). In order to facilitate the handling of the gaseous quantity in question, it is advisable to use a compressor that guarantees an increase in pressure with a view to possible storage in pressurised containers.

The operating diagram of the multistage compressor used in this configuration is shown in the following picture (Figure 44):

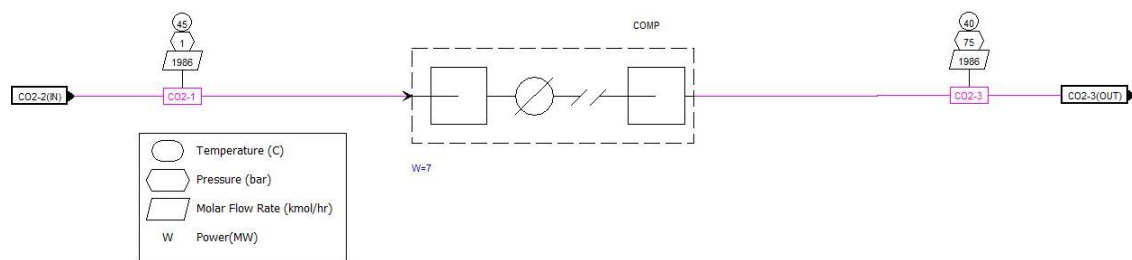


Figure 44 – CASE 2, CO2-COMP

The various compression stages ensure an increase in pressure of the  $CO_2$  flow up to a value of 75 bar (CO2-4), corresponding to the pressurisation applied in the storage vessel.

A separator (SP-CO2) therefore allows the separation of the stream generated, allocating a quantity equal to 662 kmol/hr directly to the carbonator for the subsequent carbonation reaction (CO2CARB). The remaining amount of 1324 kmol/hr (CO2-STO) is instead stored in the tank for future use. Once again, the configuration is designed to ensure a sufficient volume of material in the storage system to compensate for the assumed 16 hours of no solar radiation.

Before performing the operations inside the carbonator, the material streams involved are processed in a second network of exchangers (HE-CARB), whose role is to pre-heat the calcium carbonate stream in order to reduce the temperature difference between reactants and products involved in the reactor. The  $CO_2$  flow supplied to the HE-CARB block and subsequently employed in the carbonation reaction has a flow rate of 662 kmol/hr and a low temperature of 20 °C (CO2CARB). It comes from the storage system if under operating conditions without solar radiation (STO-CO2), otherwise it is obtained directly from the initial stream (CO2-4) generated by the calciner.

The plant scheme of the network of heat exchangers before the carbonator (HE-CARB) is represented in the following figure (Figure 45).

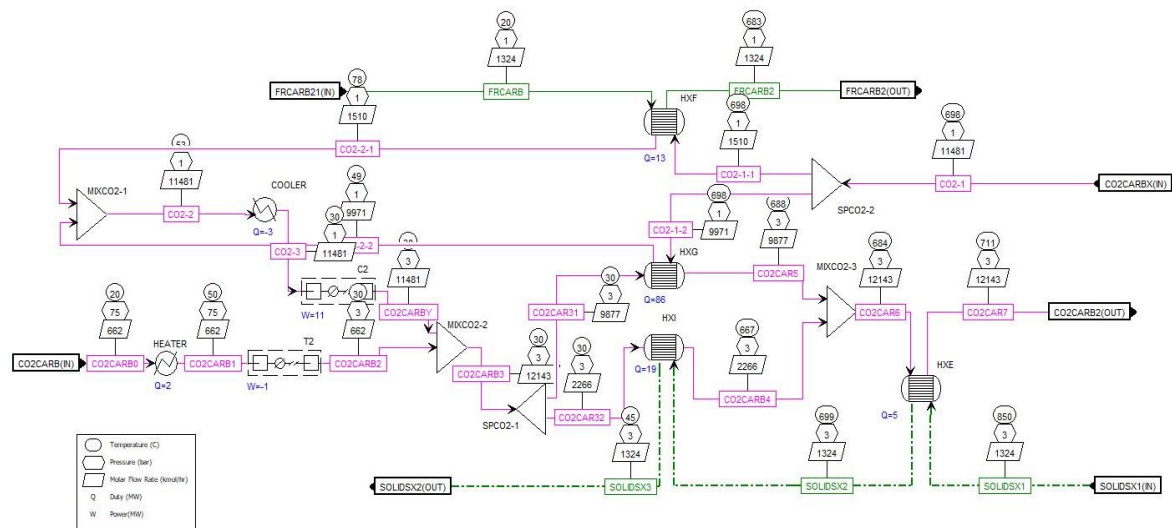


Figure 45 – CASE 2, HE-CARB

The flow of  $CO_2$  introduced into the heat exchanger network has a high pressure of 75 bar, making it possible to install a gas turbine with an operating capacity of 1,05  $MW_{el}$  to expand it in order to obtain useful power. Consequently, it is mixed with

the quantity of  $CO_2$  coming from the power block (CO2CARBX) to deal with the subsequent heat exchange processes in the solid/gas heat exchangers. In this way it is possible to exploit the thermal availability of the  $CaCO_3$  flow generated in the carbonator to preheat the  $CO_2$  which will then be used in the power cycle. In the two heat exchange stages, in fact, it raises its temperature from the initial 30 °C in the mixing phase up to the final 711 °C out of the network. In order to optimize the process, it is advisable to divide the large flow of gas obtained (CO2CARB3, 12143 kmol/hr) into two different streams. One will undergo a heat exchange in a gas/gas exchanger acquiring thermal power from the  $CO_2$  coming out of the power cycle. The other, instead, will take advantage of the residual thermal availability of the  $CaCO_3$  flow.

This is followed, consequently, by the chemical reaction of carbonation carried out inside the carbonator, whose plant scheme is shown in the figure below (Figure 46).

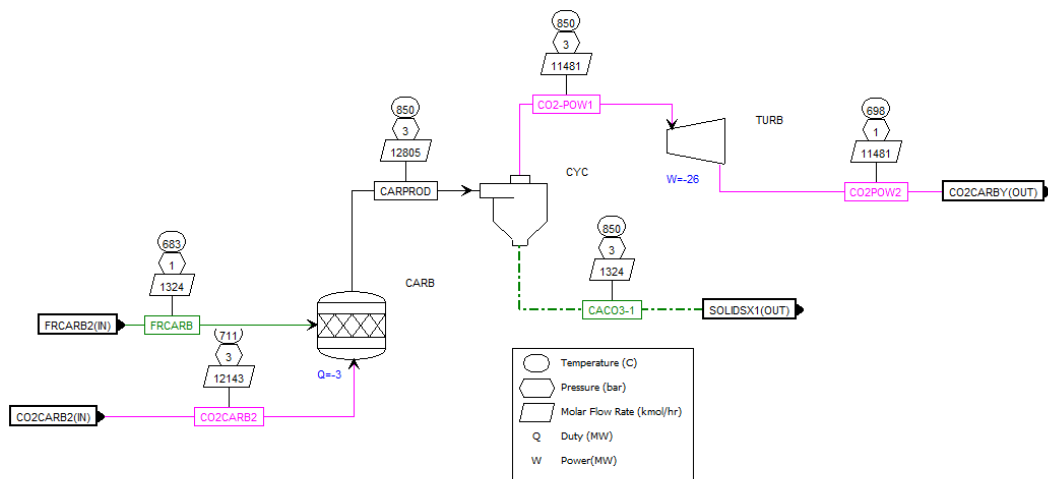


Figure 46 – CASE 2, CARB

Also in this case the carbonator is responsible for performing the chemical reaction of recombination of  $CaO$  and  $CO_2$  with consequent formation of  $CaCO_3$ . The process is exothermic and involves the generation of a high quantity of energy, ensuring the heating of the gas flow to be sent to the power cycle and to be expanded in the gas turbine.

As shown in the figure, the flow of  $CO_2$ , 12143 kmol/hr at 711 °C, coming out of the HE-CARB heat exchanger (CO2CARB2) enters the carbonator together with the flow of  $CaO$ , at 683 °C and 1324 kmol/hr.

Of the initial amount of  $CO_2$  introduced in the block, 661 kmol/hr are subjected to the reaction of carbonation, stoichiometric amount equal to that produced by the calciner. The remaining 11481 kmol/hr receive the thermal energy developed by the reaction and

achieve ideal thermodynamic conditions in order to evolve in a turbine and produce useful power. The  $CO_2$  flow then reduces its pressure to 1 bar and its temperature to 698 °C, and is then sent into the HE-CARB network and performs the subsequent heat exchange processes. The solids stream (SOLIDSX1) produced also registers a considerably high temperature (850 °C). In view of the configuration with low-temperature storage systems, cooling via heat exchange processes in the HE-CARB network is insufficient. It is therefore necessary to have an additional intercooler (HE-SOLI) that allows an ambient temperature (20 °C) to be reached and permits storage according to design.

### 3.2.3. Main differences and considerations

The two plant configurations analysed share a common operating methodology, consisting in exploiting the thermal energy generated by the carbonation reaction to provide a  $CO_2$  flow with the ideal thermodynamic qualities for power generation in a power cycle. The following table shows a comparison between the two cases through some selected comparative categories.

<i>Comparison category</i>	<i>CASE 1</i>	<i>CASE 2</i>	<i>Unit</i>
<i>Thermal power for calcination</i>	<i>100</i>	<i>100</i>	<i>MW<sub>th</sub></i>
<i>Power production: main CO2 turbine (TURB)</i>	<i>27,19</i>	<i>26,46</i>	<i>MW<sub>el</sub></i>
<i>Power production: secondary CO2 turbine (T2)</i>	<i>0,76</i>	<i>1,05</i>	<i>MW<sub>el</sub></i>
<i>Power production: steam turbine (T1-CALC)</i>	<i>3,03</i>	<i>/</i>	<i>MW<sub>el</sub></i>
<i>Power consumption: storage CO2 compressor (COMP)</i>	<i>3,95</i>	<i>7,27</i>	<i>MW<sub>el</sub></i>
<i>Power consumption: power cycle CO2 compressor (C2)</i>	<i>12,75</i>	<i>10,83</i>	<i>MW<sub>el</sub></i>
<i>Power consumption: secondary power cycle CO2 compressor (C2BIS)</i>	<i>0,51</i>	<i>/</i>	<i>MW<sub>el</sub></i>
<i>Gross Power Production</i>	<i>29,69</i>	<i>27,51</i>	<i>MW<sub>el</sub></i>
<i>Net Power Production</i>	<i>15,47</i>	<i>14,01</i>	<i>MW<sub>el</sub></i>
<i>Daytime operation hours</i>	<i>8</i>	<i>8</i>	<i>hours</i>
<i>Night-time operation hours</i>	<i>16</i>	<i>16</i>	<i>hours</i>
<i>Solids storage output temperature</i>	<i>660</i>	<i>35</i>	<i>°C</i>
<i>Solids storage duration</i>	<i>Limited</i>	<i>Unlimited</i>	<i>/</i>

*Table 5 - Comparison between CASE 1 and CASE 2*

According to the reported data, it emerges that both configurations produce a comparable amount of net power, in relation to the thermal power of  $100 \text{ MW}_{th}$  received from incident solar radiation. The product difference,  $15,47 \text{ MW}_{el}$  in CASE 1 compared to  $14,01 \text{ MW}_{el}$  in CASE 2 is most likely due to the absence of the additional steam turbine power cycle in the HE-CALC block in the second configuration. The reduced thermal availability due to low temperature storage systems, in fact, does not allow the integration of the steam generator.

The calculation of the gross and net power generated was carried out considering the differentiation between components in daytime operation only and components in night-time operation, according to the following relation.

$$P_{gross} = P_{24hr} + P_{day} \cdot \frac{8 \text{ hr}}{24 \text{ hr}} + P_{night} \cdot \frac{16 \text{ hr}}{24 \text{ hr}} \quad (3.1)$$

The net power is obtained by subtracting from the gross power the consumption associated with the compressors in operation. The power consumed by them is calculated in the same way as indicated in (3.1).

Among the most important differences, it is advisable to highlight the different storage time duration for each configuration. One of the main advantages of operating with solids containers at ambient temperature is the fact that, hypothetically, the plant structure allows storage for an almost unlimited period of time, since it would not have to handle particularly significant thermal losses. This also explains why the flow rates in CASE 2 are considerably lower than in CASE 1. As the system does not require a quick replacement in the storage tanks, it can operate with lower flow rates. Undoubtedly, the  $CO_2$  flow in the power cycle remains the same in both cases, in order to guarantee a comparable power output. It should be remembered, however, that the solution presented in CASE 2 also has obvious disadvantages, such as a lower power output due to the impossibility of integrating accessory power cycles and the increased plant complexity due to the additional heat exchange processes necessary to achieve the ideal thermodynamic conditions..

A possible improvement to increase the energy efficiency of the plant in both configurations could be achieved through the inclusion of a renovation process of the  $CaCO_3$  used in the cycle. Its continuous usage and repeated dissociation and recombination reactions lead to a progressive degradation of its properties. Specifically,  $CaO$ , sorbent in the carbonation reaction, reduces its ability to react with  $CO_2$ , leading to the subsequent accumulation of ash, impurities and  $CaSO_4^-$ . Therefore, it may be convenient to gradually replace the material in order to maintain constant the functionality of the process.

### 3.3. CSP-CaL integration on small scale: Beam-down

The technology of the Calcium Looping process is extremely versatile and flexible, and is characterized by a wide range of applications. Within the thermochemical energy storage system, it is interesting to evaluate the possibility of using it on a smaller scale. The previous configurations analyzed, in fact, refer to large solar tower systems. Calcium Looping, however, has the fundamental advantage of being able to correctly perform the calcination and carbonation cycles even in proportionally reduced conditions. Hence, the possibility of building smaller plants, with thermal power sent to the calciner significantly lower than the  $100\text{ MW}_{th}$  previously considered. The importance of this consideration is radical, not only in terms of energy, but also and above all from a plant engineering point of view, opening up the possibility of using concentrating solar systems of different types equipped with various technologies.

Many solar technologies compete with the solar tower in the construction of CSP systems. Remaining within the reduced size, however, it is worthy of deepening an emerging solution in recent years, the so-called "beam-down technology", with clear potential. There is no doubt that the study of its integration with the Calcium Looping process is stimulating and highly attractive for possible future developments of the technology.

Beam down systems belong to the class of systems characterized by the presence of a central receiver and differ from tower systems mainly in the height at which the receiver is placed. In beam down systems, in fact, the solar radiation reflected by the heliostat field is directed towards a central, elliptical, hyperboloid or plane mirrors system, whose role is to operate a second reflection and concentrate the radiation on the receiver located below, close to the ground. In this way the thermodynamic processes and the movement of the heat transfer fluid take place at a height that facilitates these operations.

The beam down technology was born mainly with the aim of finding a solution to the considerable economic costs due to the construction of the tower and the design of the vertical fluid transportation system in the same power plant. However, if on the one hand they guarantee considerable savings, on the other hand they not only require a significant economic commitment in the construction of the large central mirrors system and its support structure, but they also show a worse efficiency, especially in terms of reflection properties and associated optical losses, due to the presence of an additional reflection step compared to what occurs in solar tower systems [96]. One possibility to partially mitigate the problem in question is the use of a cavity receiver. Being a closed

receiver with a reduced aperture compared to open receivers, it would guarantee a reduction in thermal losses with consequent achievement of higher temperature values that would make the cycle performance more attractive [97].

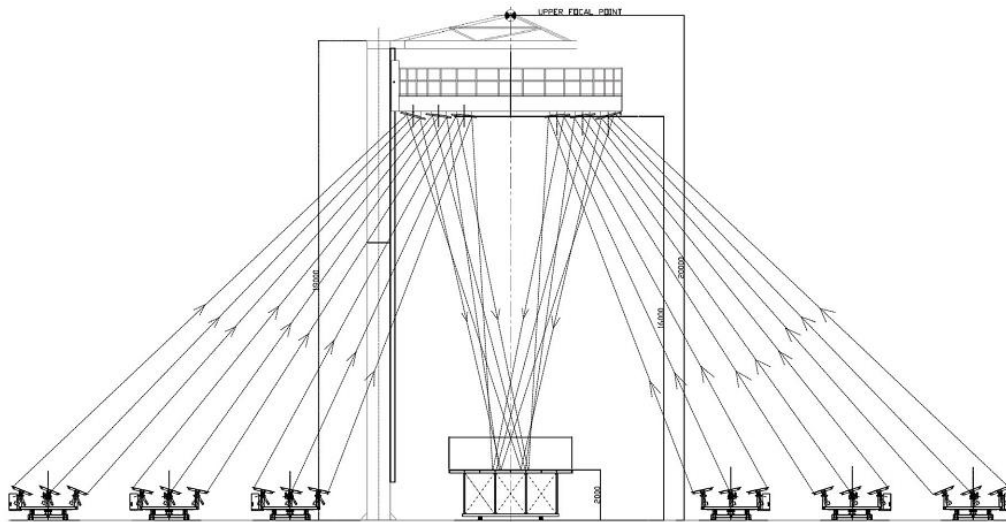


*Figure 47 - Beam-down technology operating scheme [100]*

One of the projects currently under development regarding beam down receiver technology is the Yumen Xinneng power plant. It consists of 15 mirror field modules and one beam down tower, for a total of 50 MWe. A molten salt thermal storage system and a power block with steam turbine are also integrated in the plant [98]. The company responsible for the implementation of the project, BCP Solar Technology (known as Xincheng Solar in China), is currently engaged in a study to develop second generation modules, 14 of which are expected to be sufficient to reach a total production capacity of 200 MW [98].



*Figure 48 - Yumen Xinneng CSP plant [98]*

## CHAPTER 4

### EXERGO-ECONOMIC ANALYSIS

#### 4.1. Goal and meaning of exergo-economic analysis

The exergo-economic analysis is an analytical methodology that allows to combine the exergetic study of a particular system with economic aspects, giving more completeness and universality to the results obtained.

The implementation of the process permits to obtain important information on the operation of the plant studied, evaluating its efficiency and costs, and allowing to define possible strategies for its improvement.

The method is divided into various stages of development, each of which adds significant notions, defining an effective tool for assessing the cost of inefficiencies and irreversibilities that occur in the system and the cost of individual process flows, including resources and products. In this way not only an alternative way of analysing the performance of a system emerges, but also the study of the costs formation is made in an intuitive and linear way. Starting from the energy behaviour of the system, in fact, it is possible to perceive its consequent economic impact, through a multisectorial cause effect relationship that directly connects the exergetic sector with the derived costs.

At the end of the analysis, indices such as the exergo-economic cost and the exergo-economic factor help in the perception of how each single component of the system works. In this way, it is possible to provide a preliminary study for a possible subsequent phase of plant improvement, perceiving which components are burdensome in terms of performance and which ones are burdensome in terms of cost and consequently evaluating the ways of intervention.

The following exergo-economic analysis is carried out by the computation of matrix calculations. The results are reported in the following paragraphs. The matrices and vectors involved in the calculations are fully included in the appendix.

## 4.2. Description of the systems

The exergo-economic analysis is applied below to the two Concentrated Solar Power (CSP) plant configurations with Calcium Looping integration analysed in the previous chapter. They are identified as:

- CASE 1: CSP plant with Calcium Looping, 100 MW of thermal power to the calciner and high temperature storage system;
- CASE 2: CSP plant with Calcium Looping, 100 MW of thermal power to the calciner and low temperature storage system.

### 4.2.1. CASE 1: 100 MW, high temperature storage system

Below it is represented the plant layout used in the previous chapter for the description of the configuration under analysis (*Figure 49*).

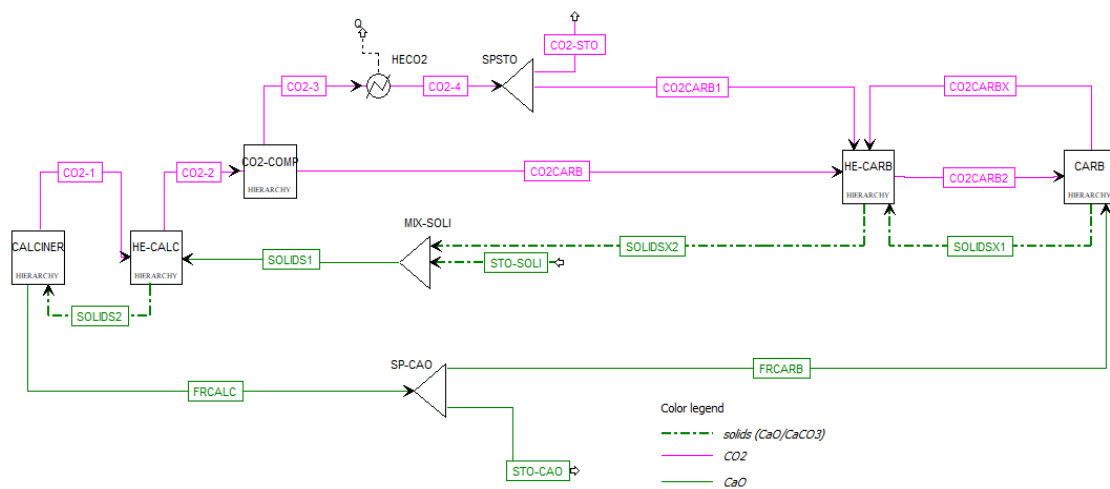


*Figure 49 - CASE 1: 100 MW, high temperature storage system*

#### 4.2.1.1. CASE 1, main assumptions

In order to streamline the otherwise complex matrix calculation, some simplifying assumptions have been made to the system. In the scheme shown in the figure (*Figure 49*), among the components included in the model there are some blocks,

respectively CALCINER, HE-CALC, CO2-COMP, HE-CARB, CARB. Each of them, as already observed in the previous chapter, contains a much more complex and articulated subsystem, especially the two blocks related to the HE-CALC and HE-CARB exchanger network. The type of method applied for the implementation of the exergo-economic analysis would require a more accurate study on each single block, making the analysis much more articulated. For this reason a simplifying hypothesis is adopted, considering the above mentioned blocks as single components. As a consequence, the mass balance is realized taking into consideration only the mass flows entering and leaving the blocks, without considering the intermediate transformations they undergo inside. As far as energy flows are concerned, each block will be assigned as many flows as the number of components inside them that operate through energy exchanges (compressors, turbines, heater, cooler). A similar hypothesis will be considered in the cost allocation phase, attributing an overall cost to the block by virtue of its individual components. The method will be discussed in more detail in the following paragraphs.

#### 4.2.1.2. CASE 1, functional and thermodynamic analysis

In the following paragraphs the various components characterizing the system are analysed individually. The process is useful to clarify the application of the above-mentioned simplifying assumptions.

- 1) Calciner (CALCINER): the "CALCINER" block is considered a single component. As noted in the previous paragraph, it comprises a reactor in which the calcination reaction takes place and a cyclone separator to differentiate the reaction products. In view of an exergo-economic analysis, the component is characterized by the following flows:

<i>Stream</i>	<i>Type</i>	<i>Direction</i>
<i>SOLIDS3</i>	<i>Mass stream</i>	<i>Input</i>
<i>FRCALC</i>	<i>Mass stream</i>	<i>Output</i>
<i>CO2-1</i>	<i>Mass stream</i>	<i>Output</i>
<i>SOLAR</i>	<i>Energy stream</i>	<i>Input</i>

*Table 6 - CASE 1, CALCINER*

It is assumed that the cyclone separator does not lead to thermal and mass losses, therefore its presence is considered negligible in the overall economy of the block;

- 2) Calciner heat exchangers systems (HE-CALC): all components necessary to ensure proper heat exchange on the calciner side are included in a block with the name HE-CALC. From the system diagram in the previous chapter it can be seen that the block includes two heat exchangers, an intercooler for CO<sub>2</sub> stream and a power cycle with steam as operating fluid, consisting of a steam turbine, a condenser and a circulation pump. The mass and energy flows that will be used to characterize the block in the exergo-economic analysis are the following:

<i>Stream</i>	<i>Type</i>	<i>Direction</i>
<i>CO2-1</i>	<i>Mass stream</i>	<i>Input</i>
<i>CO2-2</i>	<i>Mass stream</i>	<i>Output</i>
<i>SOLIDS2</i>	<i>Mass stream</i>	<i>Input</i>
<i>SOLIDS3</i>	<i>Mass stream</i>	<i>Output</i>
<i>ST (Steam turbine)</i>	<i>Energy stream</i>	<i>Output</i>

*Table 7 - CASE 1, HE-CALC*

In accordance with the simplification hypothesis mentioned above, the analysis of the heat exchanger system on the calciner side is carried out by considering the block as a single component and applying the mass and energy balance through the listed flows. In particular, the heat flux removed through the CO<sub>2</sub> intercooler falls within the category of “Losses” and, therefore, is not considered in the analysis. A similar argument for the condenser in the steam power cycle. Finally, the circulation pump is assumed to have negligible consumption compared to the other components, making it unnecessary to define an appropriate energy flow;

- 3) CO<sub>2</sub> compression system (CO2-COMP): the compression system of CO<sub>2</sub> consists of a multi-stage compressor that allows to obtain the pressure level required for the storage of the substance, a splitter and a mixer. Also in this case, the system is simplified by considering the whole block as a single component. The mass and energy flows to be used in the exergo-economic analysis are listed below:

<i>Stream</i>	<i>Type</i>	<i>Direction</i>
<i>CO2-2</i>	<i>Mass stream</i>	<i>Input</i>
<i>CO2-3</i>	<i>Mass stream</i>	<i>Output</i>
<i>CO2CARB</i>	<i>Mass stream</i>	<i>Output</i>
<i>COMP-1 (Compressor)</i>	<i>Energy stream</i>	<i>Input</i>

*Table 8 - CASE 1, CO2-COMP*

The unique energy flow included in the analysis identifies the electrical energy required to operate the compressor. Splitters and mixers are assumed to be leak-free, therefore their operation does not lead to significant changes in the results of the analysis;

- 4) CO<sub>2</sub> intercooler (HE-CO<sub>2</sub>): before entering the CO<sub>2</sub> flow into the storage system, it is necessary to cool it down. The dedicated component is an intercooler whose operating fluid is assumed to be water. The flows used in the exergo-economic analysis are described below:

<i>Stream</i>	<i>Type</i>	<i>Direction</i>
<i>CO2-3</i>	<i>Mass stream</i>	<i>Input</i>
<i>CO2-4</i>	<i>Mass stream</i>	<i>Output</i>
<i>COOL-CO2</i>	<i>Energy stream</i>	<i>Output</i>

*Table 9 – CASE 1, HE-CO2*

The "COOL-CO<sub>2</sub>" flow identifies the amount of heat removed by the intercooler. In the remainder of the analysis, it will be considered to belong to the "Losses" category.

- 5) Carbonator heat exchangers system (HE-CARB): the heat exchanger network block on the carbonator side is probably the most complex from a plant engineering point of view. It comprises three different heat exchangers that provide heat exchange between CO<sub>2</sub> and CaCO<sub>3</sub>. There are also compressors, both for CO<sub>2</sub> related to the power cycle and for CO<sub>2</sub> coming directly from the calciner. The CO<sub>2</sub> coming out of the storage is instead treated by a heater followed by a small capacity turbine. A cooler for the flow of CO<sub>2</sub> in the power cycle completes the system picture. The list of flows to be used in the exergo-economic analysis is given in the following table:

<i>Stream</i>	<i>Type</i>	<i>Direction</i>
<i>CO2CARB</i>	<i>Mass stream</i>	<i>Input</i>
<i>CO2CARB1</i>	<i>Mass stream</i>	<i>Input</i>
<i>CO2CARB2</i>	<i>Mass stream</i>	<i>Output</i>
<i>CO2CARBX</i>	<i>Mass stream</i>	<i>Input</i>
<i>SOLIDSX1</i>	<i>Mass stream</i>	<i>Input</i>
<i>SOLIDSX2</i>	<i>Mass stream</i>	<i>Output</i>
<i>T2 (Turbine)</i>	<i>Energy stream</i>	<i>Output</i>
<i>COMP-2 (Power cycle comp)</i>	<i>Energy stream</i>	<i>Input</i>
<i>COMP-2bis (CO2 calc comp)</i>	<i>Energy stream</i>	<i>Input</i>
<i>HEAT (Heater)</i>	<i>Energy stream</i>	<i>Input</i>

*Table 10 - CASE 1, HE-CARB*

Again, the intention is to treat the block as a single component. Specifically, the situation is more complex due to the dynamic nature of the configuration studied. It analyses, in fact, a system whose operation varies depending on whether or not there is availability of solar radiation. Some of the components present in the exchanger system in question, therefore, operate during the day and others during the night. It is hence necessary to divide the study of the system into two distinct periods. The difference will be discussed in more detail in the following paragraphs.

With regard to the components indicated in the table (*Table 10*), COMP2 operates in the power cycle while COMP2bis operates on the CO<sub>2</sub> flow from the Calciner. It is not considered a thermal flow for the intercooler because, as usual, it is assumed to belong to the "Losses" category. Finally, the various splitters and mixers are not treated because it is assumed that there are no losses in the processes that characterize them, making them little influential for analytical purposes;

- 6) Carbonator (CARB): the block named "CARB" contains the reactor that performs the functions of carbonator, making possible the reverse reaction of recombination of CO<sub>2</sub> and CaO in CaCO<sub>3</sub>. In addition to the reactor, the block also contains the power cycle which, through a gas turbine, is the main production source of the plant. A cyclone separator completes the list of components. Also in this case the simplifying hypothesis is adopted considering the block as a single component. The following table shows the flows used in the exergo-economic analysis:

<i>Stream</i>	<i>Type</i>	<i>Direction</i>
<i>CO2CARB2</i>	<i>Mass stream</i>	<i>Input</i>
<i>CO2CARBX</i>	<i>Mass stream</i>	<i>Output</i>
<i>SOLIDSX1</i>	<i>Mass stream</i>	<i>Output</i>
<i>FRCARB</i>	<i>Mass stream</i>	<i>Input</i>
<i>GT (Gas turbine)</i>	<i>Energy stream</i>	<i>Output</i>

*Table 11 - CASE 1, CARB*

The block is simplified by summarizing in the power generated by the turbine the main operations that occur inside it. The cyclone separator, as already happened in the calciner, is not considered in the analysis because of its negligible presence compared to the other components;

- 7) Solids mixer (MIX-SOLI): the solids mixer is the component that takes care of the remixing of the  $\text{CaCO}_3$  obtained in the calciner with the one taken from the storage system. The flows used in the exergo-economic analysis are the following:

<i>Stream</i>	<i>Type</i>	<i>Direction</i>
<i>SOLIDSX2</i>	<i>Mass stream</i>	<i>Input</i>
<i>STO-SOLI</i>	<i>Mass stream</i>	<i>Input</i>
<i>SOLIDS1</i>	<i>Mass stream</i>	<i>Output</i>

*Table 12 - CASE 1, MIX-SOLI*

The mixing process is assumed to be leak-free. Consequently, energy flows are not considered in the analysis. Predictably, the "MIX-SOLI" component will not contribute significantly in comparison to the others under examination.

- 8) CaO Splitter (SP-CAO): the splitter takes care of the division between the quantity of CaO to be sent to the storage and the quantity to be used in the carbonator for the chemical reaction. The following table shows the flows involved in the component:

<i>Stream</i>	<i>Type</i>	<i>Direction</i>
<i>FRCALC</i>	<i>Mass stream</i>	<i>Input</i>
<i>STO-CAO</i>	<i>Mass stream</i>	<i>Output</i>
<i>FRCARB</i>	<i>Mass stream</i>	<i>Output</i>

*Table 13 - CASE 1, SP-CAO*

As already indicated in the mixer, the total absence of losses is also assumed for the splitter, with a consequent negligible influence on the overall results of the system.

#### 4.2.1.3. Differences between day and night configuration

The plant configuration analysed describes a CSP plant integrated with a thermochemical storage system with Calcium Looping process. By virtue of the system's dependence on incident solar radiation, it is easy to see how its operation varies between day and night. The simulation model implemented with AspenPlus provides a static picture of the plant and does not allow the dynamics of the process to be perceived. Therefore, it is convenient to divide the analysis by differentiating the behaviour of the plant during the day from that which occurs at night. The following considerations are derived from this.

During daylight hours, in the presence of solar radiation, the system carries out the calcination reaction in the calciner, dissociating  $\text{CaCO}_3$  into  $\text{CO}_2$  and  $\text{CaO}$ . The main consideration should be made on the "SPSTO" component. It is a splitter with the aim of differentiating between  $\text{CO}_2$  flow to be destined to the storage system and the quantity to be sent to the carbonator. During the daytime hours, in fact, the flow of  $\text{CO}_2$  sent to the carbonator is "CO2CARB", coming directly from the compression system after the calciner. The SPSTO splitter is, during this period, deactivated and conveys the total amount of incoming  $\text{CO}_2$  entirely to the storage. The flow of  $\text{CO}_2$  entering the carbonator's heat exchanger system, HE-CARB, undergoes a compression process before being mixed with the  $\text{CO}_2$  from the power cycle and passing through the various heat exchange stages. In this phase, therefore, heater and low capacity turbine, components of the HE-CARB, are deactivated.

In night operation, vice versa, the only fully operational components are the carbonator and its network of heat exchangers. The calciner is deactivated and can no longer produce  $\text{CO}_2$ . As a result, the "CO2CARB" flow is in this situation zero.  $\text{CO}_2$  is supplied to the carbonator entirely from the storage system, reactivating the previously

ignored “CO2CARB1” flow. Similarly, the situation also changes in the HE-CARB exchanger system. The compressor, operating during the daytime on the CO<sub>2</sub> flow from the calciner, is no longer used. Instead, the heater and the turbine are active, which exploits the high pressure of the gas coming out of the storage.

#### 4.2.2. CASE 2: 100 MW, low temperature storage system

The second configuration used for the exergo-economic analysis is described, from an engineering point of view, in the following figure (*Figure 50*), as already observed in the previous chapter.

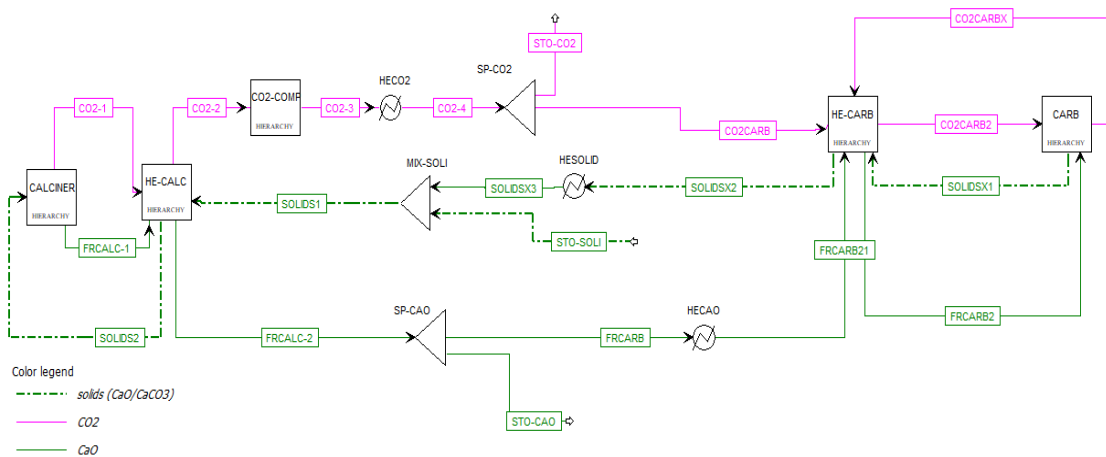


Figure 50 - CASE 2: 100 MW, low temperature storage system

##### 4.2.2.1. CASE 2, main assumptions

In order to streamline the otherwise rather articulated matrix calculation, also in this configuration, simplifying hypotheses will be adopted with a view to greater plant clarity and a differentiation of the results in order of relevance. In particular, as emerged in CASE 1, CASE 2 also denotes a scheme consisting of components and blocks. Specifically, the CALCINER, HE-CALC, CO<sub>2</sub>-COMP, HE-CARB, CARB blocks actually contain much more complex articulations which, if considered as a whole, would require a specific analysis. For the purposes of exergo-economic analysis, it is reasonable to assume that each block is a single component, using the relative input and output mass flows for the application of the mass balance, neglecting the processes that they undergo internally to the block. With regard to energy flows, they will be evaluated

taking into account each energy exchange between block and environment, both input and output. Components whose operation does not lead to significant results compared to other parts of the system will be considered negligible. Finally, the assumptions applied in this section will also be included in the cost allocation process, which is analysed in greater detail in the following paragraphs.

#### 4.2.2.2. CASE 2, functional and thermodynamic analysis

The characterization of the system is made through a study on individual blocks and components, with the aim of clarifying the application of the simplifying hypotheses and laying the foundations for the subsequent exergo-economic analysis.

- 1) Calciner (CALCINER): the "CALCINER" block is considered a single component. The block is very similar to the one analyzed in the previous case. It therefore includes a reactor in which the calcination reaction takes place and a cyclone separator to differentiate the reaction products. The mass and energy flows useful for the balance are summarised below.

<i>Stream</i>	<i>Type</i>	<i>Direction</i>
<i>SOLIDS2</i>	<i>Mass stream</i>	<i>Input</i>
<i>FRCALC-1</i>	<i>Mass stream</i>	<i>Output</i>
<i>CO2-1</i>	<i>Mass stream</i>	<i>Output</i>
<i>SOLAR</i>	<i>Energy stream</i>	<i>Input</i>

*Table 14 - CASE 2, Calciner*

The cyclone separator is an irrelevant component in terms of exergo-economic analysis when compared to the rest of the block. For this reason, in accordance with the previous paragraph, it can be overlooked.

- 2) Calciner heat exchangers systems (HE-CALC): the block includes all the components involved in the heat exchange process following the calcination reaction. Unlike CASE 1, there is no steam turbine power cycle in this situation. The flows required for the balance are, therefore, only mass flows and are listed below:

<i>Stream</i>	<i>Type</i>	<i>Direction</i>
<i>CO2-1</i>	<i>Mass stream</i>	<i>Input</i>
<i>CO2-2</i>	<i>Mass stream</i>	<i>Output</i>
<i>SOLIDS1</i>	<i>Mass stream</i>	<i>Input</i>
<i>SOLIDS2</i>	<i>Mass stream</i>	<i>Output</i>
<i>FRCALC-1</i>	<i>Mass stream</i>	<i>Input</i>
<i>FRCALC-2</i>	<i>Mass stream</i>	<i>Output</i>

*Table 15 - CASE 2, HE-CALC*

As specified in the paragraph on simplifying assumptions, the block of the heat exchanger system on the calciner side is assumed to be a single component.

- 3) CO<sub>2</sub> compression system (CO<sub>2</sub>-COMP): the block in question includes a compressor that ensures that a suitable pressure level is reached for subsequent storage. The following table (*Table 16*) lists the mass and energy flows used in the exergo-economic analysis:

<i>Stream</i>	<i>Type</i>	<i>Direction</i>
<i>CO2-2</i>	<i>Mass stream</i>	<i>Input</i>
<i>CO2-3</i>	<i>Mass stream</i>	<i>Output</i>
<i>COMP-1 (Compressor)</i>	<i>Energy stream</i>	<i>Input</i>

*Table 16 - CASE 2, CO2-COMP*

The energy flow included in the list identifies the electrical energy required to operate the compressor;

- 4) CO<sub>2</sub> intercooler (HE-CO<sub>2</sub>): Before entering the CO<sub>2</sub> flow into the storage system, a temperature reduction is carried out by means of a water intercooler. The mass and energy flows necessary for the exergo-economic analysis are shown below:

<i>Stream</i>	<i>Type</i>	<i>Direction</i>
<i>CO2-3</i>	<i>Mass stream</i>	<i>Input</i>
<i>CO2-4</i>	<i>Mass stream</i>	<i>Output</i>
<i>COOL-CO2</i>	<i>Energy stream</i>	<i>Output</i>

*Table 17 – CASE 2, HE-CO2*

The COOL-CO<sub>2</sub> energy flow represents the amount of heat subtracted from the CO<sub>2</sub> by the intercooler. Afterwards, this energy flow will be treated as one of the "Losses" of the system.

- 5) CO<sub>2</sub> splitter (SP-CO<sub>2</sub>): it is the component in charge of differentiating the quantity of CO<sub>2</sub> to be sent to the storage from that to be sent to the carbonator. Below are the flows used in the exergo-economic analysis:

<i>Stream</i>	<i>Type</i>	<i>Direction</i>
<i>CO2-4</i>	<i>Mass stream</i>	<i>Input</i>
<i>CO2-STO</i>	<i>Mass stream</i>	<i>Output</i>
<i>COOL-CARB1</i>	<i>Mass stream</i>	<i>Output</i>

*Table 18 - CASE 2, SP-CO<sub>2</sub>*

In this configuration it is chosen to include the splitter in the analysis because the system mode used does not imply a clear differentiation between daytime and night-time operation as in the previous case.

- 6) Carbonator heat exchangers system (HE-CARB): Again, the block of the heat exchanger system on the carbonator side is probably the most complex section of the plant. It comprises four heat exchangers, which ensure heat exchange between CO<sub>2</sub>, CaCO<sub>3</sub> and CaO. The flows involved in the exergo-economic analysis are listed in the table below:

<i>Stream</i>	<i>Type</i>	<i>Direction</i>
<i>CO2CARB</i>	<i>Mass stream</i>	<i>Input</i>
<i>CO2CARB1</i>	<i>Mass stream</i>	<i>Output</i>
<i>CO2CARBX</i>	<i>Mass stream</i>	<i>Input</i>
<i>SOLIDSX1</i>	<i>Mass stream</i>	<i>Input</i>
<i>SOLIDSX2</i>	<i>Mass stream</i>	<i>Output</i>
<i>FRCARB21</i>	<i>Mass stream</i>	<i>Input</i>
<i>FRCARB2</i>	<i>Mass stream</i>	<i>Output</i>
<i>T2 (Turbine)</i>	<i>Energy stream</i>	<i>Output</i>
<i>COMP-2 (Power cycle comp)</i>	<i>Energy stream</i>	<i>Input</i>
<i>HEAT (Heater)</i>	<i>Energy stream</i>	<i>Input</i>

*Table 19 - CASE 2, HE-CARB*

Also in this case, the simplifying hypothesis is adopted by summarizing it in the form of a single component. The energy flows considered refer to the various components that make up the system, including a CO<sub>2</sub> compressor for the power cycle, a heater and a turbine useful to exploit the high pressure of CO<sub>2</sub> from the calciner. As usual, intercoolers are not included in the overall analysis of the block as the amount of heat subtracted is included in the "Losses" category. Similarly, splitters and mixers are neglected as they do not have a significant effect on the overall system balance. Finally, compared to CASE 1, there are no significant differences in the operation of the block between daytime and night-time operation.

- 7) Carbonator (CARB): the block named "CARB" contains the reactor that performs the functions of carbonator, making possible the reverse reaction of recombination of CO<sub>2</sub> and CaO in CaCO<sub>3</sub>. In addition to the reactor, the block also contains the power cycle which, through a gas turbine, is the main production source of the plant. A cyclone separator completes the list of components. Also in this case the simplifying hypothesis is adopted considering the block as a single component. The following table shows the flows used in the exergo-economic analysis:

<i>Stream</i>	<i>Type</i>	<i>Direction</i>
<i>CO2CARB2</i>	<i>Mass stream</i>	<i>Input</i>
<i>CO2CARBX</i>	<i>Mass stream</i>	<i>Output</i>
<i>SOLIDSX1</i>	<i>Mass stream</i>	<i>Output</i>
<i>FRCARB</i>	<i>Mass stream</i>	<i>Input</i>
<i>GT (Gas turbine)</i>	<i>Energy stream</i>	<i>Output</i>

*Table 20 - CASE 2, CARB*

The block is simplified by summarizing in the power generated by the turbine the main operations that occur inside it. The cyclone separator, as already happened in the calciner, is not considered in the analysis because of its negligible presence compared to the other components;

- 8) Solids intercooler (HE-SOLI): the outgoing solids stream from the network of exchangers on the carbonator side has too high a temperature to be used for the storage system. For this reason an intercooler is included to subtract heat from it. The flows involved are listed below:

<i>Stream</i>	<i>Type</i>	<i>Direction</i>
<i>SOLIDSX2</i>	<i>Mass stream</i>	<i>Input</i>
<i>SOLIDSX3</i>	<i>Mass stream</i>	<i>Output</i>
<i>COOL-SOLI</i>	<i>Energy stream</i>	<i>Output</i>

*Table 21 - CASE 2, HE-SOLI*

"COOL-SOLI" identifies the amount of heat removed from the solids flow. It is included in the category "Losses".

- 9) Solids mixer (MIX-SOLI): the solids mixer is a useful component to mix the flow of solids coming out of the heat exchanger system on the carbonator side with those coming from the storage. The table shows the flows involved in the component:

<i>Stream</i>	<i>Type</i>	<i>Direction</i>
<i>SOLIDSX3</i>	<i>Mass stream</i>	<i>Input</i>
<i>STO-SOLI</i>	<i>Mass stream</i>	<i>Input</i>
<i>SOLIDS1</i>	<i>Mass stream</i>	<i>Output</i>

*Table 22 - CASE 2, MIX-SOLI*

The mixing process is assumed to be leak-free. Consequently, energy flows are not considered in the analysis. Predictably, the "MIX-SOLI" component will not contribute significantly in comparison to the others under examination.

- 10) CaO Splitter (SP-CAO): the splitter takes care of the division between the quantity of CaO to be sent to the storage and the quantity to be used in the carbonator for the chemical reaction. The following table shows the flows involved in the component:

<i>Stream</i>	<i>Type</i>	<i>Direction</i>
<i>FRCALC-2</i>	<i>Mass stream</i>	<i>Input</i>
<i>STO-CAO</i>	<i>Mass stream</i>	<i>Output</i>
<i>FRCARB</i>	<i>Mass stream</i>	<i>Output</i>

*Table 23 - CASE 2, SP-CAO*

As already indicated in the mixer, the total absence of losses is also assumed for the splitter.

- 11) CaO intercooler (HE-CAO): in order to optimize the heat exchange processes performed in HE-CARB, an intercooling via intercooler is also required for the CaO flow. The mass and energy flows are listed below:

<i>Stream</i>	<i>Type</i>	<i>Direction</i>
<i>FRCARB</i>	<i>Mass stream</i>	<i>Input</i>
<i>FRCARB21</i>	<i>Mass stream</i>	<i>Output</i>
<i>COOL-CAO</i>	<i>Energy stream</i>	<i>Output</i>

*Table 24 - CASE 2, HE-CAO*

The COOL-CAO flow represents the heat removed from solids. It is considered one of the "Losses" of the system.

#### 4.2.2.3. Differences between day and night configuration

Also in this second case it is convenient to differentiate between daytime and night-time performances. Since the system operates by exploiting the thermal power of the incident solar radiation, some components will be disabled in the absence of radiation. However, if in the configuration with high temperature storage system this difference is particularly marked, the same cannot be said of this second case.

If, in fact, in CASE 1 the CO<sub>2</sub> directed to the heat exchanger system on the carbonator side is indicated with two distinct flows according to the operating period, thus defining two different treatment modes inside the HE-CARB block, in this second case the main difference between daytime and night-time configuration occurs only in the CO<sub>2</sub> splitter. In case of presence of solar radiation, in fact, the flow is differentiated between storage system and carbonator. In case of absence, instead, the CO<sub>2</sub> univocally crosses the path from the storage system to the carbonator.

For a more precise plant analysis, however, the two separate cases will be considered. In night mode, the components in operation are HE-CARB, CARB, HE-SOLI and HE-CAO. The calciner side and all related components are therefore deactivated. For simplicity's sake, splitters and mixers are also considered deactivated, because they do not operate an effective splitting or mixing but simply connect the plant side of the carbonator with the various storage systems.

### 4.3. Irreversibility calculation

The following paragraph reports some intermediate results obtained in the exergo-economic analysis process, which are particularly useful for a better understanding of the operating methodologies of the analysed system.

Specifically, now the evaluation of the irreversibility rate characterizing each of the components listed above is performed, in each of the two configurations. By exploiting the matrix calculation, it is therefore possible to obtain information of significant importance regarding the cataloguing of the various plant components on the basis of their operational performance. The irreversibility value suggests, in fact, the correctness and efficiency with which a specific part of the system is working. It is, therefore, an initial indication through which to intuit the most effective methods to intervene on the system and improve its performance. Being intermediate results, their usefulness is subsequently completed by the integration with what will be added in the continuation of the exergo-economic analysis.

#### 4.3.1. Operational concepts

The method of calculating the irreversibilities of the various components is based on matrix operations according to the formula:

$$A \times E = I \quad (4.1)$$

Where, specifically, "*A*" refers to the so-called incidence matrix. It is a matrix of dimensions  $n \times m$ . The number  $n$  of lines corresponds to the number of system components. Columns  $m$ , on the other hand, show all flows, in mass and energy, involved in the analysis. In the two cases analysed, flows and components have been listed in the previous paragraph. The matrix is filled with "1" when a flow is entering the corresponding component, "-1" when it is leaving, "0" if there is no relation between the two. For both configurations, the relevant incidence matrices are fully reported in the appendix.

The vector "*E*", instead, of dimensions  $n \times 1$ , is the vector of the exergies. It contains the exergies of each flow. Specifically, the values are calculated taking into account the physical and chemical exergies, according to the following relation:

$$E_i = G \cdot (b_{ph,i} + e_{ch,i}) \quad (4.2)$$

In particular,  $b_{ph,i}$  indicates the physical exergy of the  $i$ -th flow, and  $e_{ch,i}$  indicates the chemical exergy of the  $i$ -th flow. The first is calculated according to the definition below:

$$b_{ph,i} = (h_i - h_{0,i}) - T_0 \cdot (s_i - s_{0,i}) \quad (4.3)$$

Where  $h_{0,i}$  and  $s_{0,i}$  are the enthalpy and entropy values under the reference conditions, while  $T_0$  represents the reference temperature. The chemical exergy of a mixture, on the other hand, is expressed by the following formula:

$$e_{ch,i} = \sum_i^n y_{0,i} \cdot e_{ch,n,i} + R \cdot T_0 \cdot \sum_i^n y_{0,i} \cdot \ln y_{0,i} \quad (4.4)$$

Specifically,  $y_{0,i}$  indicates the molar fraction of each species making up the mixture, while  $e_{ch,n,i}$  is the corresponding standard chemical exergy.

Applying the above reported relations, the exergy values are then obtained for each system flow. The enthalpy, entropy and flow rate data of the various flows are obtained from the AspenPlus simulation. The values of reference enthalpy and entropy and standard chemical exergy are instead obtained from the literature [101][102][103].

The tables below include the results relating to the calculation of the exergies of the different system flows for the two cases analysed. It should be pointed out that, since the chemical exergy values are already given in Watts, the (4.2) is actually applied in the following form:

$$E = G \cdot b_{ph,i} + e_{ch,i} \quad (4.5)$$

	<i>STREAM</i>	$b_{ph,i}$ [J/kg]	$e_{ch,i}$ [W]	$E$ [W]
1	<i>CO2-1</i>	1,97E+06	7,42E+06	4,04E+07
2	<i>CO2-2</i>	1,43E+06	7,42E+06	3,13E+07
3	<i>CO2-3</i>	1,67E+06	4,95E+06	2,35E+07
4	<i>CO2-4</i>	1,65E+06	4,95E+06	2,33E+07
5	<i>CO2-STO</i>	1,65E+06	2,47E+06	1,17E+07
6	<i>CO2CARB</i>	1,43E+06	2,47E+06	1,04E+07
7	<i>CO2CARB1</i>	1,65E+06	2,47E+06	1,17E+07
8	<i>CO2CARB2</i>	1,87E+06	6,47E+07	3,38E+08
9	<i>CO2CARBX</i>	1,78E+06	6,22E+07	3,13E+08
10	<i>SOLIDS1</i>	1,11E+06	2,78E+08	4,56E+08
11	<i>SOLIDS2</i>	1,11E+06	2,78E+08	4,56E+08
12	<i>SOLIDS3</i>	1,13E+06	2,78E+08	4,58E+08
13	<i>FRCALC</i>	1,19E+06	3,23E+08	4,93E+08
14	<i>STO-CAO</i>	1,19E+06	2,16E+08	3,29E+08
15	<i>FRCARB</i>	1,19E+06	1,08E+08	1,64E+08
16	<i>SOLIDSX1</i>	1,25E+06	9,28E+07	1,59E+08
17	<i>SOLIDSX2</i>	1,11E+06	9,28E+07	1,52E+08
18	<i>STO-SOLI</i>	1,11E+06	1,86E+08	3,04E+08
19	<i>SOLAR</i>	/	/	1,00E+08
20	<i>GT</i>	/	/	2,66E+07
21	<i>ST</i>	/	/	3,03E+06
22	<i>COMP-1</i>	/	/	4,00E+06
23	<i>COOL-CO2</i>	/	/	0,00E+00
24	<i>T2</i>	/	/	7,64E+05
25	<i>COMP-2BIS</i>	/	/	5,11E+05
26	<i>COMP-2</i>	/	/	1,27E+07
27	<i>HEAT</i>	/	/	1,57E+06

Table 25 - CASE 1, Exergy values

	<i>STREAM</i>	$b_{ph,i}$ [J/kg]	$e_{ch,i}$ [W]	$E$ [W]
1	<i>CO2-1</i>	1,97E+06	1,07E+07	5,86E+07
2	<i>CO2-2</i>	1,43E+06	1,07E+07	4,54E+07
3	<i>CO2-3</i>	1,65E+06	1,07E+07	5,07E+07
4	<i>CO2-4</i>	1,64E+06	1,07E+07	5,06E+07
5	<i>CO2-STO</i>	1,64E+06	7,16E+06	3,37E+07
6	<i>CO2CARB</i>	1,64E+06	3,58E+06	1,69E+07
7	<i>CO2CARB2</i>	1,86E+06	6,57E+07	3,42E+08
8	<i>CO2CARBX</i>	1,79E+06	6,21E+07	3,13E+08
9	<i>SOLIDS1</i>	8,52E+05	7,73E+07	1,51E+08
10	<i>SOLIDS2</i>	1,30E+06	7,73E+07	1,89E+08
11	<i>FRCALC-1</i>	1,18E+06	1,40E+08	2,13E+08
12	<i>FRCALC-2</i>	7,42E+05	1,40E+08	1,86E+08
13	<i>FRCARB</i>	7,42E+05	4,68E+07	6,21E+07
14	<i>FRCARB2</i>	1,03E+06	4,68E+07	6,80E+07
15	<i>FRCARB21</i>	7,41E+05	4,68E+07	6,21E+07
16	<i>STO-CAO</i>	7,42E+05	9,36E+07	1,24E+08
17	<i>SOLIDSX1</i>	1,31E+06	2,59E+07	6,34E+07
18	<i>SOLIDSX2</i>	8,53E+05	2,58E+07	5,03E+07
19	<i>SOLIDSX3</i>	8,53E+05	2,58E+07	5,03E+07
20	<i>STO-SOLI</i>	8,52E+05	5,15E+07	1,00E+08
21	<i>SOLAR</i>	/	/	1,00E+08
22	<i>COMP-1</i>	/	/	7,00E+06
23	<i>COOL-CO2</i>	/	/	0,00E+00
24	<i>HEAT</i>	/	/	2,00E+06
25	<i>T2</i>	/	/	1,00E+06
26	<i>COMP-2</i>	/	/	1,10E+07
27	<i>GT</i>	/	/	2,60E+07
28	<i>COOL-SOLI</i>	/	/	0,00E+00
29	<i>COOL-CAO</i>	/	/	0,00E+00

Table 26 - CASE 2, Exergy values

It should be noted that the exergy of energy flows depends on their type. Consequently, the solar radiation, indicated as "SOLAR" has an exergy exactly equal to its power (100  $MW_{th}$  in the cases analysed). For components requiring electricity consumption (heater and compressors), the exergy of the associated energy flow is assumed to be equal to the power required. The output flows from turbines have exergy corresponding to the power produced. Finally, the flows indicating the heat subtracted from the intercoolers have no exergy as they are considered "Losses".

#### 4.3.2. Irreversibility of CASE 1

The irreversibility values identified for the first case are given below, considering both day and night operation. For a better understanding of the distribution of irreversibilities in the system, the analysis is completed with a pie chart.

The following table lists the results of daytime mode operation:

<i>Components</i>	<i>Irreversibility [W]</i>	<i>Irreversibility [%]</i>
<b><i>CALCINER</i></b>	<i>2,47E+07</i>	<i>62,83</i>
<b><i>HE-CALC</i></b>	<i>3,48E+06</i>	<i>8,85</i>
<b><i>CO2-COMP</i></b>	<i>1,33E+06</i>	<i>3,40</i>
<b><i>HECO2</i></b>	<i>2,25E+05</i>	<i>0,57</i>
<b><i>HE-CARB</i></b>	<i>6,33E+06</i>	<i>16,13</i>
<b><i>CARB</i></b>	<i>3,23E+06</i>	<i>8,22</i>
<b><i>MIX-SOLI</i></b>	<i>3,58E+01</i>	<i>0,00</i>
<b><i>SP-CAO</i></b>	<i>1,27E+02</i>	<i>0,00</i>
<b><i>TOT</i></b>	<i>3,93E+07</i>	<i>100</i>

*Table 27- CASE 1, irreversibilities, daytime-mode*

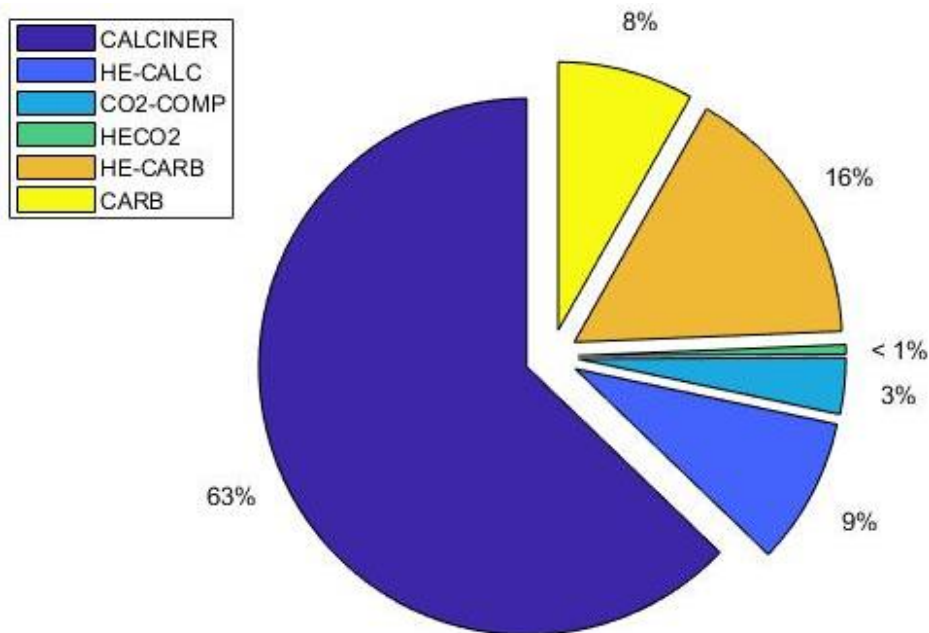


*Figure 51 - CASE 1, irreversibilities, daytime-mode*

What stands out most from the collected data is certainly the high degree of irreversibility present in the calciner in comparison to the other components of the system. It is a predictable result and can be explained taking into account the thermodynamic process that takes place in the component. The input energy flow, indicating the incident solar radiation, is essentially pure exergy, due to its origin from a system (Sun) at very high temperature. It is therefore understandable the high value of exergetic loss that develops in the component due to the reduction of the thermodynamic quality that the resource undergoes in the transfer to the calciner and during subsequent transformations.

Other components with a significant percentage of irreversibility are heat exchanger systems, both on the calciner and carbonator side. The result derives from the numerous transformations that the flows undergo inside them. Both heat exchangers and mechanical transformations of compression and expansion lead to thermal losses. Due to the plant complexity of the HE-CALC and HE-CARB blocks, the overall irreversibility value achieved is therefore quite significant.

The irreversibility value in the carbonator is also relevant. This can be attributed to thermal losses occurring in the component, both because of the chemical reaction taking place in the reactor and because of temperature differences between reactants and products.

Finally, components such as mixers and splitters have zero irreversibility. This is due to the initial assumption of no heat losses in the components in question.

The irreversibilities of the night-mode configuration are shown below:

<i>Components</i>	<i>Irreversibility [W]</i>	<i>Irreversibility [%]</i>
<b>HE-CARB</b>	<i>7,86E+06</i>	<i>70,87</i>
<b>CARB</b>	<i>3,23E+06</i>	<i>29,13</i>
<b>TOT</b>	<i>1,11E+07</i>	<i>100</i>

*Table 28 - CASE 1, irreversibilities, night-mode*

In the night configuration of CASE 1, as explained in the previous paragraphs, it is assumed that the only components with relevant operation are the carbonator and the heat exchanger system on the same side. As a result, according to the daytime configuration, the irreversibility of the HE-CARB block is greater than that of the CARB. In this situation, in particular, the deviation is more marked due to further thermal losses due to the operation of components (turbine, heater) deactivated in the daytime configuration.

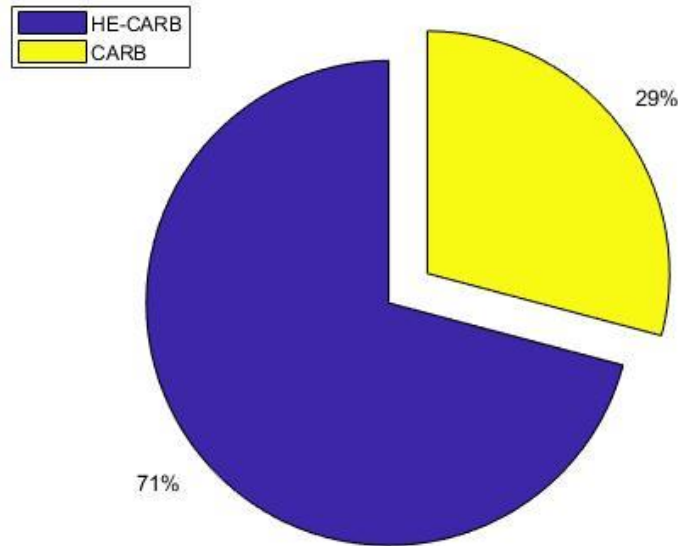


Table 1 - CASE 1, irreversibilities, night-mode

#### 4.3.3. Irreversibility of CASE 2

The irreversibility values calculated for the second case are given below, taking into account both day and night operation mode. Also in this situation, the analysis is completed by means of a pie chart to understand better the distribution of irreversibilities among the various components.

The following table lists the results for daytime operation mode:

<i>Components</i>	<i>Irreversibility [W]</i>	<i>Irreversibility [%]</i>
<i>CALCINER</i>	<i>1,75E+07</i>	<i>49,39</i>
<i>HE-CALC</i>	<i>1,42E+06</i>	<i>3,99</i>
<i>CO2-COMP</i>	<i>1,75E+06</i>	<i>4,93</i>
<i>HECO2</i>	<i>7,25E+04</i>	<i>0,20</i>
<i>SP-CO2</i>	<i>0,00E+00</i>	<i>0,00</i>
<i>HE-CARB</i>	<i>6,48E+06</i>	<i>18,24</i>
<i>CARB</i>	<i>8,21E+06</i>	<i>23,12</i>
<i>HESOLI</i>	<i>1,08E+04</i>	<i>0,03</i>
<i>MIX-SOLI</i>	<i>5,97E+03</i>	<i>0,02</i>
<i>SP-CAO</i>	<i>0,00E+00</i>	<i>0,00</i>
<i>HE-CAO</i>	<i>2,93E+04</i>	<i>0,08</i>
<i>TOT</i>	<i>3,55E+07</i>	<i>100,00</i>

Table 29 - CASE 2, irreversibilities, daytime-mode

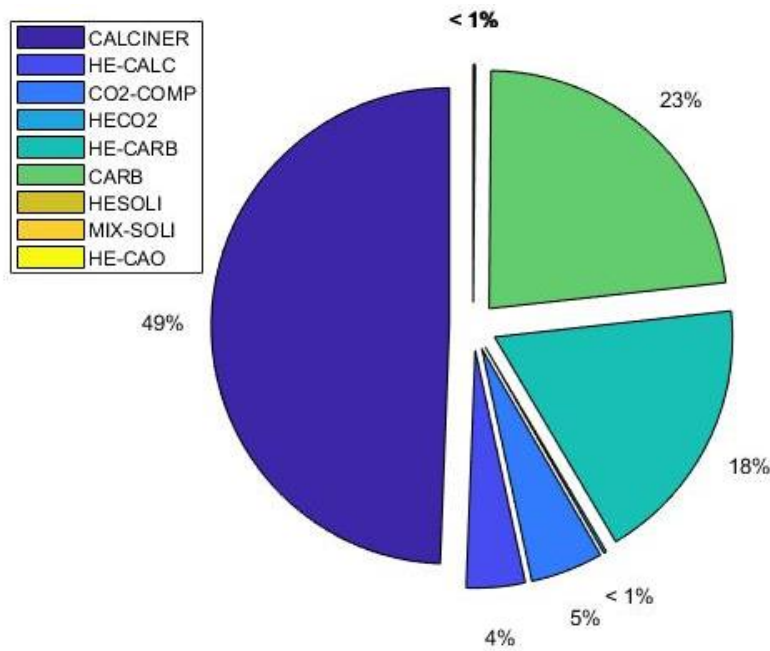


Figure 52 - CASE 2, irreversibilities, daytime-mode

Also in this second case the calciner represents the component with the highest irreversibility value. The situation is undoubtedly imputable to the same cause analysed in the previous case.

The irreversibility rates of heat exchanger systems are also relevant. As already explained above, the behaviour is certainly due to the numerous components that constitute the blocks and that involve thermodynamic transformations responsible for thermal losses.

Also significant is the high irreversibility value of the carbonator, due to the thermal losses caused by the chemical reaction and the temperature difference between reactants and products.

Even in this configuration, finally, the irreversibility of components such as mixers and splitters is assumed to be negligible, supposing the absence of thermal losses in them.

The results of the night-time performance analysis are shown below:

<i>Components</i>	<i>Irreversibility [W]</i>	<i>Irreversibility [%]</i>
<b>HE-CARB</b>	<i>6,39E+06</i>	<i>43,39</i>
<b>CARB</b>	<i>8,13E+06</i>	<i>55,23</i>
<b>HESOLI</b>	<i>1,73E+05</i>	<i>1,18</i>
<b>HE-CAO</b>	<i>2,93E+04</i>	<i>0,20</i>
<b>TOT</b>	<i>1,47E+07</i>	<i>100,00</i>

Table 30 - CASE 2, irreversibilities, night-mode

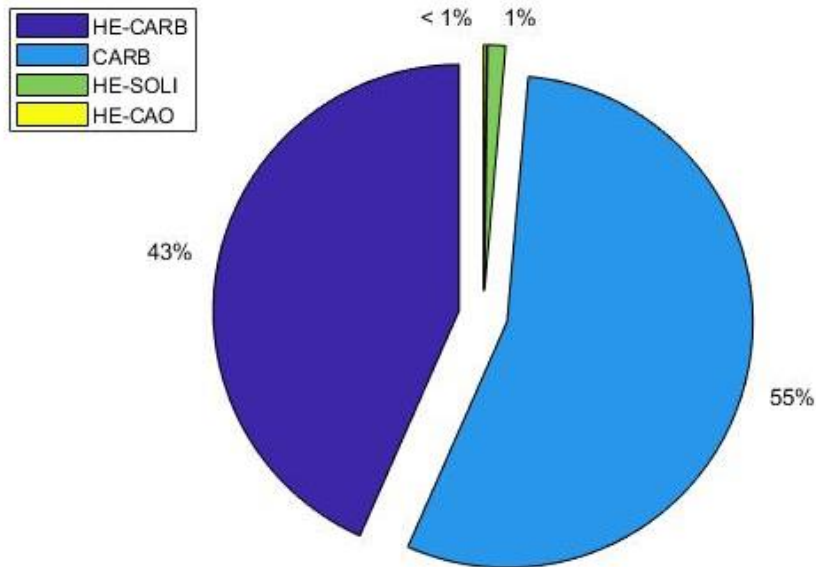


Figure 53 - CASE 2, irreversibilities, night-mode

Again, components belonging to the calciner side are considered inoperative. The main irreversibilities are distributed between the carbonator and the heat exchange system on the same side. Compared to the previous case, there are two additional components, HECAO and HESOLI, representing the intercoolers needed to cool the solids before they are fed into the storage system at ambient temperature.

#### 4.3.4. Considerations and comparisons

The two configurations analysed show common results but also important differences.

Both show that the component with the highest level of irreversibility is the calciner. This is an expected result due to the operating methodology of the component and the losses to which it goes against due to the high exergetic quality of the solar radiation.

Both CASE 1 and CASE 2 also show significant irreversibility values in heat exchange systems. This result is consistent with the system articulation. In fact, both include components in the HE-CARB and HE-CALC blocks, which result in significant heat loss rates.

The main difference, finally, is observed in the carbonator. It turns out that CASE 2 has a quite higher percentage of irreversibility. The difference may be due to the storage of solids at room temperature in CASE 2, which leads to a higher thermal loss in heating them before the carbonation reaction and to the higher temperature difference between reactants and products.

## 4.4. Exergy-cost calculation

The following paragraph provides exergetic information on the components and flows characterizing the system. In particular, through matrix calculation, it is possible to obtain the so-called "Exergy cost",  $E^*$ . It can be interpreted as an index of the amount of exergy needed to obtain a flow with a chosen exergy. Basically it allows to understand the expenditure, in exergetic terms, useful to guarantee the thermodynamic characteristics of the plant according to the chosen operating scheme.

The paragraph also sets out the basis for the subsequent exergo-economic calculation, through the construction of the cost-matrix obtained by exploiting the mass and energy balances on the individual control volumes of the various components, as described in the previous paragraphs.

### 4.4.1. Operational concepts

The process of calculation of the exergy costs vector requires the definition of a matrix, called cost-matrix, obtained from the incidence matrix used in the calculation of irreversibility and completed with a number of lines equal to that required to obtain a square matrix. In matrix terms, the operation is expressed according to the following equation:

$$\begin{bmatrix} A \\ \alpha_e \\ \alpha_x \end{bmatrix} \times E^* = \begin{bmatrix} 0 \\ \omega \\ 0 \end{bmatrix} \quad (4.6)$$

Where  $A$  is the incidence matrix used in the calculation of irreversibility,  $\alpha_e$  and  $\alpha_x$  are matrixes obtained through auxiliary equations derived from the analysis of the production structure of the individual components. The union of the three listed matrices defines the cost matrix  $A_c$ .

More in detail, the auxiliary equations useful for the matrix completion are derived using four basic rules:

- P1 rule: it is applied to the input resources to the system. When a flow enters the system as a resource, in the absence of further specifications, its exergy cost is equal to its exergy, as shown below:

$$E_i^* = E_i \quad (4.7)$$

- P2 rule: it is applied to the flows leaving the system. When a flow in exit from the system is a waste, in absence of further specifications, it can be catalogued as "Losses" and its exergy cost assumed equal to 0:

$$E_i^* = 0 \quad (4.8)$$

- P3 rule: it is a useful rule to regulate the flows indicated as resources in the individual components. In particular, if there are flows differences between the resources of a component, then the unit exergy costs of the flows in question are equal. For unit exergy cost  $k_i^*$  we mean the relationship between the exergy cost of a flow and the relative exergy:

$$k_i^* = \frac{E_i^*}{E_i} \quad (4.9)$$

- P4 rule: it is similar to P3 but deals with the products. Specifically, if among the products of a component there are sums between flows, then the unit exergy costs of the flows in question are equal. Both P3 and P4 can be expressed by the following relation:

$$\begin{aligned} k_i^* = k_j^* &\rightarrow \frac{E_i^*}{E_i} = \frac{E_j^*}{E_j} \rightarrow \\ &\rightarrow -\frac{E_j}{E_i} \cdot E_i^* + E_j^* = 0 \end{aligned} \quad (4.10)$$

P1 and P2 rules define the matrix  $\alpha_e$  while P3 and P4 rules make up the  $\alpha_x$ .

The (4.6) can be expressed in compact form as follows:

$$A_c \times E^* = Y_e \quad (4.11)$$

$Y_e$  indicates the vector of external assessments. It reports zero values at incidence matrix and  $\alpha_x$  matrix. It has values different from 0 and dependent on the exergy of the resource in correspondence of the lines introduced with the P1 rule. Finally, it is generally null in correspondence of the P2 rule unless external assessment.

Once  $A_c$  and  $Y_e$  are built, the calculation of the exergy costs vector is immediate according to the inverse formula:

$$E^* = A_c^{-1} \times Y_e \quad (4.12)$$

Below, for completeness of analysis, the exergy cost values for the two configurations treated are reported. The operators  $A_c$  and  $Y_e$  used in the matrix calculation are included in the appendix.

#### 4.4.2. Exergy costs of CASE 1

<i>STREAM</i>	<i>E* [W] - DAY</i>	<i>E* [W] - NIGHT</i>
<i>CO2-1</i>	4,44E+07	/
<i>CO2-2</i>	3,44E+07	/
<i>CO2-3</i>	2,66E+07	/
<i>CO2-STO</i>	2,66E+07	/
<i>CO2CARB</i>	1,18E+07	/
<i>CO2CARB1</i>	/	1,17E+07
<i>CO2CARB2</i>	4,60E+08	4,46E+08
<i>CO2CARBX</i>	4,26E+08	4,13E+08
<i>SOLIDS1</i>	4,81E+08	/
<i>SOLIDS2</i>	4,86E+08	/
<i>FRCALC</i>	5,41E+08	/
<i>STO-CAO</i>	3,61E+08	/
<i>FRCARB</i>	1,80E+08	1,64E+08
<i>SOLIDSX1</i>	1,86E+08	1,70E+08
<i>SOLIDSX2</i>	1,77E+08	1,62E+08
<i>STO-SOLI</i>	3,04E+08	/
<i>SOLAR</i>	1,00E+08	/
<i>GT</i>	2,80E+07	2,72E+07
<i>ST</i>	5,39E+06	/
<i>T2</i>	/	1,23E+06
<i>COMP-1</i>	4,00E+06	/
<i>COOL-CO2</i>	0,00E+00	/
<i>HEAT</i>	/	/
<i>COMP-2bis</i>	5,11E+05	1,57E+06
<i>COMP-2</i>	1,27E+07	1,27E+07

Table 31 - Exergy costs CASE 1

4.4.3. Exergy costs of CASE 2

<i>STREAM</i>	<i>E* [W] - DAY</i>	<i>E* [W] - NIGHT</i>
<i>CO2-1</i>	7,68E+07	/
<i>CO2-2</i>	3,88E+07	/
<i>CO2-3</i>	4,58E+07	/
<i>CO2-4</i>	4,58E+07	/
<i>CO2-STO</i>	3,05E+07	/
<i>CO2CARB</i>	1,53E+07	1,69E+07
<i>CO2CARB2</i>	3,10E+08	3,42E+08
<i>CO2CARBX</i>	3,15E+08	3,46E+08
<i>SOLIDS1</i>	2,04E+08	/
<i>SOLIDS2</i>	2,56E+08	/
<i>FRCALC-1</i>	2,80E+08	/
<i>FRCALC-2</i>	2,65E+08	/
<i>FRCARB</i>	8,84E+07	6,21E+07
<i>FRCARB2</i>	1,40E+08	1,09E+08
<i>FRCARB21</i>	8,84E+07	6,21E+07
<i>STO-CAO</i>	1,77E+08	/
<i>SOLIDSX1</i>	1,31E+08	1,02E+08
<i>SOLIDSX2</i>	1,04E+08	8,06E+07
<i>SOLIDSX3</i>	1,04E+08	8,06E+07
<i>STO-SOLI</i>	1,00E+08	/
<i>SOLAR</i>	1,00E+08	/
<i>COMP-1</i>	7,00E+06	/
<i>COOL-CO2</i>	0,00E+00	/
<i>HEAT</i>	2,00E+06	2,00E+06
<i>T2</i>	8,73E+06	7,94E+06
<i>COMP-2</i>	1,10E+07	1,10E+07
<i>GT</i>	4,39E+06	3,42E+06
<i>COOL-SOLI</i>	0,00E+00	0,00E+00
<i>COOL-CAO</i>	0,00E+00	0,00E+00

Table 32 - Exergy costs CASE 2

## 4.5. Cost allocation of different components

An economic analysis of the system is discussed below. It is a fundamental step to complete the exergo-economic analysis, exploiting the results of the exergetic analysis and completing them with economic aspects.

The treatment consists in a complete characterization of each component in order to calculate the total capital cost. Starting from this, through economic reasoning, it is possible to obtain the so-called "cost rate" of the various components, to be used later in the exergo-economic analysis.

### 4.5.1. Cost estimation methodology

The total capital cost of the plant is calculated using the NETL (National Energy Technology Laboratory) methodology [106], which divides the total capital cost into five levels. The first of these is the Bare Erected Cost (BEC), for whose evaluation it is applied the module costing technique through the definition of a cost functions for each device. A cost function is a relationship that estimates the purchasing cost of components depending on the operating condition. It is expressed in the general form:

$$C_{BEC} = C_p^0 \cdot F_M \cdot F_P \quad (4.13)$$

Where  $C_p^0$  indicates the purchasing cost under basic operating conditions,  $F_M$  identifies a form factor and  $F_P$  a pressure factor. In this way it is possible to obtain a purchasing cost appropriate to the specific use of the component. For components such as heat exchangers, reactors, vessels, pumps, for greater precision the following relationship is adopted:

$$C_{BEC} = C_p^0 \cdot (B_1 + B_2 \cdot F_M \cdot F_P) \quad (4.14)$$

With the introduction of corrective factors  $B_1$  and  $B_2$ .

The assessment of the purchasing cost is carried out using the data and methodologies reported in "Cost Equations and Curves for the CAPCOST Program", (Turton et al.) [104]. Before proceeding with the presentation of the results it is appropriate to list some hypotheses adopted during the analysis:

- All the data for the calculation of the purchasing cost collected in (Turton et al.) relate to the period from May to September 2001, with a CEPCI of 397. To update the data, a correction is made on the basis of the 2018 CEPCI value of 603,1 [105]. The formula used is as follows:

$$C_{2018} = C_{2001} \cdot \left( \frac{CEPCI_{2018}}{CEPCI_{2001}} \right) \quad (4.15)$$

- The data contained in (Turton et al.) correspond to a characteristic size range of the component in question, of variable type depending on the component. In case the size analysed exceeds the validity range, a corrective multiplicative factor is introduced, according to the so-called "six tenth rule", following the relationship:

$$\frac{C_1}{C_0} = \left( \frac{S_1}{S_0} \right)^{0.6} \quad (4.16)$$

In this way, the purchasing cost of the component is proportional to its characteristic size S;

- The characteristic size of heat exchangers and intercoolers is the heat exchange surface. For heat exchangers, it is precisely indicated in the results of the AspenPlus simulation. For intercoolers, instead, its value has been calculated assuming that the cooling fluid is water and assuming an inlet at ambient temperature. The heat exchange coefficient is assumed to be equal to  $0,2 \frac{kW}{m^2K}$ . Exchangers and intercoolers are considered "flat plate";
- The assessment of the purchasing cost of calciner and carbonator is made using the values reported in (Turton et al.) in the "Process vessels" category, thus considering them as generic process reactors, both of the same volume;
- Given the system configuration of the HE-CARB block in CASE 1 and the activation of some components only in daytime or night-time operation, for a more accurate evaluation of the cost-rate, the devices have been differentiated in relation to the actual period of operation. As a consequence, COMP-2bis is evaluated only for daytime operation (8 hours), T2 and HEAT, on the other hand, are in operation at night (16 hours). The rest of the components are considered operational for 24 hours.

Once the Bare Erected Cost of each component has been calculated, it is possible to proceed according to the NETL method in the individuation of the total capital cost going up in the following five levels of decomposition, as shown in the figure below (figure 6).

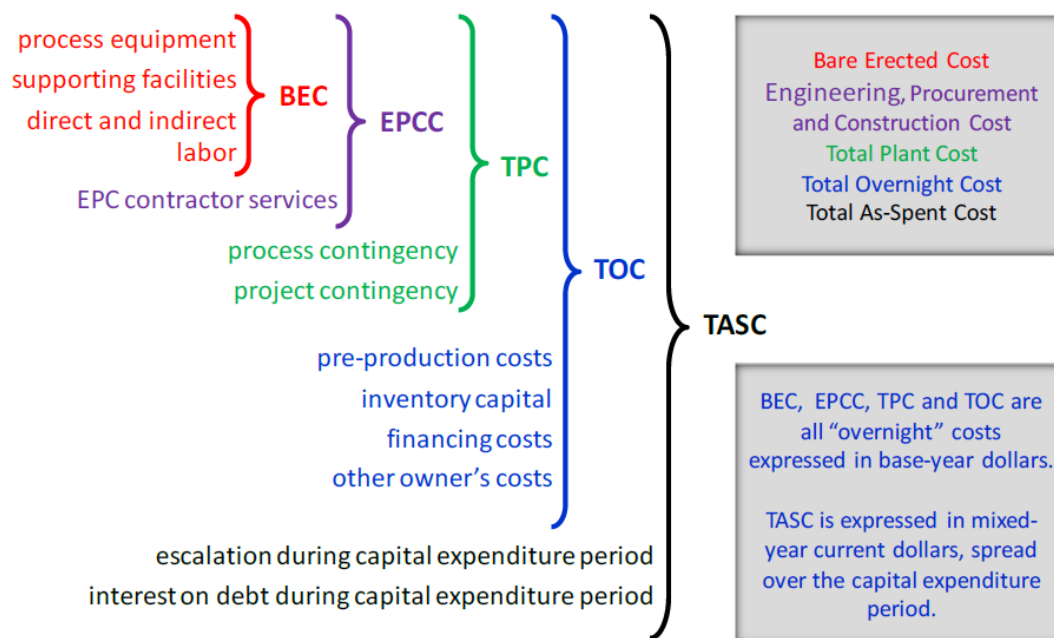


Figure 54 - Capital Cost levels, NETL [106]

How to move from one level to the next is fully explained in NETL's cost estimation methodology [106] and is summarised below:

<i>Parameter</i>	<i>Type of cost</i>	<i>Estimation from NETL report</i>	<i>Description</i>
<b>EPCC</b>		8 %	% of BEC
<b>TPC</b>	<i>Process contingencies</i>	5 %	% of EPCC
	<i>Project contingencies</i>	30 % (reactors)	
	<i>Preproduction costs</i>	15 %	
<b>TOC</b>	<i>Inventory capital</i>	2 %	% of TP
	<i>Financing cost</i>	0,5 %	
	<i>Other Owner's cost</i>	2,7 %	
<b>TASC</b>		15 %	
<b>TASC</b>		1,114	<i>Multiplying factor of TOC</i>

Table 33 - Capital Cost levels calculation, NETL [106]

In particular, the factor of 1,114 to switch from TOC to TASC was selected considering an IPP (Independent Power Producer) financial structure, articulated with 60% debt and 40% equity. This is a "high risk" choice, due to the immaturity and still low diffusion of the technology in the specific application described. For the same reason, a Process Contingencies value of 30% was chosen for calciners and carbonators. For the other more widely used components (heaters, coolers, turbines, compressors, heat exchangers) a Process Contingencies value of 5% was adopted.

Below follows the capital cost structure of the components in the two configurations analysed:

<b>COMPONENT</b>	<b>BEC [€]</b>	<b>EPCC [€]</b>	<b>TPC [€]</b>	<b>TOC [€]</b>	<b>TASC [€]</b>
<b>CALCINER</b>	306320	330826	479697	576596	642328
<b>HE-CALC</b>	4888718	5279815	6335778	7615605	8483784
<b>CO2-COMP</b>	4085461	4412298	5294757	6364298	7089828
<b>HECO2</b>	947325	1023110	1227733	1475735	1643968
<b>HE-CARB</b>   <b>Tot</b>	20874678	22544652	27053583	32518407	36225505
<b>24 hrs</b>	18431758	19906299	23887558	28712845	31986110
<b>Night</b>	1484347	1603095	1923714	2312304	2575907
<b>Day</b>	958573	1035259	1242310	1493257	1663488
<b>CARB</b>	13316503	14381824	17364144	20871701	23251075

Table 34 - CASE 1, Capital costs levels

<b>COMPONENT</b>	<b>BEC [€]</b>	<b>EPCC [€]</b>	<b>TPC [€]</b>	<b>TOC [€]</b>	<b>TASC [€]</b>
<b>CALCINER</b>	306320	330826	479697	576596	642328
<b>HE-CALC</b>	2897689	3129504	3755405	4513996	5028592
<b>CO2-COMP</b>	5891884	6363235	7635882	9178330	10224660
<b>HECO2</b>	2356918	2545471	3054565	3671588	4090149
<b>HE-CARB</b>	23146107	24997795	29997354	36056820	40167297
<b>CARB</b>	13264038	14325161	17296148	20789970	23160027
<b>HESOLI</b>	690457	745694	894833	1075589	1198206
<b>HECAO</b>	643757	695258	834309	1002840	1117164

Table 35 - CASE 2, Capital costs levels

#### 4.5.2. Economic considerations

The evaluation of the cost-rate of each component, necessary for the conclusion of the exergo-economic analysis, requires the calculation of the annuity. It can be defined as the annual payment quota obtained by dividing the total investment into tranches equally distributed over a certain period of time. Its value is obtained by the following formula:

$$annuity = TASC \cdot \frac{i \cdot (1 + i)^n}{(1 + i)^n - 1} \quad (4.17)$$

Where "n" represents the period during which payments are distributed. In this case it is assumed to be equal to the life of the plant (25 years). "i", instead, constitutes the discount rate, which, in the economic evaluation of an investment, may be assumed at the WACC (Weighted Average Cost of Capital). It can therefore be calculated as follows [107]:

$$WACC = K_e \cdot \frac{E}{D + E} + K_d \cdot \frac{D}{D + E} \quad (4.18)$$

It depends on the financial structure of the system. As previously specified, a high risk IPP structure is adopted, with Debt (D) of 60% and Equity (E) of 40%. For simplicity of treatment, the tax effects are not considered in the calculation. Factors  $K_e$  and  $K_d$  indicate the "cost of equity" and the "cost of debt" respectively. The cost of equity can be assessed according to the following report:

$$K_e = R_f + premium \quad (4.19)$$

" $R_f$ " indicates the systemic risk and is dependent on the economic background of the country concerned. Its average value in Spain, looking at the data for the last 5 years, is approximately 1,25% [108]. "*premium*", instead, depends on a number of factors, as can be seen below:

$$premium = R_s + \beta \cdot (R_m - R_f) \quad (4.20)$$

The relation (4.20) includes:

- $R_s$ : small stock premium due to reduced liquidity. It is only relevant for small investors. It is assumed to be 0 in this case;
- $\beta$ : expresses the sensitivity of the rate of return of investment to market developments. It is assumed to be of unit value;
- $R_m - R_f$ : EMRP (Equity Market Risk Premium), valued at 5.75% [109].

The cost of debt  $K_d$  is, instead, calculated according to the following formula:

$$K_d = IRS + spread \quad (4.21)$$

$IRS$  (interest rate swap) and  $spread$  are assumed to be 0,85 % and 1,36 % respectively [110]. The calculation gives a WACC for the considered financial structure of 2,89 %.

#### 4.5.3. Cost-rates of components

Once the WACC value is obtained, it is then possible to proceed with the analysis and evaluate annuity and cost rates of components ( $Z$ ). In particular, it should be remembered that the system has been calibrated ensuring an average daytime operation, in the presence of solar radiation, of 8 hours per day and an average night-time operation, in the absence of solar radiation, of 16 hours per day. The system is in operation for 365 days a year, for a total life cycle of 25 years.

Given the above assumptions, below are the annuity and cost-rate values for the two configurations analysed.

<b>COMPONENT</b>	<b>Annuity [€]</b>	<b>Z [€/s]</b>
<b>CALCINER</b>	36440	0,003
<b>HE-CALC</b>	481292	0,046
<b>CO2-COMP</b>	402212	0,038
<b>HECO2</b>	93264	0,009
	<b>Tot</b>	2055104
<b>HE-CARB</b>	<b>24 hrs</b>	1814599
	<b>Night</b>	146133
	<b>Day</b>	94371
<b>CARB</b>	1319053	0,042
<b>MIX-SOLI</b>	0	0,000
<b>SP-CAO</b>	0	0,000

Table 36 - CASE 1, annuity and cost-rates

<i>COMPONENT</i>	<i>Annuity [€]</i>	<i>Z [€/s]</i>
<i>CALCINER</i>	36440	0,003
<i>HE-CALC</i>	285276	0,027
<i>CO2-COMP</i>	580054	0,055
<i>HECO2</i>	232038	0,022
<i>SP-CO2</i>	0	0,000
<i>HE-CARB</i>	2278725	0,072
<i>CARB</i>	1313888	0,042
<i>HESOLI</i>	67975	0,002
<i>MIX-SOLI</i>	0	0,000
<i>SP-CAO</i>	0	0,000
<i>HECAO</i>	63378	0,002

*Table 37 - CASE 2, annuity and cost-rates*

#### 4.6. Exergo-economic analysis

Once the cost matrix  $A_c$  has been built and the cost-rates  $Z$  of the various components have been calculated, through a matrix calculation it is possible to evaluate the exergo-economic costs of the flows involved in the system. This analysis allows to highlight the cost distribution within the process, identifying the most intensive transformations on the basis of exergetic considerations.

The analysis is then completed by calculating the exergo-economic factor. As a complement to the calculation of irreversibility, the exergo-economic factor is a fundamental tool for understanding the performance of the various components. It not only provides information about their operations, but also identifies the area in which action can be taken to achieve a significant improvement in performance and, consequently, a lower impact on operating costs.

The results of the analysis are presented below, reporting both exergo-economic costs and exergo-economic factors.

#### 4.6.1. Operational concepts

The evaluation of exergo-economic costs follows an analytical methodology based on a matrix calculation similar to that adopted for exergy costs. The formula used is as follows:

$$A_c \times C = Z_e \quad (4.22)$$

In which, " $A_c$ " is the cost-matrix used in the calculation of exergy costs. " $C$ " is the unknown vector of exergo-economic costs.  $Z_e$ , finally, is a vector that takes into account the cost-rates of the various components and is structured as follows:

$$Z_e = \begin{bmatrix} -Z \\ C_e \\ 0 \end{bmatrix} \quad (4.23)$$

Where  $Z$  is the vector of the cost-rates seen in the previous paragraph, while  $C_e$  takes into account the cost-rates of the flows treated in P1 and P2 rules, distinguishing between resources and wastes. The (4.22) can therefore, for greater clarity, be rendered in the following extended form:

$$\begin{bmatrix} A \\ \alpha_e \\ \alpha_x \end{bmatrix} \times C = \begin{bmatrix} -Z \\ C_e \\ 0 \end{bmatrix} \quad (4.24)$$

Before reporting the results, some considerations should be made about the vector  $C_e$  and how it was built. The following assumptions are made:

- For the solar radiation entering the calciner (SOLAR), considered a resource for the system, a cost-rate equal to 0 is assumed. Being a natural resource, no cost is attributed for its use;
- The electrical energy input to the system, used for the activation of compressors and heaters, is evaluated based on the value of  $c_{el} = 0,064 \text{ €/kWh}$  [111], corresponding to the average cost per kWh of electricity in Spain. The cost rate of the related energy flows is obtained with the relation:

$$C_{el} \text{ [€/s]} = c_{el} \cdot P/3600 \quad (4.25)$$

With "P" indicating the power, in Watts, of the generic component considered;

- In the night configuration of both CASE 1 and CASE 2,  $CaO$  and  $CO_2$  flows entering the system and coming from storage systems have a cost-rate equal to the value of the corresponding flows sent to the storage systems during daytime operation;
- The calculation of the cost rate of the quantity of  $CaCO_3$  fed into the plant from outside is made considering an average material cost of 0,15 €/kg. Knowing the total amount of  $CaCO_3$  used in the life cycle of the plant, it is therefore possible to derive the relative cost rate over 25 years of use;
- Energy flows out of the system as a result of processes in the intercoolers are considered waste flows. A zero cost-rate is assumed for these.

Once the  $C_e$  vector is defined, the calculation of exergy-costs is immediate via the reverse operation:

$$C = [A_c]^{-1} \times C_e \quad (4.26)$$

The exergo-economic factor, on the other hand, is obtained according to the relation:

$$f_i = \frac{Z_i}{Z_i + C_I} \quad (4.27)$$

As  $C_I$  is a component that takes into account the effects of irreversibility on the cost, according to the equation:

$$C_I = c_{F,i} \cdot I_i \quad (4.28)$$

With  $c_{F,i}$  indicating the "cost of fuel" of the i-th component. The following are the results obtained in terms of exergo-economic costs and exergo-economic factors for the two configurations treated. Considerations and conclusions deriving from the analysis of the results are set out in the final paragraph.

4.6.2. Exergo-economic analysis of CASE 1

<i>STREAM</i>	<i>C [€/s] - DAY</i>	<i>C [€/s] - NIGHT</i>
<i>CO2-1</i>	0,012	/
<i>CO2-2</i>	0,010	/
<i>CO2-3</i>	0,082	/
<i>CO2-STO</i>	0,091	/
<i>CO2CARB</i>	0,037	/
<i>CO2CARB1</i>	/	0,091
<i>CO2CARB2</i>	4,870	5,611
<i>CO2CARBX</i>	4,515	5,201
<i>SOLIDS1</i>	0,136	/
<i>SOLIDS2</i>	0,159	/
<i>FRCALC</i>	0,150	/
<i>STO-CAO</i>	0,100	/
<i>FRCARB</i>	0,050	0,050
<i>SOLIDSX1</i>	0,115	0,124
<i>SOLIDSX2</i>	0,110	0,118
<i>STO-SOLI</i>	0,026	/
<i>SOLAR</i>	0,000	/
<i>GT</i>	0,332	0,377
<i>ST</i>	0,026	/
<i>T2</i>	/	0,019
<i>COMP-1</i>	0,071	/
<i>COOL-CO2</i>	0,000	/
<i>HEAT</i>	/	0,027
<i>COMP-2bis</i>	0,009	/
<i>COMP-2</i>	0,231	0,231

Table 38 - CASE 1, Exergo-economic costs

<i>COMPONENT</i>	<i>c<sub>F,i</sub> [€/s]</i>	<i>Z<sub>i</sub> [€/s]</i>	<i>I<sub>i</sub> [kW]</i>	<i>C<sub>I</sub> [€/s]</i>	<i>f [°]</i>
<i>CALCINER</i>	0,0010	0,004	24673	0,007	0,33
<i>HE-CALC</i>	0,0011	0,046	3476	0,001	0,98
<i>CO2-COMP</i>	0,0082	0,038	1334	0,003	0,93
<i>HECO2</i>	0,0126	0,009	225	0,001	0,92
<i>HE-CARB</i>	0,0075	0,073	6333	0,013	0,85
<i>CARB</i>	0,0519	0,042	3230	0,047	0,47

<b>MIX-SOLI</b>	0,0011	0,000	0	0,000	/
<b>SP-CAO</b>	0,0011	0,000	0	0,000	/

Table 39 - CASE 1, Exergo-economic factors

#### 4.6.3. Exergo-economic analysis of CASE 2

<b>STREAM</b>	<b>C [€/s] - DAY</b>	<b>C [€/s] - NIGHT</b>
<b>CO2-1</b>	0,127	/
<b>CO2-2</b>	0,412	/
<b>CO2-3</b>	0,596	/
<b>CO2-4</b>	0,618	/
<b>CO2-STO</b>	0,412	/
<b>CO2CARB</b>	0,206	0,206
<b>CO2CARB2</b>	4,184	4,184
<b>CO2CARBX</b>	4,227	4,230
<b>SOLIDS1</b>	0,466	/
<b>SOLIDS2</b>	0,585	/
<b>FRCALC-1</b>	0,462	/
<b>FRCALC-2</b>	0,085	/
<b>FRCARB</b>	0,028	0,083
<b>FRCARB2</b>	0,592	0,660
<b>FRCARB21</b>	0,030	0,085
<b>STO-CAO</b>	0,056	/
<b>SOLIDSX1</b>	0,552	0,615
<b>SOLIDSX2</b>	0,437	0,488
<b>SOLIDSX3</b>	0,439	0,490
<b>STO-SOLI</b>	0,027	/
<b>SOLAR</b>	0,000	/
<b>COMP-1</b>	0,129	/
<b>COOL-CO2</b>	0,000	/
<b>HEAT</b>	0,027	0,027
<b>T2</b>	0,095	0,097
<b>COMP-2</b>	0,193	0,193
<b>GT</b>	0,038	0,040
<b>COOL-SOLI</b>	0,000	0,000
<b>COOL-CAO</b>	0,000	0,000

Table 40 - CASE 2, Exergo-economic costs

<b>COMPONENT</b>	<b><math>c_{F,i}</math> [€/s]</b>	<b><math>Z_i</math> [€/s]</b>	<b><math>I_i</math> [kW]</b>	<b><math>C_I</math> [€/s]</b>	<b><math>f</math> [/]</b>
<b>CALCINER</b>	0,007	0,004	17541	0,035	0,09
<b>HE-CALC</b>	0,011	0,027	1418	0,004	0,86
<b>CO2-COMP</b>	0,066	0,055	1750	0,032	0,63
<b>HECO2</b>	0,042	0,011	73	0,001	0,93
<b>SP-CO2</b>	0,044	0,000	0	0,000	/
<b>HE-CARB</b>	0,046	0,072	6477	0,082	0,47
<b>CARB</b>	0,031	0,042	8210	0,071	0,37
<b>HE-SOLI</b>	0,031	0,002	11	0,000	0,96
<b>MIX-SOLI</b>	0,011	0,000	6	0,000	/
<b>SP-CAO</b>	0,002	0,000	0	0,000	/
<b>HE-CAO</b>	0,002	0,002	29	0,000	0,99

Table 41 - CASE 2, Exergo-economic factors

#### 4.6.4. Considerations and comparisons

The carried out exergo-economic analysis allows to deduce important information about the behaviour of the various system components in the two analysed configurations.

With reference first to the exergo-economic costs, a significant result that emerges in both configurations is the high value attributed to the  $CO_2$  flows belonging to the power cycle. The following histogram shows the evolution of the value in the two configurations (*Figure 55*). The result can be explained considering the high flow rate value of both flows, which are then used for power generation in the gas turbine. A marked exergo-economic cost difference emerges between daytime and night-time configuration in CASE 1, a trend which is not matched in CASE 2. The behaviour can be attributed to the plant articulation of CASE 1, which shows significant differences in terms of flows involved and components activated between the two periods of daily operation.

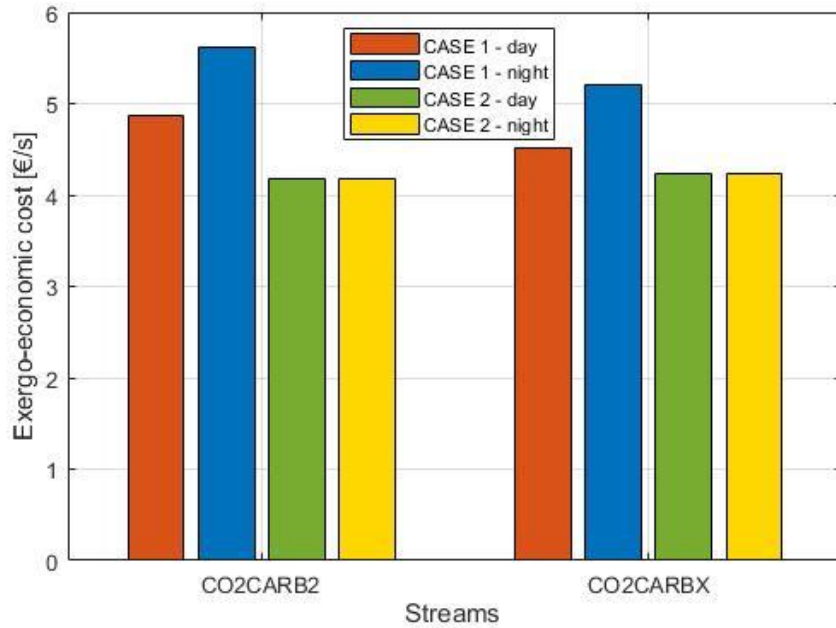


Figure 55 - Exergo-economic costs comparison

From the exergo-economic costs it then emerges how the values corresponding to the flows exchanged between the system and the environment are zero. As previously accepted, in fact, to the solar radiation entering the system, as a free and universally available natural resource, a relative cost is not assigned. Similar speech for the heat flow taken from the intercoolers and discharged to the environment. As "waste flow" and in the absence of further considerations regarding possible subsequent treatments, its exergo-economic cost is considered zero.

More significant results are obtained, instead, from the analysis of exergo-economic factors  $f$ . They are an effective tool to study the economic and energy performance of the various components and to perceive how to intervene to reduce their impact on the overall system. In virtue of the (4.27) used for the calculation, it is deduced that a high value of  $f$  indicates a prevalence of the cost component, while a low value of  $f$  imputes a non-optimal performance prevalently to the irreversibilities that occur in the process phase.

A better understanding of the results can be achieved by comparing the two cases analysed in order to observe any differences in terms of performance of the various components. In this regard, the following graph (Figure 56) shows the exergo-economic factor values for the four main components considered in the analysis: calciner (CALCINER), heat exchanger system on the calciner side (HE-CALC), heat exchanger system on the carbonator side (HE-CARB) and carbonator (CARB).

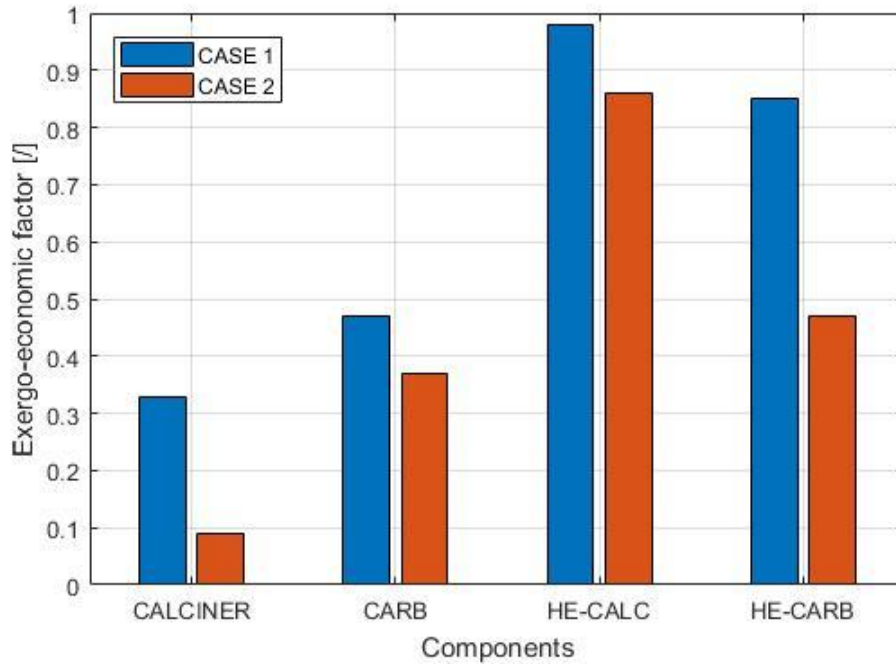


Figure 56 – Exergo-economic factors comparison

From the observation of the graph some relevant considerations emerge:

- It can be seen that the calciner is, for both cases, the component with the lowest value of exergo-economic factor. The result is in accordance with the definition of  $f$  as well as with the results found in the previous paragraphs. The calciner, in fact, is the component with the highest degree of irreversibility. It is not surprising, therefore, that the analysis suggests to intervene at exergetic level and not at economic level, also taking into account the relative low cost compared to the other components of the system. Finally, it should be pointed out that the value of  $f$  in CASE 2 is even lower. This can be explained considering that, in accordance with (4.27) and (4.28), the factor also depends on the cost of fuel  $c_{F,i}$ . Specifically, it is verified that in CASE 2 the  $c_{F,i}$  for the calciner is higher, due to the more intensive preheating processes that the solids flow has to undergo before entering the reactor, as a consequence of the low temperature storage system adopted in this configuration;
- Another component from the markedly low exergo-economic factor is the carbonator. Also in this case the result is in accordance with expectations. The thermal losses that occur during the recombination chemical reaction increase the degree of irreversibility of the component. Even in this situation, the factor is

lower in CASE 2, consistent with the explanation adopted for the calciner. The low temperature storage system, in fact, requires a higher energy expenditure for the preheating of solids, with a consequent increase in the temperature difference between reactants and products. Finally, it should be noted that the  $f$  value of the carbonator is higher than the corresponding value of the calciner in both cases due to a slightly higher overall cost of the CARB component. This is a direct consequence of the simplifying hypothesis adopted at the beginning of the chapter, due to which the gas turbine of the power cycle has been included in the calculation of the cost rate of the "CARB" block;

- In both cases it is observed that the heat exchanger system on the calciner side (HE-CALC) has a very high exergo-economic factor. Undoubtedly the result is attributable to the economic cost of the block. In both cases, the system articulation of the heat exchanger network includes a series of components that result, therefore, in an overall cost of "HE-CALC" decidedly significant, thus making the economic aspect more relevant than the irreversibilities generated in the process. The analysis therefore suggests, with a view to plant engineering improvement, to intervene on the components and on the structure of the HE-CALC block, giving priority to the reduction of the total cost generated. Finally, CASE 2 records a lower  $f$  value than CASE 1. Although still markedly high, in accordance with what has been stated, the reduction is attributable to the lower overall cost of the HE-CALC block in CASE 2, due to the absence of some components (intercooler, condenser, power cycle with steam turbine).
- The discussion on the heat exchanger system on the carbonator side, on the other hand, highlights differences between CASE 1 and CASE 2. If in the former, in fact, the particularly high exergo-economic factor suggests a prevalence of the cost factor, in the latter the trend is reversed, with the achievement of an  $f$  equal to 0.47, considerably reduced. In CASE 1 the result is justifiable considering the implant articulation of the HE-CARB block. It includes, in fact, a series of components (heat exchangers, heaters, compressors, intercoolers, turbines) that inevitably contribute to a significant overall cost, making the economic aspect predominant in the balance sheet. In CASE 2, on the other hand, a different articulation is observed. Although it includes a large number of components, there is a marked reduction in the factor, as a result of an increase in irreversibility and cost of fuel. Undoubtedly, the greater number of transformations involved in the block, also due to the presence of an extra heat exchanger compared to CASE 1, and the greater quantity of interacting flows, favour an increase in the exergetic flow destroyed during the process. Moreover,

the use of storage systems at ambient temperature leads to an increase in the cost of resources due to the preheating processes and the more demanding heat exchanges required by the system. The combination of these two factors contribute to an overall result that suggests to intervene mainly on the plant articulation of the block, making a simplification or changing the thermodynamic conditions of some transformations to reduce the percentage of irreversibility generated.

Some conclusive considerations can then be made about the other components of the system.

- Both CASE 1 and CASE 2 show that the intercoolers analysed, HE-CO<sub>2</sub> in CASE 1 and HE-CO<sub>2</sub>, HE-SOLI and HE-CAO in CASE 2, exhibit markedly high exergo-economic factor values, above 0.90. The result is reasonable, considering the high cost of the components due to the high heat transfer surface required to refine the process;
- Components such as mixers and splitters have a insignificant value of exergo-economic factor. The result is a direct consequence of having neglected the components in the analysis due to their lack of relevance compared to the contribution of the others. Since the physical processes that take place in them have been assumed to be ideally perfect with zero loss rate, the result is justifiably negligible in the overall balance sheet.

## 4.7. Sensitivity analysis and hypothesis discussion

The reuses obtained in the previous paragraphs are conditioned by some preliminary hypotheses adopted in the discussion of the analysed system and its components. In order to add value to the research, it may therefore be appropriate to conduct more in-depth analysis of some of the most questionable hypotheses. Specifically, among these, it is chosen to intervene on components such as heat exchangers and intercoolers for which a common "flat plate" typology has been assumed and an evaluation of the exchange surface through the assumption of water as operating fluid with inlet temperature equal to the ambient temperature. In addition, the issue is examined in depth by discussing the hypothesis of the cost of electricity useful for the operation of compressors and heaters. The plant is actually calibrated so that it can self-produce the energy necessary for the operation of its components. Therefore, assuming the purchase of electricity from the grid is a cautionary hypothesis, acceptable but certainly worthy of further study.

Below the results of the study are reported, with the aim of indicating how much the results of the exergo-economic analysis are affected by variations in the above mentioned parameters.

### 4.7.1. Analysis on heat exchangers

A first analysis to be carried out concerns the heat exchangers involved in the process. Up to three different types of heat exchangers are used in the CSP - CaL plant integration: gas/gas, solid/gas and solid/solid. Initially it was assumed, as a simplifying hypothesis, that all the heat exchangers involved in the process were of the "flat plate" type. Now the modification that the results could register if more accurate analyses were made on each heat exchanger used in the configurations is evaluated.

Specifically, as described in detail in (Ortiz et al.) [112], the most suitable heat exchangers for the process under analysis are the following:

- Gas/gas heat exchangers: Generally for them it would be advisable to adopt "flat plate" solutions as treated in the analysis. However, consulting some commercial catalogues on the subject [113], it is clear that the use of this type of heat exchangers is recommended for volumetric flow rates involved in the process up to  $10000 - 15000 \text{ m}^3/\text{hr}$ . The simulations carried out on AspenPlus show, however, that the flow rates of the  $\text{CO}_2$  flows used in the process are rather

higher than the limits indicated. Therefore, in order to increase the relevance of the analysis, gas/gas exchangers handling high volumetric flow rates will be considered of the "U-tube" type, more suitable for this purpose.

Applying the modification to the gas/gas exchanger of each of the two configurations, precisely the exchanger involved in the power cycle for cooling the  $CO_2$  flow used in the gas turbine, an almost similar result can be observed in the two cases, as shown in the following figure (*Figure 57*). It emerges, in particular, how the use of a component probably more appropriate to the system results, in this case, in a reduction of the HE-CARB block cost-rate in both CASE 1 and CASE 2. Undoubtedly, with a view to plant improvement, it appears that the use of a "U-tube" type for gas/gas exchangers has clear advantages in economic terms compared to the previously analysed "flat plate";

- Solid/gas heat exchangers: according to (Ortiz et al.), probably the most suitable technology for this application is the one provided by "suspension preheaters". They are a type of component widely used, especially in the cement industry. They can therefore boast secure reliability and extensive application experience. The operating methodology consists of sequentially connecting gas and solids in order to promote their separation through the use of cyclones. The reference (Turton et al.) used to calculate the purchasing cost of the various components does not, however, include any information on suspension preheaters. For this reason, the methodology discussed in (Ortiz et al.), is adopted, which involves the calculation of the component cost by evaluating separately the contribution of the heat exchanger and the contribution of the preheater stages. The evaluation of the purchasing cost  $C_{p,0}$  is carried out using the following equations:

<i>Component</i>	<i>Cost function [M€]</i>
<i>Heat exchanger (generic component)</i>	$C_{p,0} = (2546.9 \cdot A_{HE}^{0.67} \cdot P_{HE}^{0.28}) \times 10^{-6}$ (4.29)
<i>Preheater stages (solid-gas heat exchangers)</i>	$C_{p,0} = 3.98 \times 10^{-9} \cdot D_{cyc}^2 + 2.73 \times 10^{-6} \cdot D_{cyc} + 0.016$ (4.30)

*Table 42 - Solid-gas heat exchangers purchasing cost function [112]*

In which  $A_{HE}$  e  $P_{HE}$  indicate the heat exchange surface [ $m^2$ ] and the operating pressure [bar] respectively.  $D_{cyc}$ , instead, represents the diameter of the cyclone used in the preheater stages and evaluated according to the following relation [116]:

$$C_{p,0} = 647 \cdot \dot{V}^{0.422} [m^3/s] \quad (4.31)$$

Where  $\dot{V}$  represents the volume flow rate of the solids stream involved. It is then proceeded by applying the cost-functions just introduced to the solid-gas exchangers in the two configurations analysed.

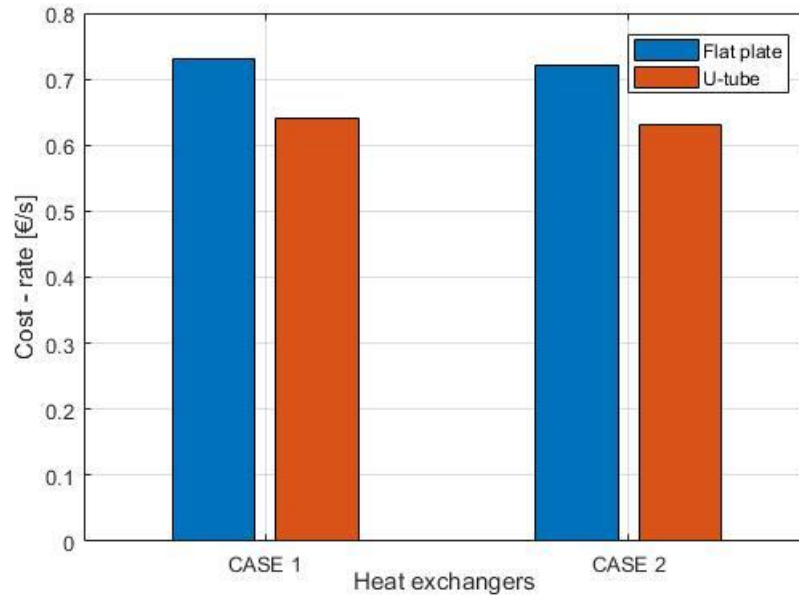


Figure 57 - Flat plate vs U-tube for gas/gas heat exchanger

In CASE 1, there are three solid-gas heat exchangers: one in the HE-CALC block and two others in the network of heat exchangers on the carbonator side. Applying the modifications, therefore, a variation of the cost-rate, and consequently of the exergo - economic factor, of both HE-CALC and HE-CARB is expected. The results show that the HE-CALC block denotes a reduction in the cost-rate from 0.46 €/s to 0.44 €/s, while the HE-CARB block reduces its cost-rate from 0.073 €/s to 0.072 €/s.

Proceeding in the same way also in the analysis of CASE 2, it emerges that the HE-CALC block reduces its cost-rate from 0.027 €/s to 0.025 €/s, while the HE-CARB block shows a variation from 0.072 €/s to 0.068 €/s.

In both situations it is observed that the improvements obtained are not significantly relevant but contribute, however, to a partial reduction in the cost-rate of components for which it was found that the cost factor was the main problem;

- Solid/solid heat exchangers: they represent the component with the most uncertain estimate in the analysis. The problem derives from the fact that, due to the relative immaturity of the process, there are currently no commercially available heat exchangers of this type and of such a dimension that they can be applied in a production plant of a so large size. In fact, this is one of the advantages of the CSP - CaL configuration with high temperature storage (CASE 1) compared to the one with ambient temperature storage (CASE 2), due to the fact that in the former case it is not necessary to operate a heat exchange between solids. In (Vorrias et al.) [115], an application model is presented consisting of the use of concentric L-valves heat exchangers, as indicated in the following figure (*Figure 58*).

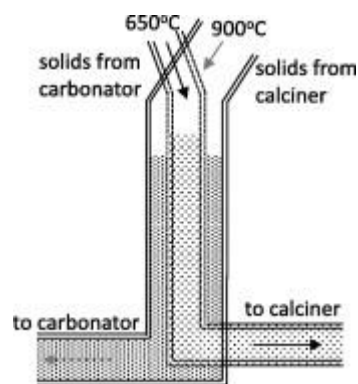


*Figure 58 - Concentric L-valves solid/solid heat exchanger [114]*

However, it is duly specified that, up to now, these are laboratory models for research purposes, not reproduced in plant dimensions. A certain degree of uncertainty therefore remains with regard to their analysis.

The only solid/solid type exchanger included in the CASE 2 configuration is incorporated in the HE-CALC block and ensures heat exchange between the flow of solids entering the calciner and the flow of  $CaO$  just produced by the dissociation reaction. By making the necessary changes to the cost function of the heat exchanger in question, with the assumption that the model described by (Vorrias et al.) is also applicable at industrial level, the result is a considerable decrease in cost, with a consequent reduction in the cost rate of the entire HE-CALC block. More specifically, it is observed a change from 0.027 €/s of the case with "flat plate" exchanger to a value of 0.013 €/s in application of the new model, with a reduction of about 50%.

Undoubtedly, this type of component, although still in the research and development phase and not completely defined, guarantees a gain, at least in terms of cost, compared to the initial hypothesis of "flat plate".

#### 4.7.2. Analysis on intercoolers

A second hypothesis to be discussed is the one concerning intercoolers. In particular, since it was not possible to obtain the heat exchange surface value directly from the simulations in AspenPlus, it was therefore necessary to calculate the value assuming that the refrigerant fluid is water and that its inlet temperature coincides with the ambient temperature. In order to improve the study of the components, a more detailed situation is now considered. In particular, intercoolers operating at sufficiently high temperatures, above approximately 35/40 °C, will be assumed to be air-cooler type heat exchangers. Their exchange surface area will therefore be assessed by considering air as a refrigerant. For intercoolers operating at lower temperatures, on the other hand, water will once again be considered as a refrigerant and a common "flat plate" type heat exchanger will be assumed.

The calculation of the heat exchange surface is consequently performed considering a refrigerating fluid inlet temperature of 20 °C. The exchange process is calibrated so that the fluid is heated to an outlet temperature 10 °C lower than the inlet temperature of the hot fluid. In this way, flexibility is given to the system allowing to adapt the flow rate of the refrigerating fluid to the amount of heat to be subtracted. In the case of water intercooler, the overall heat exchange coefficient for gas/water exchange processes is assumed to be  $U \cong 200 \text{ W/m}^2\text{K}$ . On the contrary, in the case of "air intercooler", according to (Cinocca and Cipollone) [115], an average value of global heat exchange coefficient for the air -  $\text{CO}_2$  exchange can be estimated with the value of  $U \cong 100 \text{ W/m}^2\text{K}$ .

Analyzing the two configurations, it can be observed that the intercoolers operating at sufficiently high temperatures are only two and are used in the CASE 1 configuration. These are, specifically, the intercooler installed in HE-CALC and the one operating in HE-CARB. In both cases, the replacement with 'Air-cooler' leads to an inevitable increase in the exchange area, which is roughly doubled in comparison to the previous situation, but, at the same time, a moderate decrease in the purchasing cost of the component concerned. With respect to the previous results, there is a further, albeit modest, reduction in the HE-CALC and HE-CARB cost-rate. The former undergoes a variation from 0.046 €/s to 0.045 €/s. The second, instead, considering the previous discussion on heat-exchangers, reduces its cost-rate from 0.073 €/s to 0.072 €/s.

For the other intercoolers involved in the process, both in CASE 1 and CASE 2, it appears that the outlet temperature of the hot fluid is too low to make the use of air as refrigerating fluid convenient. The low global heat exchange coefficient, in fact, would require the involvement of excessively high air flow rates, implying a significant energy consumption for the fluid handling. It is therefore preferable to maintain the initial configuration with flat plate intercoolers and water as the refrigerating fluid.

In conclusion, the results show that the use of "Air-cooler" for cooling streams operating at sufficiently high temperatures leads to an economic gain. The lower price of the component, despite the greater heat exchange surface area required, has a positive effect on the cost-rate of the block in which it is included, resulting in an improvement in the corresponding exergo-economic result.

#### 4.7.3. Main results from previous considerations

In order to understand the effect of the considerations discussed in the paragraphs just described, the observations on heat exchangers and intercoolers are applied simultaneously with the purpose of assessing their influence, in terms of variation of exergo-economic factor  $f$ , on the two main blocks involved: HE-CALC and HE-CARB.

<i>Block</i>	<i>f before modifications</i>	<i>f after modifications</i>
<i>CASE 1, HE-CALC</i>	<i>0.98</i>	<i>0.98</i>
<i>CASE 1, HE-CARB</i>	<i>0.85</i>	<i>0.83</i>
<i>CASE 2, HE-CALC</i>	<i>0.86</i>	<i>0.72</i>
<i>CASE 2, HE-CARB</i>	<i>0.47</i>	<i>0.42</i>

*Table 43 - Modifications results*

As shown in the table above (*Table 43*), variations in exergo-economic factor are considerably more significant in CASE 2 than in CASE 1. In particular, the HE-CALC block is the one that shows the biggest discrepancy, which is due to two main causes:

- In CASE 1, the components that mostly characterize the cost of the block are those belonging to the steam turbine power cycle, which were not affected by the analysis carried out previously. As a result, the interventions on exchangers and intercoolers did not show any significant influence;

- In CASE 2, the block has a solid/solid exchanger, absent in the first configuration. As a result of the previous analysis, according to the hypothesis adopted, the HE-CALC block suffers a 50% reduction in cost-rate only because of the considerations on the heat exchanger in question. This explains such a different result. Nevertheless, it is important to remark that there are no solid/solid exchangers applied with such large sizes at present. Consequently, the results in this respect are reasonably questionable and outcome from the chosen hypothesis.

On the other hand, with regard to the results on the HE-CARB block, it can be observed that in both situations there is a reduction of exergo-economic factor. The outcome demonstrates the convenience of the changes made and is consistent with the need to reduce the cost factor of the component. In CASE 2, then, the difference is more marked presumably due to the presence of an extra gas/gas heat exchanger compared to CASE 1, making the intervention applied more effective.

#### 4.7.4. Analysis on input electricity cost

Below the hypothesis addressed in paragraph 4.6.1 is discussed, according to which a cost is attributed to electricity taken from the grid, equivalent to  $c_{el} = 0,064 \text{ €/kWh}$ . The data has therefore permitted the attribution of a cost factor to energy flows indicating the electricity supplied to the system for the operation of components such as compressors and heaters, in accordance with the formula (4.25). The decision to base a discussion on this hypothesis derives from the fact that the plant characteristics and the amount of energy produced in the power cycle suggest that the system can self-produce the energy necessary for the operation of its components. This would eliminate the problem of the plant's dependence on the distribution network and would also amortize the impacts and costs of the project. On the other hand, however, it is risky to establish that a connection to the electricity grid for the possible need for energy is unnecessary, as it is reasonable to assume that there may be particular operational circumstances that prevent the plant from self-producing its own components.

In order to investigate the problem further, it might be convenient to analyse the results of the exergo-economic analysis by observing its variation according to the cost-rate of the energy vector related to the electricity supplied to the components that require it. In this regard, the exergo-economic factors of the four main components of the system (CALCINER, HE-CALC, HE-CARB and CARB) are calculated for increasing  $c_{el}$  values from a null value  $c_{el} = 0$ , in total absence of energy purchase from the grid, to  $c_{el} = 0,064 \text{ €/kWh}$ , actual cost value of electricity in Spain.

The trends obtained are presented, for both configurations, in the following graphs (*Figure 59* and *Figure 60*).

In the diagram related to CASE 1 (*Figure 59*), it emerges that generally a reduction in the cost of the electricity purchased by the plant leads to an increase in exergo-economic factors.

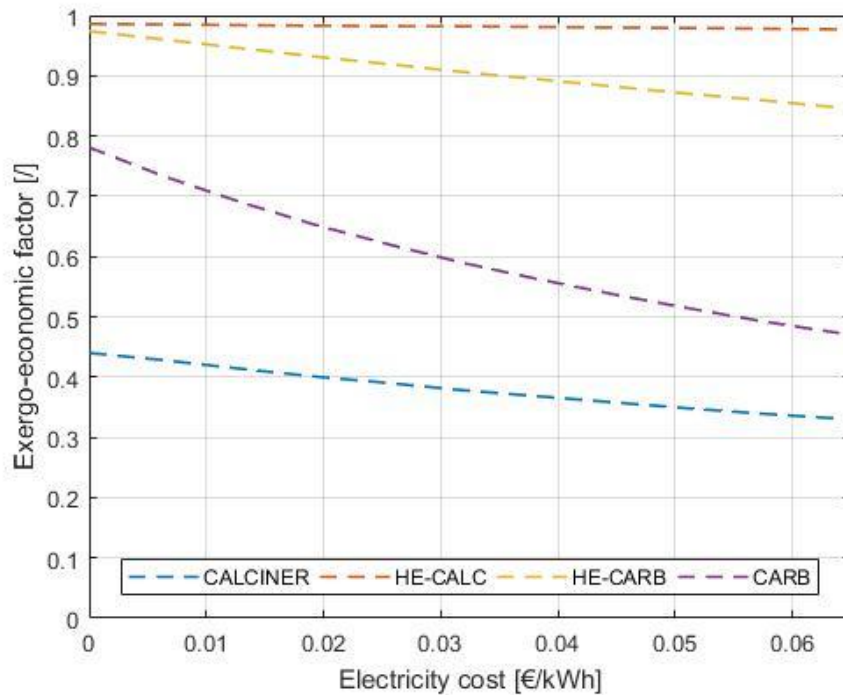


*Figure 59 - CASE 1, electricity cost variations*

The trend is attributable to a general lowering of the cost of fuel of the flows participating in the system, by virtue of the reduced cost-rate necessary to carry out the operations. The components showing a particularly significant change are the carbonator and exchanger system on the carbonator side, with a maximum deviation of 70 % and 35 % respectively. In the carbonator, in particular, such a wide variation is due to the fact that the "fuel" used for the subsequent production of electricity in the power cycle is basically the  $CO_2$  flow, for which a compressor with a high capacity ( $\sim 13 MW$ ) is operating in the HE-CARB heat exchanger system. The result is, therefore, a drastically reduced cost of fuel for the carbonator. The heat exchanger system on the calciner side (HE-CALC) does not show an equally drastic change due to the fact that the fuel considered for its operations is the  $CO_2$  coming out of the calciner, which depends on the thermal energy supplied by the incident solar radiation. Consequently, the component is not as dependent, according to the production structure considered, on the variation of the cost of the electricity consumed.

Considerably comparable results are obtained for the CASE 2 configuration, as represented in the following diagram (*Figure 60*).

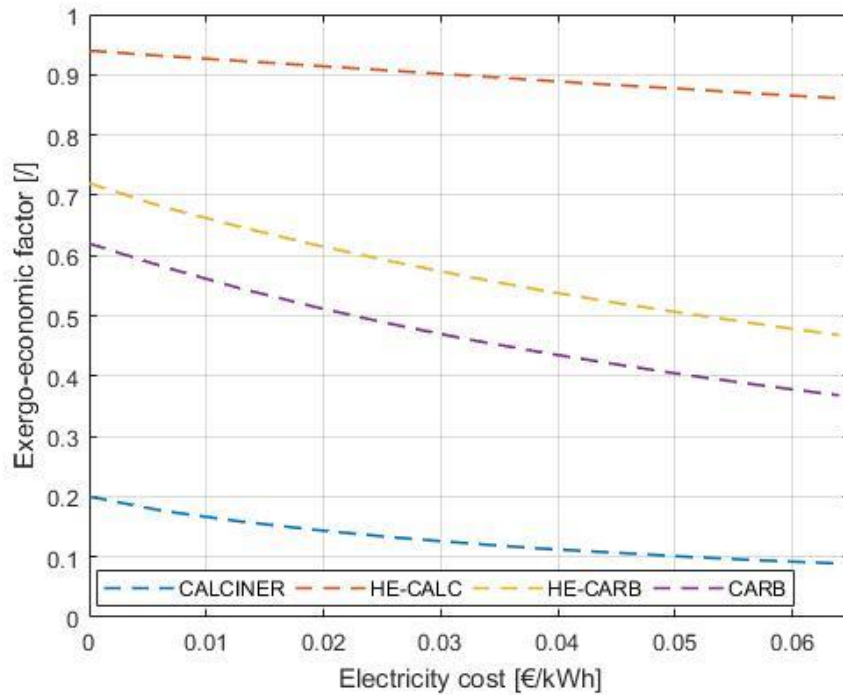


*Figure 60 - CASE 2, electricity cost variations*

Also in this case there is a behaviour influenced by the variations in the cost of electricity, whose increase leads to a reduction in the exergo-economic factor of the most important components. Specifically, if calciner, carbonator and heat exchanger systems on the carbonator side exhibit a trend that follows what already emerged in the previous analysis, some differences are encountered on the results of the heat exchanger system on the calciner side (HE-CALC). This reveals, in fact, a more pronounced reduction compared to CASE 1, with a percentage deviation in the exergo economic factor of up to 25 % overall. The discrepancy may be justified by examining the plant articulation of the block. Specifically, it may be observed that, contrary to CASE 1, in CASE 2 the heat exchanger system also involves the flow of  $CaO$  coming out of the calciner, which requires refrigeration before being sent to the low temperature storage system. Consequently the production structure of the block is significantly different compared to CASE 1, including two streams of  $CaO$ , one incoming and one outgoing, in addition. In this way, the operation of the component is more influenced by the variation in the cost of electricity, which translates into a lower cost of fuel of the solids stream coming from the carbonator and used, as a resource in this case, for the cooling of the  $CaO$ .

## CHAPTER 5

### LCA OF CSP-CaL INTEGRATION

#### 5.1. LCA, Life Cycle Assessment: main concepts

As a consequence of growing environmental challenges and the necessity to safeguard natural ecosystems and slow down the process of climate change, many industries and businesses have recently taken a keen interest in the environmental impacts generated by their activities, with the aim of orienting them towards more sustainable and socially acceptable pathways. As a direct result, many environmental management systems have been developed to facilitate the evaluation of the environmental performance of a production process or a specific activity, in order to transform it into a "greener" process by implementing strategies to contain the pollution caused. In this context, Life Cycle Assessment (LCA) is, without any doubt, an extremely effective tool.

Life Cycle Assessment is an operational methodology that allows the assessment of the environmental impacts potentially deriving from a specific activity or a specific product during its entire life cycle. The LCA is a primary tool to support the decision making process in terms of environmental sustainability and identify the best strategies to make the activity less impactful.

The procedures for a correct implementation of the method are fully defined in the ISO 14040 and ISO 14044 standards indicated by The International Standardization Organization [117]. They provide information and guidelines on the methodology, framework and operational and procedural structure to be followed for an appropriate application of the analysis.

The possibilities offered by the LCA analysis are variable and can be used for a wide variety of purposes. It is useful, for example, in the environmental characterization of a certain product or a certain process, defining, in this manner, a baseline useful to adopt subsequent decisions and achieve improvements in terms of environmental impacts. It also lends itself to the identification of possible strategies at regional or national level,

thus also acting as a valuable support in the political administration of a territory. It plays a significantly influential role in the marketing field, ensuring not only to investigate the impacts of specific products, but also to provide information to consumers and guide their purchasing decisions accordingly [120].

In general, LCA is a method that allows to study the life cycle of the process or product in question, modify it by implementing different scenarios and applying appropriate policies and, eventually, defining the most convenient one in the perspective of sustainable development. Consequently, it has a significant function in defining direction and priorities in the planning of future strategies [118].

Ultimately, the implementation of the LCA method contributes to the promotion of sustainable development by identifying the materials and processes with the greatest impact within the life cycle of a given activity. In this way, the redesign of the process is encouraged with the aim of removing those components that reduce its environmental performances. Furthermore, it represents an important indicator in the evaluation of the influence of certain life cycles on human health and resources depletion, adding useful arguments to facilitate decision-making in the selection of the most convenient option [119].

#### 5.1.1. Different LCA approaches

The application modalities and, necessarily, the results obtained following an LCA analysis may differ depending on the level of detail with which the analysis of a given life cycle is chosen. There are various methodologies through which to consider the process, depending essentially on the definition of system boundaries and the inclusion or exclusion of more or less significant parts of the life cycle.

There are various ways to set up the analysis by virtue of a considerable elasticity and dependence on the type of results required. To make a general classification of the most common approaches, it is possible to distinguish three different levels: Cradle-to-Grave, Cradle-to-Gate and Cradle-to-Cradle [118].

##### 5.1.1.1. Cradle-to-Grave

The Cradle-to-Grave approach is the most comprehensive and represents a full life cycle assessment. It includes all the processes involved, from the extraction of raw materials and their manufacturing (Cradle) to the disposal phase (Grave). In this way all impacts generated by the product or process under consideration during its full life cycle

are quantified, thus including analytical aspects that could be neglected in traditional and less detailed analyses [118].

An example of a Cradle-to-Grave approach for a life cycle is proposed in the following figure (Figure 61).

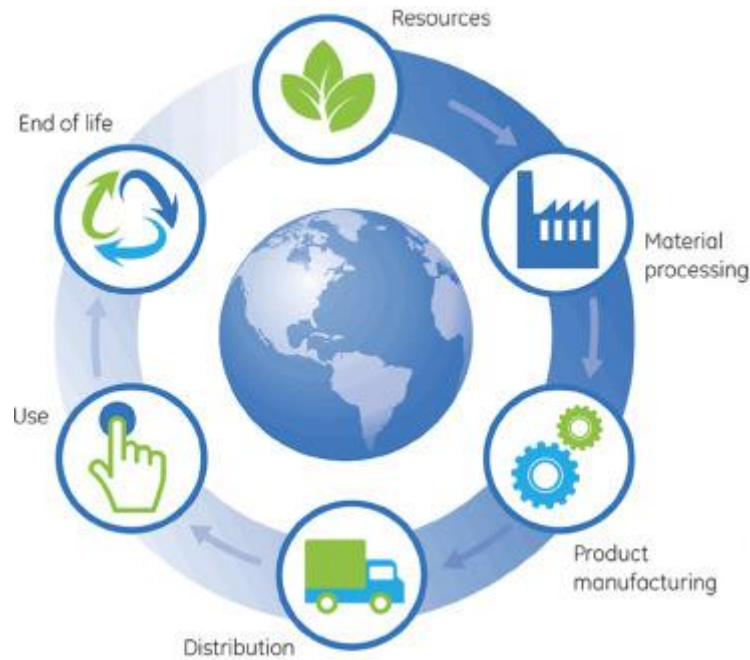


Figure 61 - LCA, Cradle-to-Grave approach [119]

#### 5.1.1.2. Cradle-to-Gate

The Cradle-to-Gate approach is more restrictive than the previous one. It comprises all the processes from extraction and manufacturing (Cradle) to the factory gate, excluding the stages of transport to the consumer, use and disposal [118], as shown in the figure below.

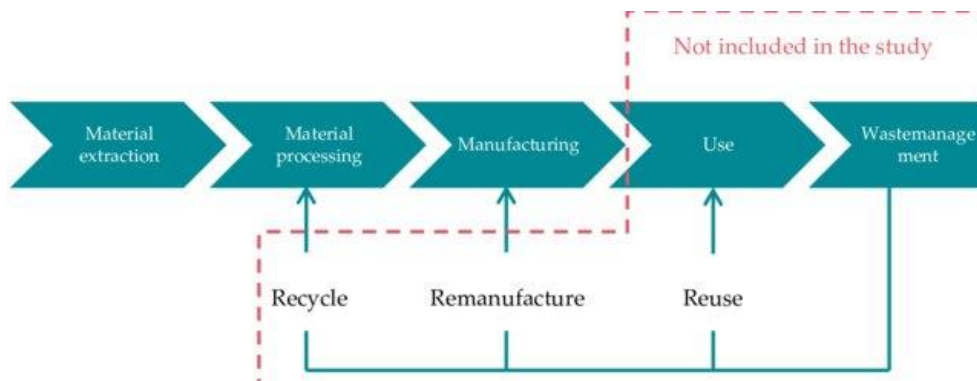


Figure 62 - LCA, Cradle to Gate approach [121]

### 5.1.1.3. Cradle-to-Cradle

The Cradle-to-Cradle approach can be intended as a complement to the well-known Cradle-to-Grave. It is essentially based on the same principle but includes processes from extraction and manufacturing (Cradle) to material recycling and reuse (Cradle). Basically, it is useful for the analysis of life cycles characterized by a final recycling process from which it is possible to obtain materials that can be used as raw materials in the same process. In this way an effective closure of the life cycle of a product or process occurs [118]. The following figure (Figure 63) shows a similar scheme to the one proposed in (Figure 61), with the addition of the "reuse" section, which defines the Cradle-to-Cradle approach.

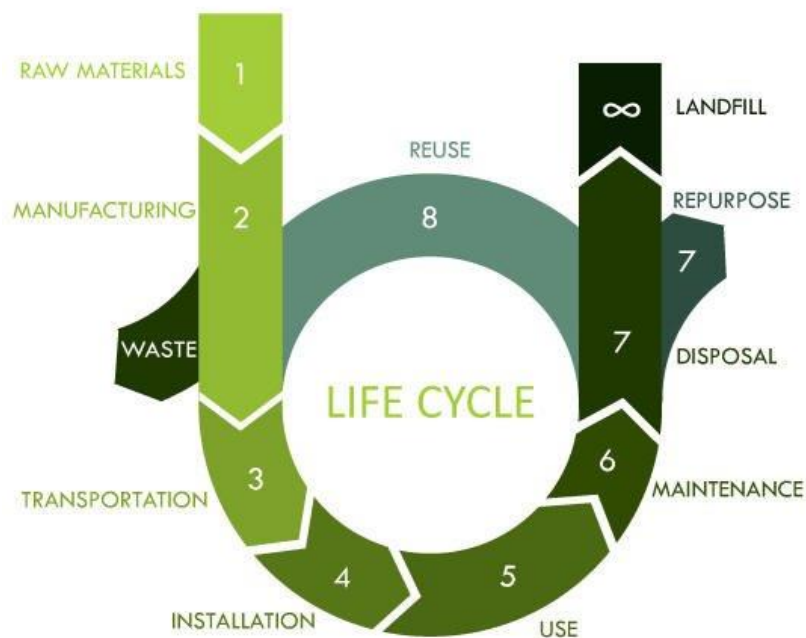


Figure 63 - LCA, Cradle-to-Cradle approach [122]

### 5.1.2. LCA recommended structure

As indicated in the standards ISO 14040 and ISO 14044, the recommended structure for the articulation of a Life Cycle Assessment is shown in the following figure (Figure 64). It consists of four main steps: Goal and Scope definition, Life Cycle Inventory (LCI), Life Cycle Impact Assessment (LCIA) and Interpretation of the results. The two-way arrows used in the figure explain another important feature of the LCA: its iterative nature and the possibility, if necessary, to repeat certain steps during the analysis to obtain the required results.

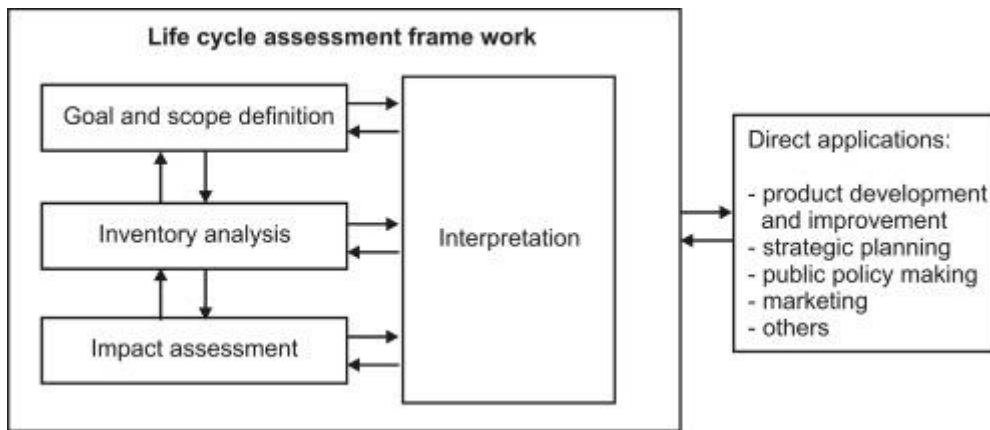


Figure 64 - LCA recommended structure [118]

### 5.1.2.1. Goal and Scope definition

Goal and Scope definition is the initial step of the LCA process. It involves the definition of the objective of the analysis and the full description of the product or process analysed.

Specifically, in the goal definition process, it is also advisable to clarify what could be possible future developments of the results obtained and in which area they could be useful. An indication of the target audience for the analysis would add further validity to the project [118].

The scoping phase, on the other hand, is of fundamental importance in order to fully indicate the subject of the analysis. It is at this stage that the system boundaries are defined, which are necessary to deduce how the analysis will be carried out and the types of processes to be included or excluded from it [119].

Moreover, another aspect of absolute relevance is the choice of the Functional Unit. It defines the unit of measurement to which the results are referred. It follows therefore that its definition is crucial as it strongly influences the quality and type of results obtained. The Functional Unit tends to be chosen using standard quantities and units of measurement (for example, for electricity generation plants, a suitable Functional Unit could be 1kWh or 1 MJ of electricity produced). This simplifies the process of comparison among different LCAs related to different processes but with the same Functional Unit. The results, in fact, are comparable because they refer to the same Functional Unit [120].

Finally, it is fundamental to choose the environmental impact categories (climate change, resources depletion, human health etc.) through which to evaluate the performance of the plant.

### 5.1.2.2. Life Cycle Inventory (LCI)

The Life Cycle Inventory phase is of fundamental importance for the realization of the LCA analysis. It consists in the construction of an "inventory" including all the actors involved in the life cycle of the analysed product or process. It is necessary, therefore, to include any inputs and outputs that are relevant in terms of environmental impact caused. Any processes or materials that do not involve the production of a given impact will generally be neglected, since they have no significant influence on the final result of the analysis [118].

The inventory structuring process is generally one of the most challenging phases of the LCA methodology and sometimes one of its weak points. The activity results, in fact, very often extremely intensive in terms of time required and resources needed to obtain all the useful data. They include, on the other hand, all relevant information from the extraction of materials to any emissions generated by a given process. The following figure (Figure 65) clarifies the general scheme of articulation of the life cycle of a certain product or process, therefore indicating all the data required in the LCI phase [118].

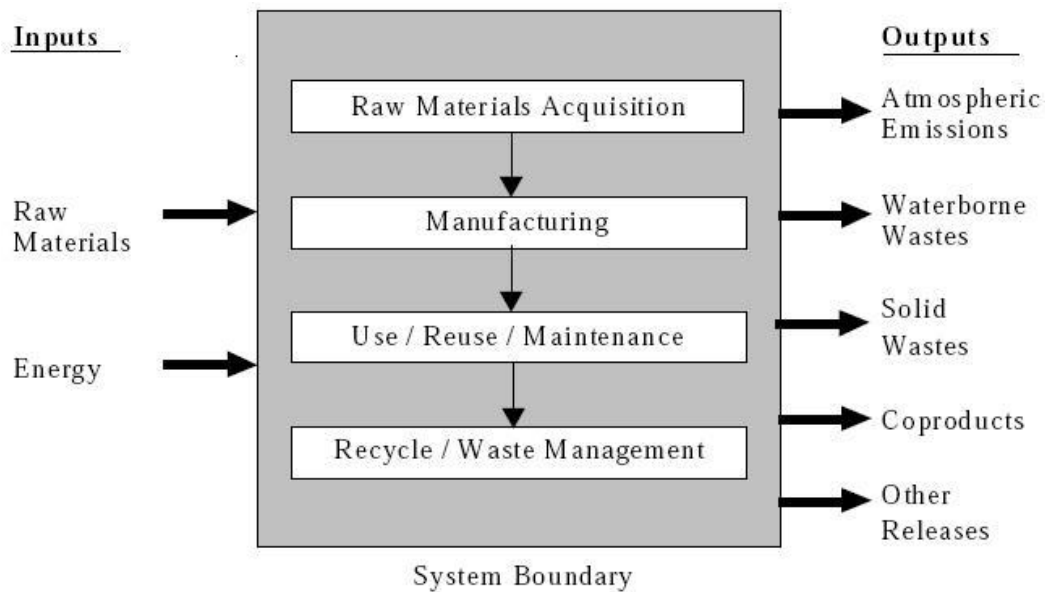


Figure 65 - Life Cycle Stages [123]

A properly articulated inventory includes both numerical data and qualitative information. Numerical data provides information on inputs and outputs of all activities involved in the life cycle, such as raw material inputs, energy or other physical inputs, products and co-products generated by processes, transport, processing and maintenance phases, quantification of emissions to the environment and waste generated. Of absolute importance in the construction of the inventory is to recalculate any numerical data

entered in order to express it consistently with the functional unit chosen in the goal and scope phase. Undoubtedly, considering the system boundaries adopted, it is necessary to conduct the data definition in compliance with mass and energy balances [118].

Qualitative information, on the other hand, is useful to include descriptions of the technologies used and the processes carried out, to clarify how the impacts generated are measured, to provide geographical location of the activities developed and to inform about the paths followed by input and output flows [120].

### 5.1.2.3. Life Cycle Impact Assessment (LCIA)

The purpose of the Life Cycle Impact Assessment (LCIA) phase is to study and describe the environmental consequences generated by the processes and activities listed in the previous Inventory phase. Starting, therefore, from the results of the LCI, it proceeds through the selection of appropriate categories of environmental impact, from which the effects of the life cycle of the product or process studied can be derived and classified [118]. The following figure explains the chronological sequence of the analysis steps.

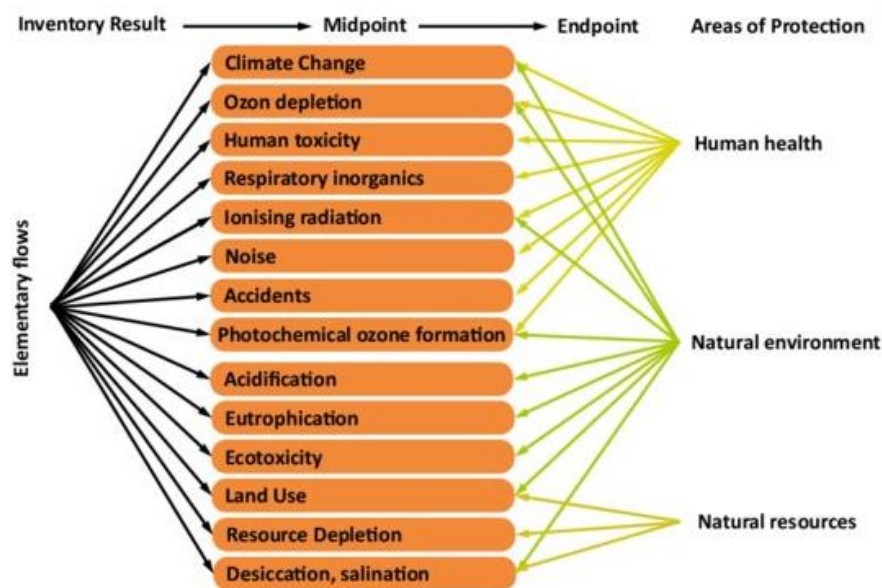


Figure 66 - Life Cycle Impact Assessment (LCIA) [124]

In accordance with the ISO standards mentioned above, the LCIA process is divided into different operational steps [117], [120]:

- 1) *Selection of Impact Categories*: first, it is necessary to identify the most significant environmental impact categories to be used in the analysis;

- 2) *Classification*: the results of the previous LCI are consequently classified in the selected impact categories;
- 3) *Characterization*: for each category, it is necessary to quantify the value of the environmental impact generated using appropriate conversion factors;
- 4) *Normalization*: if a comparison of the impacts caused by the different categories is required, the most appropriate method to proceed is to implement a normalisation of the previously identified values. In this way, it becomes possible to perform the comparative procedure;
- 5) *Weighting*: in this phase, a weight is given to each of the chosen impact categories. In this way, the evaluation of the environmental performance of a life cycle will depend on the importance given to the various categories.

If the Selection, Classification and Characterization phases are mandatory according to ISO standards, the final steps of Normalization and Weighting are optional. In particular, Normalization is mainly useful in case of comparison among categories. Weighting, on the other hand, has the disadvantage of including evaluation factors often dependent on conditions outside the pure life cycle analysis. In general, the assigned weights are derived from socio-economic and environmental evaluations that depend on public opinion, geographical location and the economic and social structure of the region analysed [121].

#### 5.1.2.4. Interpretation of the results

The final step of an LCA analysis is the interpretation of the results. It consists, naturally, in observing the results obtained in the previous steps, comparing them and drawing final conclusions summarising the information collected. The term "interpretation", in reality, implies the development of a real evaluation of the results obtained, with the aim of identifying any weaknesses, shortcomings, inconsistencies, critical points and aspects to be improved [118]. The LCA analysis is in fact based on the retrieval of a large amount of data, which very often are not all available from the same source. Some are obtained through experimental practices, others from various literature and others through hypotheses and equivalences. As a consequence, inevitably, the final results of the analysis are subject to a certain degree of uncertainty, requiring the process of interpretation.

In the ISO 14040 standard there are clear indications on how to implement the final step of interpretation, developing a critical review of the LCA and recognizing its limitations and critical points. The verification of the robustness of the results allows to make changes to the analysis according to an iterative principle whose final objective is to increase the validity of the method.

## 5.2. Goal & Scope of the analysis

The main goal of the following analysis is to evaluate the environmental impacts generated during the life cycle of a concentrated solar power plant with solar tower technology and thermochemical energy storage system based on the Calcium Looping process. In this regard, a comparative analysis is performed between two different plant configurations: plant with high temperature storage system and plant with storage system at ambient temperatures. For their characterization, the results of the simulations implemented with AspenPlus software and extensively discussed in the previous chapters are used.

### 5.2.1. Functional Unit

The two plants are characterised by slightly different electricity production and consumption. In order to simplify the comparison procedure and to provide more adaptability to the results, the analysis is conducted using  $1 \text{ MWh}_{el}$  of electricity production as functional unit over a 25-year period of operation. The choice not only makes the two plants, both assumed to be producers of the same amount of energy, comparable, but also allows comparison with any results obtained from other LCA analyses on different installations. The inventory proposed in the next paragraph shows the quantification of the main materials and processes in actual terms compared to the actual production of the two installations. When inserted in the software, they are recalculated per unit of  $\text{MWh}_{el}$  in order to adapt them to the chosen functional unit.

### 5.2.2. System Boundaries

The LCA procedure is implemented according to the "cradle-to-grave" methodology. It comprises, i.e., any process between the extraction of raw materials and the final dismantling of the plant with subsequent disposal, incineration or recycling of the waste. In the construction phase, the processes of extraction of raw materials, processing and transport to the construction site, where they undergo manufacturing and assembling processes, are considered. Maintenance operations carried out during the "use phase" of the plant are also included. As regards the end-of-life scenario, furthermore, possible recycling and landfill activities of the materials are envisaged. The percentage allocated to the relevant processes is indicated for each of them. The recycling process, however, is not properly accounted for since the products of the activity are not directly reused in the same plant. Furthermore, the impacts due to the

use of workforce and specific construction processes are excluded from the study area. Finally, the land occupation is neglected from the inventory. For simplicity, it is assumed that the plant is located in Andalusia, approximately where Gemasolar is currently located, so that the corresponding inventory can be used as a reference.

The articulation of the applied method and the resulting selected system boundaries are described in the following figure.

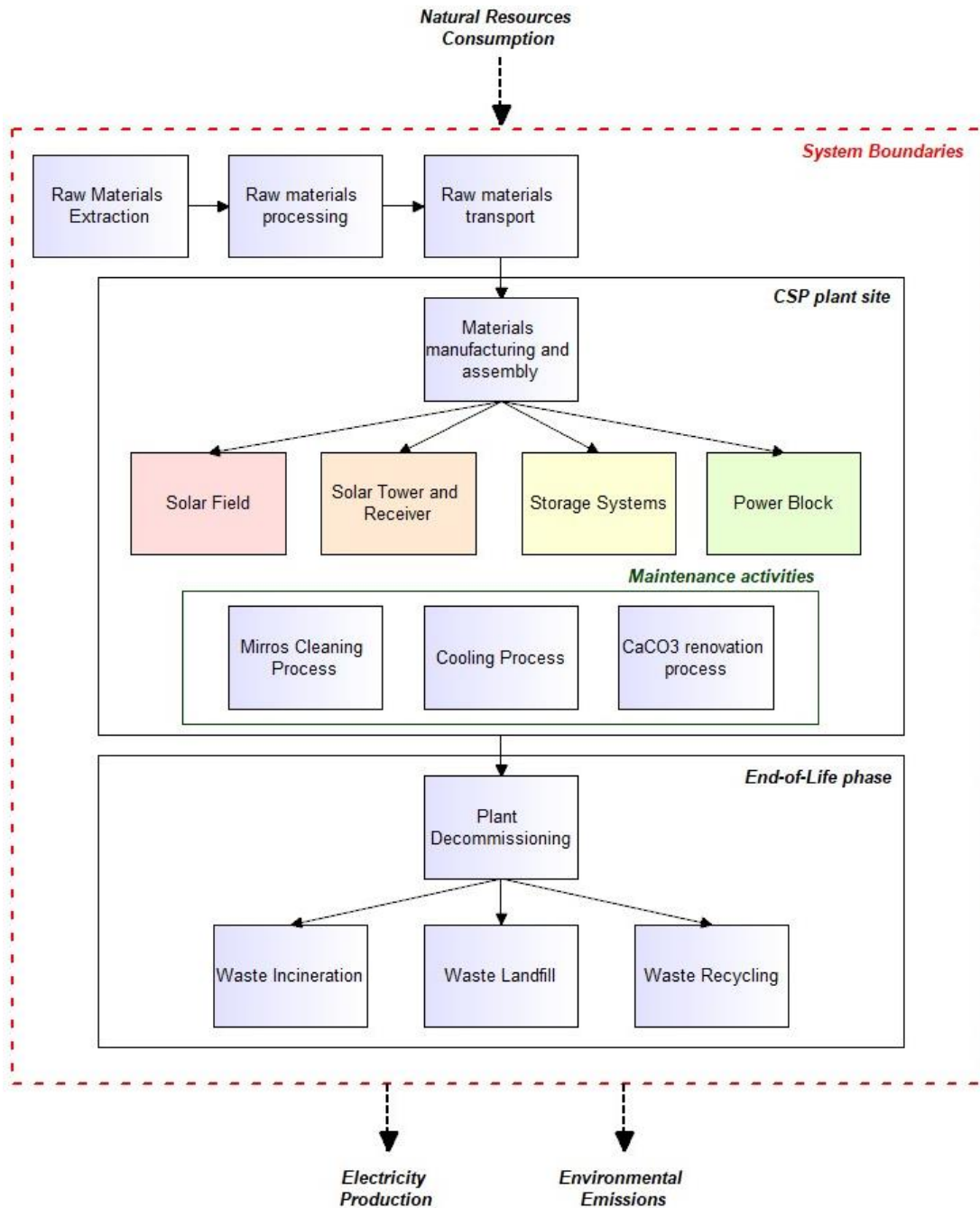


Figure 67 - Definition of system boundaries

### 5.2.3. Methodology and Indicators

The assessment of the environmental impacts produced during the analysed life cycle is carried out through the application of the IMPACT 2002+ Midpoint indicator, included in the database provided with the SimaPro 8.1 software.

IMPACT 2002+ is a combination of four methods: IMPACT 2002 (Pennington et al. 2005), Eco-indicator 99 (Goedkoop and Spriensma. 2000, 2nd version, Egalitarian Factors), CML (Guinée et al. 2002) and IPCC. It proposes a characterisation of the process studied in 15 midpoint impact categories (human toxicity, respiratory effects, ionizing radiation, ozone layer depletion, photochemical oxidation, aquatic ecotoxicity, terrestrial eco-toxicity, terrestrial acidification/nitrification, aquatic acidification, aquatic eutrophication, land occupation, global warming, non-renewable energy, mineral extraction). They are furthermore grouped into four main categories: Human Health, Ecosystem Quality, Climate Change, Resources [128].

During standardisation and weighing, the method also ensures the possibility of comparing the different categories on the basis of equivalent benchmarks. The concept of normalization is mainly useful to obtain a summary picture of the results obtained for the different impact categories, proposing the identification of the share of each category on the total damage caused. The assessment of the normalised impact factor is achieved by dividing the impact per unit of emission typical of each category by the total impact of all substances in the specific category, per unit of person and year [128].

The IMPACT 2002+ method is a Midpoint type indicator, i.e. a parameter that in a cause-effect chain related to a given impact category, lies between the inventory phase and the category endpoint. It differs, therefore, from Endpoint indicators since the latter are organised in such a way as to characterise the critical points at the endpoint of a cause-effect chain [128]. According to (Bare et al., 2000), the convenience of a Midpoint indicator rather than an Endpoint depends on the type of analysis and the quality of results desired. Midpoints tend to be preferred in the study of categories such as Climate Change and Acidification, showing higher certainty but lower relevance for decision support [129]. Endpoints, on the other hand, have a higher relevance in directing decision making, but they lack in relevance. They are particularly useful to ensure that society has an appropriate perception of the final effects of a given life cycle, such as information on Human Health and Biodiversity Change [129].

Ultimately, there is no substantial criterion to prefer one type of indicator. In general, in LCA investigations that are particularly complex and relevant to the decision-making process, one solution would be to apply the two simultaneously in order to limit gaps and exploit their strengths [129].

### 5.3. Life Cycle Inventory Analysis (LCIA)

The development of an adequate inventory to estimate the environmental impacts generated during the life cycle of a large production plant requires various resources and a combination of different databases.

The implementation of the model on SimaPro 8.1 software has been realized using the Ecoinvent v3.1 database, through which to find the necessary materials and processes. For the modelling of the heliostatic field, the solar tower, the receiver, the storage system and the power block, however, the information contained in Ecoinvent are not sufficient. It was therefore necessary to find and estimate the materials and processes involved, simplifying the structuring of the inventory with the adoption of appropriate assumptions.

In order to simplify the process, four fundamental blocks into which to divide the plant are considered: heliostatic field, solar tower and receiver, storage systems and power block. The inventory of the first two is assumed to be the same for both CASE 1 and CASE 2. For the characterization of the components making up the system, reference is made to the two AspenPlus simulations examined in the previous chapters.

#### 5.3.1. Solar Field

For the construction of the solar field inventory, analogies are used with the Gemasolar plant, CSP with Solar Tower technology, built near Seville. In particular, (Kuenlin et al., 2013) [125], proposes a comparative LCA study between various types of solar installations, including the Gemasolar system. Therefore, the inventory proposed in this study is used as reference, adopting as a modification parameter the extent of the solar field, intended as the total area of reflecting surface. The Gemasolar system records a total area of  $318000 \text{ m}^2$ . According to (Ortiz et al.), from the simulation performed with SolarPILOT, assuming the use of mirrors with a surface area of  $36 \text{ m}^2$ , a solar field with a total of 6081 mirrors results [126]. The total area can therefore be estimated in  $218916 \text{ m}^2$ . Starting from this data, it is possible to propose the inventory built by (Kuenlin et al., 2013) and obtain the following.

<i>Element</i>	<i>Ecoinvent Equivalence</i>	<i>Quantity</i>	<i>Unit</i>
<i>Solar Mirrors</i>	<i>Flat Glass, Coated {RER}</i>	$2,19 \times 10^6$	<i>kg</i>
<i>Steel Structure</i>	<i>Reinforcing Steel {RER}</i>	$7,71 \times 10^6$	<i>kg</i>
<i>Steel Structure Manufacturing</i>	<i>Metal Working, average for steel</i>	$7,71 \times 10^6$	<i>kg</i>

<i>product manufacturing {RER}</i>			
<i>Foundation Concrete</i>	<i>Concrete, sole plate and foundation {CH}</i>	$5,69 \times 10^3$	$m^3$
<i>Excavation process</i>	<i>Excavation, Hydraulic Digger {RER}</i>	$5,69 \times 10^3$	$m^3$

*Table 44 - Solar Field LCI*

For the solar field, a maintenance inventory of mirror cleaning activities is additionally created. This activity is included in the LCA as it is of considerable importance for the preservation of a certain value of plant operational performances. Also in this case, the values indicated in (Kuenlin et al., 2013) are adapted based on the size of the solar field. A complete cleaning every two weeks during the 25 years of the system's life is therefore considered. For the transport, transport by lorry for an average distance of 100 km is assumed. The following additional inventory is then obtained.

<i>Element</i>	<i>Ecoinvent Equivalence</i>	<i>Quantity</i>	<i>Unit</i>
<i>Cleaning water</i>	<i>Water, deionised, from tap water, at user {RER}</i>	$1,20 \times 10^8$	<i>kg</i>
<i>Water transport</i>	<i>Transport, freight, lorry, 7,5-16 t, EURO3 {RER}</i>	$1,20 \times 10^7$	<i>tkm</i>

*Table 45 - Solar Field LCI, Maintenance*

In addition, it is necessary to consider the impacts associated to the transport of the materials included in the inventory. For the production of the solar mirrors used in the heliostat field, the company involved in this area for the Gemasolar power plant was SENER. Having numerous establishments on Spanish territory (especially near Madrid, Valencia and Barcelona), it is reasonable to assume an average distance for the transport of solar mirrors by road of about 600 km. As far as steel and cement are concerned, an average road transport distance of 100 km is assumed due to the numerous activities involved in these sectors in Andalusia. This results in the following inventory:

<i>Element</i>	<i>Ecoinvent Equivalence</i>	<i>Quantity</i>	<i>Unit</i>
<i>Total material transport</i>	<i>Transport, freight, lorry, 7,5-16 t, EURO3 {RER}</i>	$7,31 \times 10^6$	<i>tkm</i>

*Table 46 - Solar Field LCI, Transport*

### 5.3.2. Solar Tower and receiver

The Solar Tower and receiver inventory includes all the main materials and processes required for the construction of the infrastructure. Also in this case, given the design similarities, the inventory proposed by (Kuenlin et al., 2013) is used as reference. In particular, the height of the tower is used as a comparison parameter. Gemasolar consists of a solar tower 140 meters high. In accordance with (Ortiz et al.), a 100 meter high solar tower is assumed in the modelling of the system in question [126]. Using this data it is possible to recalculate the values in the inventory used as reference [125], and obtain the following.

<i>Element</i>	<i>Ecoinvent Equivalence</i>	<i>Quantity</i>	<i>Unit</i>
<i>Steel Receiver structure</i>	<i>Steel, chromium Steel 18/8 {RER}</i>	$4,28 \times 10^3$	<i>kg</i>
<i>Receiver Manufacturing</i>	<i>Metal working, average for chromium steel product manufacturing {RER}</i>	$4,28 \times 10^3$	<i>kg</i>
<i>Cold Pipes</i>	<i>Reinforcing Steel {RER}</i>	$2,69 \times 10^3$	<i>kg</i>
<i>Cold Pipes Manufacturing</i>	<i>Metal working, average for steel product manufacturing {RER}</i>	$2,69 \times 10^3$	<i>kg</i>
<i>Hot Pipes</i>	<i>Reinforcing Steel {RER}</i>	$2,76 \times 10^3$	<i>kg</i>
<i>Hot Pipes Manufacturing</i>	<i>Metal working, average for steel product manufacturing {RER}</i>	$2,76 \times 10^3$	<i>kg</i>
<i>Tower Concrete</i>	<i>Concrete, sole plate and foundation {CH}</i>	$3,62 \times 10^3$	$m^3$
<i>Tower Excavation</i>	<i>Excavation, Hydraulic Digger {RER}</i>	$1,43 \times 10^2$	$m^3$
<i>Tower Steel</i>	<i>Reinforcing Steel {RER}</i>	$3,62 \times 10^5$	<i>kg</i>

*Table 47 - Solar Tower and Receiver LCI*

The inventory of solar towers and receivers does not include materials or processes associated with maintenance activities during the 25 years of the plant's life.

Also in this case it is necessary to consider the impacts from the transport of the materials. Specifically, for common steel and concrete the same assumptions listed in the heliostat field inventory are used. As regards the construction of central receivers and solar towers, on the other hand, SENER is once again the company commissioned with the project. Consequently, the estimate of 600 km of average road transport is adopted. This results in the following inventory:

<i>Element</i>	<i>Ecoinvent Equivalence</i>	<i>Quantity</i>	<i>Unit</i>
<i>Total material transport</i>	<i>Transport, freight lorry, 7,5-16 t, EURO3 {RER}</i>	$5,45 \times 10^6$	<i>tkm</i>

*Table 48 - Solar Tower and Receiver LCI, Transport*

### 5.3.3. Storage systems

The storage system inventory comprises all the components included in the two configurations and not directly involved in power generation in the power block. More in detail, the CALCINER, HE-CALC, CO<sub>2</sub>-COMP and any intermediate CO<sub>2</sub>, CaO and solids intercoolers are considered in this section. In the same way, impacts from the materials and production processes of the three storage systems are naturally included. The calcium carbonate extraction and transport process is also added to this inventory. Therefore, the components related to the CARB block, containing the power cycle and the main gas turbine, as well as the heat exchanger system on the carbonator side (HE-CARB) are excluded from the analysis. They will be discussed in the power block inventory.

The following assumptions were adopted in the process of defining the inventory of storage systems:

- According to (Ortiz et al.), 3409 tonnes are assumed as the amount of CaCO<sub>3</sub> supplied to the system, i.e. the volume needed to completely fill the storage system and ensure its continuous operation for the 16 hours of absence of radiation [126]. Furthermore, calcium carbonate is considered undergoing a periodic renovation of 1% per month during the 25 years of operation, in order to avoid sorbent degradation. The quantity removed will be allocated to specific disposal processes during the use-phase of LCA;
- Still using the information identified by (Ortiz et al.), it is possible to derive the impacts arising from the production of the storage systems. In particular, in “*Off-Design Model of Concentrating Solar Power Plant with Thermochemical Energy Storage Based on Calcium-Looping*”, volume estimates of stored solids are indicated, as anticipated in the previous paragraph 3.1.2. It is assumed that the storage for CaCO<sub>3</sub> and CaO are made of stainless steel, while the pressurized tank for CO<sub>2</sub> is made of chromium and molybdenum doped stainless steel. For the latter, given the absence in the Ecoinvent database of the specific alloy indicated, chromium steel 18/8 is chosen. In order to obtain the amount of material necessary for their construction, it is assumed that the external volume of the solids storage is 10% of that indicated above for high temperature storage

(CASE 1) and 5% for the case at ambient temperature (CASE 2). The quantity of material used in the construction is obtained through the following relation.

$$m_{stor} = (V_{ext} - V_{solids}) \cdot \rho \quad (5.1)$$

Where  $\rho$  indicates the density of the material used, equal to  $\rho = 7800 \text{ kg/m}^3$  for stainless steel and  $\rho = 7980 \text{ kg/m}^3$  for chromium and molybdenum doped stainless steel;

- The impact assessment of the calciner reactor is obtained by assuming a cylindrical shape of the component with reasonable dimensions of  $d_{int} = 1,7 \text{ m}$ ,  $H = 22,5 \text{ m}$ ,  $thickness = 0,1 \text{ m}$ , in accordance with *SOCRATCES* project equipment. This results in the amount of material used for its construction using the formula:

$$m_{calc} = \left[ \left( \frac{d_{int}}{2} + thickness \right)^2 - \left( \frac{d_{int}}{2} \right)^2 \right] \cdot \pi \cdot H \cdot \rho \quad (5.2)$$

Where  $\rho = 7800 \text{ kg/m}^3$  indicates the density of the main material of which it is composed, taken as stainless steel. It should be specified that calciner and carbonator are considered twin reactors, which is why the hypothesis above also applies to the evaluation of the subsequent power block;

- The assessment of the impacts related to heat exchangers is carried out using the heat exchange area as a scale parameter. The estimate of the quantity of material used in their construction is obtained by the following formula:

$$m_{HXS} = A_{HE} \cdot s \cdot \rho \cdot 1,1 \quad (5.3)$$

In which,  $A_{HE}$  indicates the heat exchange surface of each heat exchanger.  $s$ , on the other hand, indicates the thickness of the heat exchange surface. It assumes an average value of 0,002 meters for each exchanger. The factor 1.1 indicates a 10% increase on the volume calculated to consider the other components that make up the exchanger.  $\rho$ , finally, indicates the density of the material used. In particular, it is assumed that stainless steels are used for solid/gas and solid/solid type heat exchangers. For gas/gas and water/gas, where the corrosive activities are less intense, it is assumed to use carbon steel, which is cheaper than the

previous one [127]. In the Ecoinvent database, this is indicated with a low-alloyed steel equivalent;

- Turbines and compressors are evaluated by directly adapting the corresponding processes in the Ecoinvent inventory and indicating a number of items so that the sizes match. Processes of electricity production and consumption are associated with them, assuming valid, in this case, the self-productive capacity of the plant and not including a direct purchase from the electricity grid;
- In CASE 1 there is a steam turbine power cycle in the HE-CALC block. If the estimation of the turbine has been analysed in the following section, the impacts related to water use should be considered. The amount used is calculated considering the flow rate of  $3,74 \text{ kg/s}$  resulting from the AspenPlus simulation and assuming an hourly amount of  $1,35 \cdot 10^4 \text{ kg}$ . To this is added the impact resulting from transport, assumed on road for an average distance of 100 km;
- For the various materials analysed in this paragraph, a road transport with an average distance of 100 km is assumed.

The descriptive inventory of all the components included in the "storage systems" block, following the plant configuration derived from the models implemented on AspenPlus, is shown below.

<i>Element</i>	<i>Ecoinvent Equivalence</i>	<i>CASE 1</i>	<i>CASE 2</i>	<i>Unit</i>
<i>Calcium carbonate</i>	<i>Calcium carbonate &gt; 63 micron, production, at plant, EU-27</i>	$3,40 \times 10^6$	$3,40 \times 10^6$	<i>kg</i>
<i>Calcium carbonate, transport</i>	<i>Transport, freight lorry, 3,5-7,5 t, EURO3 {RER}</i>	$3,40 \times 10^6$	$3,40 \times 10^5$	<i>tkm</i>
<i>CaCO3 storage material</i>	<i>Steel, chromium Steel 18/8 {RER}</i>	$1,64 \times 10^6$	$8,19 \times 10^5$	<i>kg</i>
<i>CaCO3 storage manufacturing</i>	<i>Metal working, average for chromium steel product manufacturing {RER}</i>	$1,64 \times 10^6$	$8,19 \times 10^5$	<i>kg</i>
<i>CaO storage material</i>	<i>Steel, chromium Steel 18/8 {RER}</i>	$2,39 \times 10^6$	$1,19 \times 10^6$	<i>kg</i>
<i>CaO storage manufacturing</i>	<i>Metal working, average for chromium steel product manufacturing {RER}</i>	$2,39 \times 10^6$	$1,19 \times 10^6$	<i>kg</i>
<i>CO2 storage material</i>	<i>Steel, chromium Steel 18/8 {RER}</i>	$3,7 \times 10^5$	$3,7 \times 10^5$	<i>kg</i>
<i>CO2 storage manufacturing</i>	<i>Metal working, average for chromium steel product manufacturing {RER}</i>	$3,7 \times 10^5$	$3,7 \times 10^5$	<i>kg</i>

<i>Calciner material</i>	<i>Steel, chromium Steel 18/8 {RER}</i>	$9,90 \times 10^4$	$9,90 \times 10^4$	<i>kg</i>
<i>Calciner manufacturing</i>	<i>Metal working, average for chromium steel product manufacturing {RER}</i>	$9,90 \times 10^4$	$9,90 \times 10^4$	<i>kg</i>
<i>HX1 materials</i>	<i>Steel, chromium Steel 18/8 {RER}</i>	$9,90 \times 10^2$	$3,43 \times 10^4$	<i>kg</i>
<i>HX1 manufacturing</i>	<i>Metal working, average for chromium steel product manufacturing {RER}</i>	$9,90 \times 10^2$	$3,43 \times 10^4$	<i>kg</i>
<i>HX2 materials</i>	<i>Steel, chromium Steel 18/8 {RER}</i>	$4,51 \times 10^3$	$1,14 \times 10^4$	<i>kg</i>
<i>HX2 manufacturing</i>	<i>Metal working, average for chromium steel product manufacturing {RER}</i>	$4,51 \times 10^3$	$1,14 \times 10^4$	<i>kg</i>
<i>HE-CALC intercooler</i>	<i>Steel, low-alloyed {RER}</i>	$1,80 \times 10^3$	/	<i>kg</i>
<i>HE-CALC intercooler manufacturing</i>	<i>Metal working, average for steel product manufacturing {RER}</i>	$1,80 \times 10^3$	/	<i>kg</i>
<i>HE-CALC condenser</i>	<i>Steel, low-alloyed {RER}</i>	$5,60 \times 10^3$	/	<i>kg</i>
<i>HE-CALC condenser manufacturing</i>	<i>Metal working, average for steel product manufacturing {RER}</i>	$5,60 \times 10^3$	/	<i>kg</i>
<i>HE-CALC steam turbine</i>	<i>Gas turbine, 10 MW electrical {RER}</i>	0,3	/	<i>items</i>
<i>Electricity production</i>	<i>Electricity, high voltage {ES}</i>	$2,19 \times 10^8$	/	<i>kWh</i>
<i>HE-CALC water</i>	<i>Water, deionised, from tap water, at user {RER}</i>	$1,35 \times 10^4$	/	<i>kg</i>
<i>HE-CALC water transport</i>	<i>Transport, freight, lorry, 7,5-16 t, EURO3 {RER}</i>	$1,35 \times 10^3$	/	<i>tkm</i>
<i>CO2 compressor</i>	<i>Air compressor, screw-type compressor, 300 kW {RER}</i>	13,2	24,2	<i>items</i>
<i>CO2 Electricity consumption</i>	<i>Electricity, medium voltage {ES}</i>	$2,88 \times 10^8$	$5,31 \times 10^8$	<i>kWh</i>
<i>CO2 intercooler</i>	<i>Steel, low-alloyed {RER}</i>	$1,15 \times 10^4$	$1,53 \times 10^4$	<i>kg</i>
<i>CO2 intercooler manufacturing</i>	<i>Metal working, average for steel product manufacturing {RER}</i>	$1,15 \times 10^4$	$1,53 \times 10^4$	<i>kg</i>
<i>CaO intercooler</i>	<i>Steel, chromium Steel 18/8 {RER}</i>	/	$6,47 \times 10^3$	<i>kg</i>
<i>CaO intercooler manufacturing</i>	<i>Metal working, average for chromium steel product manufacturing {RER}</i>	/	$6,47 \times 10^3$	<i>kg</i>
<i>Solids intercooler</i>	<i>Steel, chromium Steel 18/8 {RER}</i>	/	$7,21 \times 10^3$	<i>kg</i>
<i>Solids intercooler manufacturing</i>	<i>Metal working, average for chromium steel product manufacturing {RER}</i>	/	$7,21 \times 10^3$	<i>kg</i>

Table 49 - Storage systems LCI

Also for the storage system the impact generated by the transport (the one not included in the previous table) is considered, as follows.

<i>Element</i>	<i>Ecoinvent Equivalence</i>	<i>CASE 1</i>	<i>CASE 2</i>	<i>Unit</i>
<i>Total material transport</i>	<i>Transport, freight lorry, 7,5 – 16 t, EURO3 {RER}</i>	$4,52 \times 10^5$	$2,55 \times 10^5$	<i>tkm</i>

*Table 50 - Storage systems LCI, transport*

#### 5.3.4. Power block

The power block inventory includes all components belonging to the HE-CARB and CARB systems. It comprises, therefore, all the infrastructure necessary to achieve the ideal thermodynamic conditions so that the  $CO_2$  flow can be expanded in turbines and produce useful power..

The main components of the block are heat exchangers, intercoolers, compressors, turbines and the carbonator reactor. For all these, the assumptions listed in the analysis of the storage systems block are adopted. Consequently, the following inventory is derived.

<i>Element</i>	<i>Ecoinvent Equivalence</i>	<i>CASE 1</i>	<i>CASE 2</i>	<i>Unit</i>
<i>HX1 materials</i>	<i>Steel, chromium Steel 18/8 {RER}</i>	$1,88 \times 10^3$	$1,78 \times 10^3$	<i>kg</i>
<i>HX1 manufacturing</i>	<i>Metal working, average for chromium steel product manufacturing {RER}</i>	$1,88 \times 10^3$	$1,78 \times 10^3$	<i>kg</i>
<i>HX2 materials</i>	<i>Steel, chromium Steel 18/8 {RER}</i>	$2,90 \times 10^2$	$7,96 \times 10^3$	<i>kg</i>
<i>HX2 manufacturing</i>	<i>Metal working, average for chromium steel product manufacturing {RER}</i>	$2,90 \times 10^2$	$7,96 \times 10^3$	<i>kg</i>
<i>HX3 materials</i>	<i>Steel, low-alloyed {RER}</i>	$1,26 \times 10^5$	$1,22 \times 10^5$	<i>kg</i>
<i>HX3 manufacturing</i>	<i>Metal working, average for steel product manufacturing {RER}</i>	$1,26 \times 10^5$	$1,22 \times 10^5$	<i>kg</i>
<i>HX4 materials</i>	<i>Steel, chromium Steel 18/8 {RER}</i>	/	$1,68 \times 10^4$	<i>kg</i>
<i>HX4 manufacturing</i>	<i>Metal working, average for chromium steel product manufacturing {RER}</i>	/	$1,68 \times 10^4$	<i>kg</i>
<i>Intercooler materials</i>	<i>Steel, low-alloyed {RER}</i>	$2,59 \times 10^4$	$2,14 \times 10^4$	<i>kg</i>
<i>Intercooler manufacturing</i>	<i>Metal working, average for steel product manufacturing {RER}</i>	$2,59 \times 10^4$	$2,14 \times 10^4$	<i>kg</i>

<i>HE-CARB turbine</i>	<i>Gas turbine, 10 MW electrical {RER}</i>	0,08	0,11	<i>items</i>
<i>Electricity production</i>	<i>Electricity, high voltage {ES}</i>	$1,66 \times 10^8$	$2,30 \times 10^8$	<i>kWh</i>
<i>Main turbine</i>	<i>Gas turbine, 10 MW electrical {RER}</i>	2,72	2,65	<i>items</i>
<i>Electricity production</i>	<i>Electricity, high voltage {ES}</i>	$5,95 \times 10^9$	$5,79 \times 10^9$	<i>kWh</i>
<i>Main compressor</i>	<i>Air compressor, screw-type compressor, 300 kW {RER}</i>	42,5	36	<i>items</i>
<i>Electricity consumption</i>	<i>Electricity, medium voltage {ES}</i>	$2,79 \times 10^9$	$2,37 \times 10^9$	<i>kWh</i>
<i>Small compressor</i>	<i>Air compressor, screw-type compressor, 300 kW {RER}</i>	1,7	/	<i>items</i>
<i>Electricity consumption</i>	<i>Electricity, medium voltage {ES}</i>	$3,72 \times 10^7$	/	<i>kWh</i>

Table 51 - Power block LCI

The same considerations made in the previous paragraphs are also adopted for the power block with regard to the impacts deriving from the transport of substances. This results in the following inventory.

<i>Element</i>	<i>Ecoinvent Equivalence</i>	<i>CASE 1</i>	<i>CASE 2</i>	<i>Unit</i>
<i>Total material transport</i>	<i>Transport, freight lorry, 7,5 – 16 t, EURO3 {RER}</i>	$1,54 \times 10^4$	$1,70 \times 10^4$	<i>tkm</i>

Table 52 - Power block LCI, transport

Finally, in order to take into account the impacts generated by the use of water for cooling activities in intercoolers, the following quantities consumed in both cases during the 25 years of activity are calculated. They are assumed as impacts during the maintenance phase.

<i>Element</i>	<i>Ecoinvent Equivalence</i>	<i>CASE 1</i>	<i>CASE 2</i>	<i>Unit</i>
<i>Cooling water</i>	<i>Water, decarbonised {RER}</i>	$3,70 \times 10^7$	$5,50 \times 10^7$	<i>kg</i>
<i>Cooling water transport</i>	<i>Transport, freight lorry, 7,5 – 16 t, EURO3 {RER}</i>	$3,70 \times 10^6$	$5,50 \times 10^6$	<i>tkm</i>

Table 53 - Cooling water inventory

### 5.3.5. End-of-life inventory

Using as a reference the inventory adopted by (Kuenlin et al., 2013) for the Gemasolar installation [125], an inventory that takes into account the impacts of the activities carried out in the end-of-life scenario of the installation is constructed accordingly. This results in the following list.

<b>Material</b>	<b>Ecoinvent equivalence</b>	<b>Fraction</b>
<i>Reinforcing steel</i>	<i>Steel and iron (waste treatment) {GLO}, recycling</i>	<i>90%</i>
	<i>Scrap steel {CH}, treatment of, material landfill</i>	<i>10%</i>
<i>Low-alloyed steel</i>	<i>Steel and iron (waste treatment) {GLO}, recycling</i>	<i>90%</i>
	<i>Scrap steel {CH}, treatment of, material landfill</i>	<i>10%</i>
<i>Chromium steel</i>	<i>Steel and iron (waste treatment) {GLO}, recycling</i>	<i>90%</i>
	<i>Scrap steel {CH}, treatment of, material landfill</i>	<i>10%</i>
<i>Glass</i>	<i>Waste glass {CH}, treatment of, to municipal incineration</i>	<i>100%</i>
<i>Calcium carbonate</i>	<i>Limestone residue {CH}, treatment of, inert material</i>	<i>100%</i>
<i>Other</i>	<i>Inert waste, for final disposal {CH}</i>	<i>100%</i>

*Table 54 - End-of-life LCI*

### 5.3.6. Inventory conversion factor

In respect of the Functional Unit selected, it is necessary to adapt the impact estimates indicated in the inventory listed in the previous paragraphs. The correction factor applied is calculated by proportioning the real production of the two plants studied during the total life cycle (25 years) with the functional unit of  $1 \text{ MWh}_{el}$ . This method allows to make the two configurations comparable, otherwise characterized by different production values and, consequently, by non-proportional impacts.

The equation used for the calculation of the conversion factor is the following:

$$\text{Conversion factor} = \frac{1 \text{ MWh}_{el}}{\text{Real production} [\text{MWh}_{el}]} \quad (5.4)$$

The estimation of impacts and the construction of the LCA model on the software is carried out following the realistic hypothesis of energy self-production. It is assumed that the amount of energy consumed by compressors and auxiliary components is completely covered by the total energy produced by the plant. This allows the analysis to focus on the impacts associated with the plant itself and the integrated Calcium

Looping process. The estimate of the net energy produced by the plant is evaluated considering the items of energy production and energy consumption included in the inventory. The conversion factors of the two configurations are obtained in accordance with the following table.

<i>Classification</i>	<i>CASE 1</i>	<i>CASE 2</i>	<i>Unit</i>
<i>Power block energy production</i>	$6,12 \times 10^6$	$6,02 \times 10^6$	$MWh_{el}$
<i>Power block energy consumption</i>	$2,83 \times 10^6$	$2,37 \times 10^6$	$MWh_{el}$
<i>Storage systems energy production</i>	$2,19 \times 10^5$	/	$MWh_{el}$
<i>Storage systems energy consumption</i>	$2,88 \times 10^5$	$5,31 \times 10^5$	$MWh_{el}$
<i>Net energy production</i>	$3,22 \times 10^6$	$3,12 \times 10^6$	$MWh_{el}$
<i>Conversion factor</i>	$3,11 \times 10^{-7}$	$3,21 \times 10^{-7}$	/

*Table 55 - Conversion factors evaluation*

In particular, the two configurations analysed are assumed to have the same plant structure in terms of solar field and solar tower. Therefore, the inventory related to the two mentioned blocks is adapted using an equal conversion factor for both cases. For simplicity, an intermediate factor, equal to  $3,16 \times 10^{-7}$ , between the two calculated in the previous table, is applied.

#### 5.4. Life Cycle Assessment Analysis

Once the inventory of the various components that characterize the system and the different processes involved has been built, it is possible to proceed with the insertion of data on the SimaPro software to create the analysis model.

The articulation of the process consists of some substantial steps. The initial assembly phase, in which the plant construction process is described, is followed by the use phase, with the maintenance activities foreseen during the life cycle. Finally, the model goes through the final phase of the life cycle, including the processes of decommissioning, dismantling, disposal and possibly recycling or reuse scenarios.

The following paragraphs analyse the results obtained from software simulations, reporting information in terms of environmental impact in the main impact categories provided by IMPACT 2002+ Midpoint Indicator. The values will be reported in a normalised mode, so as to ensure a comparison between the two configurations analysed.

### 5.4.1. Assembly-Phase analysis

The assembly phase, in an LCA analysis, studies the impacts resulting from the construction processes of the analysed model. With regard to the two CSP plant configurations with integration of Calcium Looping thermochemical energy storage system, the software makes it possible to evaluate first of all the impacts generated by the assembly of the individual subsystems (Power Block, Solar Field, Solar Tower and Storage System) and, consequently, the total impacts related to the construction of the plant. The processes of extraction, manufacturing and transport of the materials used, as well as their assembly on site, are included in the analysis.

The following figures propose the connection network between the main processes involved in the assembly phase of the two observed cases.

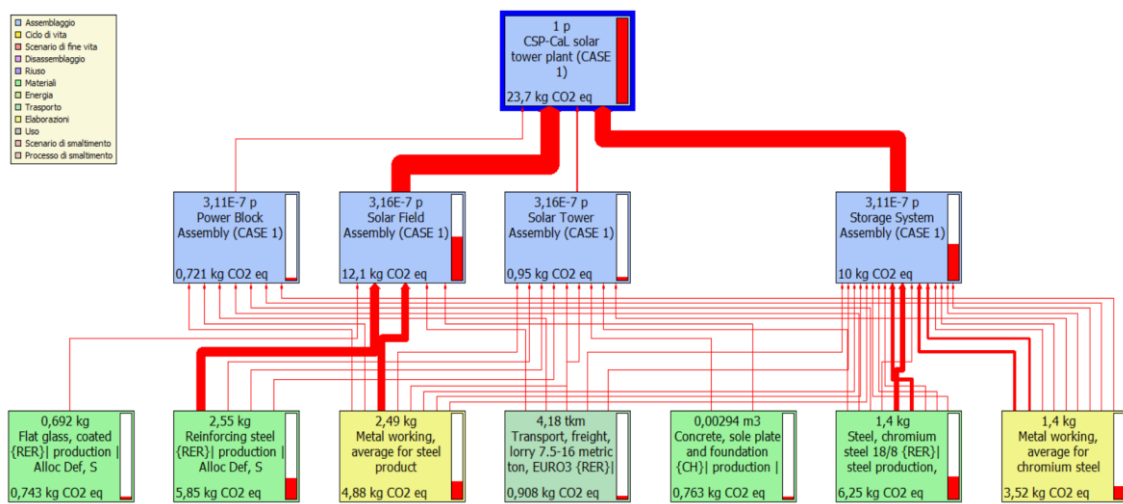


Figure 68 - Assembly-Phase CASE 1

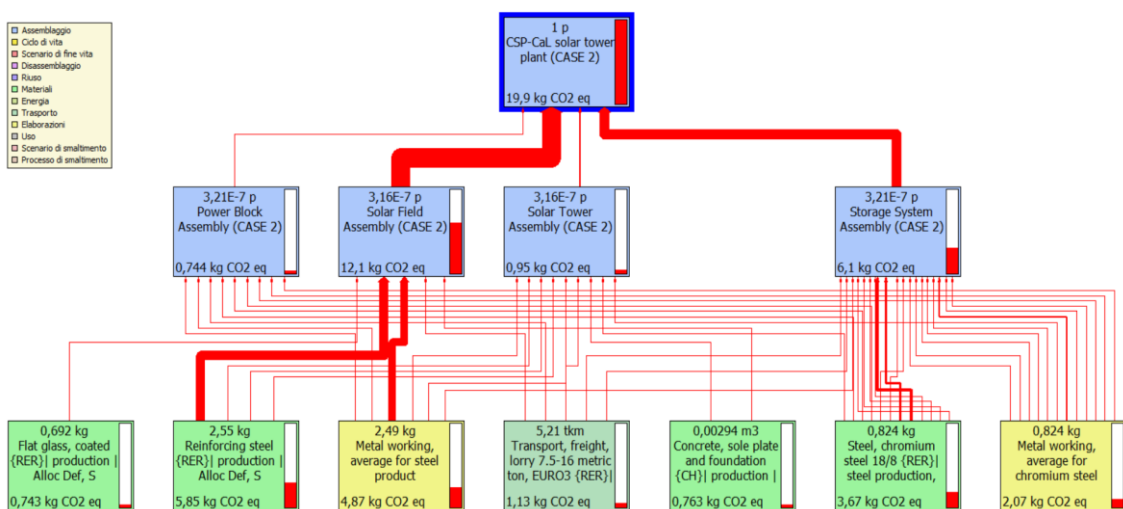


Figure 69 - Assembly-Phase CASE 2

#### 5.4.2. Use-Phase analysis and results

Once the model has been built during the assembly phase, it is possible to study its performance in terms of environmental impact in the subsequent use-phase. It includes the emissions generated during the assembly phase and additionally covers everything that is produced during the life cycle of the plant, in this case assuming a duration of 25 years of operation. This therefore comprises maintenance activities such as mirror cleaning processes, water cooling processes in the intercoolers that are part of the system and the calcium carbonate renovation process. Each of these activities also accounts for the impacts associated with subsequent disposal or processing operations resulting from the use of the plant

The information obtained from the analysis is used below to make a comparison in terms of environmental impact between the two configurations studied. Specifically, a comparison between the various categories chosen in normalized form and the study of the distribution of emissions in the various components of the system are carried out.

##### 5.4.2.1. Comparison on normalized impact categories

First of all, the two configurations are compared by analysing the overall environmental impact generated during the life cycle of the plant. For clarity and simplicity, the 15 impact categories of IMPACT 2002+ Midpoint Indicator are grouped into four main classes: Climate change, Ecosystem quality, Human health and Resources. The comparison between the two configurations is made possible by the normalization process of the results, through which the values belonging to the various categories and characterized by different units of measurement can be expressed according to a universal non-dimensional factor.

The results, shown in the following figure (*Figure 70*) certify as on average CASE 1 registers higher environmental impact values than CASE 2. A response to the trend can be identified by analysing the inventory used in the construction of the model. If, in fact, the Solar Field and Solar Tower blocks are identical in the two cases, substantial differences in the structure of the Storage System and Power Block can be individuated. Specifically, CASE 1 requires a significant amount of additional materials and construction processes due to the presence of the auxiliary power cycle with steam turbines, which is absent in CASE 2. Undoubtedly, this is reflected in the results, justifying the evident increase in impacts generated by.

In particular, the most affected by the difference is the category related to Human Health, enclosing the subcategories: carcinogens, non-carcinogens, respiratory inorganics, ionizing radiation, ozone layer depletion, respiratory organics.

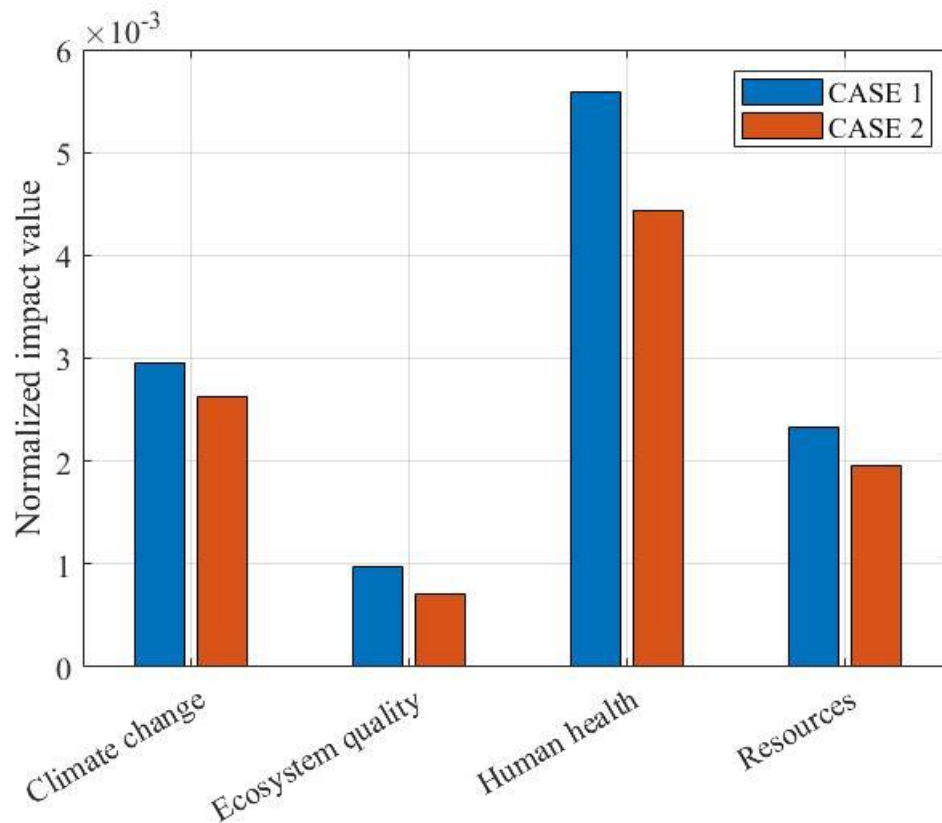


Figure 70 – Use-Phase, Normalized impact categories comparison

More in depth, from the analysis of the results, it emerges that the processes mainly responsible for the environmental impacts in this category are those related to steel production and manufacturing. Due to the increased amount of material used in CASE 1, about 40% more in accordance with the inventory and the values provided by the SimaPro software, there is no doubt that it played a substantial role in the definition of the observed impact discrepancy.

#### 5.4.2.2. Impact share from main components

The contribution of each of the four main components of the system to the total environmental impact generated is analysed below. For this type of analysis, all the impact categories provided by IMPACT 2002+ Midpoint Indicator are considered, in order to give more detail to the discussion.

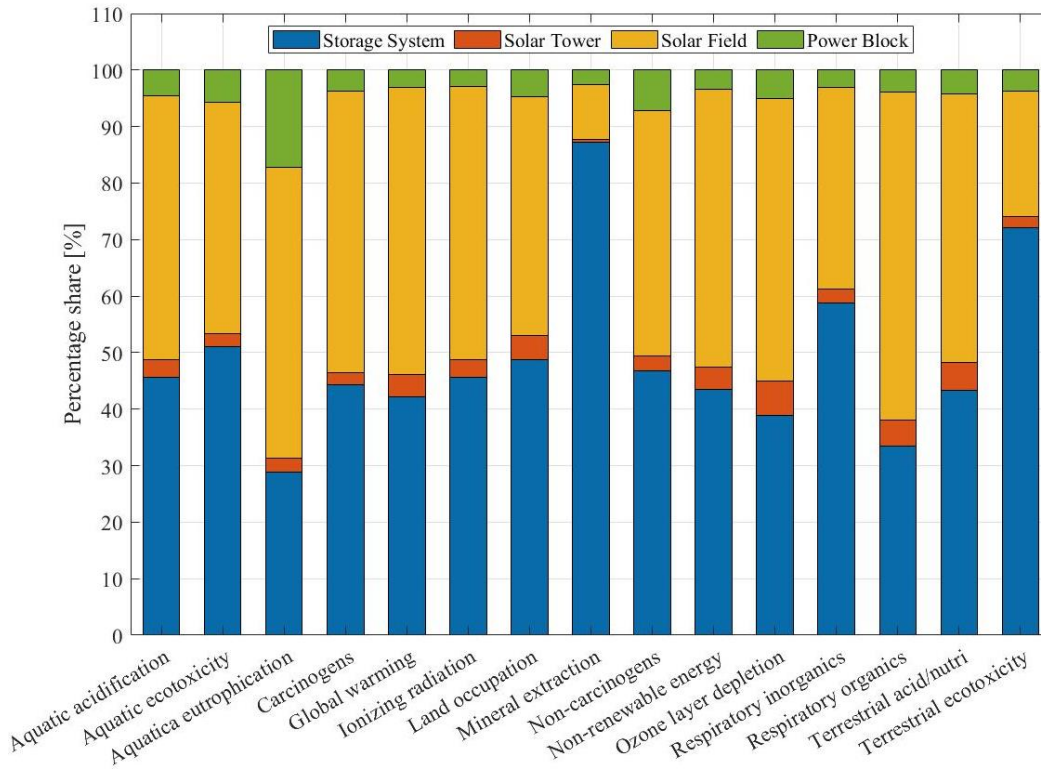


Figure 71 - Share of impact indicators from different main components, CASE 1

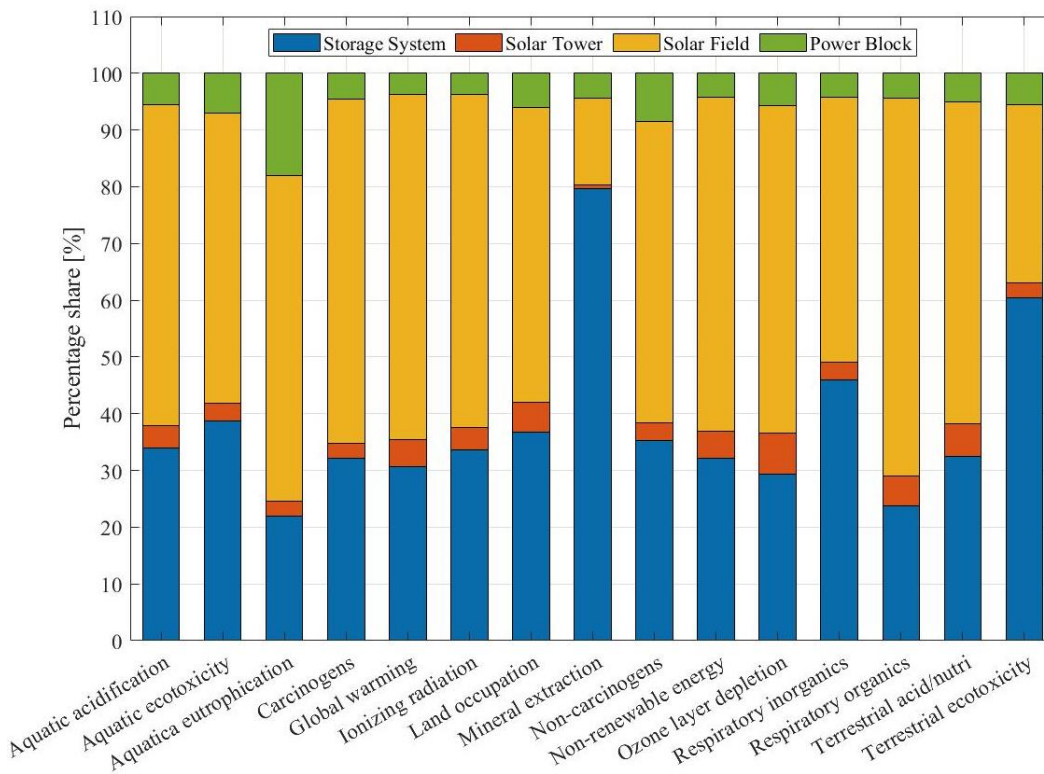


Figure 72 - Share of impact indicators from different main components, CASE 2

From the graphs shown, it can be seen that in both configurations the plant components responsible for most of the environmental impact generated are Storage System and Solar Field. On average, the solar field has greater effects in almost all impact categories. This is a result consistent with the inventory realized, due to the considerable amount of material required for the assembly of the infrastructure and the numerous processes associated with it as a consequence of the huge extension of the heliostat field. Moreover, its environmental impact item is further increased by maintenance activities related to the periodic cleaning of reflective mirrors.

The Storage System is the other component with a high environmental impact value. Also in this case, the result reflects the assumptions adopted when compiling the inventory. Having included in the block not only the three storage systems used, but also all the infrastructure and components dedicated to their operation, has undoubtedly led to a significant increase in environmental impacts generated.

In both configurations, moreover, it results that in the "Material Extraction" and "Terrestrial Ecotoxicity" categories the impact value generated by the Storage System significantly exceeds the corresponding Solar Field result. This situation is probably due to the extraction, processing and disposal of calcium carbonate, which is not included in the other components of the system.

#### 5.4.3. End-Phase analysis and results

The End-Phase, in an LCA analysis, provides an estimate of the environmental impacts generated by the end of life scenario of the studied process. Specifically for the case investigated, the End-Phase starts after the 25 years of plant operation and covers all the activities from the initial dismantling to the disposal of each material. This includes the impacts resulting from the transport of the materials to the disposal areas as well as the consumption of electricity from the grid, necessary for the completion of the dismantling phase.

Concerning the post decommissioning processes, it is assumed that 90% of the metallic materials (reinforcing steel, chromium steel and low-alloyed steel) are allocated to a recycling process, sending only the remaining 10% to landfill. Undoubtedly, being the most widely consumed type of material in the construction of the plant, recycling guarantees important gains in terms of environmental impact. The reflective mirrors glass is completely destined for municipal incineration, while for the other substances involved in the dismantling phase, mainly cement and calcium carbonate, it is considered a generic disposal process. Below it is proposed the articulation of the main end-of-life processes for both configurations studied.

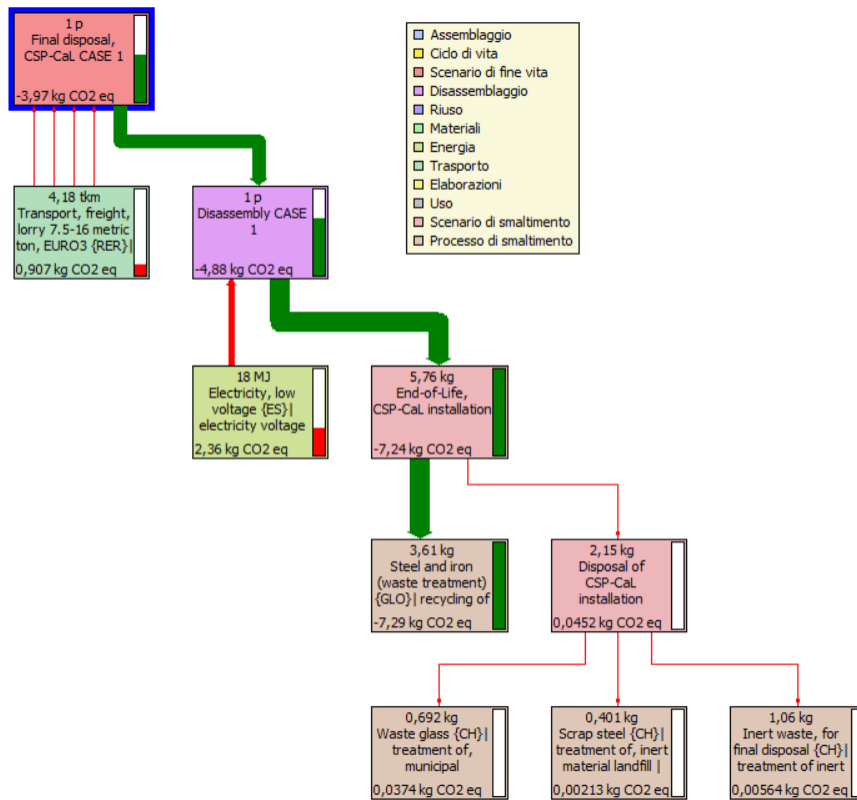


Figure 73 - End-Phase CASE 1

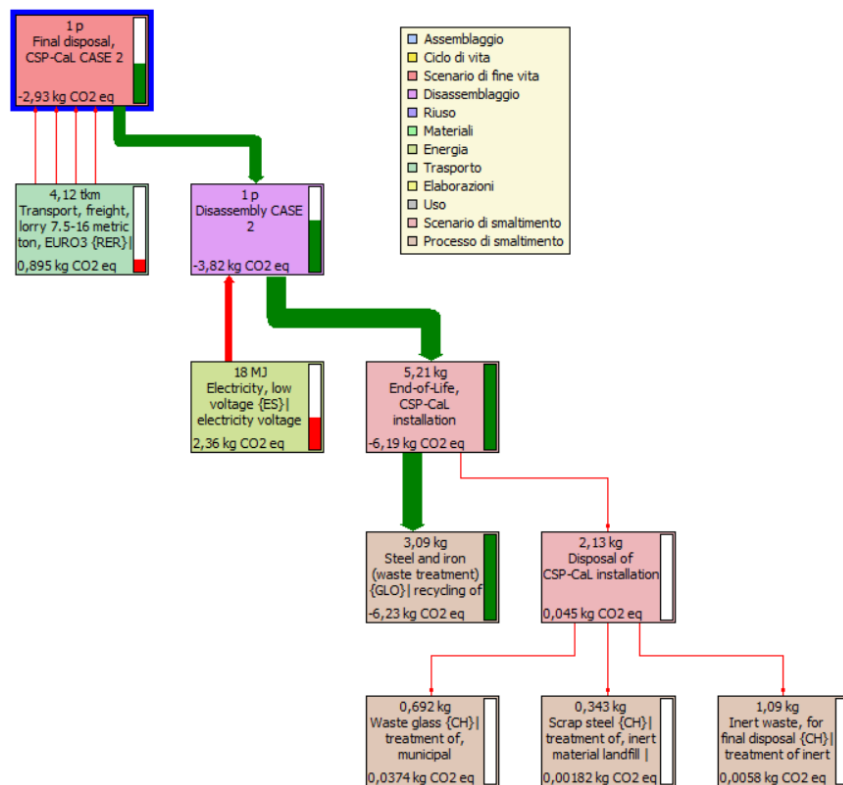


Figure 74 - End-Phase CASE 2

The graphs are calculated according to the Climate Change category, providing information about the  $CO_2$  equivalent emissions (in  $kgCO_{2,eq}$ ) released in the various processes analysed. What emerges is how recycling activity results in a positive contribution to carbon dioxide production in the atmosphere. In other words, the software suggests how the inclusion of a recycling process translates into a certain amount of saved emissions compared to what would happen in the case of landfill disposal of the material.

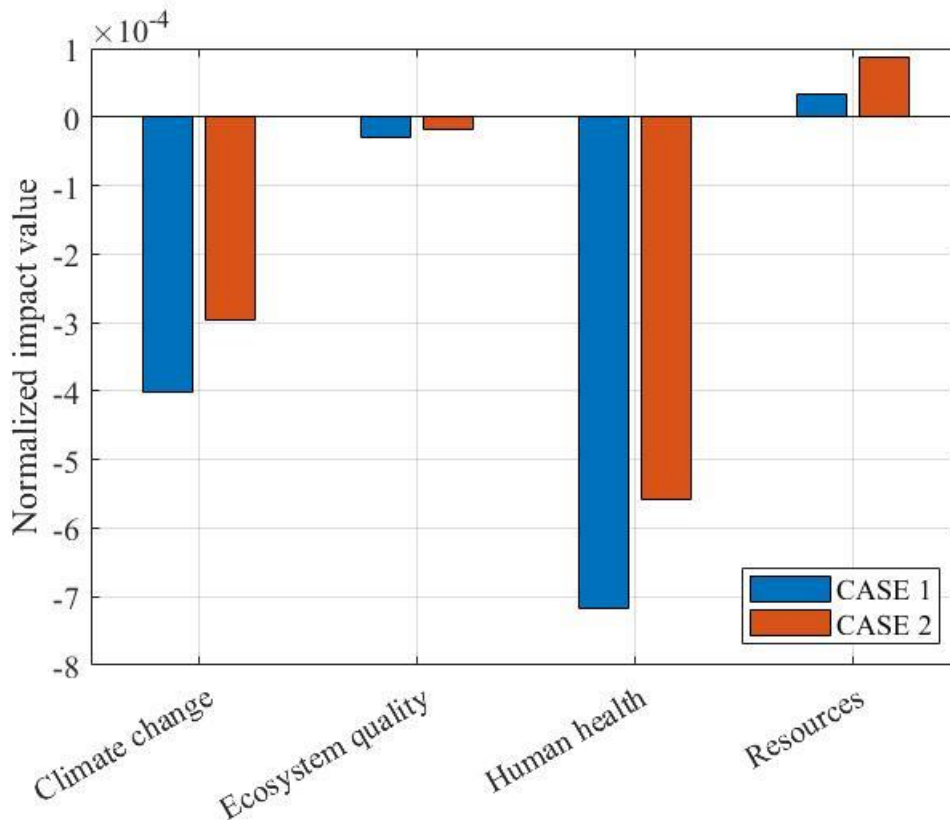


Figure 75 - End-Phase, Normalized impact categories comparison

The results obtained from the end-phase analysis, as shown in the figure (Figure 75), are in agreement with the data collected during the Use-Phase (Figure 70). Unavoidably, the impact category that benefits most from recycling processes is “Human Health”, being the one mainly affected by the effects of metallic materials and related manufacturing processes. Such a high negative environmental impact value is a direct consequence of the gain, in terms of emission reduction, obtained by the recycling process.

The only category that does not show a reduction in the environmental impact generated is “Resources”, by virtue of the fact that the End-Phase, being a final phase of the life cycle, does not directly concern the extraction of natural resources.

## 5.5. Interpretation of the results

The LCA analysis carried out allows to introduce a comparison methodology between the two CSP-CaL integration configurations studied. If, in fact, in the previous chapters they have been observed under an exergo-economic profile, in this way it is possible to insert also an environmental aspect to their description.

The results obtained from the analysis show overall better environmental performance of CASE 2 compared to CASE 1 in the Assembly-Phase, justified mainly by plant engineering differences and the absence of some components that unavoidably increase the impacts generated by the first case. Both configurations have been compared assuming an equal net energy production during the operating period, nevertheless considering however that the output guaranteed by CASE 1, under conditions of calciner irradiance equivalent to  $100 MW_{th}$ , is moderately higher than that achieved by CASE 2. Another important difference also concerns the End-Phase. If, in fact, CASE 2 is advantaged in the Assembly-Phase due to the lower amount of material required, the trend is reversed in the End-Phase, where the greater availability of substance, especially steel, favours a gain in the recycling phase, in terms of the amount of emissions saved, higher in CASE 1.

The LCA analysis, besides providing a comparison tool in environmental terms, also constitutes a strong base for the estimation of system characterization indicators, such as EPBT (Energy PayBack Time), EROI (Energy Return On (Energy) Invested) and GWP (Global Warming Potential), of relevant importance in a subsequent process of benchmarking between the type of installation treated with other different production technologies.

On the other hand, however, it is necessary to underline the limitations of the analysis. Since it is a methodology based on the construction of an inventory, there is no doubt that the assumptions adopted at that stage have a considerable influence on the final result. The treatment of production systems which do not yet exist, furthermore, adds uncertainty to the estimations made. In view of this, it is recommended to refer the results obtained to the chosen inventory and to the selected hypotheses, with the understanding that, whenever future developments of the technology were to reveal aspects neglected in this study, the final evaluations could inevitably be affected.

## CHAPTER 6

### USEFUL INDICATORS FOR FUTURE COMPARISONS

#### 6.1. Introduction

The proposal to integrate a CSP plant with a thermochemical storage system based on the Calcium Looping mechanism, although attractive, is still in the research and development phase. There are, in fact, no concrete application examples and plant solutions that exploit its potential. The characterizations carried out in the previous paragraphs provide references to the environmental and energy performance of the system, indicating its strengths and weaknesses and identifying possibilities for improvement and potential implementation. The comparison, moreover, between two different configurations of the same technology extends the application range of the system and makes it suitable for many uses

However, due to its persistent immaturity, it is appropriate to proceed with the identification of methodologies that allow the implementation of a comparison with other still existing plant technologies. In this way it is possible to update the studies carried out in the previous paragraphs and assess whether, in the light of what has emerged, it is actually worth continuing to develop the technology studied or whether, in fact, there is no evidence in favour of its deployment.

In this respect, three substantive indicators will be calculated in the following chapter, reported in standardised units of measurement in order to allow easy comparison with other similar technologies. The energy sustainability of the plant is studied using the concepts of Energy PayBack Time (EPBT) and Energy Return On Investment (EROI). Environmental performances, on the other hand, will be comparable by means of Global Warming Potential (GWP).

## 6.2. Energy PayBack Time (EPBT)

Energy payback time is a useful indicator to obtain information regarding the return of the energy invested in the construction of a certain energy production system. It provides an estimate, in terms of time, of the period required for the plant to produce a quantity of energy at least equivalent (in terms of primary energy equivalent) to that spent for its construction.

The calculation of energy payback time, in accordance with the definition provided by (Fthenakis and Kim, 2011), can be made according to the following report:

$$EPBT = \frac{E_{mat} + E_{manuf} + E_{trans} + E_{ins} + E_{EOL}}{E_{agen} - E_{aoper}} \quad (6.1)$$

Where  $E_{mat}$  indicates the primary energy demand necessary for the production of materials,  $E_{manuf}$  and  $E_{trans}$  those associated with manufacturing and transport processes.  $E_{ins}$  refers to the installation process of the materials, while  $E_{EOL}$  includes the primary energy consumption during the End-Of-Life phase of the system. Finally, in the denominator  $E_{agen}$  represents the amount of energy generated annually, from which  $E_{aoper}$ , is subtracted, indicating the energy spent annually for maintenance and operations [130].

The above definition can be made in the following more synthetic form:

$$EPBT = \frac{E_{prim,tot}}{E_{a,net}} \quad (6.2)$$

In which,  $E_{prim,tot}$  indicates the total consumption of primary energy during the life cycle of the plant, while  $E_{a,net}$  refers to the quantity of energy produced annually net of maintenance and operations expenses.

### 6.2.1. EPBT of CSP-CaL integrations

In accordance with (6.2), the calculation of the EPBT requires knowledge about the overall primary energy invested in the life cycle of a product and the net energy produced annually by the power plant.

The evaluation is based on the results obtained from the LCA analysis previously described in *Chapter 5*. Specifically, the model was created assuming a overall net

production of electricity over 25 years of operation of 1  $MWh_{el}$ , equivalent to 144 MJ of net energy produced annually.

The estimate of the total amount of primary energy spent is made through the "Cumulative Energy Demand" indicator available on the SimaPro software and applicable to the built model. The calculation is made considering the cumulative contributions of Assembly-Phase, Use-Phase and End-Phase.

The results are as follows:

	<i>CASE 1</i>	<i>CASE 2</i>	<i>Unit</i>
<i>Net annually energy produced</i>	<i>144</i>	<i>144</i>	<i>MJ</i>
<i>Total primary energy consumption</i>	<i>361,2</i>	<i>316,7</i>	<i>MJ</i>
<b><i>Energy PayBack Time (EPBT)</i></b>	<b><i>2,5</i></b>	<b><i>2,2</i></b>	<b><i>years</i></b>

*Table 56 - EPBT of CSP-CaL integrations*

#### 6.2.2. Comparison with EPBT of other systems

There are numerous references from which to obtain information about the calculation of EPBT for solar installations. Specifically, it represents a particularly used indicator for the evaluation of photovoltaic systems. In any case, it is also possible to identify, in the literature, results related to CSP installations.

The main problem in comparing data lies in their dependence on how the LCA method is implemented, the inventory chosen and the assumptions adopted. Undoubtedly, the more simplified the inventory is, the greater the deviation from the effective value will be.

A first source of information is offered by (Pelay et al., 2020), whose work offers an LCA analysis on an innovative technology based on the integration of calcium hydroxide as a thermochemical storage system in a CSP plant. Among the various configurations studied, an average EPBT variable between 90 and 130 days is reported, markedly lower than the one obtained in the previous analysis. Different values are instead identified by (Whitaker et al., 2013), whose article deals with a comparative study between different technologies of CSP solar system with molten salt thermal storage. The results demonstrate an EPBT between 13 and 16 months, still lower than that of the case studied but considerably higher compared to (Pelay et al.,2020) [131], [132].

Comparing the methodological descriptions in the above mentioned articles, a substantial difference in approach emerges. In the first case, in fact, the hypotheses

adopted exclude some processes instead considered in the study of (Whitaker et al., 2013). Moreover, it emerges that in the first study, the EPBT value is obtained from cradle-to-gate LCA analyses. Since the one addressed in this treatise is a "cradle-to-gate", there is no doubt that the processes of decommissioning, dismantling and disposal involve an increase in primary energy consumption, which translates into an increment of EPBT value. In the light of this consideration, the distance from the data collected in the literature appears to be justifiable.

Finally, on the basis of a sufficiently long operating period of 25 years, an EPBT of 2.5 and 2.2 years respectively denotes, in any case, an unquestionably advantageous energy sustainability of the project, keeping in mind, however, that the result depends on the accuracy and detail of the inventory adopted during the LCA process.

### 6.3. Energy Return On (Energy) Invested (EROI)

An important indicator used in assessing the energy sustainability of a production plant is the so-called Energy Return on Energy Invested (EROI). It provides an estimate of the profitability of an energy investment by quantifying the capability to return, in energy terms, on the expenditure made. Essentially, it makes it possible to evaluate the amount of energy gained from a given investment in relation to that spent on its implementation.

A methodology for calculating the EROI indicator, in accordance with (Bhandari et al., 2015), is represented by the following formula:

$$EROI = \frac{E_{net,tot}}{E_{prim,tot}} \quad (6.3)$$

Where,  $E_{net,tot}$  indicates the total net quantity of energy generated during the entire production period of the power plant in question, compared with a total energy expenditure over the life cycle equivalent to  $E_{prim,tot}$  [133].

Comparing (6.3) with (6.2), from the definition of EPBT it is possible to express the EROI indicator according to the following relation:

$$EROI = \frac{Lifetime}{EPBT} \quad (6.4)$$

In this way, the two indicators EROI and EPBT are proportional to each other according to the "Lifetime" factor, indicating the duration of the activity of the system studied.

From the result of EROI it is predictable the convenience of realizing a certain energy system. Undoubtedly, values of the factor lower than the unit suggest that the investment does not have the characteristics to guarantee a recovery of the energy spent. Consequently, a high value of EROI is an essential prerogative in the evaluation of a cost-effective investment.

### 6.3.1. EROI of CSP-CaL configurations

The calculation of EROI for the two configurations of CSP-CaL integration system is realized, similarly to the EPBT, using data obtained from LCA simulations implemented on SimaPro software.

After calculating the EPBT value for both configurations, the evaluation of EROI is immediate in accordance with (6.4), recalling that the analysis was carried out on the basis of an operational period of 25 years. The results are as follows:

	<i>CASE 1</i>	<i>CASE 2</i>	<i>Unit</i>
<i>Energy PayBack Time (EPBT)</i>	2,5	2,2	years
<i>Lifetime</i>	25	25	years
<i>Energy Return On Invested (EROI)</i>	<b>10,0</b>	<b>11,4</b>	/

*Table 57 - EROI of CSP-CaL configurations*

The results show that both configurations achieve a considerably higher HEROI value than the unit, certifying how in fact the system can be considered energetically convenient.

### 6.3.2. Comparison with EROI of other systems

Similarly to EPBT, EROI is a widely used indicator for the comparison between different power plants adopting various technologies. A useful reference in this respect is proposed by (Weißbach et al., 2013), in which important information about EROI values on the main solar energy production technologies can be found. Some references are also given for CSP systems. Specifically, estimates of the EROI indicator are provided for Parabolic Through ( $EROI = 21$ ) and Linear Fresnel ( $EROI = 17$ ) [134]. The order of magnitude of the EROI factor is certainly comparable with the estimates

calculated for CSP-CaL integration. The slight discrepancy with the values identified in the literature, besides obviously the choice of more or less simplifying hypotheses during the construction of the inventory, is in all probability attributable to the different CSP plant technology treated. A solar tower system, by virtue of the highly intensive construction process of Solar Field and Solar Tower, could in fact register a lower HEROI value, due to a plausible higher energy expenditure.

(Raugei et al., 2012), furthermore, provides some estimates of the EROI indicator for lignite-fired power plant ( $EROI = 12,2$ ) and coal-fired power plant ( $EROI = 24,6$ ). It should be noted that, although the values are similar in order of magnitude to those calculated in this treatise, the EROI factor may sometimes have an important weakness, as it does not include environmental aspects of pollutant emissions into the atmosphere in its definition. Consequently, the comparison between renewable resource plants and traditional production plants should be supported by specific environmental indicators in order to obtain a more detailed picture of the scenario.

## 6.4. Global Warming Potential (GWP)

The Global Warming Potential (GWP) is an important indicator for assessing the environmental performance of a particular process. It acquires usefulness in comparative procedures, making it possible not only to draw comparisons in terms of energy and production outcomes, but also to consider the environmental aspects and the corresponding impacts generated by the systems analysed.

The Global Warming Potential is typically expressed in  $kgCO_{2,eq}/MWh$  and takes into account the emissions released in each phase of the life cycle of the analysed product. Being expressed in units of energy, it represents an indicator independent of the size and actual production of the plant, making it possible to compare different installations of different sizes and using various technologies.

### 6.4.1. GWP of CSP-CaL configurations

The calculation of the Global Warming Potential is performed through the IMPACT 2002+ Midpoint Indicator on the SimaPro software. Among the impact categories analysed, in fact, appears "Global Warming", which provides the amount of emissions, in  $kgCO_{2,eq}$  released by the plant in each of the phases of its life cycle.

Having built the LCA model considering  $1 \text{ MWh}_{el}$  of electricity produced as a Functional Unit, the calculation of the GWP is immediate.

The results obtained for both configurations studied are shown in the following table.

<b>GWP</b>		<b>CASE 1</b>	<b>CASE 2</b>	<b>Unit</b>
<i>Assembly-Phase</i>		23,7	19,9	$\text{kgCO}_{2,eq}/\text{MWh}$
	<i>Power Block</i>	3%	4%	/
<i>Share of GWP in</i>	<i>Solar Field</i>	51%	60%	/
<i>Assembly-Phase</i>	<i>Solar Tower</i>	4%	5%	/
	<i>Storage System</i>	42%	31%	/
<i>Use-Phase</i>		5,6	6,2	$\text{kgCO}_{2,eq}/\text{MWh}$
<i>End-Phase</i>		-4,0	-2,9	$\text{kgCO}_{2,eq}/\text{MWh}$
<b>Total</b>		<b>25,3</b>	<b>23,2</b>	$\text{kgCO}_{2,eq}/\text{MWh}$

Table 58 - GWP of CSP-CaL integrations

What emerges from the results is how most of the GWP is attributable to the Assembly-Phase of the plant. Specifically, in both configurations, the Solar Field is the inventory item with the highest amount of emissions, as expected due to its size and the amount of material required.

The largest difference between CASE 1 and CASE 2 concerns the Storage System. The decrease of GWP in the second case is probably due to the absence of the additional power cycle with steam turbines, which involves the use of more materials during construction.

Finally, it is relevant that GWP in the End-Phase is a negative value. This is due to the presence of recycling processes, which result in savings in terms of future emissions, thanks to the reuse of a certain amount of material.

#### 6.4.2. Comparison with GWP of other systems

The Global Warming Potential is a widely used indicator in the environmental assessment of solar installations. Similarly to the EPBT, (Pelay et al., 2020) and (Whitaker et al., 2013) provide important references for a comparison process.

In particular, (Pelay et al., 2020) identifies, in the study of the various CSP plant configurations with integration of thermochemical calcium hydroxide storage system, a GWP in the range  $8 - 12 \text{ kgCO}_{2,eq}/\text{MWh}$ . The analysis of (Whitaker et al., 2013), instead, shows a markedly higher value, between  $32$  and  $42 \text{ kgCO}_{2,eq}/\text{MWh}$ . Surely the

discussions carried out for EPBT can also be shared in the analysis of the GWP in the explanation of the differences between the references analysed.

Certainly, obtaining intermediate GWP values and, above all, an order of magnitude comparable with the data identified in the literature, give them moderate validity. Undoubtedly, the inclusion of more details in the inventory and the refinement of the hypotheses adopted in its construction would favour the achievement of more accurate results. On the basis of the collected observations, however, it appears that in terms of environmental impact and atmospheric emissions, the GWP suggests that CSP installations with thermochemical storage systems are more advantageous than the traditional molten salt installations addressed by (Whitaker et al., 2013).

## 6.5. Sensitivity analysis

The EPBT, EROI and GWP values are calculated on the basis of the results of the LCA analysis carried out in Chapter 5 above and, as a result, are undoubtedly affected by a certain degree of uncertainty caused by the assumptions adopted in the phase of inventory construction. It is advisable, in this respect, to support the observations obtained with a sensitivity analysis aimed at certifying the extent to which the indicators are affected by possible variations in the adopted inventory.

The methodology adopted is based on the procedure followed by (Pelay et al., 2020), through the calculation of a "Sensitivity Indicator",  $S$ , defined by the following formula:

$$S = \frac{\Delta I_j / I_j}{\Delta x_i / x_i} \quad (6.5)$$

Where the variation of a particular inventory item used ( $\Delta x_i / x_i$ ) corresponds to a consequent variation in the impact caused ( $\Delta I_j / I_j$ ) [131].

In this way, the calculated Sensitivity Indicator allows to perceive how much the estimation of the generated impacts is influenced by the accuracy with which the inventory has been created.

Specifically, among the hypotheses adopted, those that could probably have a greater influence on the results concern the estimation of the metallic material used in the construction of the plant components, mainly those related to Storage System and Power Block, and the transport methods adopted.

The sensitivity analysis is then applied following two main directives:

- Evaluation of the influence of the quantity of steel and metal materials used in the construction phase: being the type of material most used in the construction phase and from which a considerable amount of impact originates, it is appropriate to deepen the discussion. The Sensitivity Indicator is calculated assuming a variation in the quantities involved of 20%. It is reasonable, in fact, to hypothesize that during the inventory compilation phase, some estimates may have been oversized or undersized, thus altering the amount of impact caused. Similarly, it is plausible to think that the production and manufacturing processes of metallic materials may undergo changes over time, through the adoption of environmental policies, for example, or specific emission limitations, with a consequent change in the amount of impacts generated;
- Evaluation of the influence of transport processes: in the definition of the inventory for LCA analysis, some hypotheses were considered regarding the average distance covered in the transport of the substances, as well as the category of means (EURO3) used for the transport. In view of the possibility that distance estimates are affected by a certain degree of uncertainty and in anticipation of possible measures in terms of emissions reduction from means of transport, a 50% rate of change on the inventory items related to transport processes is adopted in the calculation of the Sensitivity Indicator.

The following graph (*Figure 76*) shows the results of the sensitivity analysis performed following the hypothesis of a variation in the quantity of metallic materials used by modifying the corresponding inventory items with a rate of 20%. The study has been carried out for both GWP and Energy Indicators (EPBT, EROI).

The results show that, with regard to the Energy Indicators, the value of the Sensitivity Indicator is quite high, with percentages of around 50% for both configurations. As a result, the Energy Indicators are affected by a degree of uncertainty significantly dependent on the accuracy of the inventory concerning the metallic materials used. Undoubtedly the outcome is derived from the energy consumption caused by the metal production and manufacturing processes. For GWP, on the other hand, the analysis was divided into the main system components. If Solar Field and Storage Systems have moderately low Sensitivity Indicator values, the same cannot be said for Power Block and Solar Field. The behaviour reports a high level of uncertainty, probably due to the prevalence of metallic materials in the inventory of these two components, which is not shared by the remaining blocks due to the presence of glass for mirrors and calcium carbonate for storage.

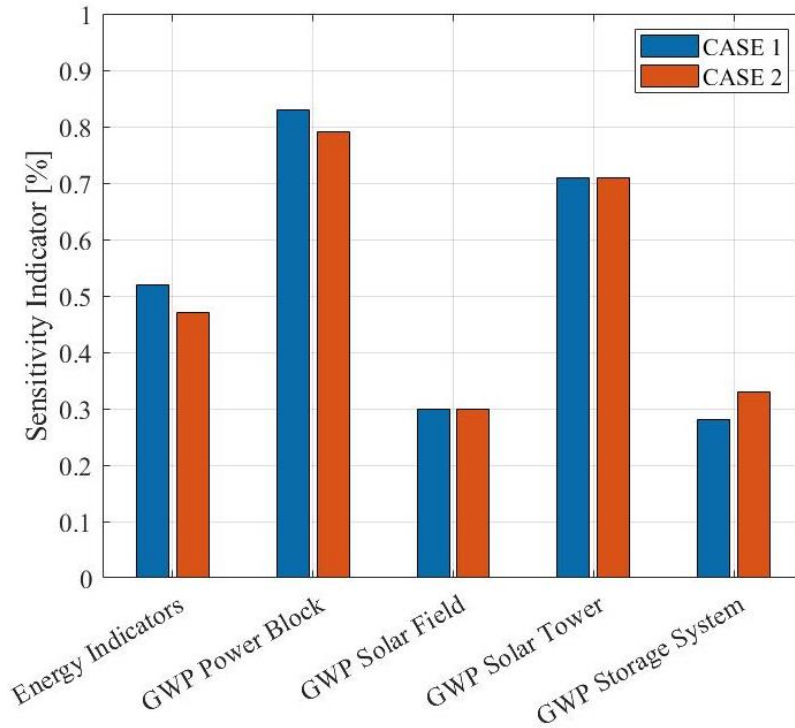


Figure 76 - Steel Materials sensitivity analysis

With regard, instead, to the influence of transport processes on the uncertainty of the indicators, the following graph shows the results of the corresponding sensitivity analysis.

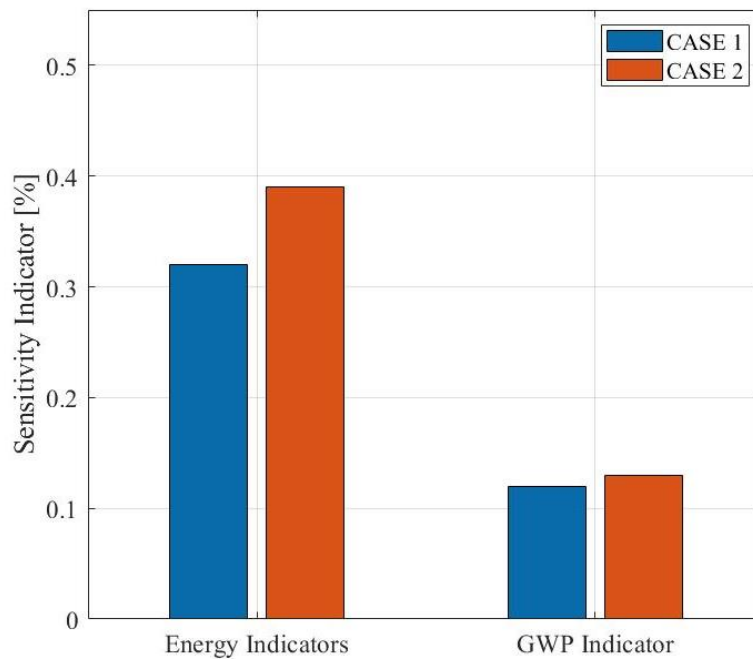


Figure 77 - Transport sensitivity analysis

What emerges from the analysis is how the transport processes influence the Energy Indicators much more than the GWP indicator. In both cases, however, despite a significant 50% change applied to the inventory, moderately reduced Sensitivity Indicator values are obtained, demonstrating that transport generates a limited percentage of impacts compared to what is observed for materials and related processes. For both categories of indicators, moreover, it emerges that the uncertainty in CASE 2 is greater than that in CASE 1. The result is a direct consequence of the fact that, on the basis of the analyses carried out and the hypotheses adopted, it appears that in total a greater quantity of transport processes is required in the second configuration.

## CONCLUSIONS

The report just described has been realized with the aim of analysing the Calcium Looping process and its adaptability as a thermochemical energy storage system in a concentration solar power plant. The main objective set with the writing of this thesis is to study the CSP-CaL concept not only from a design point of view, evaluating also the energy, exergo-economic and environmental performances of a technology still in a very early stage of development

After providing in *Chapter 1* an overview of the world energy scenario and the role played in it by energy storage systems, the main theoretical aspects of the Calcium Looping process have been addressed in *Chapter 2*. The conceptual notions studied on this occasion, especially with regard to the components needed for a possible CSP-CaL integration, have been useful in the following analysis.

Two main configurations of CSP-CaL have been studied: CSP-CaL with high temperature thermochemical energy storage system (CASE 1) and CSP-CaL with ambient temperature thermochemical energy storage system. The observation of the behaviour of the technology has been possible thanks to the use of AspenPlus software, as reported in *Chapter 3*. In both cases, it has been assumed that the thermal power supplied to the calciner by the heliostatic field was equivalent to  $100 MW_{th}$ . From the simulations performed, some important considerations emerged:

- Both configurations carry out the main process of power generation in a power block operating according to a direct gas turbine scheme, exploiting the high thermal availability of a  $CO_2$  stream with large flow-rate, heated by the exothermic reaction of carbonation and pressurized by the operation of a compressor. The output records similar results, with turbine operating capacity of  $27,2 MW_{el}$  for CASE 1 and  $26,5 MW_{el}$  for CASE 2. The first configuration, however, is articulated in such a way as to allow the integration of an additional accessory power cycle, with a steam turbine of a size of  $3 MW_{el}$ , exploiting the high thermal availability of the calcination products in a steam generator. This solution is not applicable in CASE 2 due to the large heat demand required to preheat the solids coming out of the storage at ambient temperature;

- The thermodynamic requirements necessitate the use of a solid/solid heat exchanger in CASE 2. This is a disadvantage of the configuration, due to the absence, to date, of a component of this type with a size suitable for operation in a power generation plant;
- The main result of the storage temperature variation is the actual time during which solids can be stored without excessive heat loss. This is exemplified by the reduced circulating flow rates in CASE 2, demonstrating that storage systems do not require as frequent substance replacement as CASE 1. It is a strong point of the second configuration, giving more elasticity to the system and the ability to extend its production capacity.

The models examined using AspenPlus software constituted the basis on which to set up the subsequent Exergo-economic analysis, described in *Chapter 4*. The main objective on which the process was based is to evaluate the effectiveness of the configurations analysed, studying their individual components and identifying, where possible, opportunities for improvement. The method was conducted by applying matrix calculations, whose main matrices are listed in the appendix, and using simplifying assumptions to streamline the process. The Cost Allocation phase was carried out following NETL principles and basing assumptions on the maturity and current diffusion of the technology. As described in the conclusions of Chapter 4, from the results has emerged, comparing the exergo-economic factor values of the two configurations, that in both cases the Calciner represents the component with the highest irreversibility value, presumably due to the extreme difference, in terms of exergetic quality, between the fuel of the reaction, solar radiation coming from a very high temperature source, and the products generated,  $CO_2$  and  $CaO$  around 900 °C. In the same way, it turned out that the HE-CALC and HE-CARB heat exchanger systems, respectively on the calciner side and on the carbonator side, are components with a rather high exergo-economic factor, demonstrating the high cost of the two blocks due to the high number of components contained within them. The carbonator, finally, was another component with irreversibility as the prevailing effect, probably due to the losses recorded during the chemical reaction phase, mainly due to the temperature difference between reactants and products.

Due to the fact that the process was carried out on the basis of some simplifying assumptions, the chapter has been concluded with some additional analyses aimed at improving the accuracy of the results. Specifically, it has been decided to intervene on the heat exchangers, calculating their cost factor with greater precision through a differentiation by type (gas-gas, solid-gas and solid-solid). Further intervention has been carried out on the intercoolers installed in the system, distinguishing between air-cooler

and water-cooler according to the situation. Both interventions, as discussed in detail in the conclusions of this chapter, led to an effective reduction in the cost-rate with the levelling of the exergo-economic factor values of the components, demonstrating how the use of more suitable equipment contributes to improving the exergo-economic performance of the system. Finally, a final consideration has also been spent on the energy cost of electricity input to the system. The results made it possible to perceive the variation in the exergo-economic performance of the components moving from a situation of self-production of the system with zero energy purchase to one with total dependence from the network. Undoubtedly the information was interpreted on the basis of how such a change could interfere with the calculation methodology adopted for the exergo-economic analysis.

On the basis of the two configurations studied in *Chapter 3*, moreover, an LCA analysis has been implemented, with the support of SimaPro Software, with the aim of assessing the environmental performance of the system, perceiving the impacts generated and studying the life cycle phases and the plant components that require greater consideration. The survey was set up using, as Functional Unit,  $1 MWh_{el}$ . The definition of the inventory was carried out on the basis of the Gemasolar plant, which is similar in many aspects, and supported by appropriate assumptions. The process, described in *Chapter 5*, has been divided into three main parts:

- **Assembly-Phase:** it is the descriptive phase of the process of construction and assembly of the system. The plant was considered to be composed of four main blocks: Solar Field, Solar Tower, Power Block and Storage System. All the activities of extraction, manufacturing and transport of materials have been included in the inventory related to this phase and their interconnections have been rendered by reporting the descriptive network of the two configurations;
- **Use-Phase:** It is the characteristic phase of the plant's 25-year operating period. It includes, in addition to the impacts generated by the assembly phase, those due to maintenance activities during the lifetime. The results have been reported in terms of the normalised impact produced by 4 main macro impact categories, according to the organisation provided by the IMPACT 2002+ Midpoint Indicator. In addition, in order to increase the level of detail of the analysis, the contribution of each plant component to the total score in each of the 15 impact sub-categories present in IMPACT 2002+ Midpoint Indicator has been calculated;
- **End-Phase:** It includes disassembly, disposal and recycling processes after 25 years of plant operation. The results, in these cases, show a negative impact value generated. The recycling processes, in fact, are perceived as saving a

certain amount of emissions that would otherwise be caused by the extraction and subsequent processing of raw materials.

As described in detail in the conclusions of the chapter, the results showed that, in terms of environmental impact, CASE 1 generally has higher values than CASE 2, as a likely consequence of the higher amount of material used, according to the proposed inventory, due to the presence of the secondary power cycle with steam turbine. Both configurations, on the other hand, share, in terms of category with the highest impact estimate, the "Human Health", probably as a consequence of the different production and manufacturing processes of steel and metal materials.

The results obtained from the various analyses carried out, finally, have been applied in *Chapter 6*, last chapter of the treatise, where the calculation of some useful indicators is proposed in order to obtain an evaluation of the performance of the plant also through comparison with other installations and technologies. In particular, the GWP (Global Warming Potential) stands at values of  $25,3 \text{ kgCO}_{2,eq}/\text{MWh}$  for CASE 1 and  $23,2 \text{ kgCO}_{2,eq}/\text{MWh}$  for CASE 2, comparable values and, above all, on average in line with the data obtained from the literature. Indicators useful to evaluate the energy sustainability of the project are then calculated. EPBT (Energy PayBack Time) estimates are obtained, equal to 2.5 years for CASE 1 and 2.2 years for CASE 2, and EROI (Energy Return On Energy Invested), equal to 10.0 for CASE 1 and 11.4 for CASE 2. With proper attention in relation to the difference of assumptions adopted and inventory used, also in this case the literature suggests concordance of comparable values and results. Finally, the study has been concluded with a sensitivity analysis, aimed at capturing the degree of uncertainty of the data obtained. Discussing, in particular, the accuracy of the inventory used in the LCA phase and the related hypotheses adopted, it has emerged that the results show considerable sensitivity with respect to the assumptions regarding the quantity of metallic materials used, being instead less sensitive to the uncertainty on the estimates of the transport processes.

Ultimately, the presented thesis analysed an engineering concept, simplified in the acronym CSP-CaL, by conducting a series of investigations aimed at broadening the field of study of the topic and providing diversified information. The work carried out can, in some ways, be considered a preliminary analysis. The various chapters describe, in fact, processes that currently offer various possibilities for further investigation, in order to improve the accuracy of the results and increase the validity of the data obtained. The suggestions of the Exergo-economic analysis, for example, will be used to modify and subsequently optimize the plant model adopted, taking advantage of the indications provided by the Exergo-economic factors and the exergetic behaviour of the system.

The LCA survey, on the other hand, will be subject to a progressive shoring up of details, refinement of the inventory and improvement of the hypotheses adopted in order to reduce as much as possible the degree of approximation of the analysis and add pertinence to reality. The GWP, EPBT and EROI indicators themselves will necessarily be subject to review and enhancement, taking advantage of the increasingly accurate results of previous studies as far as possible. In conclusion, the treaty provides information that can, eventually, constitute, meanwhile, starting points for further analysis, exploiting the relative novelty offered by the CSP-CaL concept and the wide range of action guaranteed by a technology still in the research and development phases, leaving considerable freedom of discussion.

# APPENDIX – MATRICES FOR EXERGO-ECONOMIC ANALYSIS

FLUXES DATA										
FLUXES		T [°C]	p [bar]	h [J/kg]	h0 [J/kg]	h[W]	s [J/kg*K]	s0 [J/kg*K]	G [kg/s]	G [kmol/s]
1	CO2-1	900,00	1,00	-7,97E+06	-8,94E+06	-1,34E+08	1529,62	4,86E+03	16,76	0,38
2	CO2-2	40,00	0,93	-8,93E+06	-8,94E+06	-1,50E+08	121,64	4,86E+03	16,76	0,38
3	CO2-3	124,27	75,75	-8,90E+06	-8,94E+06	-9,94E+07	-579,33	4,86E+03	11,17	0,25
4	CO2-4	25,00	75,00	-9,17E+06	-8,94E+06	-1,03E+08	-1421,83	4,86E+03	11,17	0,25
5	CO2-STO	25,00	75,00	-9,17E+06	-8,94E+06	-5,12E+07	-1421,83	4,86E+03	5,59	0,13
6	CO2CARB	40,00	0,93	-8,93E+06	-8,94E+06	-8,93E+06	121,64	4,86E+03	5,59	0,13
7	CO2CARB1	25,00	75,00	-9,17E+06	-8,94E+06	-5,13E+07	-1421,83	4,86E+03	5,59	0,13
8	CO2CARB2	718,81	3,05	-8,19E+06	-8,94E+06	-1,18E+09	1108,72	4,86E+03	146,17	3,32
9	CO2CARBX	694,54	1,00	-8,22E+06	-8,94E+06	-1,16E+09	1289,08	4,86E+03	140,59	3,19
10	SOLIDS1	659,62	1,14	-1,09E+07	-1,15E+07	-1,74E+09	-1005,69	717,00	159,17	2,54
11	SOLIDS2	659,62	1,14	-1,09E+07	-1,15E+07	-1,74E+09	-1005,69	717,00	159,17	2,54
12	PURGE	660,00	1,00	0,00E+00	0,00E+00	0,00E+00	0,00	0,00	0,00	0,00
13	SOLIDS3	687,39	1,11	-1,09E+07	-1,15E+07	-1,73E+09	-976,14	717,00	159,17	2,54
14	FRCALC	900,00	1,00	-1,05E+07	-1,13E+07	-1,50E+09	-636,07	680,00	142,41	2,54
15	STO-CAO	900,00	1,00	-1,05E+07	-1,13E+07	-9,98E+08	-636,07	680,00	94,94	1,69
16	FRCARB	900,00	1,00	-1,05E+07	-1,13E+07	-4,99E+08	-636,07	680,00	47,47	0,85
17	SOLIDSX1	850,00	1,20	-1,07E+07	-1,15E+07	-5,68E+08	-816,06	717,00	53,06	0,85
18	SOLIDSX2	659,62	1,14	-1,09E+07	-1,15E+07	-5,78E+08	-1005,69	717,00	53,05	0,85
19	STO-SOLI	659,62	1,14	-1,09E+07	-1,15E+07	-1,16E+09	-1005,69	717,00	106,12	1,69
20	MAKEUP	20,00	1,00	0,00E+00	0,00E+00	0,00E+00	0,00	0,00	0,00	0,00

Figure 78 - CASE 1, Thermodynamic properties

FLUXES DATA										
FLUXES		T [°C]	p [bar]	h [J/kg]	h0 [J/kg]	h[W]	s [J/kg*K]	s0 [J/kg*K]	G [kg/s]	G [kmol/s]
1	CO2-1	900,00	1,00	-7,96E+06	-8,94E+06	-1,93E+08	1529,62	4,86E+03	24,27	0,55
2	CO2-2	45,02	1,00	-8,93E+06	-8,94E+06	-2,17E+08	121,96	4,86E+03	24,27	0,55
3	CO2-3	40,00	75,00	-9,03E+06	-8,94E+06	-2,19E+08	-952,98	4,86E+03	24,27	0,55
4	CO2-4	20,00	75,00	-9,19E+06	-8,94E+06	-2,23E+08	-1493,35	4,86E+03	24,27	0,55
5	CO2-STO	20,00	75,00	-9,19E+06	-8,94E+06	-1,49E+08	-1493,35	4,86E+03	16,18	0,37
6	CO2CARB	20,00	75,00	-9,19E+06	-8,94E+06	-7,44E+07	-1493,35	4,86E+03	8,09	0,18
7	CO2CARB2	711,45	3,30	-8,20E+06	-8,94E+06	-1,22E+09	1084,55	4,86E+03	148,45	3,37
8	CO2CARBX	698,49	1,00	-8,22E+06	-8,94E+06	-1,15E+09	1294,05	4,86E+03	140,35	3,19
9	SOLIDS1	30,02	1,00	-1,18E+07	-1,17E+07	-1,02E+09	-2351,25	804,50	86,14	1,10
10	SOLIDS2	844,38	1,00	-1,10E+07	-1,17E+07	-9,44E+08	-1052,82	804,50	86,14	1,10
11	FRCALC-1	900,00	1,00	-1,05E+07	-1,13E+07	-6,50E+08	-636,07	680,00	61,86	1,10
12	FRCALC-2	50,02	1,00	-1,13E+07	-1,13E+07	-6,99E+08	-1819,20	680,00	61,86	1,10
13	FRCARB	50,02	1,00	-1,13E+07	-1,13E+07	-2,33E+08	-1819,20	680,00	20,62	0,37
14	FRCARB2	683,49	1,00	-1,07E+07	-1,13E+07	-2,21E+08	-831,90	680,00	20,62	0,37
15	FRCARB21	20,00	1,00	-1,13E+07	-1,13E+07	-2,37E+08	-1904,99	680,00	20,62	0,37
16	STO-CAO	50,02	1,00	-1,13E+07	-1,13E+07	-4,66E+08	-1819,20	680,00	41,24	0,74
17	SOLIDSX1	850,00	3,00	-1,10E+07	-1,17E+07	-3,14E+08	-1047,00	804,50	28,71	0,37
18	SOLIDSX2	45,00	3,00	-1,18E+07	-1,17E+07	-3,38E+08	-2310,30	804,50	28,71	0,37
19	SOLIDSX3	20,00	3,00	-1,18E+07	-1,17E+07	-3,38E+08	-2379,48	804,50	28,71	0,37
20	STO-SOLI	35,00	1,00	-1,18E+07	-1,17E+07	-6,77E+08	-2337,49	804,50	57,43	0,74

Figure 79 - CASE 2, Thermodynamic properties

FLUXES EXERGY				
FLUXES	bph [J/kg]	ech [W]	E [W]	
1	CO2-1	1,97E+06	7,42E+06	4,04E+07
2	CO2-2	1,43E+06	7,42E+06	3,13E+07
3	CO2-3	1,67E+06	4,95E+06	2,35E+07
4	CO2-4	1,65E+06	4,95E+06	2,33E+07
5	CO2-STO	1,65E+06	2,47E+06	1,17E+07
6	CO2CARB	1,43E+06	2,47E+06	1,04E+07
7	CO2CARB1	1,65E+06	2,47E+06	1,17E+07
8	CO2CARB2	1,87E+06	6,47E+07	3,38E+08
9	CO2CARBX	1,78E+06	6,22E+07	3,13E+08
10	SOLIDS1	1,11E+06	2,78E+08	4,56E+08
11	SOLIDS2	1,11E+06	2,78E+08	4,56E+08
12	SOLIDS3	1,13E+06	2,78E+08	4,58E+08
13	FRCALC	1,19E+06	3,23E+08	4,93E+08
14	STO-CAO	1,19E+06	2,16E+08	3,29E+08
15	FRCARB	1,19E+06	1,08E+08	1,64E+08
16	SOLDSX1	1,25E+06	9,28E+07	1,59E+08
17	SOLDSX2	1,11E+06	9,28E+07	1,52E+08
18	STO-SOLI	1,11E+06	1,86E+08	3,04E+08
19	SOLAR	/	/	1,00E+08
20	GT	/	/	2,66E+07
21	ST	/	/	3,03E+06
22	COMP-1	/	/	4,00E+06
23	COOL-CO2	/	/	0,00E+00
24	T2	/	/	7,64E+05
25	C2BIS	/	/	5,11E+05
26	COMP-2	/	/	1,27E+07

Figure 80 - CASE 1, Exergy calculation

FLUXES EXERGY				
FLUXES	bph [J/kg]	ech [W]	E [W]	
1	CO2-1	1,97E+06	1,07E+07	5,86E+07
2	CO2-2	1,43E+06	1,07E+07	4,54E+07
3	CO2-3	1,65E+06	1,07E+07	5,07E+07
4	CO2-4	1,64E+06	1,07E+07	5,06E+07
5	CO2-STO	1,64E+06	7,16E+06	3,37E+07
6	CO2CARB	1,64E+06	3,58E+06	1,69E+07
7	CO2CARB2	1,86E+06	6,57E+07	3,42E+08
8	CO2CARBX	1,79E+06	6,21E+07	3,13E+08
9	SOLIDS1	8,52E+05	7,73E+07	1,51E+08
10	SOLIDS2	1,30E+06	7,73E+07	1,89E+08
11	FRCALC-1	1,18E+06	1,40E+08	2,13E+08
12	FRCALC-2	7,42E+05	1,40E+08	1,86E+08
13	FRCARB	7,42E+05	4,68E+07	6,21E+07
14	FRCARB2	1,03E+06	4,68E+07	6,80E+07
15	FRCARB21	7,41E+05	4,68E+07	6,21E+07
16	STO-CAO	7,42E+05	9,36E+07	1,24E+08
17	SOLDSX1	1,31E+06	2,59E+07	6,34E+07
18	SOLDSX2	8,53E+05	2,58E+07	5,03E+07
19	SOLDSX3	8,53E+05	2,58E+07	5,03E+07
20	STO-SOLI	8,52E+05	5,15E+07	1,00E+08
21	SOLAR	/	/	1,00E+08
22	COMP-1	/	/	7,00E+06
23	COOL-CO2	/	/	0,00E+00
24	HEATER	/	/	2,00E+06
25	T2	/	/	1,00E+06
26	COMP-2	/	/	1,10E+07
27	GT	/	/	2,60E+07
28	COOL-SOLI	/	/	0,00E+00
29	COOL-CAO	/	/	0,00E+00

Figure 81 - CASE 2, Exergy calculation

		MASS FLUXES															ENERGY FLUXES						
		1	2	3	4	5	6	7	8	9	10	11	12	13	14	15	16	17	18	19	20	21	22
COMPONENTS		CO2-1	CO2-2	CO2-3	CO2-STO	CO2CARB	CO2CARB2	CO2CARBX	SOLIDS1	SOLIDS2	FR-CALC	STO-CAO	FR-CARB	SOLIDSX1	SOLIDSX2	STO-SOLI	SOLAR	GT	ST	COMP-1	COOL-CO2	HEAT-2	COMP-2
1	CALCNER	-1	0	0	0	0	0	0	0	1	-1	0	0	0	0	0	1	0	0	0	0	0	0
2	HE-CALC	1	-1	0	0	0	0	0	1	-1	0	0	0	0	0	0	0	0	-1	0	0	0	0
3	CO2-COMP	0	1	-1	0	-1	0	0	0	0	0	0	0	0	0	0	0	0	0	1	0	0	0
4	HECO2	0	0	1	-1	0	0	0	0	0	0	0	0	0	0	0	0	0	0	0	-1	0	0
5	HE-CARB	0	0	0	0	1	-1	1	0	0	0	0	0	1	-1	0	0	0	0	0	0	0	1
6	CARB	0	0	0	0	0	1	-1	0	0	0	1	-1	-1	0	0	0	-1	0	0	0	0	0
7	MIX-SOLI	0	0	0	0	0	0	0	-1	0	0	0	0	0	1	1	0	0	0	0	0	0	0
8	SP-CAO	0	0	0	0	0	0	0	0	0	1	-1	-1	0	0	0	0	0	0	0	0	0	0
	Qsun	0	0	0	0	0	0	0	0	0	0	0	0	0	0	0	1	0	0	0	0	0	0
	Qcomp1	0	0	0	0	0	0	0	0	0	0	0	0	0	0	0	0	0	0	1	0	0	0
	STO-SOLI	0	0	0	0	0	0	0	0	0	0	0	0	0	0	1	0	0	0	0	0	0	0
	Qcomp2	0	0	0	0	0	0	0	0	0	0	0	0	0	0	0	0	0	0	0	0	0	1
	Qheat	0	0	0	0	0	0	0	0	0	0	0	0	0	0	0	0	0	0	0	0	0	0
P2	HXCO2	0	0	0	0	0	0	0	0	0	0	0	0	0	0	0	0	0	0	0	0	1	0
	HE-CALC (P3)	0/78	-1	0	0	0	0	0	0	0	0	0	0	0	0	0	0	0	0	0	0	0	0
P3	HE-CARB (P3)	0	0	0	0	0	0	0	0	0	0	0	0	0.95	-1	0	0	0	0	0	0	0	0
	CARB (P3)	0	0	0	0	0	0.93	-1	0	0	0	0	0	0	0	0	0	0	0	0	0	0	0
	CALCNER (P4)	-1	0	0	0	0	0	0	0	0	0.08	0	0	0	0	0	0	0	0	0	0	0	0
	HE-CALC (P4)	0	0	0	0	0	0	0	1	-1	0	0	0	0	0	0	0	0	0.85	0	0	0	0
	CO2-COMP (P4)	0	0	0/44	0	-1	0	0	0	0	0	0	0	0	0	0	0	0	0	0	0	0	0
	CARB (P4)	0	0	0	0	0	0	0	0	0	0	0	1	-1	0	0	0	0.20	0	0	0	0	0
	SP-CAO (P4)	0	0	0	0	0	0	0	0	0	0.50	-1	0	0	0	0	0	0	0	0	0	0	0

Figure 82 - CASE 1, Cost matrix



	A	K1	K2	K3	Cp0	FM	C1	C2	C3	FP	B1	B2	COST	\$1	cost1	CEPCI 2001	CEPCI 2018	Cost 2015	
<b>CALCINER</b>																			
REACTOR	51.04	350	0.45	0.11	37732.14	3.10	/	/	/	0.82	1.49	1.52	201640.08	51.04	201640.08	397.00	603.10	306320.23	
<b>HE-CALC</b>																			
HX1	57.88	467	-0.16	0.15	74328.74	1.00	/	/	/	1.00	0.96	1.21	161293.36	57.88	161293.36	397.00	603.10	245027.77	
HX2	263.04	467	-0.16	0.15	156603.36	1.00	/	/	/	1.00	0.96	1.21	339829.29	263.04	339829.29	397.00	603.10	516249.48	
STEAM TURB	3096.00	2.71	1.44	-0.18	36895.58	5.90	/	/	/	1.00	/	/	2176849.73	3096.00	2176849.73	397.00	603.10	3306947.28	
COOLER	104.00	467	-0.16	0.15	95704.65	1.00	/	/	/	1.00	0.96	1.21	207679.08	104.00	207679.08	397.00	603.10	315494.34	
CONDENSER	4000.00	403	0.23	0.05	332423.41	1.00	/	/	/	1.00	/	/	332423.41	4000.00	332423.41	397.00	603.10	504998.89	
TOT																			4888717.76
<b>CO2-COMP</b>																			
COMP	3000.00	229	1.36	-0.10	600197.98	3.80	/	/	/	1.00	/	/	2280752.32	3948.16	2689318.37	397.00	603.10	4085460.73	
<b>HE-CO2</b>																			
HEAT-EX	666.07	467	-0.16	0.15	287389.20	1.00	/	/	/	1.00	0.96	1.21	623591.16	666.07	623591.16	397.00	603.10	947324.50	
<b>HE-CARB</b>																			
COOLER	1000.00	467	-0.16	0.15	388955.57	1.00	/	/	/	1.00	/	/	388955.57	1580.61	511911.44	397.00	603.10	77666.98	
COMP1	3000.00	229	1.36	-0.10	600197.98	3.80	/	/	/	1.00	/	/	2280752.32	13000.00	5497577.79	397.00	603.10	8351609.98	
HX1	100.00	446	-0.53	0.40	97994.12	2.40	/	/	/	1.00	/	/	235185.88	109.56	248429.09	397.00	603.10	377399.46	
HX2	1000.00	467	-0.16	0.15	389762.45	2.40	/	/	/	1.00	/	/	935429.89	7266.34	3074685.29	397.00	603.10	4670888.42	
HX3	16.22	446	-0.53	0.40	25420.90	2.40	/	/	/	1.00	/	/	61010.15	16.22	61010.15	397.00	603.10	92683.18	
TURB	764.10	2.71	1.44	-0.17	269045.49	3.40	/	/	/	1.00	/	/	914754.67	764.10	914754.67	397.00	603.10	1389643.68	
HEATER	1572.83	208	0.91	-0.02	54356.67	1.00	-0.02	0.06	-0.01	1.15	/	/	62340.18	1572.83	62340.18	397.00	603.10	94703.68	
COMP2	510.08	229	1.36	-0.10	166051.45	3.80	/	/	/	1.00	/	/	630995.51	510.08	630995.51	397.00	603.10	958572.78	
TOT																			16713168.17
<b>CARB</b>																			
REACTOR	333.26	350	0.45	0.11	205309.28	3.10	/	/	/	1.14	1.49	1.52	1405591.94	333.26	1405591.94	397.00	603.10	2135295.96	
TURB	4000.00	2.71	1.44	-0.17	462236.34	5.90	/	/	/	1.00	/	/	2727194.41	26640.00	8507474.11	397.00	603.10	12924074.64	
TOT																			15059370.61

Figure 84 - CASE 1, Cost of components calculation

	A	K1	K2	K3	Cp0	Fm	C1	C2	C3	FP	B1	B2	COST	s1	cost1	CEPCI 2001	CEPCI 2018	Cost 2015	
<b>CALCIMER</b>																			
REACTOR	5104	3.50	0.45	0.11	37732.14	3.10	/	/	/	0.82	1.49	1.52	201640.08	51.04	201640.08	397.00	603.10	306320.23	
<b>HE-CALC</b>																			
HX1	666.95	4.67	-0.16	0.15	288202.07	1.00	/	/	/	1.00	0.96	1.21	625398.49	666.95	625398.49	397.00	603.10	950070.10	
HX2	1000.00	4.67	-0.16	0.15	389762.45	1.00	/	/	/	1.00	0.96	1.21	845784.52	2000.21	1282050.38	397.00	603.10	1947618.59	
TOT																			2897688.69
<b>CO2-COMP</b>																			
COMP	3000.00	2.29	1.36	-0.10	600197.98	3.80	/	/	/	1.00	/	/	2280752.32	7268.03	3878425.01	397.00	603.10	5891884.44	
<b>HE-CO2</b>																			
HEAT-EX	888.09	4.67	-0.16	0.15	355229.86	1.00	/	/	/	1.00	0.96	1.21	770848.80	888.09	770848.80	397.00	603.10	1171030.01	
<b>HE-CARB</b>																			
COOLER	1000.00	4.67	-0.16	0.15	388955.57	1.00	/	/	/	1.00	0.96	1.21	844033.60	1240.14	960379.88	397.00	603.10	1489954.92	
COMP	3000.00	2.29	1.36	-0.10	600197.98	3.80	/	/	/	1.00	/	/	2280752.32	10839.10	4929482.23	397.00	603.10	788891.27	
HX1	103.99	4.67	-0.16	0.15	95568.81	2.40	/	/	/	1.00	0.96	1.21	369277.89	109.56	381012.78	397.00	603.10	578813.12	
HX2	464.03	4.67	-0.16	0.15	223670.24	2.40	/	/	/	1.00	0.96	1.21	864261.79	464.03	864261.79	397.00	603.10	1312997.75	
HX3	1000.00	4.67	-0.16	0.15	388955.57	2.40	/	/	/	1.00	0.96	1.21	1502924.34	7089.49	4867501.73	397.00	603.10	794433.98	
HX4	977.36	4.67	-0.16	0.15	382150.48	3.80	/	/	/	1.00	0.96	1.21	2123992.36	977.36	2123992.36	397.00	603.10	326649.35	
TURB	1052.82	2.71	1.44	-0.17	308449.39	3.40	/	/	/	1.00	/	/	1048727.92	1052.82	1048727.92	397.00	603.10	1593168.28	
HEATER	1525.64	2.08	0.91	-0.02	53125.04	1.00	-0.02	0.06	-0.01	1.15	/	/	60927.66	1525.64	60927.66	397.00	603.10	9257.87	
TOT																			23146106.55
<b>CARB</b>																			
REACTOR	5104	3.50	0.45	0.11	37732.14	3.10	/	/	/	1.14	1.49	1.52	258322.40	51.04	258322.40	397.00	603.10	392428.82	
TURB	4000.00	2.71	1.44	-0.17	462236.34	5.90	/	/	/	1.00	/	/	2727194.41	26460.00	8472937.59	397.00	603.10	12871608.72	
TOT																			13264037.54
<b>HE-SOU</b>																			
HEAT-EX	420.22	4.67	-0.16	0.15	209449.01	1.00	/	/	/	1.00	0.96	1.21	454504.35	420.22	454504.35	397.00	603.10	690457.36	
<b>HE-CAO</b>																			
HEAT-EX	377.20	4.67	-0.16	0.15	195282.63	1.00	/	/	/	1.00	0.96	1.21	423763.32	377.20	423763.32	397.00	603.10	643757.32	

Figure 85 - CASE 2, Cost of components calculation



## AKNOWLEDGEMENTS – RINGRAZIAMENTI

Un sincero ringraziamento, innanzitutto, lo dedico al Professor Ricardo Chacartegui, con il quale ho lavorato su questa tesi. Ha saputo essere un amico prima ancora di un professore. Mi ha accolto a Siviglia con straordinaria simpatia e disponibilità e, con Carlos, Estela e tutto il team, ha saputo farmi sentire a casa.

La mia esperienza non sarebbe stata possibile senza l'impegno del Professor Vittorio Verda. Parte di ciò che ho imparato lo devo anche a lui.

Il mio più grande ringraziamento va ai miei genitori. A mia Madre, per essere stata, in questi anni di studio, la mia prima confidente, il mio più grande supporto e la mia più saggia guida. A mio Padre, per esserci stato ogni singolo istante. Sei il mio punto di riferimento. Spero, un giorno, di diventare l'uomo che sei tu ora e di continuare a renderti orgoglioso di me.

Questa tesi è per voi.

Voglio ringraziare mia sorella Francesca, probabilmente la persona a cui voglio più bene in questo mondo. E mio cugino Gianmarco, un vero fratello a cui starò sempre accanto. Spero di essere, per voi, fonte di ispirazione. Siete essenziali.

Ringrazio i miei nonni, a cui voglio un bene immenso, e tutta la mia famiglia, grazie alla quale tornare a casa era e sarà sempre la più grande gioia.

Ovviamente non avrei potuto affrontare questo percorso senza i miei amici. Andrea, Carlo, Pier, Sky, Spagna, Marco, Fede, Manuel e tutti gli altri. Vi dedico una parte del mio traguardo. Riempite le mie giornate e mi fate sentire parte di una famiglia. Spero di poter condividere per sempre ogni momento con voi.

Ringrazio tutti i miei compagni di studio e le persone stupende incontrate nei miei anni a Torino, Budapest e Siviglia. Ringrazio Pedro, un vero amico, e Nicoletta, il più grande regalo che il Poli potesse farmi. Sapere di non poter tornare a Torino insieme a te per affrontare i disagi, le sessioni, lo studio, il divertimento e il nonsense che caratterizzava le nostre giornate mi lascia un grade vuoto. Ci sarò sempre per te.

Infine, un ringraziamento speciale lo dedico ad Annalaura. Sa sopportarmi, sa capirmi, sa apprezzarmi, sa consolarmi, sa incoraggiarmi ma, soprattutto, sa amarmi. Mi completi e mi rendi felice, non posso chiedere altro. Sei la mia persona.



## References

### CHAPTER 1

- [1]. Energy Production & Changing Energy Sources - Our World in Data. <https://ourworldindata.org/energy-production-and-changing-energy-sources>. Accessed 29 Dec. 2019;
- [2]. Smil, Vaclav. Energy Transitions: Global and National Perspectives (Expanded and Updated Edition). no. 4, 2017, doi:10.1037/0096-1523.30.4.746;
- [3]. Specific Carbon Dioxide Emissions of Various Fuels. [https://www.volker-quaschning.de/datserv/CO2-spez/index\\_e.php](https://www.volker-quaschning.de/datserv/CO2-spez/index_e.php). Accessed 29 Dec. 2019;
- [4]. CO<sub>2</sub> and Greenhouse Gas Emissions - Our World in Data. <https://ourworldindata.org/co2-and-other-greenhouse-gas-emissions>. Accessed 29 Dec. 2019;
- [5]. CO<sub>2</sub> Emissions | Global Carbon Atlas. <http://www.globalcarbonatlas.org/en/CO2-emissions>. Accessed 29 Dec. 2019;
- [6]. Global Warming of 1.5 oC —. <https://www.ipcc.ch/sr15/>. Accessed 29 Dec. 2019;
- [7]. Renewable Energy - Our World in Data. <https://ourworldindata.org/renewable-energy>. Accessed 29 Dec. 2019;
- [8]. Statistical Review of World Energy | Energy Economics | Home. <https://www.bp.com/en/global/corporate/energy-economics/statistical-review-of-world-energy.html>. Accessed 29 Dec. 2019;

- [9]. Răboacă, Maria Simona, et al. “Concentrating Solar Power Technologies.” *Energies*, vol. 12, no. 6, MDPI AG, Mar. 2019, p. 1048, doi:10.3390/en12061048;
- [10]. Abdi, Hamdi, et al. “Energy Storage Systems.” *Distributed Generation Systems: Design, Operation and Grid Integration*, Elsevier, 2017, pp. 333–68, doi:10.1016/B978-0-12-804208-3.00007-8.
- [11]. Wagner, Léonard. “Overview of Energy Storage Technologies.” *Future Energy: Improved, Sustainable and Clean Options for Our Planet*, Elsevier Inc., 2013, pp. 613–31, doi:10.1016/B978-0-08-099424-6.00027-2.
- [12]. Ould Amrouche, S., et al. “Overview of Energy Storage in Renewable Energy Systems.” *International Journal of Hydrogen Energy*, vol. 41, no. 45, Elsevier Ltd, Dec. 2016, pp. 20914–27, doi:10.1016/j.ijhydene.2016.06.243.
- [13]. Dinçer, Ibrahim, and Marc A. Rosen. “Thermal Energy Storage: Systems and Applications, Second Edition.” *Thermal Energy Storage: Systems and Applications, Second Edition*, John Wiley and Sons, 2010, doi:10.1002/9780470970751.
- [14]. Alva, Guruprasad, et al. “An Overview of Thermal Energy Storage Systems.” *Energy*, vol. 144, Elsevier Ltd, 2018, pp. 341–78, doi:10.1016/j.energy.2017.12.037.
- [15]. Tian, Y., and C. Y. Zhao. “A Review of Solar Collectors and Thermal Energy Storage in Solar Thermal Applications.” *Applied Energy*, vol. 104, 2013, pp. 538–53, doi:10.1016/j.apenergy.2012.11.051.
- [16]. Pardo, P., et al. “A Review on High Temperature Thermochemical Heat Energy Storage.” *Renewable and Sustainable Energy Reviews*, vol. 32, Apr. 2014, pp. 591–610, doi:10.1016/j.rser.2013.12.014.
- [17]. Abedin, Ali H. “A Critical Review of Thermochemical Energy Storage Systems.” *The Open Renewable Energy Journal*, vol. 4, no. 1, 2011, pp. 42–46, doi:10.2174/1876387101004010042.

## CHAPTER 2

- [18]. Huang, Chin Ming, et al. “Development of Post-Combustion CO<sub>2</sub> Capture with CaO/CaCO<sub>3</sub> Looping in a Bench Scale Plant.” *Energy Procedia*, vol. 4, Elsevier Ltd, 2011, pp. 1268–75, doi:10.1016/j.egypro.2011.01.183.
- [19]. Berstad, David, et al. “Post-Combustion CO<sub>2</sub> Capture from a Natural Gas Combined Cycle by CaO/CaCO<sub>3</sub> Looping.” *International Journal of Greenhouse Gas Control*, vol. 11, Nov. 2012, pp. 25–33, doi:10.1016/j.ijggc.2012.07.021.
- [20]. IEA (2018), *World Energy Balances*, <https://www.iea.org/statistics/co2emissions/>. All rights reserved.
- [21]. Chacartegui, R.; Alovizio, A.; Ortiz, C.; Valverde, J. M.; Verda, V.; Becerra, J. “A. Thermochemical Energy Storage of Concentrated Solar Power by Integration of the Calcium Looping Process and a CO<sub>2</sub> Power Cycle”. *Appl. Energy* 2016, 173, 589–605;
- [22]. Edwards, Susan E. B., and Vlatko Materić. “Calcium Looping in Solar Power Generation Plants.” *Solar Energy*, vol. 86, no. 9, Sept. 2012, pp. 2494–503, doi:10.1016/j.solener.2012.05.019.
- [23]. Rodriguez, N., et al. “Heat Requirements in a Calciner of CaCO<sub>3</sub> Integrated in a CO<sub>2</sub> Capture System Using CaO.” *Chemical Engineering Journal*, vol. 138, no. 1–3, May 2008, pp. 148–54, doi:10.1016/j.cej.2007.06.005.
- [24]. Zhou, Xing, et al. “Pressurized Catalytic Calcium Looping Hydrogen Generation from Coal with In-Situ CO<sub>2</sub> Capture.” *Energy Conversion and Management*, vol. 198, Elsevier BV, Oct. 2019, p. 111899, doi:10.1016/j.enconman.2019.111899.
- [25]. O.A. Jimoh, P.U Okoye, T.G. Mathew, H.B. Hussin, K.S. Ariffin, “Calcium extraction and synthesis of precipitated calcium carbonate from Mg-rich dolomite”, *Materials Today: Proceedings*, 2019, 1093-1099;

- [26]. Romeo LM, Lara Y, Lisbona P, Martínez A. “Economical assessment of competitive enhanced limestones for CO<sub>2</sub> capture cycles in power plants”. *Fuel Process Technol* 2009;90:803–11;
- [27]. Berger, E. E. “Effect of Steam on the Decomposition of Limestone.” *Industrial and Engineering Chemistry*, vol. 19, no. 5, May 1927, pp. 594–96;
- [28]. Valverde, Jose Manuel, and Santiago Medina. “Reduction of Calcination Temperature in the Calcium Looping Process for CO<sub>2</sub> Capture by Using Helium: In Situ XRD Analysis.” *ACS Sustainable Chemistry and Engineering*, vol. 4, no. 12, American Chemical Society, Dec. 2016, pp. 7090–97;
- [29]. Kyaw, Kyaw, et al. “Study of Carbonation of CaO for High Temperature Thermal Energy Storage.” *Journal of Chemical Engineering of Japan*, vol. 31, no. 2, Society of Chemical Engineers, Japan, 1998, pp. 281–84, doi:10.1252/jcej.31.281.
- [30]. “Carbonation of Limestone Derived CaO for Thermochemical Energy Storage: From Kinetics to process Integration in Concentrating Solar Plants” – C. Ortiz, J.M: Valverde, R. Chacartegui, L.A. Perez-Maqueda.
- [31]. Hanak, D. P.; Anthony, E. J.; Manovic, V. “A Review of Developments in Pilot-Plant Testing and Modelling of Calcium Looping Process for CO<sub>2</sub> Capture from Power Generation Systems”. *Energy Environ. Sci.* 2015, 8 (8), 2199–2249
- [32]. Beruto, D. T., et al. “Microstructure, Kinetic, Structure, Thermodynamic Analysis for Calcite Decomposition: Free-Surface and Powder Bed Experiments.” *Thermochimica Acta*, vol. 424, no. 1–2, Dec. 2004, pp. 99–109, doi:10.1016/j.tca.2004.05.027.
- [33]. Hanak, Dawid P., et al. “Calcium Looping with Inherent Energy Storage for Decarbonisation of Coal-Fired Power Plant.” *Energy and Environmental Science*, vol. 9, no. 3, Royal Society of Chemistry, Mar. 2016, pp. 971–83, doi:10.1039/c5ee02950c.

- [34]. Abedin, Ali H. "A Critical Review of Thermochemical Energy Storage Systems." *The Open Renewable Energy Journal*, vol. 4, no. 1, Bentham Science Publishers Ltd., Aug. 2011, pp. 42–46, doi:10.2174/1876387101004010042.
- [35]. Ortega-Fernández, Iñigo, et al. "Thermophysical Characterization of a By-Product from the Steel Industry to Be Used as a Sustainable and Low-Cost Thermal Energy Storage Material." *Energy*, vol. 89, Elsevier Ltd, Sept. 2015, pp. 601–09.
- [36]. Abanades, J. Carlos, and Diego Alvarez. "Conversion Limits in the Reaction of CO<sub>2</sub> with Lime." *Energy and Fuels*, vol. 17, no. 2, 2003, pp. 308–15, doi:10.1021/ef020152a.
- [37]. Grasa, Gemma S., and J. Carlos Abanades. "CO<sub>2</sub> Capture Capacity of CaO in Long Series of Carbonation/Calcination Cycles." *Industrial and Engineering Chemistry Research*, vol. 45, no. 26, 2006, pp. 8846–51, doi:10.1021/ie0606946.
- [38]. Blamey, J., et al. "The Calcium Looping Cycle for Large-Scale CO<sub>2</sub> Capture." *Progress in Energy and Combustion Science*, vol. 36, no. 2, Elsevier Ltd, 2010, pp. 260–79, doi:10.1016/j.pecs.2009.10.001.
- [39]. Champagne, Scott, et al. "Influence of Steam Injection during Calcination on the Reactivity of CaO-Based Sorbent for Carbon Capture." *Industrial and Engineering Chemistry Research*, vol. 52, no. 6, American Chemical Society, Feb. 2013, pp. 2241–46, doi:10.1021/ie3012787.
- [40]. Valverde, J. M., et al. "Limestone Calcination Nearby Equilibrium: Kinetics, CaO Crystal Structure, Sintering and Reactivity." *Journal of Physical Chemistry C*, vol. 119, no. 4, American Chemical Society, Jan. 2015, pp. 1623–41, doi:10.1021/jp508745u.
- [41]. Ortiz, C.; Chacartegui, R.; Valverde, J. M.; Alovísio, A.; Becerra, J. A. "Power Cycles Integration in Concentrated Solar Power Plants with Energy Storage Based on Calcium Looping". *Energy Convers. Manage.* 2017, 149, 815–829;

- [42]. Tregambi, Claudio, et al. "A Model of Integrated Calcium Looping for CO<sub>2</sub> Capture and Concentrated Solar Power." *Solar Energy*, vol. 120, Elsevier Ltd, Oct. 2015, pp. 208–20, doi:10.1016/j.solener.2015.07.017.
- [43]. Alovio, A., et al. "Optimizing the CSP-Calcium Looping Integration for Thermochemical Energy Storage." *Energy Conversion and Management*, vol. 136, Elsevier Ltd, Mar. 2017, pp. 85–98, doi:10.1016/j.enconman.2016.12.093.
- [44]. Ortiz, C., et al. "The Calcium-Looping (CaCO<sub>3</sub>/CaO) Process for Thermochemical Energy Storage in Concentrating Solar Power Plants." *Renewable and Sustainable Energy Reviews*, vol. 113, Elsevier Ltd, 1 Oct. 2019, doi:10.1016/j.rser.2019.109252.
- [45]. Perejón, Antonio, et al. "The Calcium-Looping Technology for CO<sub>2</sub> Capture: On the Important Roles of Energy Integration and Sorbent Behavior." *Applied Energy*, vol. 162, Elsevier Ltd, 15 Jan. 2016, pp. 787–807, doi:10.1016/j.apenergy.2015.10.121.
- [46]. Valverde, Jose Manuel, and Santiago Medina. "Reduction of Calcination Temperature in the Calcium Looping Process for CO<sub>2</sub> Capture by Using Helium: In Situ XRD Analysis." *ACS Sustainable Chemistry and Engineering*, vol. 4, no. 12, American Chemical Society, Dec. 2016, pp. 7090–97, doi:10.1021/acssuschemeng.6b01966.
- [47]. Schorcht, Frauke, et al. "Best Available Techniques (BAT) Reference Document for the Production of Cement, Lime and Magnesium Oxide." European Commission, 2013, doi:10.2788/12850.
- [48]. Pardo, P., et al. "A Review on High Temperature Thermochemical Heat Energy Storage." *Renewable and Sustainable Energy Reviews*, vol. 32, Apr. 2014, pp. 591–610, doi:10.1016/j.rser.2013.12.014.
- [49]. Shimizu, T., et al. "A Twin Fluid-Bed Reactor for Removal of CO<sub>2</sub> from Combustion Processes." *Chemical Engineering Research and Design*, vol. 77, no. 1, 1999, pp. 62–68, doi:10.1205/026387699525882.

- [50]. Hanak, Dawid P., et al. "A Review of Developments in Pilot-Plant Testing and Modelling of Calcium Looping Process for CO<sub>2</sub> Capture from Power Generation Systems." *Energy and Environmental Science*, vol. 8, no. 8, Royal Society of Chemistry, 29 July 2015, pp. 2199–249, doi:10.1039/c5ee01228g.
- [51]. Valverde Millán, José Manuel. "Fluidization of Fine Powders - Cohesive vs Dynamical Aggregation." *Géotechnique*, vol. 29, no. 1, 2012, pp. 47–65, doi:10.1007/978-94-007-5587-1.
- [52]. Flamant, Gilles, et al. "Experimental Aspects of the Thermochemical Conversion of Solar Energy; Decarbonation of CaCO<sub>3</sub>." *Solar Energy*, vol. 24, no. 4, 1980, pp. 385–95, doi:10.1016/0038-092X(80)90301-1.
- [53]. Edwards, Susan E. B., and Vlatko Materić. "Calcium Looping in Solar Power Generation Plants." *Solar Energy*, vol. 86, no. 9, Sept. 2012, pp. 2494–503, doi:10.1016/j.solener.2012.05.019.
- [54]. Charitos, Alexander, et al. "Experimental Validation of the Calcium Looping CO<sub>2</sub> Capture Process with Two Circulating Fluidized Bed Carbonator Reactors." *Industrial and Engineering Chemistry Research*, vol. 50, no. 16, American Chemical Society, Aug. 2011, pp. 9685–95, doi:10.1021/ie200579f.
- [55]. Valverde, J. M., et al. "Enhancement of CO<sub>2</sub> Capture at Ca-Looping Conditions by High-Intensity Acoustic Fields." *Applied Energy*, vol. 111, Elsevier Ltd, 2013, pp. 538–49, doi:10.1016/j.apenergy.2013.05.012.
- [56]. Romano, Matteo C. "Modeling the Carbonator of a Ca-Looping Process for CO<sub>2</sub> Capture from Power Plant Flue Gas." *Chemical Engineering Science*, vol. 69, no. 1, Elsevier, 2012, pp. 257–69, doi:10.1016/j.ces.2011.10.041.
- [57]. Ortiz, C., et al. "A New Model of the Carbonator Reactor in the Calcium Looping Technology for Post-Combustion CO<sub>2</sub> Capture." *Fuel*, vol. 160, Elsevier Ltd, Aug. 2015, pp. 328–38, doi:10.1016/j.fuel.2015.07.095.
- [58]. Pacio, J., Singer, C., Wetzels, T., & Uhlig, R. (2013). Thermodynamic evaluation of liquid metals as heat transfer fluids in concentrated solar power

plants. *Applied Thermal Engineering*, 60(1–2), 295–302.  
<https://doi.org/10.1016/j.applthermaleng.2013.07.010>

- [59]. Nurhan Adil Ozturk, “Investigation of flow characteristics in heat exchangers of various geometries”, October, 2011.
- [60]. Lovella, Y. G., et al. “Multi-Objective Optimization of the Thermal and Hydraulic Design of a Heat Exchanger of the Type Shell and Tubes.” *ECOS 2015 - 28th International Conference on Efficiency, Cost, Optimization, Simulation and Environmental Impact of Energy Systems*, no. July, 2015.
- [61]. Wasilewski, Marek. “Analysis of the Effects of Temperature and the Share of Solid and Gas Phases on the Process of Separation in a Cyclone Suspension Preheater.” *Separation and Purification Technology*, vol. 168, Elsevier B.V., Aug. 2016, pp. 114–23, doi:10.1016/j.seppur.2016.05.033.
- [62]. De Lena, E., et al. “Process Integration Study of Tail-End Ca-Looping Process for CO<sub>2</sub> Capture in Cement Plants.” *International Journal of Greenhouse Gas Control*, vol. 67, Elsevier Ltd, Dec. 2017, pp. 71–92, doi:10.1016/j.ijggc.2017.10.005.
- [63]. Spinelli, M., et al. “Integration of Ca-Looping Systems for CO<sub>2</sub> Capture in Cement Plants.” *Energy Procedia*, vol. 114, Elsevier Ltd, 2017, pp. 6206–14, doi:10.1016/j.egypro.2017.03.1758.
- [64]. Zement, Rohrbach. “Combined Utilization of Oil Shale Energy and Oil Shale Minerals within Production of Cement and Other Hydraulic Binders.” *Production*, vol. 20, no. 3, 2003, pp. 347–55.
- [65]. Kyaw, Kyaw, et al. “Study of Carbonation of CaO for High Temperature Thermal Energy Storage.” *Journal of Chemical Engineering of Japan*, vol. 31, no. 2, Society of Chemical Engineers, Japan, 1998, pp. 281–84, doi:10.1252/jcej.31.281.
- [66]. Muto, Andrew, and Tim Hansen. “Demonstration of High-Temperature Calcium-Based Thermochemical Energy Storage System for Use with

- Concentrating Solar Power Facilities.” DOE OSTI.GOV, 2019, doi:10.2172/1501361.
- [67]. Ortiz, Carlos, et al. “Off-Design Model of Concentrating Solar Power Plant with Thermochemical Energy Storage Based on Calcium-Looping.” AIP Conference Proceedings, vol. 2126, no. July, 2019, doi:10.1063/1.5117755.
- [68]. Akhbarifar, Sepideh, and Mansour Shirvani. “Improving Cyclone Efficiency for Small Particles.” Chemical Engineering Research and Design, vol. 147, Institution of Chemical Engineers, July 2019, pp. 483–92, doi:10.1016/j.cherd.2019.05.026.
- [69]. Jo, Youngmin, et al. “Development of a Post Cyclone to Improve the Efficiency of Reverse Flow Cyclones.” Powder Technology, vol. 113, no. 1–2, Nov. 2000, pp. 97–108, doi:10.1016/S0032-5910(00)00206-0.
- [70]. De Souza, Francisco José, et al. “Simulation of the Performance of Small Cyclone Separators through the Use of Post Cyclones (PoC) and Annular Overflow Ducts.” Separation and Purification Technology, vol. 142, Elsevier, Mar. 2015, pp. 71–82, doi:10.1016/j.seppur.2014.12.032.
- [71]. Ibhadode, Osezua O., et al. “Performance Characterization of Gas-Solid Cyclone for Separation of Particle from Syngas Produced from Food Waste Gasifier Plant.” European Journal of Sustainable Development Research, vol. 1, no. 2, Modestum Limited, Dec. 2017, doi:10.20897/ejosdr.201713.
- [72]. Ho, Clifford K. “A Review of High-Temperature Particle Receivers for Concentrating Solar Power.” Applied Thermal Engineering, vol. 109, Elsevier Ltd, 25 Oct. 2016, pp. 958–69, doi:10.1016/j.applthermaleng.2016.04.103.
- [73]. Zhang, Shirong, and Xiaohua Xia. “Optimal Control of Operation Efficiency of Belt Conveyor Systems.” Applied Energy, vol. 87, no. 6, Elsevier Ltd, 2010, pp. 1929–37, doi:10.1016/j.apenergy.2010.01.006.
- [74]. Olds, Robert, et al. A Radical Approach to the Vertical Conveyance of Bulk Materials : The Olds Elevator. no. January 2004, 2006, pp. 1–11.

- [75]. Bahadori, Alireza. "Solids Handling Systems and Dryers." *Essentials of Oil and Gas Utilities*, Elsevier, 2016, pp. 423–88, doi:10.1016/b978-0-12-803088-2.00010-9.
- [76]. Hanak, Dawid P., and Vasilije Manovic. "Calcium Looping with Supercritical CO<sub>2</sub> Cycle for Decarbonisation of Coal-Fired Power Plant." *Energy*, vol. 102, Elsevier Ltd, 2016, pp. 343–53, doi:10.1016/j.energy.2016.02.079.
- [77]. Fernández, Angel G., et al. "Mainstreaming Commercial CSP Systems: A Technology Review." *Renewable Energy*, Elsevier Ltd, 1 Sept. 2019, pp. 152–76, doi:10.1016/j.renene.2019.03.049
- [78]. Christian, Joshua, and Clifford Ho. "Alternative Designs of a High Efficiency, North-Facing, Solid Particle Receiver." *Energy Procedia*, vol. 49, Elsevier Ltd, 2014, pp. 314–23, doi:10.1016/j.egypro.2014.03.034.
- [79]. Ho, Clifford K., et al. "On-Sun Testing of an Advanced Falling Particle Receiver System." *AIP Conference Proceedings*, vol. 1734, American Institute of Physics Inc., 2016, doi:10.1063/1.4949074.
- [80]. Xiao, Gang, et al. "Optical and Thermal Performance of a High-Temperature Spiral Solar Particle Receiver." *Solar Energy*, vol. 109, Elsevier Ltd, Nov. 2014, pp. 200–13, doi:10.1016/j.solener.2014.08.037.
- [81]. Prosin, T., et al. "Solar Gas Turbine Systems with Centrifugal Particle Receivers, for Remote Power Generation." *Energy Procedia*, vol. 69, no. 0, Elsevier B.V., 2015, pp. 1382–92, doi:10.1016/j.egypro.2015.03.131.
- [82]. Prosin, T., et al. "Hybrid Solar and Coal-Fired Steam Power Plant with Air Preheating Using a Centrifugal Solid Particle Receiver." *Energy Procedia*, vol. 69, no. 0, Elsevier B.V., 2015, pp. 1371–81, doi:10.1016/j.egypro.2015.03.134.
- [83]. Wu, W., et al. "Proof of Concept Test of a Centrifugal Particle Receiver." *Energy Procedia*, vol. 49, Elsevier Ltd, 2014, pp. 560–68, doi:10.1016/j.egypro.2014.03.060.

- [84]. Meier, Anton, et al. "Multitube Rotary Kiln for the Industrial Solar Production of Lime." *Journal of Solar Energy Engineering, Transactions of the ASME*, vol. 127, no. 3, Aug. 2005, pp. 386–95, doi:10.1115/1.1979517.
- [85]. Abanades, Stéphane, and Laurie André. "Design and Demonstration of a High Temperature Solar-Heated Rotary Tube Reactor for Continuous Particles Calcination." *Applied Energy*, vol. 212, Elsevier Ltd, Feb. 2018, pp. 1310–20, doi:10.1016/j.apenergy.2018.01.019.
- [86]. Ma, Zhiwen, et al. "Fluidized Bed Technology for Concentrating Solar Power With Thermal Energy Storage." *Journal of Solar Energy Engineering*, vol. 136, no. 3, Aug. 2014, doi:10.1115/1.4027262.
- [87]. Briongos, J. V., et al. "Two-Phase Heat Transfer Model of a Beam-down Gas-Solid Fluidized Bed Solar Particle Receiver." *Solar Energy*, vol. 171, no. January, Elsevier, 2018, pp. 740–50, doi:10.1016/j.solener.2018.07.016.
- [88]. Matsubara, K., et al. "High-Temperature Fluidized Receiver for Concentrated Solar Radiation by a Beam-down Reflector System." *Energy Procedia*, 2014, doi:10.1016/j.egypro.2014.03.048.
- [89]. Sakadjian, B., et al. "Fluidized-Bed Technology Enabling the Integration of High Temperature Solar Receiver CSP Systems with Steam and Advanced Power Cycles." *Energy Procedia*, vol. 69, 2015, pp. 1404–11, doi:10.1016/j.egypro.2015.03.126.

## CHAPTER 3

- [90]. Ho, C., et al. "Technology Advancements for next Generation Falling Particle Receivers." *Energy Procedia*, vol. 49, Elsevier Ltd, 2014, pp. 398–407, doi:10.1016/j.egypro.2014.03.043.

- [91]. Corona, Blanca, et al. “Environmental Assessment of a HYSOL CSP Plant Compared to a Conventional Tower CSP Plant.” *Procedia Computer Science*, vol. 83, no. Hcsp\_Oes, Elsevier Masson SAS, 2016, pp. 1110–17, doi:10.1016/j.procs.2016.04.231
- [92]. Fernández, Angel G., et al. “Mainstreaming Commercial CSP Systems: A Technology Review.” *Renewable Energy*, vol. 140, Elsevier Ltd, 1 Sept. 2019, pp. 152–76, doi:10.1016/j.renene.2019.03.049.
- [93]. Tian, Y., and C. Y. Zhao. “A Review of Solar Collectors and Thermal Energy Storage in Solar Thermal Applications.” *Applied Energy*, vol. 104, Elsevier Ltd, Apr. 2013, pp. 538–53, doi:10.1016/j.apenergy.2012.11.051.
- [94]. Alexopoulos, Spiros, and Bernhard Hoffschmidt. “Solar Tower Power Plant in Germany and Future Perspectives of the Development of the Technology in Greece and Cyprus.” *Renewable Energy*, 2010, doi:10.1016/j.renene.2009.11.003.
- [95]. Ortiz, Carlos, et al. “Off-Design Model of Concentrating Solar Power Plant with Thermochemical Energy Storage Based on Calcium-Looping.” *AIP Conference Proceedings*, vol. 2126, no. July, 2019, doi:10.1063/1.5117755.
- [96]. Vant-Hull, L. “Issues with Beam-down Concepts.” *Energy Procedia*, vol. 49, Elsevier B.V., 2014, pp. 257–64, doi:10.1016/j.egypro.2014.03.028.
- [97]. Mokhtar, Marwan Basem. “The Beam-Down Solar Thermal Concentrator : Experimental Characterization and Modeling.” *Mit.Edu*, 2011, pp. 1–117, [http://web.mit.edu/parmstr/www/Theses/Mokhtar 2011.pdf](http://web.mit.edu/parmstr/www/Theses/Mokhtar%202011.pdf).
- [98]. Three Solar Modules of World’s First Commercial Beam-down Tower Concentrated Solar Power Project to Be Connected to Grid – HELIOSCSP. <http://helioscsp.com/three-solar-modules-of-worlds-first-commercial-beam-down-tower-concentrated-solar-power-project-to-be-connected-to-grid/>.
- [99]. China Beam-down CSP Pioneer Predicts 30% Cost Reduction | New Energy Update. [https://analysis.newenergyupdate.com/csp-today/china-beam-down-csp-pioneer-predicts-30-cost-reduction?utm\\_campaign=NEP](https://analysis.newenergyupdate.com/csp-today/china-beam-down-csp-pioneer-predicts-30-cost-reduction?utm_campaign=NEP) CSP

30OCT19

Newsletter2&utm\_medium=email&utm\_source=Eloqua&elqTrackId=2bacaac87ba448ce959cfbdef9557190&elq=59c0b94d592d486b958dbbe2b667b81e&elqaid=48911&elqat=1&elqCampaignId=29830.

- [100]. H. Hasuike, M. Yuasa, H. Wada, K. Ezawa, K. Oku, T. Kawaguchi, N. Mori, W. Hamakawa, H. Kaneko, and Y. Tamaura, “Demonstration of Tokyo Tech Beam-Down Solar Concentration Power System in 100kW Pilot Plant,” Proceedings of 15th International Symposium on Concentrated Solar Power and Chemical Energy Technologies, Germany: 2009.

## CHAPTER 4

- [101]. Rivero, R., and M. Garfias. “Standard Chemical Exergy of Elements Updated.” *Energy*, vol. 31, no. 15, Elsevier Ltd, 2006, pp. 3310–26, doi:10.1016/j.energy.2006.03.020;
- [102]. Dincer, Ibrahim, and Marc A. Rosen. “Chemical Exergy.” *Exergy*, Elsevier, 2013, pp. 31–49, doi:10.1016/b978-0-08-097089-9.00003-6;
- [103]. Bagatti, Corradi, Desco, Ropa, *Immagini della chimica* – ed. Arancione, *Tabella: Entalpia ed entropia standard* © Zanichelli Editore SpA, 2014;
- [104]. Turton, Richard, et al. “Cost Equations and Curves for the CAPCOST Program.” *Analysis, Synthesis and Design of Chemical Processes*, 2012.
- [105]. Chemical Engineering Plant Cost Index: 2018 Annual Value - Chemical Engineering | Page 1. <https://www.chemengonline.com/2019-cepci-updates-january-prelim-and-december-2018-final/>.
- [106]. NETL, *Cost Estimation Methodology for NETL Assessment of Power Plant Performance*, 2011.

- [107]. Weighted Average Cost of Capital – WACC Definition.  
<https://www.investopedia.com/terms/w/wacc.asp>. Accessed 14 Jan. 2020.
- [108]. Spain Government Bond 10Y.  
<https://tradingeconomics.com/spain/government-bond-yield>.
- [109]. KMPG, Equity Market Risk Premium – Research Summary, 2019,  
<https://assets.kpmg/content/dam/kpmg/nl/pdf/2019/advisory/equity-market-risk-premium-research-summary-31032019.pdf>
- [110]. Spain-Germany 10 Year Bond Spread.  
[https://ycharts.com/indicators/spaingermany\\_10\\_year\\_bond\\_spread](https://ycharts.com/indicators/spaingermany_10_year_bond_spread).
- [111]. Mercados y Precios | ESIOS Electricidad · Datos · Transparencia.  
<https://www.esios.ree.es/es/mercados-y-precios>.
- [112]. Ortiz, C., et al. “The Calcium-Looping (CaCO<sub>3</sub>/CaO) Process for Thermochemical Energy Storage in Concentrating Solar Power Plants.” *Renewable and Sustainable Energy Reviews*, vol. 113, Elsevier Ltd, 1 Oct. 2019, doi:10.1016/j.rser.2019.109252.
- [113]. Brochures & Operating Manuals for Plate Heat Exchangers | Kelvion.  
<https://www.kelvion.com/company/fairs-media/downloads/plate-heat-exchangers/>.
- [114]. Vorrias, Ilias, et al. “Calcium Looping for CO<sub>2</sub> Capture from a Lignite Fired Power Plant.” *Fuel*, vol. 113, Elsevier Ltd, 2013, pp. 826–36, doi:10.1016/j.fuel.2012.12.087.
- [115]. Cinocca, Andrea, and Roberto Cipollone. *Un Modello Matematico Di Supporto Alle Tecnologie Del Solare Termodinamico a Concentrazione*. no. September, 2011.
- [116]. De Lena, Spinelli et al., “Techno-economic analysis of calcium looping processes for low CO<sub>2</sub> emission cement plants”, *International Journal of Greenhouse Gas Control*, vol.82, Elsevier Ltd, March 2019, doi: 10.1016/j.ijggc.2019.01.005.

## CHAPTER 5

- [117]. Finkbeiner, Matthias, et al. “The New International Standards for Life Cycle Assessment: ISO 14040 and ISO 14044.” *International Journal of Life Cycle Assessment*, vol. 11, no. 2, Springer, 25 Mar. 2006, pp. 80–85, doi:10.1065/lca2006.02.002.
- [118]. Muralikrishna, I. V., and V. Manickam. “Environmental Management Life Cycle Assessment.” *Environmental Management*, 2017, pp. 57–75, doi:10.1016/B978-0-12-811989-1.00005-1.
- [119]. Brusseau, M. L. “Sustainable Development and Other Solutions to Pollution and Global Change.” *Environmental and Pollution Science*, 3rd ed., Elsevier Inc., 2019, doi:10.1016/b978-0-12-814719-1.00032-x.
- [120]. Simonen, Kathrina. “Life Cycle Assessment.” *Life Cycle Assessment*, 2014, pp. 1–159, doi:10.4324/9781315778730.
- [121]. Molin, Elvira, and Michael Martin. *Assessing the Energy and Environmental Performance of Vertical Hydroponic Farming In Cooperation with Grönska Stadsodling*. 2018, www.ivl.se.
- [122]. Ayesha Shaik Mohiddin, “*Environmental Life Cycle Assessment of a Standalone Hybrid Energy Storage System for Rural Electrification*”, 2018.
- [123]. EPA – United States Environmental Protection Agency, *Life Cycle Assessment: Principles and Practice*, 2006
- [124]. Arce, Alicia. Andrea Immendörfer ( Lead Author ) | *The NETfficient Handbook: Aggregated Energy Storage for Smarter Communities Grid Integration of Distributed Energy Storage Using an Aggregation P ... The NETfficient Handbook: Aggregated Energy Storage for Smarter Co.* no. December, 2018.

- [125]. Kuenlin A, Augsburg G, Gerber L, Maréchal François. (2013). *Life cycle assessment and environomic optimization of concentrating solar thermal power plants*. Proceedings of the 26th International Conference on Efficiency, Cost, Optimization, Simulation and Environmental Impact of Energy Systems, ECOS 2013. Guilin, China, July 16–19, 2013.
- [126]. Ortiz, Carlos, et al. “Off-Design Model of Concentrating Solar Power Plant with Thermochemical Energy Storage Based on Calcium-Looping.” AIP Conference Proceedings, vol. 2126, no. July, 2019, doi:10.1063/1.5117755.
- [127]. Pelay, Ugo, et al. Life Cycle Assessment of Thermochemical Energy Storage Integration Concepts for a Concentrating Solar Power Plant. no. October 2019, 2020, doi:10.1002/ep.13388.
- [128]. Jolliet, Olivier, et al. “IMPACT 2002+: A New Life Cycle Impact Assessment Methodology.” International Journal of Life Cycle Assessment, vol. 8, no. 6, 2003, pp. 324–30, doi:10.1007/BF02978505.
- [129]. Bare, Jane C., et al. “Midpoints versus Endpoints: The Sacrifices and Benefits.” The International Journal of Life Cycle Assessment, vol. 5, no. 6, 2000, pp. 319–26, doi:10.1007/bf02978665.

## CHAPTER 6

- [130]. Fthenakis, V. M., and H. C. Kim. “Photovoltaics: Life-Cycle Analyses.” *Solar Energy*, vol. 85, no. 8, Pergamon, Aug. 2011, pp. 1609–28, doi:10.1016/j.solener.2009.10.002.
- [131]. Pelay, Ugo, et al. *Life Cycle Assessment of Thermochemical Energy Storage Integration Concepts for a Concentrating Solar Power Plant*. no. October 2019, 2020, doi:10.1002/ep.13388.

- [132]. Whitaker, Michael B., et al. “Life Cycle Assessment of a Power Tower Concentrating Solar Plant and the Impacts of Key Design Alternatives.” *Environmental Science and Technology*, vol. 47, no. 11, 2013, pp. 5896–903, doi:10.1021/es400821x.
- [133]. Bhandari, Khagendra P., et al. “Energy Payback Time (EPBT) and Energy Return on Energy Invested (EROI) of Solar Photovoltaic Systems: A Systematic Review and Meta-Analysis.” *Renewable and Sustainable Energy Reviews*, vol. 47, Elsevier, 2015, pp. 133–41, doi:10.1016/j.rser.2015.02.057.
- [134]. Weißbach, D., et al. “Energy Intensities, EROIs (Energy Returned on Invested), and Energy Payback Times of Electricity Generating Power Plants.” *Energy*, vol. 52, Elsevier Ltd, 2013, pp. 210–21, doi:10.1016/j.energy.2013.01.029.
- [135]. Raugei, Marco, et al. “The Energy Return on Energy Investment (EROI) of Photovoltaics: Methodology and Comparisons with Fossil Fuel Life Cycles.” *Energy Policy*, vol. 45, Elsevier, June 2012, pp. 576–82, doi:10.1016/j.enpol.2012.03.008.